Fall 2020

The Trophic Ecology of Coral Reef Sponges in Caribbean Mesophotic Ecosystems

Keir John Macartney
University of New Hampshire, Durham

The Trophic Ecology of Coral Reef Sponges in Caribbean Mesophotic Ecosystems

BY

Keir J. Macartney

Bachelor of Marine Biology (Honours), University of St Andrews, 2016

DISSERTATION

Submitted to the University of New Hampshire

in Partial Fulfillment of

the Requirements for the Degree of

Doctor of Philosophy

In

Molecular and Evolutionary Systems Biology

September 2020

This dissertation was examined and approved in partial fulfillment of the requirements for the degree of Ph.D. in Molecular and Evolutionary Systems Biology by:

Dissertation Director, Michael P. Lesser, Ph.D.,
Research Professor Emeritus, Molecular, Cellular and Biomedical Sciences,
University of New Hampshire

Marc Slattery, Ph.D.,
Professor, Pharmacognosy and Environmental Toxicology in BioMolecular Sciences,
University of Mississippi

Winsor Watson III, Ph.D.,
Professor Emeritus, Biological Sciences,
University of New Hampshire

David Plachetzki, Ph.D.,
Associate Professor, Molecular, Cellular and Biomedical Sciences,
University of New Hampshire

Stephen H. Jones, Ph.D.,
Associate Research Professor, Natural Resources and the Environment
University of New Hampshire

On August 21, 2020

Approval signatures are on file with the University of New Hampshire Graduate School.

Dedication

I would like to dedicate this work to my family. Your unrelenting support and encouragement towards my passion for marine biology put me firmly on the path to this moment. I could not have completed this work without you.

Acknowledgements

First, I want to thank my advisor, Dr. Michael Lesser, for his unwavering guidance and patience during my four years at UNH. I was as green as they come when I arrived at UNH to begin my graduate studies, but your support helped guide me through the many challenges that came up. None of this would have been possible without your Jedi-like wisdom. I would also like to thank my co-advisor, Dr. Marc Slattery, for his guidance on fieldwork and writing. The challenging questions you asked me about my work helped me think more critically about many topics. I would also like to thank the other members of my dissertation committee; Dr. Windsor Watson, Dr. David Plachetzki, Dr. Stephen Jones and Dr. Marianne Litvaitus. I appreciate the wisdom and advice you provided during meetings and for your comments on my work.

I would like to thank the many other faculty members, postdoctoral researchers and UNH students who helped me with analyses and field work. To Dr. Deborah Gochfeld and Dr. Andia Chavez, thank you for your continued assistance during the many trips to the field and for your assistance in the wet laboratory. To Dr. Kathleen Morrow, thank you very much for your comments on many of my early presentations for conferences and showing me the ropes in laboratory. Thank you to Dr. M. Sabrina Pankey, for your extreme patience with the vast number of questions I had about molecular and statistical analyses, your continued support in all thing's laboratory related and for the many helpful comments you have given me on manuscripts or presentations. Thank you to Liz Kintzing for keeping an eye on me during the many technical dives required for this dissertation and for fixing the many problems that cropped up in my CCR unit while we were in the field. Thank you to Amelia Clayshute for her tireless work on the proximate biochemical compositions of sponges. Thank you to Derek Rothenheber, Nate Ennis, Cooper Park, Devon O'Rourke for giving me advice on bioinformatic analyses. I would like to thank Meghan Hartwick for her help in navigating the fine points of formatting this dissertation and her advice on statistical methods. Thank you to Alaina Weinheimer for her continued patience with my endless questions about bioinformatics and the many scripts she helped me write. You kept me sane during the writing of this dissertation. Thanks to Matt Strobel, Jacob Koile and Jon Streter for cracking a couple of cold ones open with me when I needed a morale boost. I also want to thank the scientists at Mote Marine Laboratory and the University of St Andrews. In particular, thank you to Dr. Erinn Muller and Prof. Christopher Todd for inspiring me to pursue a graduate degree in this field.

Lastly, I would also like to thank my family. To my Dad, thank you for all you have done to support me throughout the last few years. To my brother and sister, thanks for taking the time to encourage me when I was struggling. Without the love and support from my family this would not have been possible.

All sample collections complied with the laws of the Cayman Islands and the United States of America. Support was provided by NSF Biological Oceanography (OCE–1632348/1632333), NOAA NIUST (14U752) and the University of New Hampshire Marine Biology Small Grants fund.

Table of Contents

List of Tables

List of Figures

Abstract

Emergent sponges are crucial to the functional ecology of coral reef ecosystems, playing key roles in benthic-pelagic coupling, biogeochemical cycling of key nutrients, and provision of food and habitat to a variety of coral reef fauna. In mesophotic coral reef ecosystems (MCEs), sponges show a repeatable pattern of increasing abundance and diversity with increasing depth. Mesophotic coral reef ecosystems are typically found between 30 – 150 m and are characterized by depth-dependent gradients in photosynthetically active radiation (PAR), and trophic resources such as increases in particulate organic matter (POM) and decreases in dissolved organic matter (DOM). Increased concentrations of POM appear to support increases in open reef sponge abundance, growth rates and diversity in MCEs, however the role of bottom-up control compared to top-down control of sponge distributions is contested in the literature. Given the importance of sponges on MCEs, increasing our understanding of what regulates their distribution and abundances is crucial in understanding MCEs function as a whole. To address this knowledge gap, we conducted a series of studies to assess the role of bottom-up forcing on the trophic ecology of sponges. We hypothesized that sponges on MCEs would be more abundant and have higher growth rates relative to their shallow conspecifics due to increased POM consumption. First, we used both bulk stable isotope analysis (SIA) and compound-specific isotope analysis of amino acids (CSIA-AA) of $\delta^{13}C$ and $\delta^{15}N$ to disentangle the host and microbiome signal, in order to better understand dietary changes between shallow and mesophotic depths, the trophic position of sponges and the potential translocation of resynthesized amino acids by the sponges microbiomes (Chapter 1). We then conducted a reciprocal transplant experiment and natural growth experiment with *Agelas tubulata* between

shallow (22 m) and mesophotic (61 m) depths in order to quantify growth rates, feeding on POM and DOM and nutrient cycling between depths (Chapter 2). As it our data appears to show that a sponge's growth is controlled by gradients in POM and DOM concentrations, we then conducted a "natural" experiment along a shallow to mesophotic depth gradient. We collected tissue samples of four sponges to assess their microbiome community structure and function, SIA and proximate biochemical composition (Chapter 3). While these open reef sponges show increases in abundance and growth rate in MCEs due to increased POM consumption, low light adapted sponges such as the sclerosponge, *Ceratoporella nicholsoni,* are also abundant in mesophotic habitats. We quantified percent cover between a shallow and mesophotic depths and took tissue samples for 16s rRNA metabarcoding and stable isotope analyses (Chapter 4). The collective findings in these studies show that bottom-up forcing is the principle factor influencing the distribution, abundances and growth rates of emergent sponges due to the increased concentrations of more bioavailable POM on MCEs. While there is species-specific translocation of resynthesized amino acids by sponges, the total contributions by heterotrophic microbes through DOM consumption to sponge energetic budgets is still unknown. Species-specific changes in microbial community composition and function were observed in these studies, indicating that gradients in PAR or trophic resources can influence the microbiome of sponges between depths. This has important implications for both sponge trophic strategy and biogeochemical cycling of carbon and nitrogen between shallow and mesophotic depths We also found that cryptic and low light sponges in MCE may not be influenced by the increases in POM and warrant further study given the abundances of these sponges on Caribbean MCEs.

Chapter 1

Trophic Ecology of Caribbean Sponges in the Mesophotic Zone

Keir J. Macartney[1], Marc Slattery[2], Michael P. Lesser[1]

Article in revision at *Limnology and Oceanography*

[1]University of New Hampshire, Department of Molecular, Cellular and Biomedical Sciences and School of Marine Science and Ocean Engineering, Durham, NH 03824 USA

Corresponding author: kjm1049@wildcats.unh.edu – Keir Macartney (ORCID ID: 0000-0002-9461-0445)

mpl@unh.edu – Dr. Michael Lesser (ORCID ID: 0000-0002-0741-3102)

[2]University of Mississippi, Department of BioMolecular Science, Oxford, MS 38677 USA

slattery@olemiss.edu – Dr. Marc Slattery (ORCID ID: 0000-0001-8325-3262)

Keywords: sponges, stable isotopes, mesophotic, particulate organic material, dissolved organic material, compound-specific isotope analysis, microbiome

Abstract

Sponges are a crucial component of Caribbean coral reef ecosystem structure and function. In the Caribbean, many sponges show a predictable increase in percent cover or abundance as depth increases from shallow (<30 m) to mesophotic (30-150 m) depths. Given that sponge abundances are predicted to increase in the Caribbean as coral cover declines, understanding ecological factors that control their distribution is critical. Here we assess if sponge cover increases as depth increases into the mesophotic zone for three common Caribbean reef sponges, *Xestospongia muta*, *Agelas tubulata* and *Plakortis angulospiculatus*, and use stable isotope analyses to determine whether shifts in trophic resource utilization along a shallow to mesophotic gradient occurred. The ecological surveys show that all target sponges significantly increase in percent cover as depth increases. Using bulk stable isotope analysis, we show that as depth increases there are increases in the $\delta^{13}C$ and $\delta^{15}N$ values, reflecting that all sponges examined consumed more heterotrophic picoplankton, with low C:N ratios in the mesophotic. However, compound-specific isotope analysis of amino acids (CSIA-AA) shows that there are species-specific increases in $\delta^{13}C_{AA}$ and $\delta^{15}N_{AA}$ values. It appears that sponges consume similar diets along the depth gradient, with variable changes in isotopic composition due to their unique microbiomes. There were species-specific increases in $\delta^{15}N_{AA}$ values along the depth gradient, which is contrary to our bulk results, as in *A. tubulata*, no increases in $\delta^{15}N_{AA}$ were observed. Based on the CSIA-AA results, it may not be a change in diet quality (i.e., lower C:N ratio picoplankton) that drives changes in sponge abundances, but an increase in quantity of that available particulate organic matter (POM). The $\delta^{13}C_{AA}$ and $\delta^{15}N_{AA}$ values of these sponges also reflect species-specific patterns of host utilization of both POM and dissolved organic matter (DOM), its subsequent re-synthesis, and translocation, by their microbiomes.

Introduction

As coral reefs around the world continue to show declines in biodiversity and health (Gardner et al. 2003, Hoegh-Guldberg et al. 2007, Hughes et al. 2017, 2018) there has been increased interest in understanding processes affecting the structure and function of coral reef communities in the Anthropocene (Waters et al. 2016). The decline in coral cover due to anthropogenic stressors such as pollution, ocean acidification and increases in sea surface temperature (e.g., Hoegh-Guldberg et al. 2007) has resulted in ecological phase shifts in the benthic communities of many coral reefs (McManus et al. 2000). These community shifts are predicted to cause an increase in the abundance of sponges, and changes in the functional attributes of coral reefs as sponge biomass exceeds coral biomass Caribbean-wide (McMurray et al. 2010, Bell et al. 2013, 2018). In the Caribbean, sponges provide an important source of food and habitat for a variety of coral reef species (Diaz & Rutzler 2001, Wulff 2001, Bell 2008). Sponges also play an important role in benthic food webs through benthic-pelagic coupling due to their consumption of live particulate organic material (POM) (Pile 1997, Lesser 2006, Lesser & Slattery 2013) and dissolved organic material (DOM) (de Goeji et al. 2008, 2013, 2017, Mueller et al. 2014), thus coupling water column productivity to benthic secondary productivity (Gili & Coma 1998, Lesser, 2006).

The role of bottom-up (i.e., nutrient availability) versus top-down (i.e., predation) control of sponge distribution, abundance and growth has been debated in the literature (Pawlik et al. 2013, Pawlik et al. 2016, Lesser & Slattery 2013, Slattery & Lesser 2015, Wulff 2017, Scott & Pawlik 2018, Pawlik et al. 2018, Lesser & Slattery 2018, Lesser et al. 2019a). but most of the data on this topic has come from studies of the trophic ecology of sponges on shallow coral reefs (de Goeij et al. 2017).. In contrast, studies in the mesophotic zone, while increasing (Loya et al.

2016), are not as common (Lesser et al. 2018). The mesophotic zone is found between 30-150 m and is defined primarily by gradients of abiotic factors, particularly irradiance (Lesser et al. 2018, Lesser & Slattery 2018). Along the shallow to mesophotic depth gradient, mesophotic sponges exhibit increased growth rates, abundances, and diversity (Lesser 2006, Trussel et al. 2006, Lesser & Slattery 2013, 2018, Slattery & Lesser 2015). Additionally, their primary particulate food sources, auto- and heterotrophic picoplankton, increase with depth (Lesser 2006, Lesser & Slattery 2013). As sponges consume particulate and dissolved food in proportion to its availability (Lesser 2006, de Goeij et al. 2008, Slattery & Lesser 2015), mesophotic sponges should consume more POM with increasing depth (e.g. Slattery and Lesser 2015). Despite the fact that dissolved organic carbon (DOC) declines with increasing depth (Lesser et al. 2019), it has been suggested that carbon, including both particulate organic carbon (POC) and DOC, is not limiting for sponges along the shallow to mesophotic depth range (Lesser et al. 2018, Lesser & Slattery 2018). Nitrogen, however, is much more likely to be a limiting nutrient for sponge growth (e.g. Hadas et al. 2009). Heterotrophic picoplankton, with low C:N ratios, increase with increasing depth and may supply the nitrogen required for the observed increase in growth rates and biomass of mesophotic sponges (Lesser et al. 2018). These patterns suggest that sponge populations are strongly influenced by bottom-up processes (Lesser & Slattery 2013, Slattery & Lesser 2015, de Goeij et al. 2017).

One of the most common analytical tools used for studying the trophic ecology of an organism is bulk stable isotopic analysis (SIA), particularly the stable isotopes $\delta^{15}N$ and $\delta^{13}C$ (Fry 2006). However, sponges present a unique problem for SIA-based studies of their trophic ecology due to the presence of a diverse microbiome in their tissues and their consumption of free-living microbes in the plankton (Schmitt et al. 2012, Hentschel et al. 2012, Pita et al. 2018).

For sponges, the bulk $\delta^{13}C$ and $\delta^{5}N$ values become enriched as depth increases into the mesophotic zone (Slattery et al. 2011, Morrow et al. 2016), indicating a shift in diet from autotrophic to heterotrophic resources in sponge diets at mesophotic depths. Using compound-specific isotope analysis of amino acids (CSIA-AA) may provide increased resolution, compared to bulk SIA, of sponge trophic ecology along environmental gradients. This is important as bulk SIA represents a mixed signal of host, microbes and the trophic resources they consume. Because of the unique fractionation patterns of $\delta^{15}N$ and $\delta^{13}C$ stable isotopes for different amino acids (AAs), the $\delta^{13}C$ composition of essential amino acids (EAAs) can be used to effectively "fingerprint" the biosynthetic origin of source carbon due to the highly conserved modes of carbon acquisition in bacteria, algae and fungi (Larsen 2009, 2013, McMahon et al. 2016). Additionally, the $\delta^{15}N$ composition of "source" (e.g. phenylalanine) vs "trophic" (e.g. glutamic acid) AAs are informative for both the estimation of trophic position (TP) and the $\delta^{15}N$ composition of AAs at the base of the food web. Source AAs (SAA) undergo minimal to no fractionation as they are transferred through a food web (Phe = ~ 0.5‰) (Chikaraishi et al. 2009), whereas the $\delta^{15}N$ of trophic AAs (TAA) becomes enriched by as much as ~7-8‰ per trophic level (McClelland & Montoya 2002, Chikaraishi et al. 2009, McMahon et al. 2015). Additionally, ΣV values, a measure of bacterial resynthesis and translocation of organic matter, has been successfully used on sponge microbe interactions (Shih et al. 2020) to assess the reliance of sponges on translocated organic material versus feeding from the water column, and will be applied here using the CSIA-AA data on sponges from shallow to mesophotic depths.

Agelas tubulata, Xestospongia muta and *Plakortis angulospiculatus* are three common sponges on coral reefs throughout the Caribbean, and all are considered to be high microbial abundance (HMA) sponges (Gloeckner et al. 2014). While HMA sponges are known to filter

feed upon picoplankton (e.g., Lesser 2006) it is generally accepted that because of their high microbial densities they efficiently utilize DOM as well (Maldonado et al. 2012). Here we assess if the percent cover of these three sponge species increases as depth increases into the mesophotic zone on Little Cayman Island, and use SIA and CSIA-AA to quantify shifts in trophic resource utilization along a shallow to mesophotic depth gradient. We hypothesize that sponges will increase in cover with increasing depth and rely upon the increasing concentration of POM with increasing depth and this will be reflected in both their isotopic signatures and diet reconstruction modeling. Additionally, variability in the utilization of DOM by the sponge microbiome with depth will affect the transfer of re-synthesized organic material to the host.

Materials and methods

Target sponge abundance surveys, sample collection and processing

Replicate samples (n = 3) of *Agelas tubulata*, *Xestospongia muta* and *Plakortis angulospiculatus* were collected using open circuit technical diving at 10, 18, 30, 61 and 91 m at Rock Bottom Wall, Little Cayman, Cayman Islands (19º 42'7.36" N, 80º 3'24.94" W) in the Spring of 2009. The abiotic environment (i.e., light, temperature) of this site from shallow to mesophotic depths is described in Morrow et al. (2016), while from an oceanographic perspective this site is occasionally impacted by internal waves (Lesser et al. 2009). To quantify sponge cover with increasing depth the percent cover of the target species was estimated using replicate (n=10) 1 m^2 quadrats positioned at random points along transect lines (n=3-9 at each depth) of 20 x 2 m at each depth. The survey data for *P. angulospiculatus* presented are from Slattery et al. (2016) and reanalyzed for this study. At each depth, all sponges were sampled by cutting a "pie-slice" of sponge tissue from the apical lip of the osculum including both pinacoderm and mesohyl as

described in Morrow et al. (2016). Samples were transported on ice to the laboratory and immediately frozen. All samples were transported frozen to the University of New Hampshire where they were freeze-dried and ground to a powder for stable isotope analyses.

Bulk stable isotope analysis

Bulk stable isotope data for *X. muta* and *P. angulospiculatius* were taken from Morrow et al. (2016), and for *Agelas tubulata* the data are from Slattery et al. (2011) and reanalyzed here to compare to the CSIA-AA analyses. Briefly, subsamples from each piece of sponge tissue, sampled as described above, were sent to the Marine Biological Laboratory (Woods Hole, MA) for the bulk analysis of particulate C and N, as well as the natural abundance of the stable isotopes $\delta^{15}N$ and $\delta^{13}C$. Samples were analyzed using a Europa ANCA-SL elemental analyzer-gas chromatograph attached to a continuous-flow Europa 20-20 gas source stable isotope ratio mass spectrometer. The carbon isotope results are reported relative to Vienna Pee Dee Belemnite, nitrogen isotope results are reported relative to atmospheric air, and both are expressed using the delta (δ) notation in units per mil (‰).

Compound specific isotope analysis of amino acids

Sponge samples were sent to the Isotope Biogeochemistry Laboratory at the University of Hawai‘i at Mānoa for $\delta^{15}N$ and $\delta^{13}C$ analysis of individual amino acids. Both $\delta^{15}N$ and $\delta^{13}C$, were quantified using gas chromatography/combustion-isotope ratio mass spectrometry (GC/C-IRMS) after amino acid extraction and derivatization. Samples were analyzed using either a Thermo Scientific Delta V Plus or a Thermo Scientific MAT 253 mass spectrometer interfaced

with a Thermo Finnigan Trace GC gas chromatograph via a Thermo Finnigan GC-C III. The amino acids measured using this technique were alanine (Ala), glycine (Gly), threonine (Thr), serine (Ser), valine (Val), leucine (Leu), isoleucine (Iso), proline (Pro), aspartic acid (Asp), phenylalanine (Phe) and lysine (Lys). The terminal amide groups in glutamine (Gln) and aspartame (Asn) were cleaved during the chemical isolation of amino acids. This resulted in the conversion of these amino acids to glutamic acid (Glu) and aspartic acid (Asp), respectively. Thus, the isotope value of the combined Glu + Gln was measured (termed Glx), and the isotope value of a combined Asn + Asp was measured (termed Asx). Averaged AA $\delta^{13}C$ and $\delta^{15}N$ values from these analyses can be found in tables S2 and S3.

Statistical analyses

Statistical analyses were conducted using PRIMER (version 7) or JMP (v. 14), and R (version 3.4.3). Differences in percent cover of sponges as a function of depth was assessed with linear regression. Differences in bulk SIA values between species were assessed using ANOVA, and differences between SIA values along the depth gradient were assessed using linear regression. In order to assess relative contributions of common sponge source end members to sponge diet, a fully Bayesian approach using the SIAR4 program (Parnell et al. 2010) within R was utilized on bulk SIA $\delta^{13}C$ and $\delta^{15}N$ values. The coral DOM source data were taken from van Duyl (2011), macroalgal DOM and coral reef POM data were taken from van Duyl (2018) as were the trophic enrichment factors of $0.5 \pm 0.5\%$ (SD) for $\delta^{13}C$ and $3.0 \pm 0.5\%$ (SD) for $\delta^{15}N$ and used as described in Lesser et al. (2020). Separate model runs (500,000 iterations with 50,000 discarded for burn-in) were conducted for each sponge species. For the effects of depth in the mixing model both $\delta^{13}C$ and $\delta^{15}N$ stable isotope values for *Lobophora variegata* (Slattery & Lesser

2014) and *Montastraea cavernosa*, *Montastraea annularis* (now *Orbicella annularis*) and *Agaricia agaricities* (Lesser et al. 2010, Muscatine et al. 1989, 1994) were included as averaged source end members for algal and coral DOM for their respective depths. The end member sources used, their locations, and justification are available in Appendix 1.

The $\delta^{13}C$ values of each amino acid in all sponge samples were normalized to the mean value of all AAs in the sample ($\delta^{13}C_{norAA}$ = $\delta^{13}C_{AA}$ (of interest)-mean all AAs in sample) as described for the multivariate statistics required for the $\delta^{13}C$ fingerprinting approach described in Larsen et al. (2013). To assess if CSIA-AA can be used to separate bacterial isotopic values from sponge isotopic values, a principal component analysis (PCA) and linear discriminant analysis (LDA) were conducted on $\delta^{13}C_{norEAA}$ from the sponges at each depth using source end member data from Larsen et al. (2013) and McMahon et al. (2016). For the CSIA $\delta^{13}C_{EAA}$ diet reconstruction, 5 EAA were used (Thr, Phe, Leu, Iso, Val) and coral reef source data (Red Sea) for those 5 EAA were taken from McMahon et al. (2016). These represent some of the only source CSIA data available for coral reefs (see Appendix 1 for justification). Separate model runs (500,000 iterations with 50,000 discarded for burn-in) were conducted for each sponge species in SIAR4 (Parnell 2010) using a non-zero trophic discrimination factor of 0.1% ± 0.1% for the CSIA-AA data (*sensu* McMahon et al. 2016).

Differences in mean of all $\delta^{13}C_{AA/EAA}$ and $\delta^{15}N_{AA/SAA/TAA}$, TP, and ΣV values between depths within each species were assessed using linear regression with depth as a continuous variable (significance level of α=0.05). Differences in mean $\delta^{13}C_{AA/EAA}$ and $\delta^{15}N_{AA/SAA/TAA}$, TP and ΣV values between species were also assessed using analysis of variance (ANOVA) with Tukey's HSD *post hoc* tests as needed (significance level of α=0.05). Any data not meeting the assumptions of normality were log-transformed before analyses. The trophic position of sponges

at each depth was calculated with $\delta^{15}N_{Phe}$ and $\delta^{15}N_{Glx}$ using a sponge species-specific enrichment factor calculated as described in Chikaraishi et al. (2014) using the formula:

$$TP_{Glx/Phe} = [(\delta^{15}N_{Glx} - \delta^{15}N_{Phe} + \beta)/TDF] + 1$$

where β represents the isotopic difference between $\delta^{15}N_{Glu}$ and $\delta^{15}N_{Phe}$ in aquatic cyanobacteria and algae (-3.4 ± 0.9‰). Species-specific discrimination factors (TDF) were calculated by subtracting the mean $\delta^{15}N_{SAA}$ from the mean $\delta^{15}N_{TAA}$ of each sponge, then the mean value of that calculation from each set of samples was calculated for use as the species-specific discrimination factor (*X. muta* = 8.077, *P. angulospiculatus* = 7.318, *A. tubulata* = 4.75). The ΣV value was calculated as outlined in McCarthy et al. (2007) and as described by Shih et al. (2020), using the average deviation of seven trophic $\delta^{15}N_{AA}$ values (Ala, Glu, Leu, Iso, Pro, Asx, Glx) for all samples as follows:

$$\Sigma V = 1/n \; \Sigma \; \text{Abs} \; (X_{AA})$$

where X of each trophic AA = ($\delta^{15}N_{AA}$ – AVG $\delta^{15}N_{AA}$ (Ala, Glu, Leu, Iso, Pro, Asx, Glx)), and n = the total number of $\delta^{15}N_{AA}$ used in the calculation.

Results

Sponge environment and survey results

From Morrow et al. (2016) vertical profiles of PAR for Little Cayman showed that the maximum surface irradiances were ~ 2400 µmol quanta m^{-2} s^{-1}, and a K_{dPAR} for the water column that ranged from 0.056 to 0.057 m^{-1}. Vertical profiles of temperature showed a well-mixed water column down to ~25 m at Little Cayman with surface temperature ~ 28.5°C at the surface and ~24.5°C at 91 m. For the percent cover of sponges with depth a significant increase was observed for *X. muta* ($t(28) = 8.60$, P = <0.0001), *A. tubulata* ($t(28) = 6.50$, P = <0.0001) and *P. angulospiculatus* ($t(28) = 8.61$, P = <0.0001) (Fig. 1) with the largest increase in percent cover coming at, or after, ~60 m depth for all species.

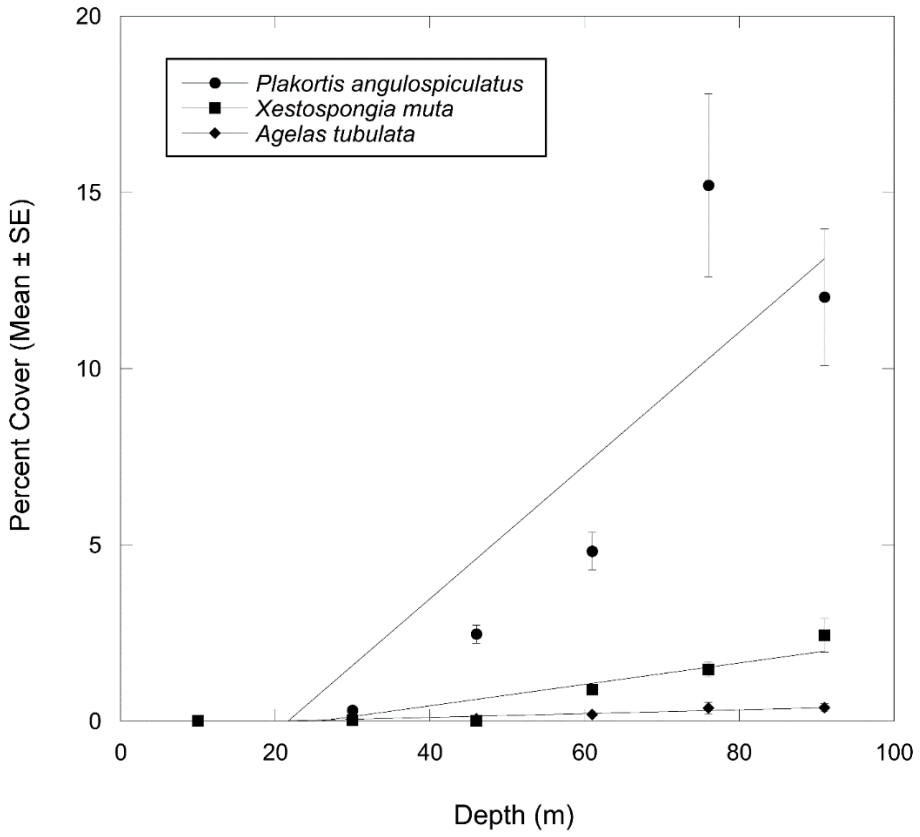

Figure 1. Percent cover per m^2 (mean ± SE) plot of sponges at 10, 18, 30, 61 and 91 m. Regression analysis for effect of depth were all significant: *Plakortis angulospeculatus*, y=-4.0968 + 0.18922x, R^2=0.787 ($t(28) = 8.61$, P = <0.0001), *Agelas tubulata*, y=-0.1105 + 0.0054x, R^2=0.893 ($t(28) = 6.50$, P = <0.0001), *Xestospongia muta*, y=-0.7867 + 0.0305x, R^2=0.831 ($t(28) = 8.60$, P = <0.0001).

Bulk stable isotope analyses:

The bulk stable isotopes of the three sponges show species-specific differences but all show a pattern of enrichment with increasing depth into the mesophotic zone (Fig. 2, Table 1). There were significant differences between all species in tissue $\delta^{13}C$ (ANOVA: F = 63.1331, P = <0.0001, Tukey's HSD: P=<0.05), and $\delta^{15}N$ (ANOVA: F = 53.996P = <0.0001, Tukey's HSD: P=<0.05). There was also a significant effect observed, using regression analyses of the data in Table 1, of depth on the bulk tissue $\delta^{13}C$ ($t(10) = 6.39$, P = <0.0001) and $\delta^{15}N$ ($t(10) = 3.07$, P = 0.012) for *X. muta*, *A. tubulata* $\delta^{13}C$ (t(10) = 4.20, P = 0.001) and $\delta^{15}N$ (t(10) = 4.21, P = 0.001) and *P. angulospiculatus* $\delta^{13}C$ ($t(10) = -3.01$, P = 0.007) and $\delta^{15}N$ ($t(10) = -260$, P = 0.009).

The diet reconstruction using a Bayesian based mixed modelling with bulk SIA data showed high variability in the mean contribution of different food sources to the diet of each sponge species based on 95% confidence intervals of mean contribution to diet (Fig. 3a, Table S1). In *X. muta*, algal DOM contributed the majority of the sponge diet at all depths (50-74%), with POM appearing to reduce its contribution with depth decreasing from 26% at shallow depths to 11% at mesophotic depths. Conversely, in *A. tubulata* POM is a significant contributor (11-37%) to its diet that increases with depth, while for *P. angulospiculatus*, algal DOM again contributed to the majority of the sponge diet at all depths (40-74%), but POM increases in its contribution as depth increases, from 8% in the shallow depths to 16% at mesophotic depths.

Table 1. Means (±SE) of $\delta^{13}C_{EAA}$, $\delta^{15}N_{SAA,}$ trophic position (TP) and ΣV value data for the target species and all.

Species	Depth	Bulk δ13C	Bulk δ15N	δ13C$_{EAA}$	δ15N SAA	δ15N$_{TAA}$	TP phe-glu	ΣV value
Xestospongia muta	**10 m**	-19.77 (0.15)	3.53 (0.10)	-19.96 (0.53)	0.11 (0.21)	8.85(0.28)	2.03 (0.10)	1.65(0.04)
Xestospongia muta	**30 m**	-19.07 (0.08)	4.33 (0.09)	-19.41 (0.37)	-0.04 (0.44)	8.91 (0.95)	1.96 (0.19)	1.77 (0.01)
Xestospongia muta	**61 m**	-18.37 (0.23)	4.07 (0.10)	-19.73 (0.11)	0.74 (0.09)	8.79 (0.49)	1.85 (0.04)	1.43 (0.03)
Xestospongia muta	**91 m**	-17.67 (0.07)	5.13 (0.21)	-18.89 (0.33)	2.36 (0.29)	9.72 (0.21)	1.86 (0.05)	1.86 (0.01)
Agelas tubulata	**18 m**	-15.93 (0.23)	4.77 (0.33)	-19.48 (0.47)	1.40 (0.21)	5.96 (0.13)	1.74 (0.05)	0.85 (0.11)
Agelas tubulata	**30 m**	-15.80 (0.13)	5.03 (0.52)	-18.8 (0.25)	1.7 (0.28)	6.20 (0.35)	1.75 (0.10)	0.82 (0.11)
Agelas tubulata	**61 m**	-15.56 (0.35)	5.87 (0.12)	-18.92 (0.10)	2.175 (0.21)	6.89 (0.41)	1.90 (0.12)	0.98 (0.12)
Agelas tubulata	**91 m**	-15.00 (0.26)	6.40 (0.25)	-18.1 (1.16)	1.2 (0.57)	6.43 (0.31)	1.96 (0.19)	0.94 (0.08)
Plakortis angulospiculatus	**10 m**	-19.04 (0.14)	2.41 (0.21)	-19.12 (0.21)	-1.23 (0.59)	5.61 (0.25)	1.66 (0.02)	1.47 (0.07)
Plakortis angulospiculatus	**30 m**	-18.96 (0.05)	2.48 (0.08)	-19.75 (0.14)	0.133 (0.24)	6.69 (0.50)	1.56 (0.02)	1.5 (0.05)
Plakortis angulospiculatus	**61 m**	-18.76 (0.06)	2.62 (0.22)	-18.83 (0.35)	-0.55 (0.33)	6.98 (0.16)	1.40 (0.23)	1.48 (0.08)
Plakortis angulospiculatus	**91 m**	-18.66 (0.19)	2.70 (0.07)	-17.71 (0.16)	-0.175 (0.44)	8.15 (0.08)	1.63 (0.23)	1.79 (0.09)

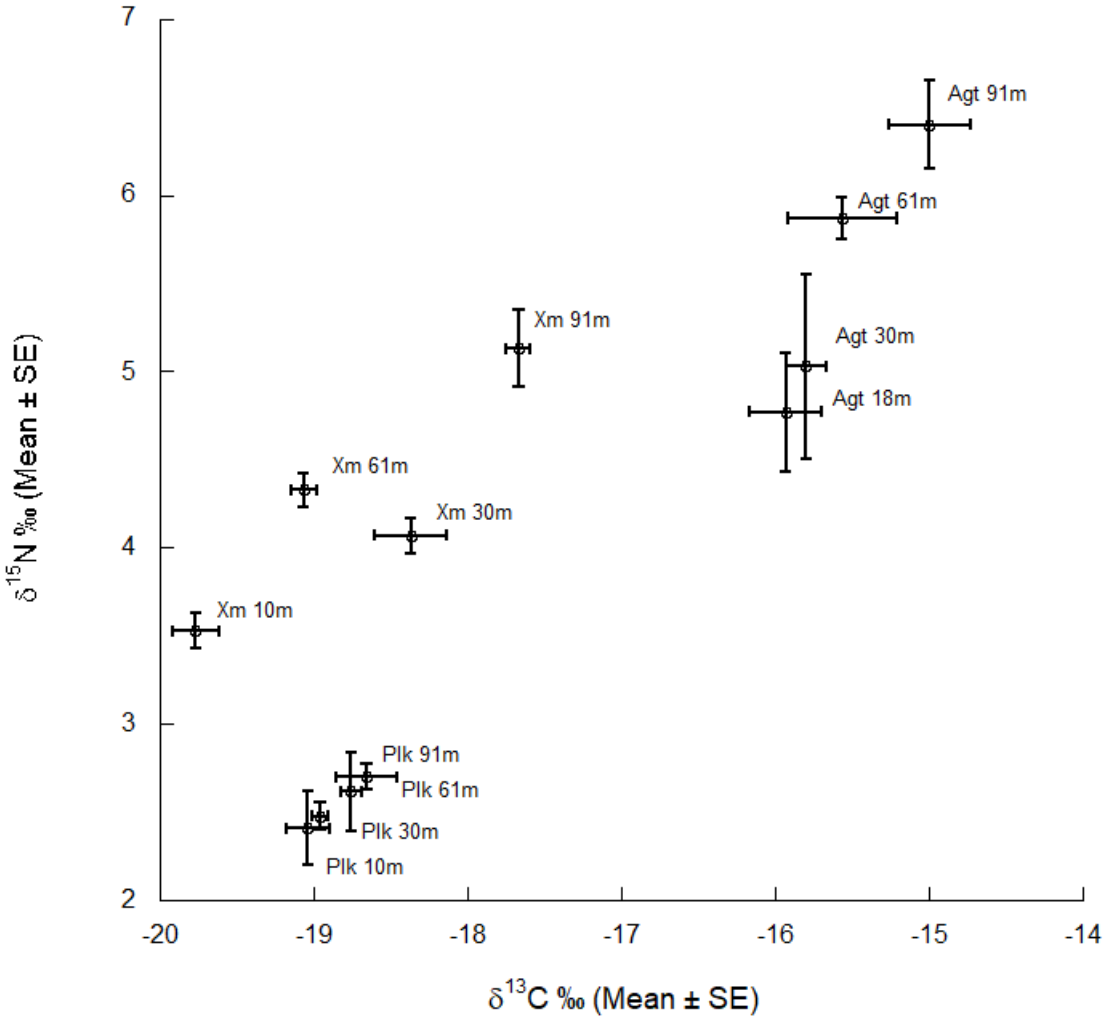

Figure 2. Bivariate plot for bulk stable isotope data for $\delta^{13}C$ and $\delta^{15}N$ from *Xestospongia muta* (Xm), *Plakortis angulospiculatus* (Plk) and *Agelas tubulata* (Agt).

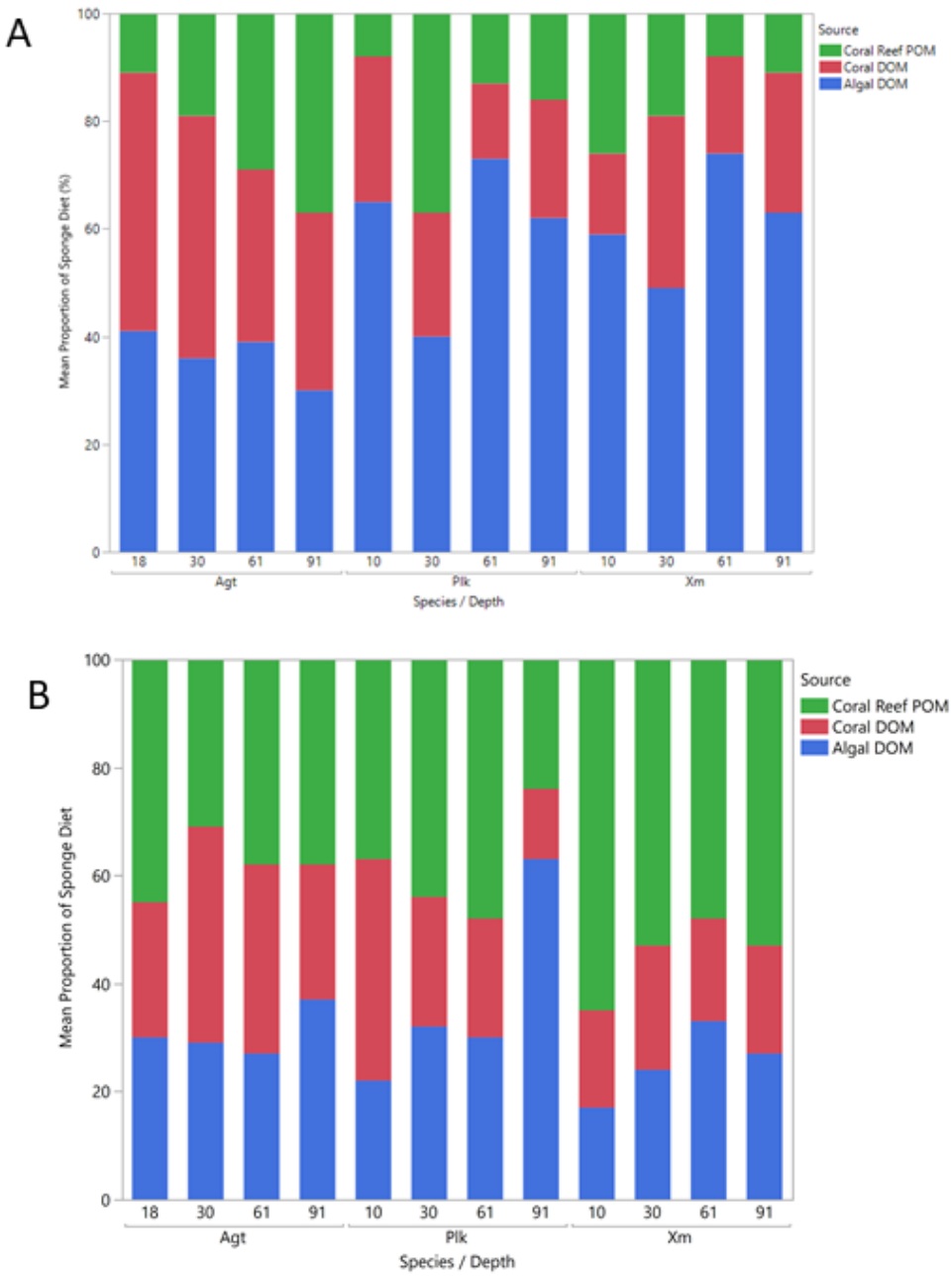

Figure 3. Diet reconstruction of the sponges, using a Bayesian based mixing model, describing the mean percent contribution of algal DOM, coral DOM and coral reef POM in the diet of sponges at 10, 18, 30, 61 and 91 m using **A)** bulk SIA data or **B)** CSIA-AA data. *Agelas tubulata* (Agt), *Plakortis angulospiculatus* (Plk) and *Xestospongia muta* (Xm).

Compound specific isotope analyses of amino acids

The $\delta^{13}C_{EAA}$ fingerprinting analysis, using the Larsen et al. (2013) $\delta^{13}C_{EAA}$ training data set, showed that sponges' group separately from most other organisms, but by sponge species (Fig. 4). In both analyses, sponges with known symbionts are differentiated from their potential food sources such as microalgae, fungus, and bacteria, with microalgae grouping closely with macroalgae. The LDA was used to assess biosynthetic origin of sponge carbon, and the LDA predicted source end-member groups with 91% accuracy. All sponges are predominantly classified with bacteria, detritus, microalgae or macroalgae but not POM (plankton collection using 5 μm mesh net) (Fig. 5).

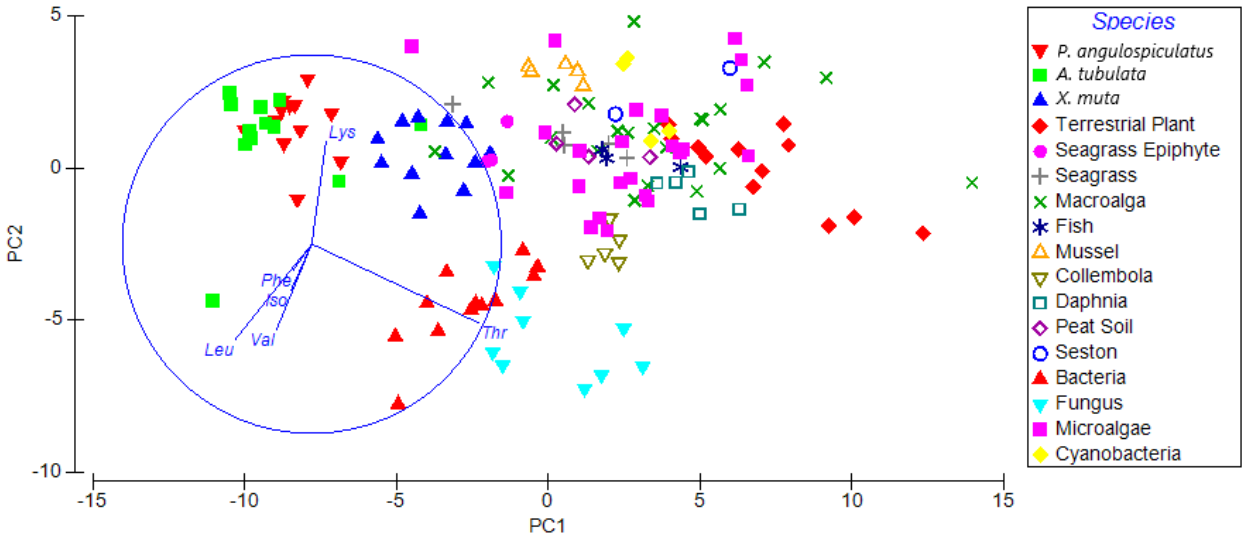

Figure 4. Fingerprinting method for separating functional groups based on principal component analysis of CSIA $\delta^{13}C_{norEAA}$ data. Sponge $\delta^{13}C_{norEAA}$ values are unique, species-specific and well separated compared to potential food resources of prokaryotic and eukaryotic origin, as well as other filter feeding organisms (e.g. mussels).

To quantify changes in trophic strategy between depths, an ANOVA was used on species and linear regression was applied to the mean values of all $\delta^{13}C_{EAA}$, $\delta^{15}N_{SAA,}$ $\delta^{15}N_{TAA,}$ TP and ΣV measurements between depths for each species (Table 1, Fig. 6). There were no significant differences in $\delta^{13}C_{EAA}$ between species (ANOVA: F = 2.2217, P = 0.124). There were significant differences in $\delta^{15}N_{SAA}$ (ANOVA: F = 17.1226, P = <0.0001), with *P. angulospiculatus* significantly lower than both *X. muta* and *A. tubulata* (Tukey's HSD: P<0.05), and significant differences in $\delta^{15}N_{TAA}$ (ANOVA: F = 32.403, P = <0.0001), with *X. muta* significantly greater than *P. angulospiculatus* and *A. tubulata* (Tukey's HSD: P=<0.05).

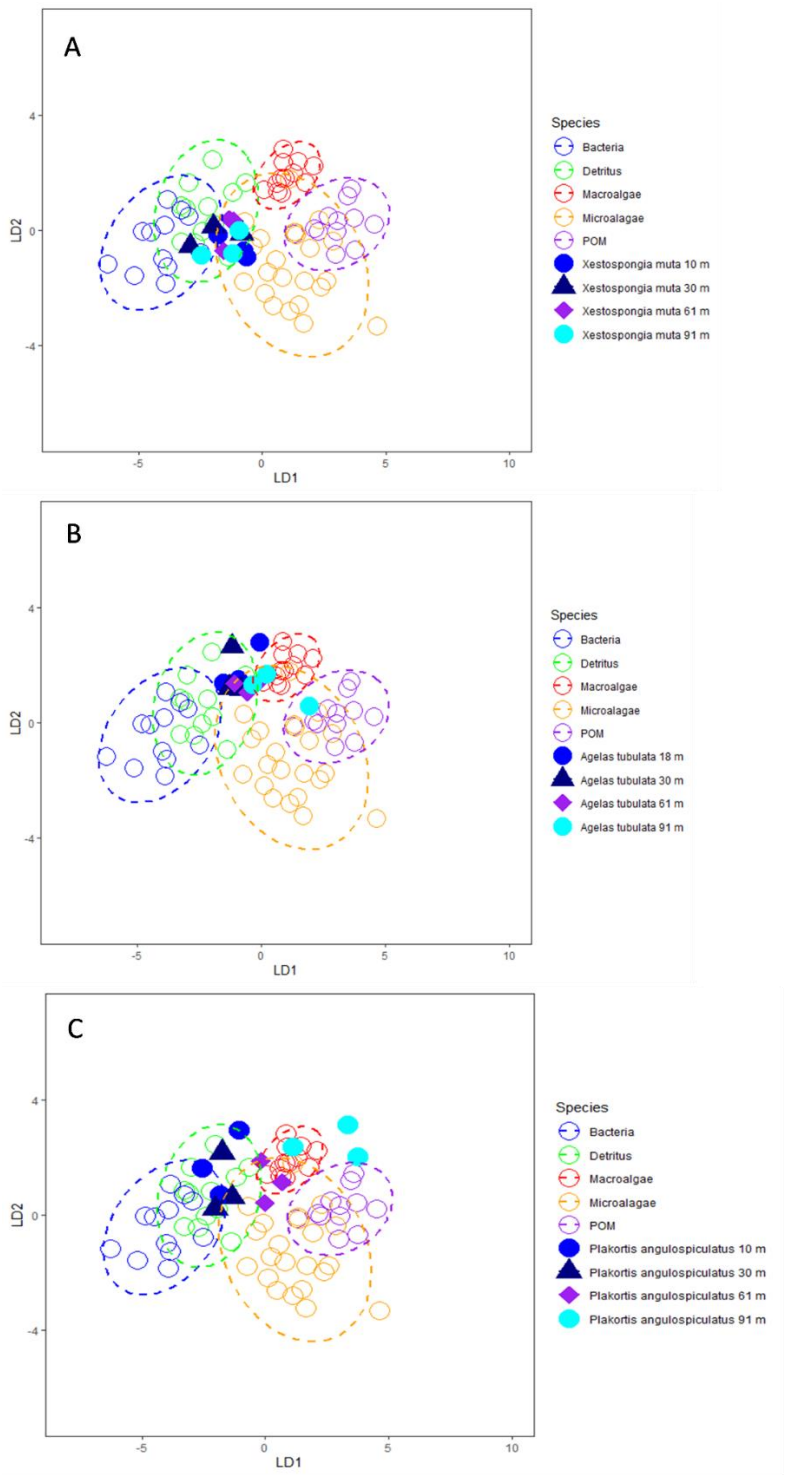

Figure 5. Linear discriminant analysis plots from CSIA $\delta^{13}C_{norEAA}$ data from **A)** *Agelas tubulata* **B)** *X. muta* and **C)** *P. angulospiculatus.* Source end member data was taken from the Larsen et al. (2013) CSIA $\delta^{13}C_{norEAA}$ and from McMahon et al. (2016).

Significant differences were detected (ANOVA: F = 11.432, P = 0.0002) in TP between species with *P. angulospiculatus* significantly lower than *A. tubulata* and *X. muta* (Tukey's HSD: P=<0.05). There were significant differences between species for ΣV values, with higher values indicating more microbial repossessing and translocation of organic matter to the host (ANOVA: F = 69.702, P = <0.0001). *Post-hoc* comparisons revealed that *A. tubulata* was significantly lower than *X. muta* and *P. angulospiculatus* (Tukey's HSD: P=<0.05) (Table 1).

Using regression analysis there was no significant effect of depth on $\delta^{13}C_{EAA}$ ($t(10) = 1.73$, P = 0.114), $\delta^{15}N_{TAA}$ ($t(10) = 1.08$, P = 0.305), TP ($t(10) = -1.29$, P = 0.225) or ΣV value ($t(10) =$ 0.63, P = 0.541) for *X. muta*, (Table 1). But there was a significant effect of depth on $\delta^{15}N_{SAA}$ ($t(10) = 4.97$, P = <0.0001) (Table 1). For *A. tubulata* there was no significant effect of depth on $\delta^{13}C_{EAA}$ ($t(10) = 1.51$, P = 0.163), $\delta^{15}N_{SAA}$ (t(10) = -0.18, P = 0.864), $\delta^{15}N_{TAA}$ (t(10) = 1.38, P = 0.197), TP ($t(10) = 1.61$, P = 0.138) or ΣV value ($t(10) = 0.99$, P = 0.3471) (Table 1). For *P. angulospiculatus* there was no significant effect of depth on $\delta^{15}N_{SAA}$ ($t(10) = 1.02$, P = 0.332) or TP ($t(10) = -0.41$, P = 0.689), while there was a significant effect of depth on $\delta^{13}C_{EAA}$ ($t(10) =$ 3.71, P = 0.004), $\delta^{15}N_{TAA}$ ($t(10) = 5.78$, P = 0.001), and ΣV value ($t(10) = 2.55$, P = 0.0287) (Table 1).

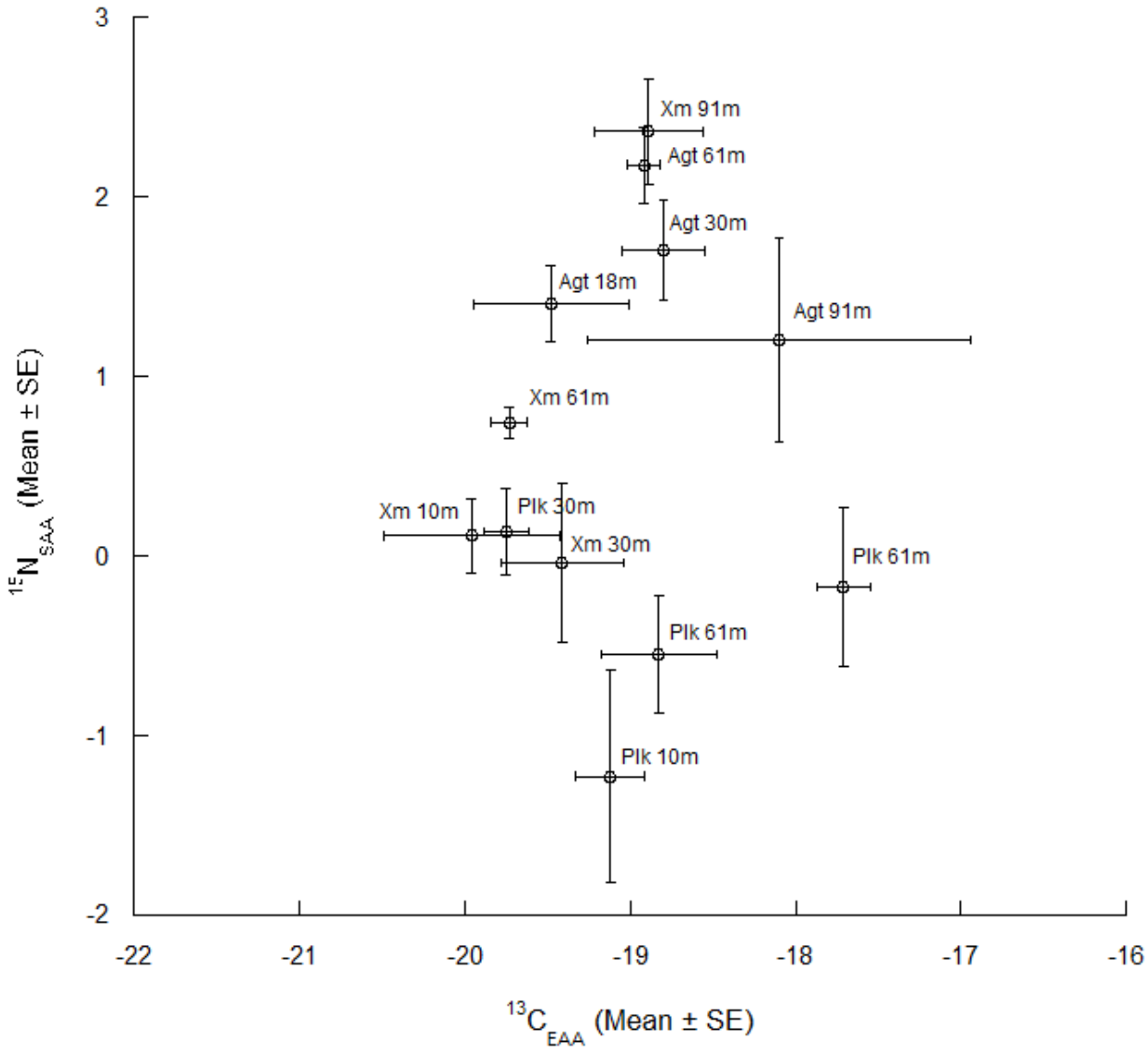

Figure 6. Bivariate plot for CSIA $\delta^{13}C_{EAA}$ and $\delta^{15}N_{SAA}$ stable isotope data from *Xestospongia muta* (Xm), *Plakortis angulospiculatus* (Plk) and *Agelas tubulata* (Agt).

Similar to SIA, the diet reconstruction using a Bayesian based mixing model and $\delta^{13}C_{EAA}$ showed high variability in the mean contribution of different food sources to the diet of each sponge species based on the 95% confidence intervals of the mean of each components contribution to the diet of sponges using the CSIA-AA data (Fig. 3b, Table S1). However, the

diet reconstruction using CSIA-AA data does show a greater contribution of POM in the diet of these sponges. For instance, in *X. muta* the diet is heavily reliant on POM, a 48-65% contribution that does not vary significantly with depth. For *A. tubulata* the CSIA-AA data show a 31-45% POM contribution that does not vary significantly with depth, and for *P. angulospiculatus* the data show a 23-47% POM contribution that does not vary significantly with depth.

Discussion

The sponge species used for this study show an increase in percent cover from shallow to mesophotic depths in Little Cayman consistent with sponges from multiple locations in the Caribbean (Lesser & Slattery 2018), and the Pacific (Slattery & Lesser 2012, Lesser & Slattery 2018). The increase in sponge cover also occurs at the beginning of the lower mesophotic (~60 m) and is consistent with recent observations of global faunal breaks for mesophotic taxa on coral reefs (Lesser et al. 2018, 2019a). Sponges are more abundant (Fig. 1), grow faster and have increased scope for growth as depth increases in the Caribbean from shallow to mesophotic depths (Trussell et al. 2006, Lesser 2006, Slattery & Lesser 2011, 2012, Lesser et al. 2018, Lesser & Slattery, 2018). This is due to the increase in particulate trophic resources available to them with increasing depth (Lesser 2006, Slattery & Lesser 2011, Lesser et al. 2018, 2019a, 2020, Lesser & Slattery, 2018). Specifically, particulate nitrogen availability increases with depth (Lesser et al. 2019) and may play a key role in the patterns of sponge distribution in the Caribbean mesophotic zone (de Goeij et al. 2017).

The bulk SIA data from the three sponges in this study shows a pattern of species-specific enrichment as depth increases (Fig. 2). The $\delta^{13}C$ values reflect the consumption of both

photoautotrophically produced DOM and photoautotrophic and heterotrophic POM (Table 1, $\delta^{13}C$ marine picoplankton: -19 to -24‰, DOM: -16 to -23‰) (Fry 2006, Slattery & Lesser 2011, Hansell 2014, van Duyl et al. 2011, 2018). They also represent fractionation processes, such as carbon or nitrogen cycling, and photoautotrophy, facilitated by the species-specific microbiomes of these sponges. The data show that heterotrophy increases with increasing depth as lighter isotopes are favored during waste excretion leading to enrichment in $\delta^{15}N$ values at higher trophic levels (i.e. more of the heavier isotope leads to an increase in $\delta^{15}N$ values). The increases in both $\delta^{13}C$ and $\delta^{15}N$ suggest an increased reliance on heterotrophic bacterioplankton into the mesophotic zone (Lesser 2006, Trussell et al. 2006, Slattery & Lesser 2011). Concurrent decreases in photoautotrophically produced DOM could also drive these increases, as sponges consume resources proportionally to their availability in the water column (Lesser 2006, Slattery & Lesser 2015).

While the bulk SIA diet reconstruction (Fig. 3a) shows an increased reliance on POM as depth increases for *A. tubulata* and *P. angulospiculatus*, the dependence on algal DOM is still significant into the mesophotic zone. *Xestospongia muta*, surprisingly, shows a decreasing reliance on POM into the mesophotic zone with a higher percent of algal DOM in its diet which could reflect an increasing incorporation of photosynthate from its cyanobacterial symbionts (Morrow et al. 2016). The diet reconstruction also shows that both sponge cells and the microbiome are utilizing DOM, as sponge cells take up coral DOM preferentially while the microbiome appears to prefer algal DOM (Rix et al. 2017). Based on this model, the reliance on algal DOM shows that these sponges rely heavily on their microbial symbionts for DOM consumption and reprocessing. This diet reconstruction relies on the isotopic signatures of the end members in the model, and our end member values come largely from the literature but the

use of these data in our diet reconstructions is justifiable (see Supplemental 1). This is because Bayesian mixing models, unlike other isotopic mixing models (e.g., linear), includes the uncertainty of the end member, as well as its geographic variation making the model more generalizable to the species used in this study across the Caribbean (Layman et al. 2012). Additionally, using mixing models on sponge diets will always be problematic to some degree because of the temporal mismatch between a long-lived consumer and short-lived prey and their respective isotopic turnover rates (Moore and Semmens 2008). The CSIA-AA model (Fig. 3b) shows that POM is a larger component of the sponge's diet compared to the results of the bulk SIA model. The mean contributions seen for *X. muta* follow a similar pattern as seen in the bulk model, potentially driven by changes in photosynthate production by cyanobacterial symbionts with depth. For *A. tubulata* and *P. angulospiculatus*, POM contributes to approximately a third of their overall diet. There is a large amount of variability in the CSIA-AA model outputs (Table S1). This may be a result of both small sample sizes of sponges and the use of source end-member data collected from shallow reefs in the Red Sea (McMahon et al. 2016) as opposed to having direct data from the Caribbean. Additionally, the lack of $\delta^{15}N_{SAA}$ may also obscure small-scale changes between depths in this model. With the lack of CSIA-AA data in general for Caribbean source-end members, it must be noted that these multivariate and Bayesian mixing models have increased variability as a result of the use of data from different locations and time scales, but are based on the best available data at the time of the study. Increased sampling of $\delta^{13}C_{EAA}$ and $\delta^{15}N_{SAA}$ from Caribbean source end members will be important in increasing overall accuracy in these analyses.

Additional analyses of the CSIA-AA data, using the $\delta^{13}C_{norEAA}$ fingerprinting method based on the Larsen et al. (2013) training dataset and data from McMahon et al. (2016), reveals that

sponge $\delta^{13}C_{norEAA}$ values are both unique to sponges and species-specific when compared to the $\delta^{13}C_{norEAA}$ of a wide range of both prokaryotic and eukaryotic organisms (Fig 4). Sponges were unambiguously separated from their principal planktonic food sources such as cyanobacteria and free-living bacteria (Fig. 4). This was possible despite the fact that sponges host a microbiome consisting of these groups in their tissues. This suggests fundamental differences in the microbial communities of sponges versus the bacterioplankton of the surrounding seawater that can be distinguished using CSIA-AA. For instance, there are multiple aerobic or anaerobic microenvironments within a sponge (Hoffmann et al. 2005, Taylor et al. 2007, Fiore et al. 2010) that are linked to the metabolic diversity found in sponge microbiomes (Hentschel et al. 2012, Fiore et al. 2015, Slaby et al. 2017, Pita et al. 2018) a wide range of $\delta^{13}C_{norEAA}$ values from these metabolic pathways could be contributing to the observed ability to discriminate between the sponge microbiome and the ambient bacterioplankton communities.

An LDA (Fig. 5) of $\delta^{13}C_{norEAA}$ was also used to assess which source end-member a sponge sample classified most closely with. All sponges classify between bacteria, detritus and macroalgae (a proxy for DOM), indicating a reliance on a mixed diet of POM and DOM at all depths. The LDA shows species specific patterns which are likely a result of the species-specific microbiomes utilization of DOM and in the case of *X. muta*, a loss of cyanobacterial photosynthate due to reductions in cyanobacterial symbionts with depth (Morrow et al. 2016). The DOM consumed by sponges could be used for microbial production of essential amino acids, as essential amino acids are derived from microbial, algal or plant organic material and cannot be synthesized *de novo* in animals (Larsen et al. 2009, 2013, McMahon et al. 2016). The microbiome may then translocate (*sensu* Fiore et al. 2015) specific nutrients to the host (Shih et al. 2020) or be consumed directly through phagocytosis (*sensu* Leys et al. 2017) to be used for

sponge growth. It is evident that DOM is an important component of the diets of these sponges but as the LDA classifies the most likely source for each sponge sample, it may not detect finer scale patterns such as changes in the quantity of particular source-end member (i.e. an increase in lower C:N ratio bacterioplankton available as depth increases).

To examine fine scale changes in diet, the mean $\delta^{13}C_{EAA}$, $\delta^{15}N_{SAA,}$ $\delta^{15}N_{TAA,}$ ΣV and TP values between depths for each species, as well as CSIA-AA diet reconstructions, have the potential to provide valuable information into the overall diet of an organism and the metabolic processes of a host and its microbiome at each depth (McCarthy et al. 2007, Larsen et al. 2013, Vokshoori et al. 2014, McMahon et al. 2016). The mean $\delta^{13}C_{EAA}$ of these sponges reflect a diet of both picoplankton and DOM (Fig. 6, Table 1), but the species-specific patterns observed in the bulk data (Fig. 2) were not observed. These sponges appear to be feeding in the same trophic niche at each depth based on the diet reconstructions using $\delta^{13}C_{EAA}$. This suggests that selective feeding is not occurring here, but instead non-selective filtering and utilization of the DOM and POM resources, based on their availability, occurs at all depths. Since available resources change with depth, such as increased heterotrophic bacterioplankton in the mesophotic zone (Lesser 2006, Lesser et al. 2018, 2019), it is highly probable that the patterns of enrichments in mesophotic sponge $\delta^{13}C_{EAA}$ are driven by this change in food availability. The enrichments in $\delta^{13}C_{EAA}$ do not appear to be driven by depth related changes in the community structure in the microbiome of these sponges, as *A. tubulata* shows no significant change in microbiome community structure along the depth gradient (Olson & Gao 2013, Macartney & Lesser, unpublished). The $\delta^{13}C_{EAA}$, however, does follow a similar pattern with depth in *X. muta* and *P. angulospiculatus* where significant changes in their microbiome communities from shallow to mesophotic depths were observed (Olson & Gao 2013, Morrow et al. 2016, Macartney & Lesser,

unpublished). Given that sponge species that do, and do not, exhibit changes in their microbiome communities still show a pattern of enrichment in $\delta^{13}C_{EAA}$ with depth, a functional analysis (i.e., isotope tracer studies) would be needed to fully resolve the role of the microbiome on $\delta^{13}C_{EAA}$ values. Recently, however, Shih et al. (2020) showed that the $\delta^{13}C_{EAA}$ and $\delta^{15}N_{SAA}$ of host and symbiont cells in the sponge, *Mycale grandis* are not significantly different, and that their high ΣV values, a measure of bacterial re-synthesis and translocation of organic material (i.e., amino acids), indicated that these sponges obtained a significant amount of their nutrition directly from their symbionts.

All three of the sponge species examined show a isotopic depletion (i.e. more of the lighter isotope and therefore a decrease in the $\delta^{15}N$ value) in their $\delta^{15}N_{SAA}$ values which indicates that all sponges are consuming resources produced by diazotrophs during nitrogen fixation (-2 to 2‰) (Fig. 6, Table 1, Table S3). While the potential for nitrogen fixation has been reported in sponges previously (Mohammed et al. 2008, Fiore et al. 2013), sponge tissues appear well oxygenated during pumping (Schlappy et al. 2010, Fiore et al. 2013, Leys et al. 2017) which would normally inhibit nitrogen fixation as the enzyme nitrogenase is sensitive to oxygen (Fiore et al. 2010). A more parsimonious explanation for this isotopically depleted signal would be consumption of isotopically light picoplankton and DOM, which are present at all depths, but decreases in abundance with depth (Lesser 2006). Sponges are known to consume unicellular picoplankton such as *Crocosphaera* sp. and *Cyanothece* sp. that fix nitrogen (Bauercachs et al. 2009), which would also influence the depleted value observed here. Populations of unicellular cyanobacteria decrease, while *Prochlorococcus* and heterotrophic prokaryotes increase into the mesophotic (Lesser 2006, Lesser et al. 2019a). *Prochlorococcus*, and most marine species of *Synechoccocus*, are not known to fix nitrogen and their $\delta^{15}N$ value likely reflects the $\delta^{15}N$

isotopic values of DIN in the water column (~3 to 6‰) (Slattery & Lesser 2011, Ren et al. 2012). However, anoxic compartments do occur in sponge tissues, so a combined effect of microbiome-associated nitrogen fixation and feeding on isotopically lighter picoplankton cannot be ruled out. Interestingly, the $\delta^{15}N_{SAA}$ of *P. angulospiculatus* and *A. tubulata* do not undergo significant increases with depth indicating that increases in the bulk $\delta^{15}N$ may be a result of microbial transformations or changes in trophic resources stable isotope composition instead of increased consumption of heterotrophic bacteria. This is contrary to multiple feeding studies (Lesser 2006, Trussell 2006), but it is clear that POM as a resource increases with depth (Chapter 2, Lesser 2006, Trussell et al. 2006, Lesser et al. 2020), so while these sponges CSIA-AA results may not reflect increased heterotrophic picoplankton and thus increased diet quality, they are still likely feeding on increased quantities of POM as depth increases. The observed $\delta^{15}N_{TAA}$ values from all sponges show evidence of isotopic enrichment consistent with one trophic level fractionation (Hannides et al. 2009, Chickariashi et al. 2009, 2014), validating that sponges consume both picoplankton and DOM. The increased values of $\delta^{15}N_{TAA}$ values along the depth gradient observed in *P. angulospiculatus* and *X. muta* (Table 1) also indicate that there is increased trophic enrichment as depth increases, and a decrease in the consumption of photoautotrophically derived nutrients.

The ΣV value of a sponge sample can be used as a proxy for the microbial resynthesis of amino acids within the sponge (McCarthy et al. 2007, Shih et al. 2020). The microbiomes of sponges and sponge cells are known to consume DOM as it is pumped through the host sponge (Rix et al. 2017). The byproducts of metabolizing DOM or photosynthesis by the microbiome are known to be translocated to host cells or through direct symbiont consumption via phagocytosis in the mesohyl (Wilkinson 1979, Taylor et al. 2007, Fiore et al. 2015, Leys et al. 2017, Pita et al.

2018). The ΣV values for all sponges in this study are below 2 which is similar to values seen in zooplankton (McCarthy et al. 2007, Shih et al. 2020) (Table 1). This indicates that while DOM re-synthesis by the microbiome and subsequent transfer to the host is occurring in these sponges, the sponge host is still obtaining food from heterotrophic feeding on picoplankton. The higher ΣV values in *X. muta* and *P. angulospiculatus* compared to *A. tubulata* (Table 1) suggests that they rely more on microbial reprocessing of DOM for nutrients at all depths, as seen in *X. muta*'s symbiosis with cyanobacteria (Morrow et al. 2016). In particular, the significant increase in *P. angulospiculatus* ΣV values with depth suggests that this sponge relies more on their microbial symbionts with depth for DOM consumption and reprocessing relative to shallow conspecifics and may be more dependent on DOM compared to the other sponges in this study. This also appears to be reflected in its TP values which are lower compared to the other sponges. Additionally, their microbiomes may play a larger role in processing waste products that the sponge produces from heterotrophic feeding, such as ammonia. Many sponges are known to have ammonia oxidizing bacteria present in their mesohyl and genomic evidence shows waste uptake in several common sponge symbionts (Hentschel et al. 2012, Pita et al. 2018). This study did not separate microbial symbionts from sponge tissues, however, data from Shih et al. (2020) showed no significant difference in CSIA-AA isotopic composition between sponge tissues and its microbiome. The TP values of the sponges' in this study range between 1-2 (Table 1), indicating that they are primary consumers on Caribbean coral reefs (Hannides et al. 2009, Mompean et al. 2015, Landry et al. 2017) that utilize both POM and DOM. Taken together, the ΣV and TP values provide evidence of consumption of POM and DOM by the host at all depths.

Conclusions

Based on the bulk SIA data from this study, mesophotic sponges have increased reliance on POM consumption based on the enrichment patterns of $\delta^{13}C$ and $\delta^{15}N$. However, these patterns also suggest that these sponges may have varying trophic strategies (i.e. feeding on different source end members) or that their microbiomes influence the results. The CSIA-AA data shows that these sponges feed in the same trophic niche at each depth, consuming DOM and POM in proportion to its availability at all depths but with varying contributions of nutrition from their microbiomes through microbial reprocessing of DOM. Consumption of DOM is crucial for sponge nutrition but the increased quality of POM (i.e. low C:N ratio bacterioplankton) and increased quantity of that diet at depth appears to drive the increase in sponge growth rates. However, the species-specific CSIA-AA results indicate that it is potentially the increased quantity but not quality that is more important for sponges here. While the enrichments in mean $\delta^{13}C_{EAA}$ and $\delta^{15}N_{SAA}$ are lower as depth increases compared to bulk data, this is to be expected due to the lack of fractionation processes and low sampling sizes in this study (Larsen et al. 2009, 2013). The ΣV values from these sponges show that these sponges utilize resynthesized amino acids from their microbiome to varying degrees but also that these sponges rely on both DOM and POM for their carbon and nitrogen budgets at all depths assessed here. This study provides comprehensive evidence that CSIA-AA has the potential to increase our understanding of Caribbean mesophotic coral reef trophic ecology and sets a baseline that can be expanded upon with additional studies of sponge microbiome community structure, increased source-end member sampling, and *in-situ* feeding measurements of sponges in the mesophotic zone.

Acknowledgements

We thank K. Morrow, E. Kintzing, C. Fiore, D. Gochfeld and J. Jarett for field and laboratory support. We thank S. Pankey for comments on sponge microbiomes and statistical analysis. We thank Dr. Brian Popp and Natalie Wallsgrove at the University of Hawaii Biogeochemical Stable Isotope Facility for conducting the CSIA of Amino Acids. All sample collections complied with the laws of the Cayman Islands and the United States of America. This project was funded by the National Science Foundation (OCE 1632348) and NOAA NIUST (14U752). The authors declare no competing conflicts of interest.

Literature Cited

Arthur KE, Kelez S, Larsen T, Choy CA, Popp BN (2014) Tracing the biosynthetic source of essential amino acids in marine turtles using 13C fingerprints. Ecology 95:1285–1293.

Bauersachs T, Schouten S, Compaoré J, Wollenzien U, Stal LJ, Damsteé JSS (2009) Nitrogen isotopic fractionation associated with growth on dinitrogen gas and nitrate by cyanobacteria. Limnol Oceanogr 54:1403–1411.

Bell JJ (2008) The functional roles of marine sponges. Estuar Coast Shelf Sci 79:341–353.

Bell JJ, Davy SK, Jones T, Taylor MW, Webster NS (2013) Could some coral reefs become sponge reefs as our climate changes? Glob Chang Biol 19:2613–2624.

Bell JJ, Rovellini A, Davy SK, Taylor MW, Fulton EA, Dunn MR, Bennett HM, Kandler NM, Luter HM, Webster NS (2018) Climate change alterations to ecosystem dominance: how might sponge-dominated reefs function? Ecology 99:1920–1931.

Chikaraishi Y, Ogawa NO, Kashiyama Y, Takano Y, Suga H, Tomitani A, Miyashita H, Kitazato H, Ohkouchi N (2009) Determination of aquatic food-web structure based on compound-specific nitrogen isotopic composition of amino acids. Limnol Oceanogr Methods 7:740–750.

Chikaraishi Y, Steffan SA, Ogawa NO, Ishikawa NF, Sasaki Y, Tsuchiya M, Ohkouchi N (2014) High-resolution food webs based on nitrogen isotopic composition of amino acids. Ecol Evol 4:2423–2449.

van Duyl FC, Moodley L, Nieuwland G, van Ijzerloo L, van Soest RWM, Houtekamer M, Meesters EH, Middelburg JJ (2011) Coral cavity sponges depend on reef-derived food resources: stable isotope and fatty acid constraints. Mar Biol 158:1653–1666.

van Duyl FC Mueller B, Meesters EH (2018) Spatiotemporal variation in stable isotope signatures (13C and 15N) of sponges on the Saba Bank. PeerJ 6:e5460.

Erwin PM, Thacker RW (2007) Incidence and identity of photosynthetic symbionts in Caribbean coral reef sponge assemblages. J Mar Biol Assoc United Kingdom 87:1683–1692.

Fiore CL, Baker DM, Lesser MP (2013) Nitrogen Biogeochemistry in the Caribbean Sponge, *Xestospongia muta*: A Source or Sink of Dissolved Inorganic Nitrogen? PLoS One 8:e72961.

Fiore CL, Jarett JK, Olson ND, Lesser MP (2010) Nitrogen fixation and nitrogen transformations in marine symbioses. Trends Microbiol 18:455–463.

Fiore CL, Labrie M, Jarett JK, Lesser MP (2015) Transcriptional activity of the giant barrel sponge, *Xestospongia muta* holobiont: molecular evidence for metabolic interchange. Front Microbiol 6:364.

Fry B (2006) Using Stable Isotope Tracers. In: *Stable Isotope Ecology*. Springer New York, p 40–75

Gardner TA (2003) Long-Term Region-Wide Declines in Caribbean Corals. Science (80-) 301:958–960.

Gili J-M, Coma R (1998) Benthic suspension feeders: their paramount role in littoral marine food webs. Trends Ecol Evol 13:316–321.

Gloeckner V, Wehrl M, Moitinho-Silva L, Gernert C, Schupp P, Pawlik JR, Lindquist NL, Erpenbeck D, Wörheide G, Hentschell U (2014) The HMA-LMA dichotomy revisited: an electronmicroscopical survey of 56 sponge species. Bio Bull 227:78-88.

de Goeij JM, Lesser MP, Pawlik JR (2017) Nutrient Fluxes and Ecological Functions of Coral Reef Sponges in a Changing Ocean. In: *Climate Change, Ocean Acidification and Sponges*. Springer International Publishing, p 373–410

de Goeij JM, van Oevelen D, Vermeij MJA, Osinga R, Middelburg JJ, de Goeij AFPM, Admiraal W (2013) Surviving in a marine desert: the sponge loop retains resources within coral reefs. Science (80-) 342:108–110.

Hadas E, Shpigel M, Ilan M (2009) Particulate organic matter as a food source for a coral reef sponge. J Exp Biol 212:3643–3650.

Hannides CCS, Popp BN, Landry MR, Graham BS (2009) Quantification of zooplankton trophic position in the North Pacific Subtropical Gyre using stable nitrogen isotopes. Limnol Oceanogr 54:50–61.

Hansell DA and Carlson CA (2014). *Biogeochemistry of marine dissolved organic matter*. Academic Press.

Hentschel U, Piel J, Degnan SM, Taylor MW (2012) Genomic insights into the marine sponge microbiome. Nat Rev Microbiol 10:641–654.

Hoegh-Guldberg O, Mumby PJ, Hooten AJ, Steneck RS, Greenfield P, Gomez E, Harvell CD, Sale PF, Edwards AJ, Caldeira K, Knowlton N, Eakin CM, Iglesias-Prieto R, Muthiga N, Bradbury RH, Dubi A, Hatziolos ME (2007) Coral reefs under rapid climate change and ocean acidification. Science 318:1737–1742.

Hughes TP (2003) Climate Change, Human Impacts, and the Resilience of Coral Reefs. Science 301:929–933.

Hughes TP, Barnes ML, Bellwood DR, Cinner JE, Cumming GS, Jackson JBC, Kleypas J, van de Leemput IA, Lough JM, Morrison TH, Palumbi SR, van Nes EH, Scheffer M (2017) Coral reefs in the Anthropocene. Nature 546:82–90.

Hughes TP, Kerry JT, Baird AH, Connolly SR, Dietzel A, Eakin CM, Heron SF, Hoey AS, Hoogenboom MO, Liu G, McWilliam MJ, Pears RJ, Pratchett MS, Skirving WJ, Stella JS, Torda G (2018) Global warming transforms coral reef assemblages. Nature 556:492–496.

Kamke J, Sczyrba A, Ivanova N, Schwientek P, Rinke C, Mavromatis K, Woyke T, Hentschel U (2013) Single-cell genomics reveals complex carbohydrate degradation patterns in poribacterial symbionts of marine sponges. ISME J 7:2287–2300.

Landry MR, Décima MR (2017) Protistan microzooplankton and the trophic position of tuna: quantifying the trophic link between micro- and mesozooplankton in marine foodwebs. ICES J Mar Sci 74:1885–1892.

Larsen T, Taylor DL, Leigh MB, OBrien DM (2009) Stable isotope fingerprinting: a novel method for identifying plant, fungal, or bacterial origins of amino acids. Ecology 90:3526–3535.

Larsen T, Ventura M, Andersen N, O'Brien DM, Piatkowski U, McCarthy MD (2013) Tracing Carbon Sources through Aquatic and Terrestrial Food Webs Using Amino Acid Stable Isotope Fingerprinting. PLoS One 8:e73441.

Layman CA, Araujo MS, Boucek R, Hammerschlag-Peyer CM, Harrison E, Jud ZR, & Post DM (2012) Applying stable isotopes to examine food-web structure: an overview of analytical tools. Biological Reviews *87*(3): 545-562.

Lesser MP (2006) Benthic-pelagic coupling on coral reefs: Feeding and growth of Caribbean sponges. J Exp Mar Bio Ecol 328:277–288.

Lesser MP, Slattery M, Stat M, Ojimi M, Gates RD, Grottoli A (2010) Photoacclimatization by the coral *Montastraea cavernosa* in the mesophotic zone: light, food, and genetics. Ecology 91:990-1003.

Lesser MP, Slattery M (2013) Ecology of Caribbean Sponges: Are Top-Down or Bottom-Up Processes More Important? PLoS One 8:e79799.

Lesser MP, Slattery M (2018) Sponge density increases with depth throughout the Caribbean. Ecosphere 9:e02525.

Lesser MP, Slattery M, Laverick JH, Macartney KJ, Bridge TC (2019a) Global community breaks at 60 m on mesophotic coral reefs. Glob Ecol Biogeogr 28:1403–1416.

Lesser MP, Slattery M, Leichter JJ (2009) Ecology of mesophotic coral reefs. J Exp Mar Bio Ecol 375:1–8.

Lesser MP, Slattery M, Mobley CD (2018) Biodiversity and functional ecology of mesophotic coral reefs. Ann Rev Ecol Evol Syst 49:49–71.

Lesser MP, Mueller B, Pankey MS, Macartney KJ, Slattery M, de Goeij JM (2020) Depth-dependent detritus production in the sponge, *Halisarca caerulea*. Limnol Oceaogr doi: 10.1002/lno.11384.

Loya Y, Eyal G, Treibitz T, Lesser MP, Appeldoorn R (2016) Theme section on mesophotic coral ecosystems: advances in knowledge and future perspectives. Coral Reefs 35:1–9.

Maldonado M, Ribes M, van Duyl FC (2012) Nutrient fluxes through sponges: biology, budgets, and ecological implications. Adv Mar Biol 62:113–182.

McCarthy MD, Benner R, Lee C, Fogel ML (2007) Amino acid nitrogen isotopic fractionation patterns as indicators of heterotrophy in plankton, particulate, and dissolved organic matter. Geochim Cosmochim Acta 71:4727–4744.

McClelland JW, Montoya JP (2002) Trophic relationships and the nitrogen isotopic composition of amino acids in plankton. Ecology 83:2173-2180.

McMahon KW, Polito MJ, Abel S, McCarthy MD, Thorrold SR (2015) Carbon and nitrogen isotope fractionation of amino acids in an avian marine predator, the gentoo penguin (*Pygoscelis papua*). Ecol Evol 5:1278–1290.

McMahon KW, Thorrold SR, Houghton LA, Berumen ML (2016) Tracing carbon flow through coral reef food webs using a compound-specific stable isotope approach. Oecologia 180:809–821.

McManus J (2000) Coral reef fishing and coral-algal phase shifts: implications for global reef status. ICES J Mar Sci 57:572–578.

McMurray SE, Henkel TP, Pawlik JR (2010) Demographics of increasing populations of the giant barrel sponge *Xestospongia muta* in the Florida Keys. Ecology 91:560–570.

McMurray SE, Johnson ZI, Hunt DE, Pawlik JR, Finelli CM (2016) Selective feeding by the giant barrel sponge enhances foraging efficiency. Limnol Oceanogr 61:1271–1286.

McMurray SE, Stubler AD, Erwin PM, Finelli CM, Pawlik JR (2018) A test of the sponge-loop hypothesis for emergent Caribbean reef sponges. Mar Ecol Prog Ser 588:1–14.

Moore JW & Semmens BX (2008) Incorporating uncertainty and prior information into stable isotope mixing models. Ecology letters, *11*(5): 470-480.

Mompeán C, Bode A, Gier E, McCarthy MD (2016) Bulk vs. amino acid stable N isotope estimations of metabolic status and contributions of nitrogen fixation to size-fractionated zooplankton biomass in the subtropical N Atlantic. Deep Sea Res I Oceanogr Res Pap 114:137–148.

Morrow KM, Fiore CL, Lesser MP (2016) Environmental drivers of microbial community shifts in the giant barrel sponge, *Xestospongia muta*, over a shallow to mesophotic depth gradient. Environ Microbiol 18:2025–2038.

Mueller B, de Goeij JM, Vermeij MJA, Mulders Y, van der Ent E, Ribes M, van Duyl FC (2014) Natural diet of coral-excavating sponges consists mainly of dissolved organic carbon (DOC). PLoS One 9:e90152.

Muscatine L, Porter JW, Kaplan IR (1989) Resource partitioning by reef corals as determined from stable isotope composition. Mar Biol 100:185–193.

Muscatine L, Porter JW, Kaplan IR (1989) Resource partitioning by reef corals as determined from stable isotope composition - I. $\delta^{13}C$ of zooxanthellae and animal tissue vs depth. Mar Biol 100:185–193.

Olson JB, Gao X (2013) Characterizing the bacterial associates of three Caribbean sponges along a gradient from shallow to mesophotic depths. FEMS Microbiol Ecol 85:74–84.

Parnell AC, Inger R, Bearhop S, Jackson AL (2010) Source partitioning using Stable isotopes: coping with too much variation. PLoS One 5:e9672.

Pawlik JR, Loh T-L, McMurray SE (2018) A review of bottom-up vs. top-down control of sponges on Caribbean fore-reefs: what's old, what's new, and future directions. PeerJ 6:e4343.

Pawlik JR, Loh T-L, McMurray SE, Finelli CM (2013) Sponge communities on Caribbean coral reefs are structured by factors that are top-down, not bottom-up. PLoS One 8:e62573.

Pawlik JR, McMurray SE, Erwin P, Zea S (2015) Trophic ecology of sponges from shallow to mesophotic depths (3 to 150 m): Comment on Pawlik et al. (2015). Mar Ecol Prog Ser 527:275–279.

Pita L, Rix L, Slaby BM, Franke A, Hentschel U (2018) The sponge holobiont in a changing ocean: from microbes to ecosystems. Microbiome 6:46.

Ren H, Sigman DM, Thunell RC, Prokopenko MG (2012) Nitrogen isotopic composition of planktonic foraminifera from the modern ocean and recent sediments. Limnol Oceanogr 57:1011–1024.

Rix L, de Goeij JM, Mueller CE, Struck U, Middelburg JJ, van Duyl FC, Al-Horani FA, Wild C, Naumann MS, van Oevelen D (2016) Coral mucus fuels the sponge loop in warm- and cold-water coral reef ecosystems. Sci Rep 6.

Schmitt S, Tsai P, Bell J, Fromont J, Ilan M, Lindquist N, Perez T, Rodrigo A, Schupp PJ, Vacelet J, Webster N, Hentschel U, Taylor MW (2011) Assessing the complex sponge microbiota: core, variable and species-specific bacterial communities in marine sponges. ISME J 6:564–576.

Scott AR, Pawlik JR (2018) A review of the sponge increase hypothesis for Caribbean mesophotic reefs. Mar Biodivers 49:1073–1083.

Shih JL, Selph KE, Wall CB, Wallsgrove NJ, Lesser MP, Popp BN (2020) Trophic tcology of the Tropical Pacific sponge *Mycale grandis* inferred from amino acid compound-specific isotopic analyses. Microb Ecol 79:495-510.

Slaby BM, Hackl T, Horn H, Bayer K, Hentschel U (2017) Metagenomic binning of a marine sponge microbiome reveals unity in defense but metabolic specialization. ISME J 11:2465–2478.

Slattery M, Lesser MP, Brazeau D, Stokes MD, Leichter JJ (2011) Connectivity and stability of mesophotic coral reefs. J Exp Mar Bio Ecol 408:32–41.

Slattery M, & Lesser MP (2012). Mesophotic coral reefs: a global model of community structure and function. Proc 12th Intl Coral Reef Symp 1:9-13.

Slattery M, Lesser MP. 2014. Allelopathy in the tropical alga *Lobophora variegata* (Phaeophyceae): mechanistic basis for a phase shift on mesophotic coral reefs? J Phycol 50:493-505.

Slattery M, Lesser M P (2015) Trophic ecology of sponges from shallow to mesophotic depths (3 to 150 m): Comment on Pawlik et al. (2015) . Mar Ecol Prog Ser 527:275–279.

Taylor MW, Radax R, Steger D, Wagner M (2007) Sponge-associated microorganisms: evolution, ecology, and biotechnological potential. Microbiol Mol Biol Rev 71:295–347.

Trussell GC, Lesser MP, Patterson MR, Genovese SJ (2006) Depth-specific differences in growth of the reef sponge *Callyspongia vaginalis*: role of bottom-up effects. Mar Ecol Prog Ser 323:149–158.

Vokhshoori NL, Larsen T, McCarthy MD (2014) Reconstructing 13C isoscapes of phytoplankton production in a coastal upwelling system with amino acid isotope values of littoral mussels. Mar Ecol Prog Ser 504:59–72.

Waters CN, Zalasiewicz J, Summerhayes C, Barnosky AD, Poirier C, Ga~uszka A, Cearreta A, Edgeworth M, Ellis EC, Ellis M, Jeandel C, Leinfelder R, McNeill JR, d. Richter D, Steffen W, Syvitski J, Vidas D, Wagreich M, Williams M, Zhisheng A, Grinevald J, Odada E, Oreskes N, Wolfe AP (2016) The Anthropocene is functionally and stratigraphically distinct from the Holocene. Science 351:137.

Wilkinson CR (1979) Nutrient translocation from symbiotic cyanobacteria to coral reef sponges. In: C Levi, N Boury-Esnault (eds).Biologie des Spongiaires,pp 373–380, Coli. Int. C.N.R.S., Paris, No. 291.

Wulff J (2017) Bottom-up and top-down controls on coral reef sponges: disentangling within-habitat and between-habitat processes. Ecology 98:1130–1139.

Wulff JL (2006) A simple model of growth form-dependent recovery from disease in coral reef sponges, and implications for monitoring. Coral Reefs 25:419–426.

Wulff JL (2001) Assessing and monitoring coral reef sponges: why and how? Bull Mar Sci 69:831-846

Table 2 (S1). Contributions of most likely coral reef source end members to sponge diet using both a bulk SIA and CSIA-AA approach. Bayesian means (± SD) of source contributions (%) to sponge diets based on SIAR4**.**

Species	Depth	Data Type	Macroalgae	Coral	Coral Reef POM	Data Type	Macroalgae	Coral	Coral Reef POM
Xestospongia. muta	**10 m**	**Bulk SIA**	59 (36)	15 (19)	26 (27)	**CSIA**	17 (18)	18 (21)	65 (28)
Xestospongia. muta	**30 m**	**Bulk SIA**	49 (34)	32 (28)	19 (21)	**CSIA**	24 (22)	22 (24)	53 (28)
Xestospongia. muta	**61 m**	**Bulk SIA**	74 (25)	18 (24)	8 (11)	**CSIA**	33 (22)	18 (20)	48 (23)
Xestospongia. muta	**91 m**	**Bulk SIA**	63 (31)	26 (32)	11 (13)	**CSIA**	27 (25)	20 (19)	53 (24)
Agelas tubulata	**18 m**	**Bulk SIA**	41 (23)	48 (23)	11 (11)	**CSIA**	30 (25)	25 (22)	45 (26)
Agelas tubulata	**30 m**	**Bulk SIA**	36 (29)	45 (32)	19 (16)	**CSIA**	29 (24)	40 (23)	31 (19)
Agelas tubulata	**61 m**	**Bulk SIA**	39 (27)	32 (37)	29 (19)	**CSIA**	27 (28)	35 (24)	38 (22)
Agelas tubulata	**91 m**	**Bulk SIA**	30 (13)	33 (14)	37 (11)	**CSIA**	37 (27)	24 (21)	38 (23)
Plakortis angulospiculatus	**10 m**	**Bulk SIA**	65 (35)	27 (25)	8 (14)	**CSIA**	22 (21)	41 (19)	37 (15)
Plakortis angulospiculatus	**30 m**	**Bulk SIA**	39 (39)	23 (29)	37 (45)	**CSIA**	32 (27)	23 (20)	44 (23)
Plakortis angulospiculatus	**61 m**	**Bulk SIA**	73 (40)	14 (26)	13 (23)	**CSIA**	30 (25)	22 (19)	47 (21)
Plakortis angulospiculatus	**91 m**	**Bulk SIA**	62 (34)	22 (27)	16 (21)	**CSIA**	63 (21)	13 (15)	23 (19)

Table 3 (S2). Averaged $\delta^{13}C$ CSIA-AA values (± SE) for the target sponge species along the depth gradient.

Species	Depth	Ala	Gly	Thr	Ser	Val	Leu	Iso	Pro	Asx	Glx	Phe	Lys
Xestospongia muta	10 m	-15.2 (1)	-10.8 (1)	-13.73 (0.26)		-22.73 (0.56)	-23.06 (0.78)	-18.6 (0.2)		-13.43 (1.04)	-13.03 (1.36)	-24.13 (0.71)	-17.5 (0.72)
Xestospongia muta	30 m	-15.3 (0.85)	-10.66 (1.12)	-14.6 (0.36)		-22.43 (0.23)	-21.96 (0.85)	-18.83 (0.2)		-12.96 (0.35)	-11.73 (0.8)	-22.46 (0.73)	-16.2 (0.2)
Xestospongia muta	61 m	-15.93 (0.21)	-11.23 (0.72)	-15.6 (0.75)		-22.33 (0.13)	-22.06 (0.06)	-18.5 (0.11)		-14.53 (0.51)	-12.76 (0.37)	-22.43 (0.31)	-17.46 (0.31)
Xestospongia muta	91 m	-14.8 (0.16)	-9.7 (0.87)	-13.7 (0.7)		-21.7 (0.48)	-21.4 (0.17)	-17.6 (0.25)		-14.63 (0.26)	-12.96 (0.28)	-22 (0.19)	-18.13 (0.24)
Agelas tubulata	18 m	-17.56 (0.54)	-20.26 (1.19)	-20.93 (0.84)	-13.43 (0.55)	-20.7 (1.26)	-20.23 (1.57)	-17.66 (1.38)	-16.46 (0.49)	-17.06 (0.61)	-15.73 (1.3)	-21.83 (1.03)	-15.56 (1.11)
Agelas tubulata	30 m	-15.96 (0.08)	-18.1 (0.15)	-19.8 (0.2)	-10.3 (0.51)	-20.56 (0.21)	-19.86 (0.33)	-17.43 (0.54)	-14.63 (0.12)	-14.56 (0.12)	-12.63 (0.08)	-20.16 (0.4)	-14.96 (0.26)
Agelas tubulata	61 m	-15.46 (0.47)	-16.73 (0.46)	-19.8 (0.51)	-10.6 (1.3)	-20.93 (0.06)	-20.43 (0.08)	-17.13 (0.28)	-14.4 (0.25)	-14.4 (0.25)	-12.33 (0.48)	-20.8 (0.4)	-14.43 (0.37)
Agelas tubulata	91 m	-14.86 (1.61)	-15.33 (2.33)	-16.43 (1.59)	-8.8 (1.27)	-19.9 (1.73)	-21.03 (1.91)	-16.16 (1.23)	-14.56 (0.89)	-14.26 (0.97)	-14.26 (1.47)	-20.7 (0.87)	-14.36 (0.77)
Plakortis angulospiculatus	10 m	-16.73 (0.63)	-9.3 (0.62)	-18.43 (1.03)	-0.4 (1.3)	-20.76 (0.28)	-20.13 (0.34)	-18.5 (0.36)	-15.9 (0.15)	-14.23 (0.37)	-12.1 (0.11)	-20.46 (0.2)	-16.43 (0.34)
Plakortis angulospiculatus	30 m	-17.36 (0.21)	-11.93 (0.52)	-19.36 (0.16)	-3.43 (0.44)	-22.13 (0.68)	-21.06 (0.28)	-18.8 (0.2)	-15.66 (0.29)	-14.23 (0.23)	-11.7 (0.32)	-21.56 (0.2)	-15.56 (0.32)
Plakortis angulospiculatus	61 m	-14.13 (1.08)	-7.53 (1.25)	-17.73 (0.87)	-6.5 (0.85)	-20.3 (0.66)	-20.83 (0.32)	-16.46 (0.06)	-14.5 (0.4)	-13.5 (1.02)	-10.16 (0.75)	-21.3 (0.15)	-16.36 (0.49)
Plakortis angulospiculatus	91 m	-11.33 (1.41)	-5.13 (0.73)	-16.66 (0.49)	-5.5 (0.2)	-17.36 (0.18)	-20.56 (0.73)	-14.13 (0.42)	-13.86 (0.12)	-11.3 (0.15)	-9.3 (0.32)	-21 (0.15)	-16.56 (0.52)

Table 4 (S3). Averaged $\delta^{15}N$ CSIA-AA values (± SE) for the target sponge species along the depth gradient.

Species	Depth	Ala	Gly	Thr	Ser	Val	Leu	Iso	Pro	Asx	Glx	Phe	Lys
Xestospongia muta	10 m	10.63 (2.16)	-1.86 (1.46)	10.4 (5.06)	8.4 (7.5)	9.93 (10.06)	-1.7 (1.76)	0.29 (0.12)	0.36 (0.48)	0.11 (0.37)	0.7 (0.05)	0.39 (0.39)	0.45 (0.03)
Xestospongia muta	30 m	11.2 (3.36)	-1.6 (2.46)	10.9 (5.1)	8.1 (7.46)	9.73 (9.93)	-1.26 (1.1)	0.97 (0.74)	0.1 (0.49)	1.26 (0.95)	1.53 (0.43)	0.8 (0.82)	0.76 (0.1)
Xestospongia muta	61 m	9.86 (2.53)	-1.7 (2.3)	11.06 (5.33)	8.36 (7.5)	9.53 (9.86)	-0.43 (1.9)	0.53 (0.42)	1.4 (0.23)	1.23 (0.6)	0.73 (0.51)	0.35 (0.18)	0.16 (0.1)
Xestospongia muta	91 m	11 (4.53)	-0.63 (3.63)	10.65 (5.63)	8.85 (8.96)	10.8 (12.3)	1.9 (2.83)	0.16 (1.04)	0.86 (0.37)	0.36 (0.67)	0.28 (0.29)	0.28 (0.43)	0.1 (0.21)
Agelas tubulata	18 m	6.16 (2.83)	-6.76 (3.13)	9.2 (3.9)	5.46 (4.7)	5.56 (6.73)	-0.2 (0.13)	0.61 (0.14)	0.12 (0.31)	0.3 (0.2)	0.43 (0.05)	0.13 (0.17)	0.4 (0.12)
Agelas tubulata	30 m	6.36 (3.4)	-7.03 (3.4)	9.33 (4.16)	5.23 (5.26)	6.13 (6.93)	-0.03 (0.03)	0.29 (0.25)	0.63 (0.83)	0.56 (0.61)	0.66 (0.14)	0.26 (0.43)	0.43 (0.12)
Agelas tubulata	61 m	7.2 (3.66)	-6.06 (4.7)	10 (4.6)	5.9 (5.73)	6.93 (7.9)	0.2 (0.13)	0.11 (0.18)	0.29 (0.83)	0.77 (0.37)	0.8 (0.29)	0.38 (0.55)	0.1 (0.37)
Agelas tubulata	91 m	6.63 (3.2)	-5.96 (2.63)	9.6 (4.63)	5.43 (5.13)	6.23 (7.4)	-0.6 (0.43)	1.08 (0.4)	0.17 (0.92)	0.25 (0.38)	0.31 (0.18)	0.14 (0.3)	1.1 (0.73)
Plakortis angulospiculatus	10 m	8.03 (0.36)	-4.73 (0.63)	7.3 (3.4)	6.43 (3.2)	5.96 (5)	-3.23 (1.43)	0.84 (0.73)	0.24 (0.48)	0.55 (0.26)	0.08 (0.37)	0.23 (0.55)	0.61 (0.58)
Plakortis angulospiculatus	30 m	9.8 (1.8)	-2.6 (0.53)	7.26 (3.93)	6.96 (4.73)	7.2 (6.93)	-0.63 (0.1)	0.83 (0.37)	0.15 (0.28)	0.86 (0.47)	0.65 (0.29)	0.34 (0.26)	0.33 (0.1)
Plakortis angulospiculatus	61 m	9.26 (0.63)	-2.93 (2)	8.63 (4.43)	8.1 (5.16)	7.23 (6.06)	-0.26 (0.56)	0.8 (0.43)	0.21 (0.2)	0.43 (0.32)	0.2 (0.14)	0.24 (0.14)	1.09 (0.37)
Plakortis angulospiculatus	91 m	10.83 (2.53)	-4.16 (1.03)	10.6 (6.06)	9.93 (5.2)	7.83 (6.6)	-1.46 (0.73)	0.27 (0.74)	0.68 (0.16)	0.35 (0.29)	0.41 (0.25)	0.12 (0.15)	0.83 (0.29)

APPENDIX 1

Supplemental Information on Compound Specific Isotopic Analysis of Amino Acids (CSIA-AA)

In CSIA-AA both $\delta^{15}N$ (trophic versus source amino acids) and $\delta^{13}C$ (essential versus non-essential amino acids) values can be used effectively to unravel trophic sources and metabolic processes with better resolution than bulk tissue isotope analysis because the confounding influence of trophic fractionation is largely absent. In particular, interpreting the trophic position from the $\delta^{15}N$ values of bulk tissues is complicated by the fact that these values are a consequence of two variables; variation in $\delta^{15}N$ values of N available to primary producers and the mean number of steps the consumer is removed from feeding on those primary producers (Vander Zanden and Rasmussen 2001, Martínez del Rio et al. 2009). CSIA-AA avoids these shortcomings of bulk tissue analyses. In CSIA-AA the "source" amino acids (e.g., phenylalanine) of consumer tissues largely retain the $\delta^{15}N$ values of the N sources at the base of the food web, whereas "trophic" amino acids (e.g., glutamic acid) become ^{15}N enriched by approximately 7-8‰ per trophic level (McClelland and Montoya 2002, Chikaraishi et al. 2009). A key advantage of CSIA-AA is that consumer tissue alone is sufficient to obtain integrated information on the $\delta^{15}N$ values of the base of the food web as well as trophic position. Algae, bacteria and fungi have highly conserved modes of carbon acquisition and amino acid biosynthesis that produce unique, and specific, patterns of essential amino acid carbon isotopic fractionation (Keil and Fogel 2001, Ziegler and Fogel 2003) that can be used to "fingerprint" their biosynthetic origin (Scott et al. 2006, Larsen et al. 2009, 2012, 2013). This "fingerprinting" approach (see McMahon et al. 2016 for use in tracing carbon through a coral reef food web), and the isotopic fingerprints of different essential amino acid carbon source end members are faithfully maintained through a food web. Thus, carbon and nitrogen CSIA-AA can resolve between heterotrophic and photoautotrophic sources of DOC/DON and POC/PON (McCarthy et

al. 2004) in sponges and results in a significant increase in the power to resolve autotrophy from heterotrophy and trophic position over environmental gradients compared to bulk isotope analyses.

Justification for Assumptions Made in the SIAR4 Models

The Bayesian mixed modelling of the relative contributions of trophic resources to sponge diets was dependent on several assumptions due to a lack of onsite source end-member data. One such assumption was the use of isotopic values of end members from studies undertaken at different locations than our study site, Little Cayman. While we essentially agree that using isotopic measurements of source end members from the same location would be ideal, we are confident that using the isotopic values from the same species, but from different locations, *a priori* does not change the bulk SIA outputs of the mixing model in this study. For DOM we used the source SI data on macrophytes and corals from Curacao, Saba Bank, Belize and the Bahamas. As an example, if you take the following $\delta^{13}C$ and $\delta^{15}N$ data (mean ± SD) for the macroalgae below as *individual* runs into the SIAR model;

Dictyota spp. from van Duyl 2018; -16.60‰ (1.17) and 0.47‰ (0.60) Curacao
Lobophora variegata from van Duyl 2018; -14.23‰ (2.10) and 1.12‰ (0.93) Curacao
Sargassum spp. from van Duyl 2018; -16.31‰ (2.36) and 1.31‰ (1.32) Curacao
Lobophora variegata from Lesser and Slattery 2014; -18.7‰ (1.39) and 0.77‰ (0.05) Bahamas
Dictyota spp. from Carreón-Palau et al 2013; -14.0‰ (2.7) and -0.09‰ (0.68) Belize

The model output of the percentage contribution by algal DOM to sponge diets is statistically indistinguishable using any of these sources. Therefore, the SIA values that are typical for brown macrophyte sources of DOM in the Caribbean do not have sufficient inherent variability to have affected the interpretation of how much DOM was in the diet of the sponges under study and presented in the manuscript.

For coral DOM (i.e., mucous) the values from van Duyl et al. (2011, Table 2) were used and consisted of four species of coral common throughout the Caribbean. Again, similar to the algal DOM sources discussed above the variability between coral species and locations does not introduce sufficient variation that significantly changes the model outputs for the proportion of coral DOM in the diet of sponges. The isotopic signature of $\delta^{13}C$ for particulate organic material (POM) ranges from -14‰ to-25‰ and for $\delta^{15}N$ it is 3–6‰ from multiple locations in Florida and the Caribbean basin (Land et al. 1975, Owens 1987, Peterson and Fry 1987, Lamb and Swart 2008, Maier et al., 2010, Freeman and Thacker 2011, van Duyl et al. 2011). Our POM values (mean ± SD) of -24.91‰ (1.77) for $\delta^{13}C$ and 4.33‰ (1.24) for $\delta^{15}N$ used in the SIAR model come from van Duyl et al. (2018). These values are also consistent with a large dataset compiled by Briand et al. (2015) from New Caledonia. Again, the site to site variability overlaps and do not produce results in the model output that are statistically different from the outputs using the van Duyl et al. (2018) POM source data. Given this, the use of these DOM and POM sources in the SIAR model provide a more than reasonable database for assessing the percentage contribution of these sources in the diet of sponges. For the CSIA-AA mixed model, there is very little coral reef source-end member data available for CSIA-AA, so this model is based on the best available data. We have made this clear in the manuscript and have included it to illustrate

the potential uses this technique has in understanding sponge trophic ecology. Lastly, this same approach using bulk SIA data was recently published (Lesser et al. 2020)

A second assumption is that the variation of source end-member values may change with depth, as fractionation may be affected by the changing abiotic factors (i.e. irradiance) along the same depth gradient. We did not find that there is sufficient variability associated with changing depth (i.e., irradiances) that could affect the model outputs. The end-member values used in the model were similar to those discussed above from van Duyl et al. (2018) and Briand et al (2015). Larger fractionations in $\delta^{13}C$ and $\delta^{15}N$ can occur beyond ~200m in POM, as observed in Benner et al. (1997) and Eadie & Jeffery (1973) but between 0-100 m the $\delta^{13}C$ and $\delta^{15}N$ values in Caribbean POM are not significantly different. For coral derived DOM values Reynaud et al. (2002) found no effect of irradiance on $\delta^{15}N$ values of zooxanthellae or host tissues such that the DOM signal for $\delta^{15}N$ would not be affected by depth. Similarly, Lesser et al. (2010) found no significant effect of depth on the $\delta^{15}N$ of *M. cavernosa* for tissue or zooxanthellae, and those $\delta^{15}N$ values were similar to the values for mucous in van Duyl et al. (2011). So, it is unlikely that depth would affect the $\delta^{15}N$ signature of DOM from corals. For carbon isotopic signatures Lesser et al. (2010) did see a decrease in $\delta^{13}C$ tissue signatures with increasing depth as did Alamaru et al. (2009) for corals from the Red Sea. The range from shallow (3 m) to mesophotic (91 m) was -12.6‰ to -19.3‰ ($\delta^{15}N$ was invariant with depth as discussed above). Similarly, we have $\delta^{15}N$ and $\delta^{13}C$ data for *Lobophora* from the Bahamas (Slattery and Lesser 2014) and both the $\delta^{13}C$ and $\delta^{15}N$ values are invariant across the shallow to mesophotic depth range and were incorporated into the model at their respective depths. We also incorporated source values for *Montastraea cavernosa, M. annularis* (now known as *Orbicella annularis*) and *Agaricia*

agaricites from Muscatine et al. (1989, 1994) along a depth gradient to the source pool from their respective depths.

The third assumption made for the Bayesian mixed modelling was the disentangling of sponge tissue $\delta^{15}N$ and $\delta^{13}C$ values from symbiont $\delta^{15}N$ and $\delta^{13}C$ values. Despite suggestions that one cannot determine sponge diets without separating host tissues from their microbial symbionts bulk tissue analyses of sponges do, in fact, reveal many aspects of a sponge's diet (e.g., Weisz 2007). In this manuscript we recognize this important fact in the introduction and why CSIA-AA may be more informative. We also know that for dissolved inorganic C and N, and most organic sources as well, the primary uptake in sponges is facilitated by symbiotic microbes followed by translocation to the host (Fiore et al. 2013). For many, but not all, sponges this results in little, or no, differences in $\delta^{13}C$ between host and microbes because of the small amount of fractionation (0.5 to 1.0 per mil) for C isotopes (see Freeman and Thacker 2011). Recently, but using CSIA-AA isotope signatures (Shih et al. 2019), it has been shown that sponge host and bacterial isotopic signatures are not different from each other suggesting that the sponge microbiome is reworking organic matter taken into the holobiont and passing amino acids directly to the sponge host.

Given that there are small differences in the isotopic signature between the host and symbionts for some species of sponge, and large differences between many species as well as changes with depth (Fig. 2) we believe that the issue of host versus microbiome isotopic signatures does not confound the ecological interpretation of our results at this time. This is especially the case since here in this manuscript we are arguing for the greater utility of CSIA-AA analyses. We agree that the separation of host from symbiont cells is important when trying to understand the kinetics of uptake for various substrates, but not a prerequisite for

understanding the trophic ecology of sponges in the field. Lastly, we specifically say that one of the stated reasons for taking the CSIA-AA approach is to address whether the technique can disentangle the host versus bacterial isotopic signatures without physically separating those components (see M+M *Statistical Analyses*) and see the fingerprinting data which show that sponges can be distinguished from the bacterioplankton (heterotrophic bacteria and microalgae) due to their unique signature from CSIA-AA. Lastly, changes in host isotopic signatures occur in the absence of changes in the microbiome strongly suggesting an important role for the sponge host in its diet.

Source Data for Bulk SIA and CSIA SIAR4 Models

The values below represent the pooled and averaged bulk SIA values from multiple depth dependent sources to address the potential variation in source end member $\delta^{15}N$ and $\delta^{13}C$ values due to depth and location. Models for each depth were completed in separate runs of 500,000 iterations with 50,000 discarded for burn-in. Coral DOM consists of *Montastraea cavernosa, M. annularis* (now known as *Orbicella annularis*) and *Agaricia agaricites* from Muscatine et al. (1989, 1994) van Duyl et al. (2011) and Lesser et al. (2010). Algal DOM consists of *Lobophora variegata* and *Dictyota spp*. from van Duyl et al. (2018) and Slattery & Lesser (2014). POM data was taken from van Duyl et al. (2018).

Species	Depth	Mean 13c	SD	Mean 15n	SD
Coral DOM	10-18m	-14.23	0.98	2.22	0.80
Coral DOM	30m	-16.74	2.07	1.35	0.95
Coral DOM	61m	-18.92	2.53	2.51	0.95
Coral DOM	91m	-18.96	2.61	2.51	0.95
Algal DOM	10-18m	-18.70	1.36	0.77	0.29
Algal DOM	30m	-17.53	0.81	0.70	0.01
Algal DOM	61m	-18.64	0.78	0.93	0.38
Algal DOM	91m	-18.64	0.78	0.93	0.38
POM	10-18m	-24.91	1.77	4.33	1.24
POM	30m	-24.91	1.77	4.33	1.24
POM	61m	-24.91	1.77	4.33	1.24
POM	91m	-24.91	1.77	4.33	1.24

The values below represent the source end members used for the CSIA diet reconstruction. Source end-member values δ_{13CEAA} for coral, macroalgae and POM were taken from Red Sea oceanic coral reef values provided in McMahon et al. (2016) supplemental documents. These represent some of the only available coral reef source end members available at the time of publication and are thus used to illustrate the utility of CSIA-AA data in diet reconstructions.

Source	Thr	Thr SD	Iso	Iso SD	Val	Val SD	Phe	Phe SD	Leu	Leu SD
POM	-10.4	1	-16.6	0.8	-20.5	1.3	-24.1	0.5	-25.3	0.3
Algal DOM	-9.6	1	-14.5	1	-16.5	1	-19.2	1.7	-19.4	0.9
Coral DOM	-5.5	1.3	-12.2	0.9	-22.1	1.2	-18	0.4	-22.1	0.8

Appendix References

Benner R, Biddanda B, Black B, & McCarthy, M (1997). Abundance, size distribution, and stable carbon and nitrogen isotopic compositions of marine organic matter isolated by tangential-flow ultrafiltration. Marine Chemistry, 57*:* 243-263.

Boecklen WJ, Yarnes CT, Cook BA, James AC (2011) On the use of stable isotopes in trophic ecology.Ann Rev Ecol Syst 42: 411-440.

Briand MJ, Bonnet X, Goiran C, Guillou G, & Letourneur Y (2015). Major sources of organic matter in a complex coral reef lagoon: identification from isotopic signatures (δ13C and δ15N). PloS one, 10: e0131555.

Carreón-Palau L, Parrish CC, del Angel-Rodríguez JA, Pérez-Espana H, & Aguiñiga-García S (2013). Revealing organic carbon sources fueling a coral reef food web in the Gulf of Mexico using stable isotopes and fatty acids. Limnology and Oceanography, *58*(2), 593-612.

Chikaraishi Y, Ogawa NO, Kashiyama Y, Takano Y, Suga H, Tomitani A, Miyashita H, Kitazato H,Ohkouchi N (2009) Determination of aquatic food-web structure based on compound-specific nitrogen isotopic composition of amino acids. Limnology and Oceanography: Methods 7: 740-750.

Eadie, B. J., & Jeffrey, L. M. (1973). δ13C analyses of oceanic particulate organic matter. Marine Chemistry, 1*:* 199-209.

Fiore CL, Baker DM, Lesser MP (2013) Nitrogen Biogeochemistry in the Caribbean Sponge, *Xestospongia muta*: A Source or Sink of Dissolved Inorganic Nitrogen? PLoS One 8: e72961

Freeman, C. J., & Thacker, R. W. (2011). Complex interactions between marine sponges and their symbiotic microbial communities. Limnology and Oceanography, 56: 1577-1586.

Keil RG, Fogel ML (2001) Reworking of amino acid in marine sediments: Stable carbon isotopic composition of amino acids in sediments along the Washington coast. Limnology and Oceanography46: 14-23.

Lamb K, & Swart PK. (2008). The carbon and nitrogen isotopic values of particulate organic material from the Florida Keys: a temporal and spatial study. *Coral Reefs*, *27*(2), 351-362.

Larsen T, Taylor DL, Leigh MB, O'Brien DM (2009) Stable isotope fingerprinting: a novel method for identifying plant, fungal, or bacterial origins of amino acids. Ecology 90: 3526-3535.

Larsen T, Ventura M, Andersen N, O'Brien DM, Piatkowski U, McCarthy MD (2013) Tracing carbon sources through aquatic and terrestrial food webs using amino acid stable isotope fingerprinting. PLoS ONE 8: e73441.

Larsen T, Wooller MJ, Fogel ML, O'Brien DM (2012) Can amino acid carbon isotope ratios distinguish primary producers in a mangrove ecosystem? Rapid Communications in Mass Spectrometry 26: 1541-1548.

Lesser MP, Mueller B, Pankey MS, Macartney KJ, Slattery M, de Goeij JM (2020) Depth-dependent detritus production in the sponge, *Halisarca caerulea*. Limnol Oceanogr doi: 10.1002/lno.11384

Lesser MP, Slattery M, Stat M, Ojimi M, Gates RD, & Grottoli A (2010). Photoacclimatization by the coral Montastraea cavernosa in the mesophotic zone: light, food, and genetics. Ecology, 91, 990-1003.

Maier C, Weinbauer MG, & Pätzold J (2010). Stable isotopes reveal limitations in C and N assimilation in the Caribbean reef corals *Madracis auretenra*, *M. carmabi* and *M. formosa*. Marine Ecology Progress Series, 412: 103-112.

Martínez del Rio C, Wolf N, Carleton SA, Gannes LZ (2009) Isotopic ecology ten years after a call for more laboratory experiments. Biological Reviews 84: 91-11.

McCarthy MD, Benner R, Lee C, Hedges JI, Fogel M (2004) Amino acid carbon isotopic fractionation patterns in oceanic dissolved organic matter: an unaltered photoautotrophic source for dissolved organic nitrogen in the ocean? Mar Chem 92: 123–134.

McClelland JW, Montoya JP (2002) Trophic relationships and the nitrogen isotopic composition of amino acids. Ecology 83: 2173–2180.

McMahon KW, Thorrold SR, Houghton LA, Berumen ML (2016) Tracing carbon flow through coral reef food webs using a compound-specific stable isotope approach. Oecologia 180: 809-821.

Muscatine L, Porter JW, Kaplan IR (1989) Resource partitioning by reef corals as determined from stable isotope composition. Mar Biol 100:185–193.

Muscatine L, Porter JW, Kaplan IR (1989) Resource partitioning by reef corals as determined from stable isotope composition - I. $\delta^{13}C$ of zooxanthellae and animal tissue vs depth. Mar Biol 100: 185–193.

Peterson, B. J., & Fry, B. (1987). Stable isotopes in ecosystem studies. Ann Rev Ecol Syst, 18: 293-320.

Reynaud S, Ferrier-Pages C, Sambrotto R, Juillet-Leclerc A, Jaubert, J, & Gattuso JP (2002). Effect of feeding on the carbon and oxygen isotopic composition in the tissues and skeleton of the zooxanthellate coral Stylophora pistillata. Marine Ecology Progress Series, 238: 81-89.

Scott JH, O'Brien DM, Emerson D, Sun H, McDonald GD, Salgado A, Fogel ML (2006) An examination of the carbon isotope effects associated with amino acid biosynthesis. Astrobiology 6: 867–880.

Shih JL, Selph KE, Wall CB, Wallsgrove NJ, Lesser MP, Popp BN (2020) Trophic ecology of the Tropical Pacific sponge *Mycale grandis* inferred from amino acid compound-specific isotopic analyses. Microb Ecol 79:495-510.

Slattery M, & Lesser MP (2014). Allelopathy in the tropical alga *Lobophora variegata* (P haeophyceae): mechanistic basis for a phase shift on mesophotic coral reefs?. Journal of Phycology, 50: 493-505.

van Duyl, F. C., Moodley, L., Nieuwland, G., van Ijzerloo, L., van Soest, R. W., Houtekamer, M., & Middelburg, J. J. (2011). Coral cavity sponges depend on reef-derived food resources: stable isotope and fatty acid constraints. Marine Biology, 158: 1653-1666.

Van Duyl FC, Mueller B, & Meesters EH (2018). Spatio–temporal variation in stable isotope signatures (δ13C and δ15N) of sponges on the Saba Bank. PeerJ, 6: e5460.

Vander Zanden J and Rasmussen JB (2001) Variation in δ15N and δ13C trophic fractionation: Implications for aquatic food web studies. Limnology and Oceanography 46: 2061-2066.

Weisz JB, Hentschel U, Lindquist N, & Martens CS (2007). Linking abundance and diversity of sponge-associated microbial communities to metabolic differences in host sponges. Mar Biol, 152: 475-483.

Ziegler SE, Fogel ML (2003) Seasonal and diel relationships between the isotopic compositions of dissolved and particulate organic matter in freshwater ecosystems. Biogeochemistry 64:25-52.

Chapter 2

Growth and Feeding in the Sponge, *Agelas tubulata*, From Shallow to Mesophotic Depths on Grand Cayman

Article formatted for submission to *Ecological Monographs*

Keir J. Macartney[1*], Amelia Clayshute[2], Marc Slattery[2], Michael P. Lesser[3]

[1]University of New Hampshire, Department of Molecular, Cellular and Biomedical Sciences, Durham, NH 03824 USA

[2]University of Mississippi, Department of BioMolecular Science, Oxford, MS 38677 USA

[3]University of New Hampshire, Department of Molecular, Cellular and Biomedical Sciences and School of Marine Science and Ocean Engineering, Durham, NH 03824 USA

*Corresponding author; kjm1049@wildcats.unh.edu

Abstract

On Caribbean coral reefs, sponges are important members of the benthic community and play multiple roles in ecosystem structure and function. They have a particularly important role in benthic pelagic coupling on coral reefs, consuming particulate organic matter (POM) and dissolved organic matter (DOM) and in turn providing food in the form of sponge biomass or he release of detritus for a variety of coral reef organisms. Throughout the Caribbean sponges show consistent increases in their abundance and growth rates as depth increases into the mesophotic zone (30-150 m). This has been hypothesized to be driven by bottom-up forces, particularly the increased supply of nitrogen rich POM in mesophotic coral reef ecosystems (MCEs). In chapter 1 we observed that sponges increased in percent cover in MCEs and that increased consumption of POM as depth increases supports the increased biomass of sponges. Here we tested if the emergent sponge *Agelas tubulata* exhibits increased growth rates on MCEs relative to shallow reefs at Grand Cayman Island and if it is driven by bottom-up forcing. We observed increased growth rates in mesophotic *A. tubulata* compared to shallow conspecifics despite variability in feeding on both POM and DOM. Mesophotic sponges, however, were consistently exposed to greater amounts of POM, which was seasonally variable unlike DOM. Despite the variability in the feeding, both the stable isotopic signatures and mixing models of diet composition support the growth results. These observations are consistent with the hypothesis that mesophotic sponges have higher growth rates due to increased POM availability and consumption over time. These sponges also appear to be important sources of inorganic nutrients such as NO_x and NH_4 at both shallow and mesophotic depths, while mesophotic *A. tubulata* were sources and shallow *A. tubulata* were sinks of PO_4.

Introduction

One of the dominant members of the benthic fauna on Caribbean coral reefs are sponges, which increase in abundance and biodiversity with increasing depth from shallow to mesophotic depths (10-150 m) (Trussell et al. 2006; Lesser et al. 2009, 2018, 2019 a; Lesser and Slattery 2013, 2018). Sponges have multiple functional roles on coral reefs such as providing food and habitat for many ecologically and economically important coral reef species (Diaz and Rützler 2001; Bell 2008), reef stabilization (Bell 2008) and benthic-pelagic coupling (Pile et al. 1997; Lesser 2006; Perea-Blázquez et al. 2012; Lesser and Slattery 2013; Slattery and Lesser 2015). Sponges are conspicuous on mesophotic coral reefs (MCEs), defined as coral reefs occurring from 30-150 m (Lesser et al. 2009, 2018; Loya et al. 2016; Slattery and Lesser 2019) with communities structured primarily by depth-dependent changes in irradiance and dissolved and particulate food (Lesser et al. 2009, 2018, 2019, 2020). Upper MCE (~30-60 m) communities may be important refuges for a variety of shallow reef benthic fauna, while lower MCEs (~60-150 m) harbor unique endemic species that make-up a significant percentage of the community in the lower MCE (Lesser et al. 2018, 2019). Given the importance of sponges and the potential role of MCEs as refuges, understanding what factors regulate sponge distributions along the shallow to mesophotic depth gradient will inform predictions on their population dynamics in the future (*sensu* Lesser and Slattery 2020).

Benthic-pelagic coupling by suspension feeders through the consumption of particulate organic matter (POM) and dissolved organic matter (DOM) supports a large proportion of benthic secondary production (Gili and Coma 1998, de Goeig et al. 2017), and the motile fauna that depends on these resources for food and habitat (Dayton et al. 1974; Diaz and Rützler 2001; Saier 2002; Boudreaux et al. 2006; Bell 2008). Additionally, filter feeders play important roles in

the biogeochemistry of inorganic nutrients in both the water column and the benthos (Fiore et al. 2013a; Griffiths et al. 2017). The linkage between the planktonic communities and the community structure of benthic suspension feeders, and how abiotic factors such as near benthic flow fields influence both active and passive suspension feeders (Gili 2001), results in a variety of diverse marine benthic communities (Gili & Coma 1998). One example is the changes in community structure in rocky coralligenous aggregations in the Mediterranean, where increased flow rates facilitate a highly diverse community due to the increased flux of particulate food supply and where biomass and diversity declines significantly as current induced flow rates, and subsequent food delivery, declines (Gili & Coma 1998). Additionally, the distribution of active versus passive suspension feeders in the Mediterranean is determined by both food supply and flow rates, with sponges, as active suspension feeders, able to exploit areas of low flow compared to passive suspension feeders with the resulting communities determined by the variability in currents (Coppari et al. 2016). Food supply is also known to structure benthic communities in polar regions (Dayton et al. 1974; Cattaneo-Vietti et al. 1999; Orejas et al. 2000; Gili et al. 2001). In Antarctica, near shore and deep-water communities have diverse and dense communities of suspension feeders. Seasonal pulses in particulate food drive increased seasonal growth rates in these suspension feeders (Cattaneo-Vietti et al. 1999; Orejas et al. 2000; Gili et al. 2001), and in particular for sponges and bivalve molluscs. Additionally, different physiological strategies based on seasonal pulses of food appear to govern the distributions of different species in polar environments (Cattaneo-Vietti et al. 1999; Orejas et al. 2000; Gili et al. 2001). Suspension feeders can utilize picoplankton and detritus to support metabolic rates that occur during the resource depleted winter, and then increase their feeding and growth during the plankton rich spring and summer months (Orejas et al. 2000). Feeding on picoplankton, which is

available year-round, has also been hypothesized to satisfy the energy requirements of polar ascidians (e.g., Lesser and Slattery 2015).

Bottom-up forcing has been observed in sea anemone and mussel populations in the Gulf of Maine, where the concentrations of particulate food, combined with ambient flow rates, is important in structuring populations of the passive suspension feeding sea anemone, *Metridium senile* on offshore sites, and the active suspension feeding mussel, *Modiolus modiolus* on inshore sites (Lesser et al. 1994). Additionally, the growth rates of the blue mussel, *Mytilus edulis* in Californian waters were found to be correlated with increased chlorophyll *a* concentration (Page & Hubbard 1987). The trend of bottom-up control on growth rates and biomass accumulation was also found in mussel populations in Oregon, USA where mussel growth rates and recruitment was higher in areas with greater pelagic water productivity (Menge 1994, 2000). While predation or competition (i.e., top-down processes) does ultimately influence community structure and diversity of sessile benthic communities (Menge & Sutherland 1976; Summerson & Peterson 1984; Wulff 2017), it is clear that bottom-up forcing via food availability is a critical factor in the regulation of community structure and diversity of benthic suspension feeders in marine ecosystems (Menge 2000; Gili & Coma 1998; Lesser 2006).

Similarly, the role of food availability to suspension feeders is important on tropical coral reefs. Tropical coral reefs host a wide array of both passive and active suspension feeders. Compared to temperate waters, productivity is low but constant on coral reefs and as a result POM supply is relatively low in these marine ecosystems, and a variety of adaptations such as symbiosis of algal or cyanobacterial symbionts with corals and sponges has evolved (Stanely, 2006; Bourne et al. 2016; Morrow et al. 2016; Fiore et al. 2020). However, it is clear that for sponges, food supply is a major factor influencing their abundance and diversity (Lesser 2006,

Trussell et al. 2006, Wulff 2017). The roles of bottom-up and top-down control of tropical coral reef sponge distributions has been debated widely in the published literature (Pawlik et al. 2013, 2018; Slattery and Lesser 2015; Slattery et al. 2016; Wulff 2017; Lesser et al. 2018, 2020; Lesser and Slattery 2018; Scott and Pawlik 2019). Based on current knowledge, it has been repeatedly observed that bottom-up control is the primary driver of increasing sponge abundances and biomass into the mesophotic zone while acknowledging that top-down processes also play a role in their ultimate ecological distributions (Lesser 2006; Trussell et al. 2006; Lesser & Slattery 2013, 2018; Slattery & Lesser 2015; Lesser & Slattery 2018; Lesser et al. 2018, 2019, 2020). As depth increases, POM, particularly heterotrophic picoplankton, increases while a concurrent decrease in DOM has been observed (Lesser 2006; Trussell et al. 2006; Lesser et al. 2019, 2020). Heterotrophic picoplankton and prochlorophytes have low C:N ratios compared to cyanobacteria, which results in increased nitrogen availability with increased depth (Ducklow et al. 1993; Campbell et al. 1994; Lesser 2006). Additionally, it has been shown that picoplankton can provide most of the organic nitrogen for sponges on coral reefs (Ribes et al. 2003), and as sponges consume picoplankton in proportion to its abundance, the increased consumption of this resource at mesophotic depths appears to strongly influence the increased abundances and growth rates of sponges with increasing depth (Lesser 2006; Trussell et al. 2006; Lesser and Slattery 2013, 2018; Slattery and Lesser 2015). Increased consumption of picoplankton is also associated with increased growth rates in the sponges *Callyspongia vaginalis, Agelas conifera* (now correctly identified as *A. tubulata*) and *Aplysina fistularis* (Lesser 2006), while a reciprocal transplant by Trussell et al. (2006) using *C. vaginalis* between 12 m and 25 m, showed unequivocally that increased growth rates occur in deeper sponges and sponges transplants from shallow to deep habitats where more picoplankton was observed resulted in energy surpluses for

deep sponges. Trussel et al. (2006) did not measure DOM uptake for their experimental sponge, *Callyspongia vaginalis*, but the dependence on DOM for *C. vaginalis* is minimal (McMurray et al. 2018).

Additionally, stable isotope values of $\delta^{13}C$ and $\delta^{15}N$, signatures of the integration of what organisms consume over time, became less depleted from shallow to mesophotic depths for both *Xestopsongia muta* (Morrow et al. 2016) and *Agelas tubulata* indicating that these species increasingly rely on heterotrophy with increasing depth (Slattery et al. 2011). Interestingly, Slattery et al. (2016) also found that the sponge *Plakortis angulospiculatus* displayed phenotypic variability in chemical defense between shallow and mesophotic specimens. Shallow *P. angulospiculatus* were more chemically defended compared to their mesophotic conspecifics but mesophotic *P. angulospiculatus* regenerated tissue faster. This plasticity between chemical defenses and the capacity to repair tissue damage is believed to be the result of increased trophic resources available to the mesophotic populations for repair processes compared to shallow populations.

The studies above provide strong evidence for bottom-up processes controlling sponge distributions but also reinforces the need to integrate both traditional feeding measurements with environmental data and biochemical methods to provide, within a robust experimental framework, evidence to support what trophic processes influence sponge distributions. Sponges are well known to consume DOM, and the microbiome of high microbial abundance sponges (HMA) can process DOM and potentially translocate products from those processes (e.g., dissolved free amino acids) to their host (de Goeij et al. 2008, 2013, 2017; Freeman and Thacker 2011; Maldonado et al. 2012; Thacker and Freeman 2012; Fiore et al. 2013, 2020; Shih et al. 2020). However, many of these studies quantified DOC but not DON, and while DON is

generally an order of magnitude lower in terms of availability compared to DOC (Lesser et al. 2019), it should nevertheless be included to get a better understanding of sponge DOM consumption and reprocessing. The simultaneous quantification of DOM and POM consumption will provide a more complete assessment of the trophic ecology of sponges.

The sponge used in this study was *Agelas tubulata*, which is commonly found along the shallow to mesophotic depth gradient in the Cayman Islands. *Agelas tubulata* is a chemically defended (Pawlik 2011; Rohde et al. 2015), HMA sponge that is known to feed on both DOM and POM (Lesser 2006; Slattery and Lesser 2015; de Goeij et al. 2017). Here we present a reciprocal transplant experiment between shallow and mesophotic depths using *A. tubulata* to assess changes in growth rates, trophic resource consumption, carbon and nitrogen stable isotopes and proximate biochemical composition between shallow and mesophotic depths. This experiment exposes the transplanted sponges to all potential abiotic and biotic factors, including predation. We hypothesize that the growth rates will be higher in mesophotic control sponges and the shallow to mesophotic transplant sponges due to the increased availability of PON at those depths and that this will be reflected in their stable isotopic signatures and biochemical composition.

Methods

Study site

Both the reciprocal transplant and natural growth measurements were conducted at the Kittiwake Anchor Buoy site, Grand Cayman (Lat: 19.362756, Long: -81.402437). This site exhibits a sloping spur and groove reef structure between 15 – 61 m, at which point reef topography turns

into a vertical wall. Both transplant sites were located on bare coral rock, and not located on live coral or sand channels.

Light and temperature data

Temperature data was collected along a depth gradient (0, 15, 21, 30, 46, 61, 76 and 91 m) beginning in January 2018 using Hobo Water Temperature Pro V2 loggers attached directly to the substrate using cable ties. Sensors were checked and data downloaded every 6 mo. A drop package was used to obtain profiles of photosynthetically active radiation (PAR: 400-700 nm), for downwelling (E_d) irradiance, as a function of depth using a single channel PAR recorder (RBRsoloPAR; RBR Ltd., Ottawa Canada) fitted with a calibrated LiCor cosine-corrected, planar, sensor (LI 192SA) combined with a Sea-Bird SBE39 plus temperature and depth profiler. Profiles from the surface to ~100 m depth were taken between 11 AM and 1 PM on partly (25-40%) cloudy days.

Reciprocal transplant and natural growth experiment

To assess changes in growth rates and resource consumption a reciprocal transplant experiment, beginning January 2018, was established between 22 m and 61 m. A total of 20 sponge PVC frames (n = 10 per depth, Fig. S1) were affixed to the reef substrate using eye bolts epoxied into the substrate with cable ties placed through the eye bolt and PVC frame. *Agelas tubulata* with more than three tubes were identified and tagged with cow tags (n = 5 at 22 and 61 m) and used as the source sponges for the transplant study. Five sponge tubes were cut (~8-19 cm tall) from these sponges and transplanted from deep (61 m) to shallow (22 m) (DS), and shallow to deep

(SD). Deep to deep (DD) and shallow to shallow (SS) controls (n = 5 each) were also cut and transplanted back to their respective depths as disturbance controls. All samples were identified with a cattle tag on the sponge frame and a plastic growth tag inserted 1 cm below the osculum lip (Fig. S1). Subsequent measurements from the point of tag insertion to the top of each sponge tube were taken to the nearest 0.1 cm in July 2018, January 2019 and June 2019 and used to calculate apical growth rates. Total length and osculum wall thickness (total maximum diameter minus inner diameter) were also measured to the nearest 0.1 cm. Growth rates were assessed in several ways including apical, total length and osculum wall thickness in cm mo^{-1}. Transplanted sponges were removed from the reef after final measurements at 18 mo. All sponges were kept in a shaded cooler submerged in seawater until returned to shore for processing of samples for biochemical and stable isotope analysis. Any samples collected for biochemical and stable isotope analyses were immediately frozen at -20°C and transported frozen to the University of Mississippi or the University of New Hampshire, where they were frozen at -80°C until analysis. Unmanipulated *Agelas tubulata* along the study depth gradient (15 to 61 m) (n = 33) were also tagged to provide information on the natural growth rates, assessed as apical growth, across the depths of the transplant experiment. Both transplanted sponges and tagged natural growth sponges were revisited every 6 mo and growth metrics measured. Additionally, any bite scars observed for each treatment were counted as a relative measure of predation on the experimental sponges.

Ambient food availability

To quantify total POM and DOM availability along the shallow to mesophotic depth gradient replicate samples (n = 3 per depth) were collected at 0, 15, 22, 30, 46, 61, 76 and 91 m in July

2018 and January 2019. Acid-washed 180 mL syringes were filled by divers at approximately 1 m from the reef substrate taking care not to disturb sediment and detritus. To quantify POM, the samples were returned to the laboratory and 5 ml aliquoted and fixed at a final concentration of 0.5% electron microscopy grade paraformaldehyde and frozen at 0℃. Samples were shipped frozen to the University of New Hampshire and stored at -80℃. Samples were shipped frozen on dry ice to the Bigelow Laboratory of Marine Science, J.J. MacIsaac Facility for Aquatic Cytometry and stored in liquid nitrogen (-196℃). Each sample was analyzed using flow cytometry for total cell abundances as described, and modified, by Lomas et al. (2010) using a Becton Dickinson Influx flow cytometer equipped with a 15 mW, 488 nm, aircooled Argon ion laser. Both Chl *a* (692 ± 20 nm) and phycoerythrin (PE, 585 ± 15 nm) bandpass filters were used and the instrument was calibrated daily with 3.46 µm Rainbow Beads (Spherotech Inc. Lake Forest, Illinois, USA). Each sample was run for 3–5 min (~0.2–0.3 ml total volume analyzed), with log-amplified Chl *a* and PE fluorescence, as well as forward and right-angle scatter signals, recorded and analyzed using FlowJo 9.8 Software (Becton Dickinson, San Jose, CA). Pico-autotrophs were identified as either *Synechococcus*, *Prochlorococcus* or picoeukaryotes based upon cell size and the presence or absence of phycoerythrin. For picoautotrophs the concentration of cells in each population were enumerated and converted to cell abundances by the volume-analyzed method (Sieracki et al., 1993). For heterotrophic bacterial abundance samples were diluted 1:10 and stained using SYBR™ Green I Nucleic Acid Stain (Thermofisher Scientific) at room temperature for 15 min (Marie et al. 2005). Samples were analyzed on a BioRad ZE5 Cell Analyzer using a 488 nm (100 mW) blue excitation laser for a total volume of 100 µl. Files were analyzed from scatter plots based on green (525/35 BP filter) fluorescence and right-angle light scatter (side scatter – SSC) using FlowJo 10 Software (Becton Dickinson,

San Jose, CA). Heterotrophic bacteria counts were gated based on cell size and presence of green fluorescence.

All counted cells were converted to their carbon and nitrogen equivalents (*sensu* Lesser et al. 2019) to provide the concentrations of live particulate organic carbon (POC) and particulate organic nitrogen (PON) available to the sponges. The following conversion values were used: heterotrophic bacteria: 20 fg C/cell (Ducklow et al. 1993); *Prochlorococcus*: 53 fg C/cell (Morel et al. 1993); *Synechococcus*: 470 fg C/cell (Campbell et al. 1994); heterotrophic bacteria: 3.3 fg N/cell (Fagerbakke et al. 1996); *Prochlorococcus*: 9.4 fg N/cell; and *Synechococcus*: 35 fg N/cell (Bertilsson et al. 2003). For phytoplankton, the carbon and nitrogen contents were computed where $C = 0.433$ (biovolume, $\mu m^3)^{0.863}$ and $N = 0.883$ (biovolume, $\mu m^3)^{0.837}$ (Verity et al. 1992).

To quantify DOM, 40 ml aliquots were collected from the same water samples used for flow cytometry analyses. These samples were filtered through a 0.2 µm GF/F filter and immediately frozen at 0°C and transported frozen to the University of New Hampshire. The filtered seawater samples were analyzed at the UNH Water Quality Analysis Laboratory. Dissolved organic carbon (DOC, µmol C l^{-1}) and dissolved organic nitrogen (DON, µmol N l^{-1}) were quantified using high-temperature catalytic oxidation and high-temperature oxidation with chemiluminescent detection, respectively. Dissolved inorganic nitrogen (DIN) as NO_x (i.e., NO_3^- + NO_2^-), ammonium (NH_4), phosphate (PO_4) and silicon dioxide (SiO_2) were analyzed using a SmartChem 200 automated colorimetric chemistry analyzer (Westco, Brookfield, Connecticut, USA) or a Seal AQ2 (Seal Analytical, Mequon, WI, USA) discrete colorimetric analyzer. Standard EPA protocols for each compound (NO_x: #353.2, NH_4: #350.1, PO_4: #365, SiO_2: #370.1) were used.

Sponge feeding measurements

To assess sponge feeding, paired ambient and excurrent water samples were collected from each sponge, transplants and controls, in July 2018 and January 2019. Ambient water samples were collected approximately 10 cm from the base of a sponge tube and excurrent samples were collected approximately halfway down the osculum of the sponge using acid-washed 180 mL syringes and surgical tubing (*sensu* Lesser et al., 2006). POM and DOM were quantified as described above. After feeding samples were collected, sponge pumping rates were assessed. Fluorescein dye was placed at the base of the tube and time of appearance of the dye at the osculum measured (s^{-1}). Morphometrics on each sponge were collected to calculate the volume of a cylinder (= plug volume) using total length of the tube and osculum width to the nearest 0.1 cm. In order to calculate a Q value (volumetric flux, ml s^{-1}), the cross-sectional area (cm^2) of the sponge osculum was calculated and multiplied by the dye front speed (cm s^{-1}) that was calculated by dividing the total tube length of the sponge by the dye speed (Trussell et al. 2006). This method assumes plug flow through the sponge tube, and a visual assessment of the dye fronts produced during measurements confirms plug flow in the sampled sponges.

To calculate sponge feeding on POM, filtration efficiency was calculated for each sponge by dividing the concentrations of total cells in the sponge ex-current water samples by the concentration of total cells in the ambient water samples taken adjacent to the sponge and multiplied by 100. Total cells consumed for each class (i.e., prochlorophytes, *Synecochoccus*, eukaryotic phytoplankton and heterotrophic bacteria) of cells was computed by multiplying the ambient concentration of cells (cells ml^{-1}) by the filtration efficiency of cells and the individual sponge Q value (ml s^{-1}). All filtered cells were then converted to carbon or nitrogen equivalents as described above. Rates of both carbon or nitrogen uptake (ug s^{-1}) were calculated by

multiplying cells filtered by the relevant groups carbon or nitrogen equivalent per cell and then converted to its molar equivalents (µmol s^{-1}). Similarly, to calculate sponge feeding on DOM, filtration efficiency was calculated for each sponge by dividing the concentrations of total DON or DOC in the sponge ex-current water samples by the concentration of total DON or DOC in the ambient water samples taken adjacent to the sponge and multiplied by 100. Instantaneous (s^{-1}) total DON or DOC consumed was computed by multiplying the ambient concentration of DON or DOC (µmol l^{-1}) by the filtration efficiency and the individual sponge Q value (l s^{-1}). The dry mass of each sponge (g) was calculated using a tissue density of 0.14 g ml^{-1} for *Agelas tubulata* (Weisz et al. 2008).

Stable isotope analyses

Sub samples of *Agelas tubulata* tissue were collected under sterile conditions using a sterile razor from experimental sponges in June 2019 at the end of the experiment. Tissue samples were dried at 55℃ for 24 h before pulverizing into a powder using a mortar and pestle. Samples of pulverized tissue were sent to the Marine Biological Laboratory (Woods Hole, MA) for the bulk analysis of particulate C and N as well as the natural abundance of the stable isotopes $\delta^{15}N$ and $\delta^{13}C$. Prior to analysis samples were acidified using 1N HCL. Our analysis on the effect of acidification on $\delta^{15}N$ tissue values (*sensu* Vafeiadou et al. 2013) shows no significant effects of acidification in our hands as previously reported (Jaschinski et al. 2008; Kolasinski et al. 2008). Samples were analyzed using a Europa ANCA-SL elemental analyzer-gas chromatograph attached to a continuous-flow Europa 20-20 gas source stable isotope ratio mass spectrometer. The carbon isotope results are reported relative to Vienna Pee Dee Belemnite and nitrogen

isotope results are reported relative to atmospheric air and both are expressed using the delta (δ) notation in units per mil (‰). The analytical precision of the instrument is ± 0.1‰, and the mean precision of sample replicates for $\delta^{13}C$ was ± 0.4 ‰ and $\delta^{15}N$ was ± 0.2 ‰.

Proximate Biochemical Composition

For the samples collected in June 2019 sample wet mass and volume were also recorded, freeze dried, pulverized, and dry sample mass recorded. Carbohydrates were extracted via incubation of 10 mg freeze dried tissue in 5 ml 5% trichlororacetic acid (TCA) for 4 h. Concentration of carbohydrates was determined using the phenol-sulfuric acid method in microplate format described in Masuko et al. (2005). Briefly, 50 µl of TCA digested sample solution or glucose standard, 150 µl of sulfuric acid, and 30 µl of 5% phenol was pipetted in triplicate on a 96 well plate and incubated for 10-15 min at 90°C. Absorbance at 490 nm was then measured using a microplate reader. A standard curve was derived from glucose standards and used to calculate the concentration of carbohydrates in samples. Protein was extracted via incubation of 10 mg of freeze-dried tissue in 5 ml of 1 M sodium hydroxide (NaOH) for 24 h. Soluble protein concentration was then analyzed using the Bradford Method (Bradford, 1976). 40 µl of NaOH digested sample or BioRad Bovine Serum Albumin (BSA) standard was mixed with 2 ml of BioRad Quick StartTM Bradford reagent. Absorbance at 600 nm was measured using a spectrophotometer. A standard curve was derived from BSA standards and used to calculate the concentration of protein in samples. Lipids were extracted using a modified version of the protocol described by Freeman et al. (1957). A 50 mg sample of freeze-dried tissue was sonicated for 15 min in a 2:1 chloroform to methanol solution and then filtered into a 50 ml

conical tube containing ~20 ml of distilled water. The bottom organic layer was then pipetted into a pre-weighed scintillation vial. This process was repeated twice per sample. The methanol-chloroform solution was then evaporated off over a period of 12 h via vacuum centrifugation. Inorganic tissue constituents (i.e., ash) were measured using methods described by McClintock et al. (1992). A 100 mg sample of freeze-dried sponge tissue was placed in a pre-weighed aluminum foil weigh-boat that was baked at 500°C in a muffle furnace for 5 h to obtain the ash content of each sample. All concentrations of proximate biochemical composition were normalized to ash-free dry weight (AFDW).

Statistical analyses

All statistical analyses were completed in either JMP (v. 14) or R (v. 3.6.2). Mean monthly and yearly temperatures were tested for any effects of depth using ANOVA and the effect of depth on PAR was assessed using non-linear regression. Sponge growth rates for the transplant experiment were assessed using one-way ANOVA with treatment as a fixed factor while the growth rate of naturally occurring sponges were quantified using linear regression. To assess differences between depths and years in the concentration of available POM and DOM, an analysis of covariance (ANCOVA) was run using depth as a fixed factor and year as the covariate. In order to assess differences in sponge pumping rates and sponge consumption of POM and DOM between treatments, an analysis of covariance (ANCOVA) was run with treatment as the primary factor and sponge dry mass as the covariate to remove the potential allometric effects of sponge size on sponge pumping and food intake. Because all analyses showed that the slopes were non-homogeneous, a requirement for ANCOVA, individual regression slopes from each treatment were used to weight individual sponge pumping or feeding

rates to a sponge of standard dry mass (Packard and Boardman, 1988; Lesser & Kruse, 2004). The weighted pumping or feeding rates were then analyzed using ANOVA with experimental treatment as a fixed factor.

The statistical analyses for treatment effects on SIA and proximate biochemical compositions were carried out utilizing ANOVA. Any variables not meeting the assumptions of normality were log transformed before analysis. Any significant global effects of treatment detected by ANOVA were followed-up with *post-hoc* multiple comparison tests using Tukey's HSD tests.

Results

Light and temperature

There was a significant effect of depth on mean monthly temperature (ANOVA: $F_{11, 2303} = 233.5$, $P<0.0001$) (Fig. 7, Table S1). In July 2018, the mean monthly temperature was 29.25°C (± 0.45 SD) at 22 m and 28.09°C (± 0.19 SD) at 61 m. In January 2019, mean month temperature was 27.10°C (± 1.14 SD) at 22 m and 27.39°C (± 0.32 SD) at 61 m. The attenuation of E_d with depth was typical for tropical Case I or II waters (Lesser et al. 2009) (Fig. S2). At 22 m E_d was ~198 µmol quanta m^{-2} s^{-1} and at 61 m E_d was ~96 µmol quanta m^{-2} s^{-1}.

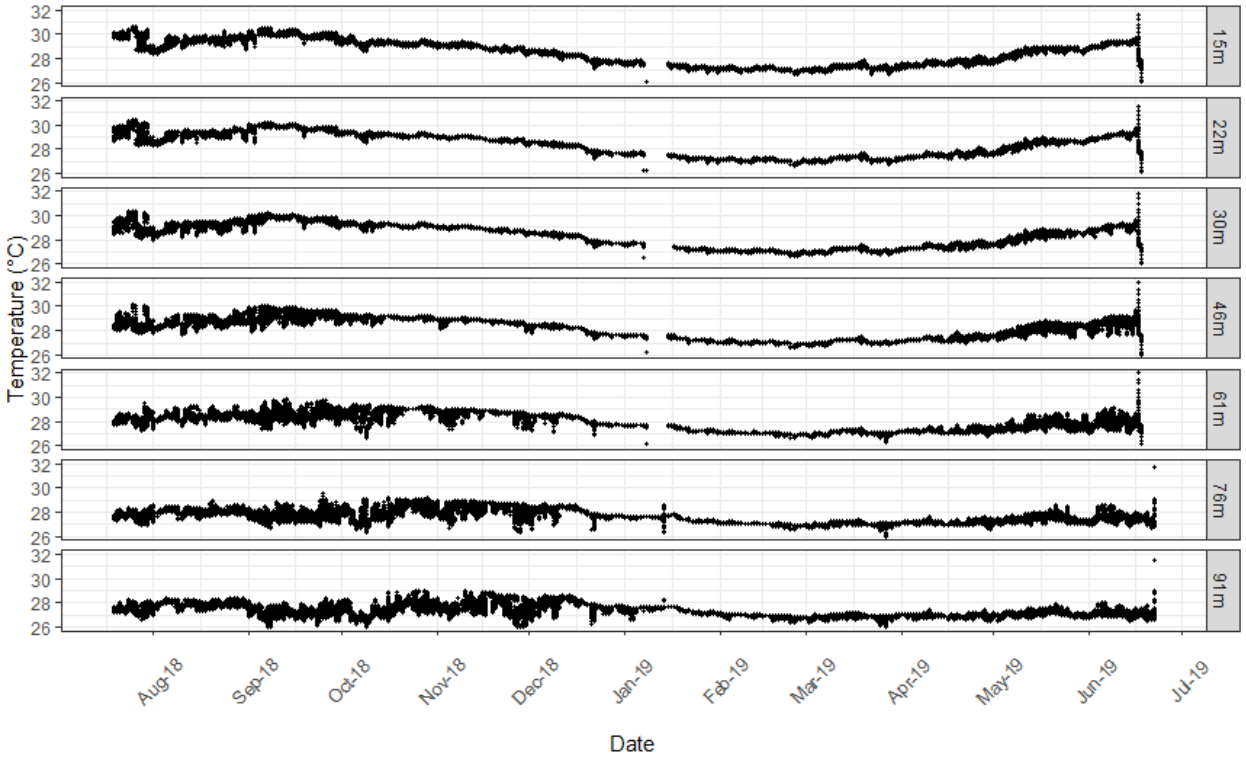

Figure 7. Daily temperature (°C) measurements between July 2018 and July 2019 along the shallow to mesophotic depth gradient at the experimental site.

Transplant experiment and natural growth of sponges

There was a significant effect of treatment on apical growth rates (ANOVA: $F_{3,16} = 8.51$, P = 0.001). Sponges from the DD and SD treatments had a significantly higher mean growth rate (DD = 0.12 ± 0.01 [SE] cm mo^{-1}, SD = 0.11 ± 0.02 [SE] cm mo^{-1}) than DS transplants (DS = 0.02 ± 0.01 [SE] cm mo^{-1}) (Tukey's HSD = <0.05) (Fig. 8 a), which had the lowest growth rates of all treatments. Samples from the SS treatment showed an intermediate mean growth rate (SS = 0.07 ± 0.04 [SE] cm mo^{-1}) that was not significantly different from any other treatment group (Fig. 8 a). There was a significant effect of treatment on osculum wall width (ANOVA: $F_{3,16}$ = 4.27, P = 0.021). Sponges from the DD treatment had significantly greater osculum wall width

growth rates (DD = 0.11 ± 0.02 [SE] cm mo^{-1}) than the sponges from SS treatment (SS = 0.04 ± 0.005 [SE] cm mo^{-1}) (Tukey's HSD = <0.05) (Fig. 8 b). Treatment also had a significant effect on the total length of sponges (ANOVA: $F_{3,16} = 4.25$, P = 0.025) with DD sponges (DD = 0.23 ± 0.012 [SE] cm mo^{-1}) displaying significantly higher growth rates compared to DS transplants (DS = -0.17 ± 0.16 [SE] cm mo^{-1}) (Tukey's HSD = <0.05) (Fig. 8 c). There was also a significant effect of depth on the apical growth rates of naturally occurring, non-experimental, sponges ($t(25) = 6.31$, P = 0.0188), as well as growth rates based on total length ($t(31) = 12.62$, P = 0.0012) using linear regression, with deeper sponges displaying the highest growth rates (Fig. 9 a, b). There was no significant effect of depth on osculum wall width growth rates ($t(25) = 0.23$, P = 0.6334) (Fig. 9 c).

Ambient levels of POM and DOM

For POC (µmol C l^{-1}) the assumptions of ANCOVA were satisfied and the analysis showed that both depth (ANOVA: $F_{1,15} = 9.67$, P = 0.009) and year (ANOVA: $F_{1,15} = 88.03$, P <0.0001) had a significant effect on POC concentrations which increased with increasing depth (Fig. 10 a). As depth increased into the mesophotic zone the available POC increased with the July 2018 sampling period showing significantly overall greater POC concentrations compared to January 2019 (Fig. 10 a). The regression lines for PON (µmol N l^{-1}) were not homogeneous (ANOVA: depth x year interaction, $F_{1,15} = 6.76$, P = 0.023) so while PON increased significantly with depth (ANOVA: $F_{1,15} = 37.42$, P <0.0001), the effect of year was assessed using a separate ANOVA after Bonferroni correction for multiple tests on dependent values to avoid Type I errors. Using a more stringent P=0.025 value a significant effect (ANOVA: $F_{1,15} = 88.03$, P = 0.006) for year

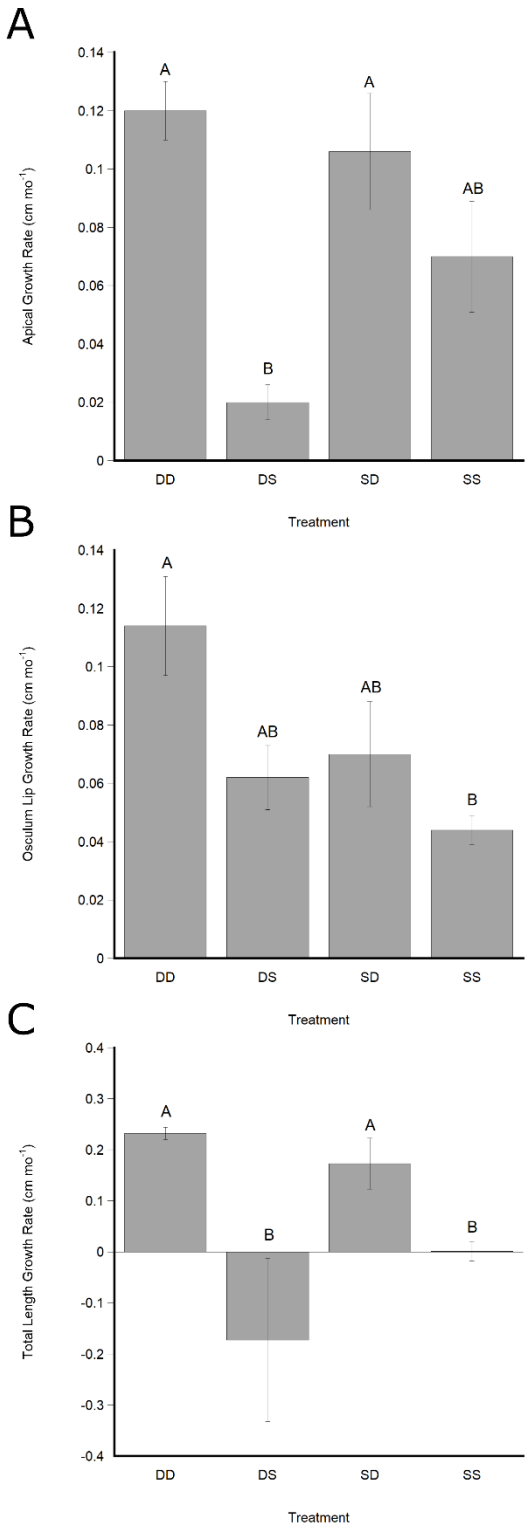

Figure 8. Experimental transplant effects between treatments on mean (± SE) **A)** apical growth rate, **B)** osculum wall thickness growth rate and **C)** total length growth rate. Treatments with common superscripts are not significantly different from each other (Tukey's HSD, $P<0.05$)

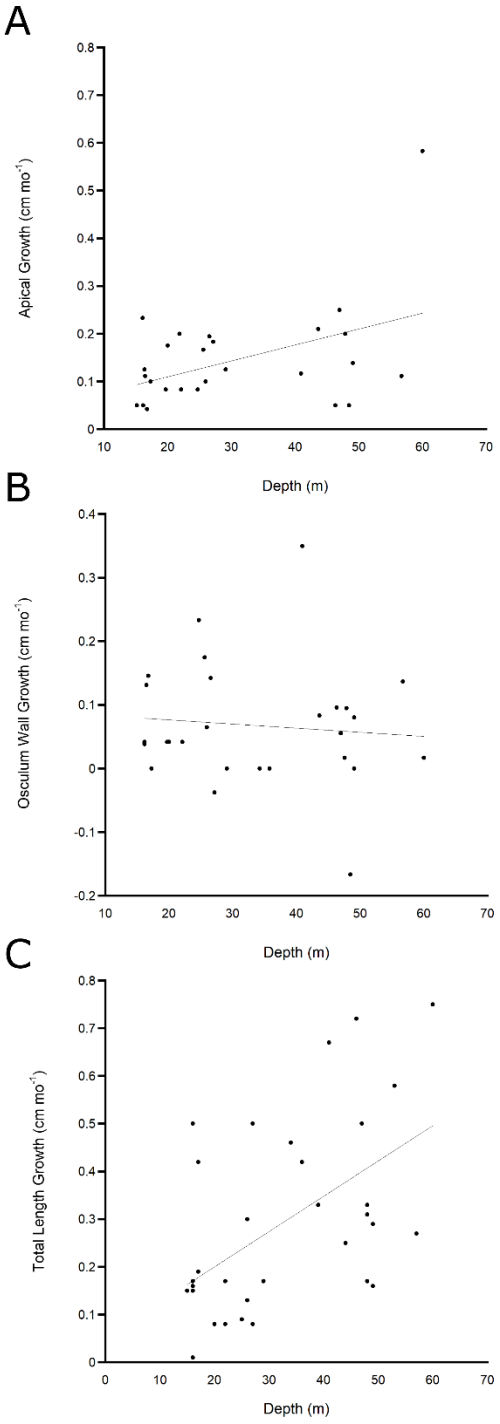

Figure 9. Effects of depth (m) on **A)** apical growth rate ($y = 0.042267 + 0.003351x$, $R^2 = 0.20188$, $P = 0.0188$), **B)** osculum wall thickness growth rate ($y = 0.08968 + 0.006567x$, $R^2 = 0.0092$, $P = 0.6334$) and **C)** total length growth rate ($y = 0.051545 + 0.007405x$, $R^2 = 0.28094$, $P = 0.0012$) on the sponge *Agelas tubulata.*

was observed (Fig. 10 b), with PON significantly greater in July 2018 compared to January 2019 (Fig. 10 b). For DOC (μmol C l^{-1}) the assumptions of ANCOVA were satisfied and the analysis showed that only depth (ANOVA: $F_{1,15} = 29.17$, $P = 0.0002$) had a significant effect of decreasing DOC with depth (Fig. 10 c) while year was not significant (ANOVA: $F_{1,15} = 1.05$, $P = 0.326$). For DON (μmol N l^{-1}) the assumptions of ANCOVA were also satisfied and the analysis showed only a significant (ANOVA: $F_{1,15} = 55.81$, $P < 0.0001$) effect of decreasing DON with depth (Fig. 10 d), while the effect of year on DON concentration was not significant (ANOVA: $F_{1,15} = 0.30$, $P = 0.594$). The regression lines for NO_x (μmol l^{-1}) were not homogeneous (ANOVA: depth x year interaction, $F_{3,47} = 6.36$, $P <0.0001$) so while NO_x increased significantly with depth (ANOVA: $F_{3,47} = 234.36$, $P <0.0001$), the effect of year was assessed using a separate ANOVA after Bonferroni correction for multiple tests on dependent values to avoid Type I errors. Using a more stringent P=0.025 value a significant effect (ANOVA: $F_{1,47} = 16.39$, $P = 0.0002$) for year was observed (Fig. 11), with NO_x significantly greater in January 2019 compared to July 2018 (Fig. 11). The regression lines for PO_4 (Fig. 11 b) were not homogenous (ANOVA: depth x year interaction, $F_{3,47} = 4.37$, $P = 0.0349$), but there was no significant effect of depth (ANOVA: $F_{1,47} = 0.8423$, $P = 0.363$) or year (ANOVA: $F_{1,47} = 0.04$, $P = 0.984$) on PO_4 with increasing depth. The assumptions for ANCOVA were meet for the analysis of SiO_2 (Fig. 11 c) but no significant effect of depth (ANOVA: $F_{1,47} = 0.625$, $P = 0.28$) or year (ANOVA: $F_{1,47} = 0.62$, $P = 0.434$) was observed.

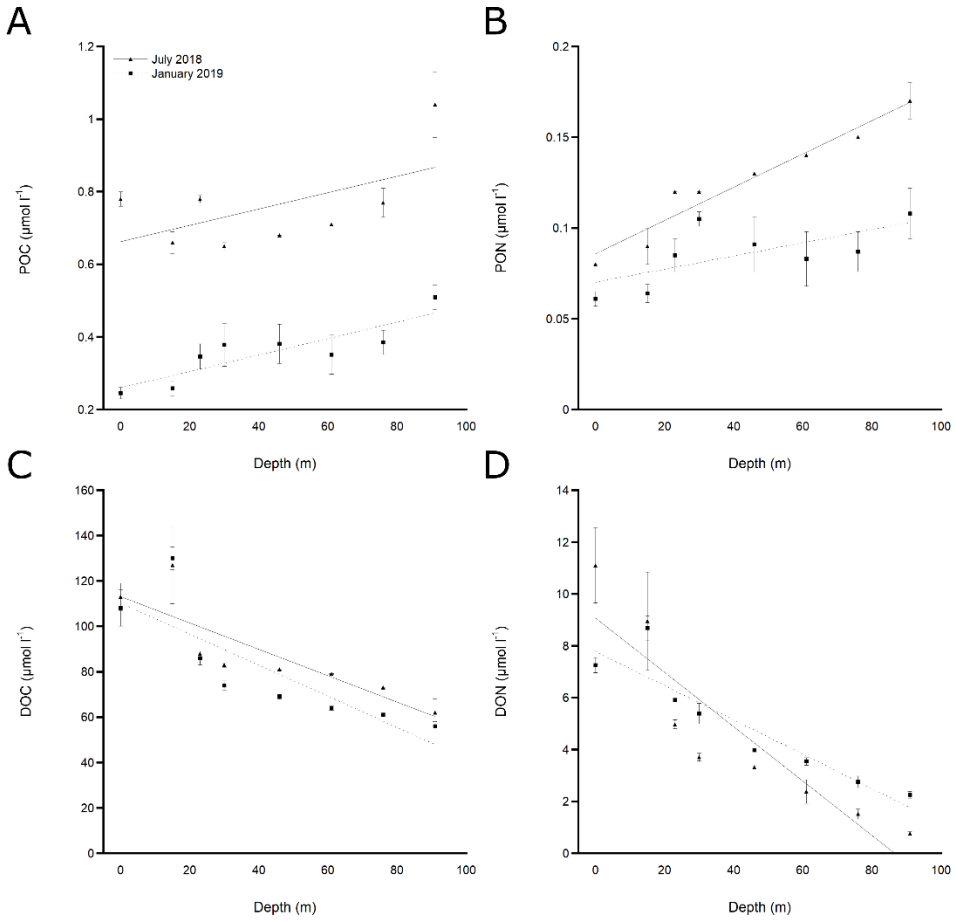

Figure 10. Effects of depth on mean (± SE) ambient levels of **A)** particulate organic carbon (POC) (July 2018: y = 0.6625 + 0.002261x, R^2 = 0.318, P <0.0001; January 2019: y = 0.25962 + 0.00225x, R^2 = 0.752, P <0.0001), **B)** particulate organic nitrogen (PON) (July 2018: y = 0.0858 + 0.000916x, R^2 = 0.938, P <0.0001; January 2019: y = 0.0699 + 0.000362x, R^2 = 0.458, P <0.0001), **C)** dissolved organic carbon (DOC) (July 2018: y = 113.1 – 0.5813x, R^2 = 0.731, P <0.0001; January 2019: y = 110.28 – 0.6848x, R^2 = 0.698, P <0.0001) and **D)** dissolved organic nitrogen (DON) (July 2018: y = 9.0764 – 0.1049x, R^2 = 0.821, P <0.0001; January 2019: y = 7.8 – 0.06625x, R^2 = 0.857, P <0.0001).

Sponge pumping, consumption of POM and DOM, and nutrient fluxes

Rates of sponge pumping (Q value, ml s^{-1}) was analyzed using ANCOVA with mass (g) as the covariate. The assumptions of ANCOVA were met and the analysis showed no significant effect of treatment on sponge pumping in July 2018 (ANOVA: $F_{3,19}$ = 1.25, P = 0.335) or January 2019 (ANOVA: $F_{3,17}$ = 0.62, P = 0.618) (Fig. S3).

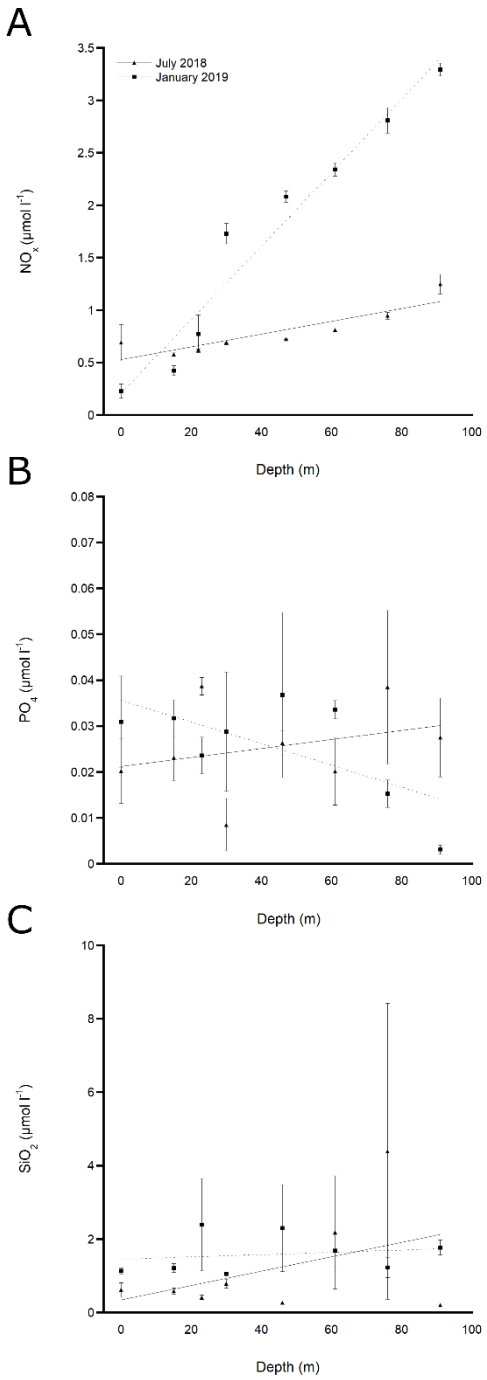

Figure 11. Effects of depth on mean (± SE) ambient levels of **A)** dissolved inorganic nitrogen ($NO_x = NO_2 + NO_3$) (July 2018: y = 0.528 + 0.00606x, R^2 = 0.772, P <0.0001; January 2019: y = 0.2123 + 0.03503x, R^2 = 0.857, P <0.0001), **B)** phosphate (PO_4) (July 2018: y = 0.02115 + 0.000098x, R^2 = 0.095, P = 0.385; January 2019: y = 0.03561 – 0.000237x, R^2 = 0.442, P = 0.126) and **C)** silica dioxide (SiO_2) (July 2018: y = 0.34 + 0.0196x, R^2 = 0.183, P = 0.563; January 2019: y = 1.4603 + 0.00312x, R^2 = 0.034, P = 0.287).

For the feeding studies in both July 2018 and January 2019 there were violations in the assumptions (i.e., homogeneity of slopes) of ANCOVA for all dependent variables. As a result, all analyses were conducted using a weighted ANCOVA approach as described above. There were significant treatment effects for POC uptake (μmol C s^{-1}) in July 2018 (ANOVA: $F_{3,17}$ = 3.96, P = 0.031) with the SS treatment having the highest rate among treatments (Fig. 12 a). *Post-hoc* multiple comparisons showed that the only significant pair-wise difference was between the SS and DS treatments (Tukey's HSD: P<0.05). For PON uptake (μmol N s^{-1}) there were no treatment effects (ANOVA: $F_{3,17}$ = 3.21, P = 0.056) (Fig. 12 b). For DOC (μmol C s^{-1}) there were significant treatment effects (ANOVA: $F_{3,17}$ = 3.63, P = 0.040) with the SD treatment having the highest rate among treatments (Fig. 12 c). *Post-hoc* multiple comparisons showed that the only significant pair-wise difference was between the SD and DS treatments (Tukey's HSD: P<0.05) (Fig. 12 c). Similarly, for DON uptake (μmol N s^{-1}) there were significant treatment effects (ANOVA: $F_{3,17}$ = 4.37, P = 0.023) with the SS treatment having the highest rate among treatments (Fig. 12 d). *Post-hoc* multiple comparisons showed that the only significant pair-wise difference was between the SS and DS treatments (Tukey's HSD: P<0.05). There were no significant differences in natural feeding treatments between shallow and mesophotic sponges for POC, (ANOVA: $F_{1,5}$ = 0.3255, P = 0.598), PON (ANOVA: $F_{1,5}$ = 0.341, P = 0.590), DOC (ANOVA: $F_{1,5}$ = 7.7, P = 0.0501), DON (ANOVA: $F_{1,5}$ = 2.09, P = 0.221) or detritus (ANOVA: $F_{1,5}$ = 1,51, P = 0.277) (Table 5).

Table 5. Adjusted feeding rates on naturally occurring (i.e., non-experimental) *Agelas tubulata* on Grand Cayman. Mass, and all rate measurements, were not significantly different (ANOVA: P>0.05) between depths which were binned into shallow (~ 22 m) and deep (~ 61 m) sponges for analysis. These sponges correspond to the populations where SS and DD samples were collected.

Depth	Volume Flux (Q: ml s^{-1})	DOC (µmol l^{-1})	DON (µmol l^{-1})	POC (µmol l^{-1})	PON (µmol l^{-1})	Detritus (cell ml^{-1})
Shallow	269.212	2.679	0.414	0.127	0.022	19174956.079
Shallow	185.629	6.664	0.572	0.159	0.028	22627939.961
Shallow	178.055	2.041	0.330	0.225	0.037	4506438.600
Deep	477.706	18.174	1.335	0.221	0.040	48450272.400
Deep	172.991	8.806	0.347	0.116	0.020	15173728.351
Deep	331.238	10.916	0.913	0.264	0.047	7221530.664

There were no significant effects of treatment for weighted NO_x fluxes in July (ANOVA: $F_{3,17} = 1.22$, P = 0.337) or January (ANOVA: $F_{3,17} = 2.667$, P = 0.088), NH_4 in July (ANOVA: $F_{3,17} = 2.98$, P = 0.073) or January (ANOVA: $F_{3,17} = 1.79$, P = 0.193), PO_4 in July (ANOVA: $F_{3,17} = 0.27$, P = 0.84) or January (ANOVA: $F_{3,17} = 2.17$, P = 0.14) and SiO_2 in July (ANOVA: $F_{3,17} = 0.40$, P = 0.752) or January (ANOVA: $F_{3,17} = 0.739$, P = 0.55). These were then binned based on their final depth of occurrence for experimental sponges (22 m = SS and DS treatments and 61 m = DD and SD treatments), and only NH_4 showed an effect of depth in July 2018, with the deeper sponges producing greater fluxes of NH_4 (ANOVA: $F_{1,17} = 5.79$, P = 0.028) (Table S2). There was a significant effect of year for DIN flux (ANOVA: $F_{3,32} = 3.56$, P = 0.0385) with sponges in January 2019 having higher rates of DIN production compared to July 2018.

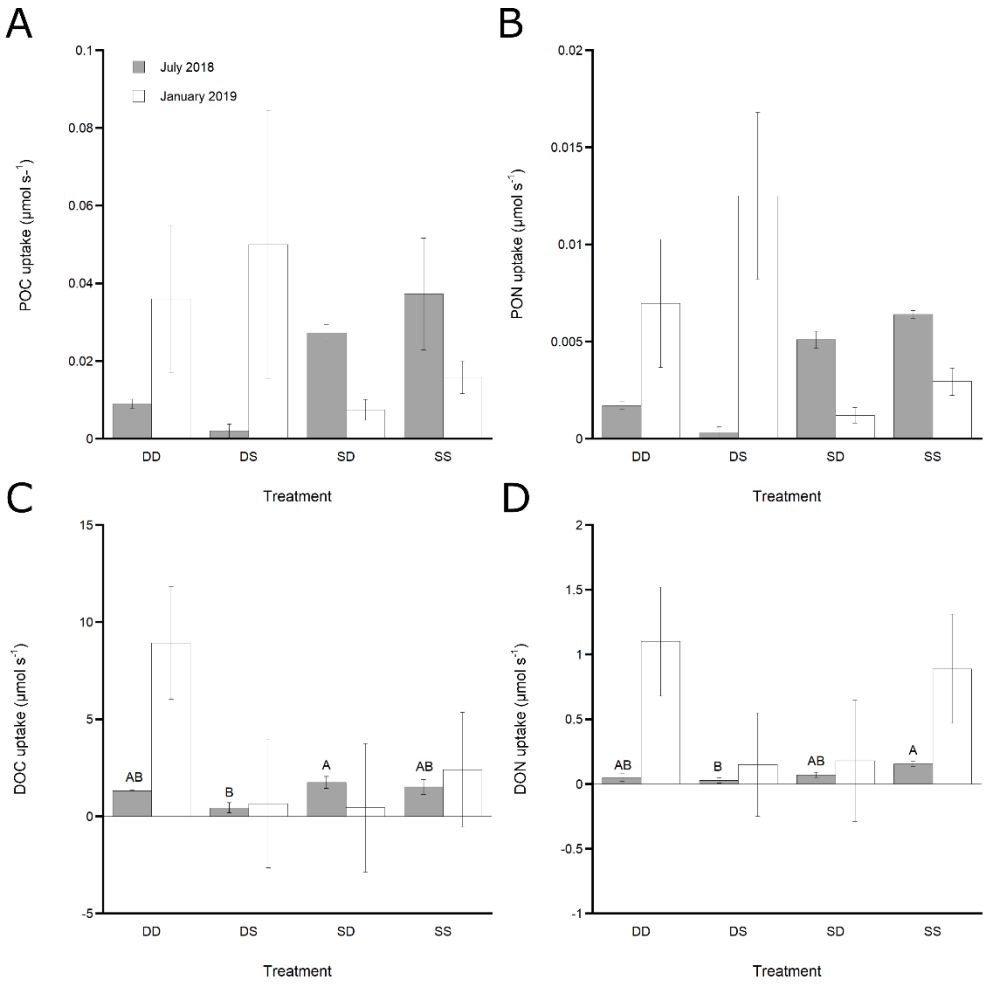

Figure 12. Mean (± SE) of **A)** Particulate organic carbon (POC) uptake weighted to remove effects of sponge mass (g AFDW). **B)** Particulate organic nitrogen (PON) uptake weighted to remove effects of sponge mass (g AFDW). **C)** Dissolved organic carbon (DOC) uptake weighted to remove effects of sponge mass (g AFDW). **D)** Dissolved organic nitrogen (DON) uptake weighted to remove effects of sponge mass (g AFDW). Treatments with common superscripts are not significantly different from each other (Tukey's HSD, $P<0.05$)

Stable isotope analyses

For *Agelas tubulata* there were no significant differences for $\delta^{13}C$ (ANOVA: $F_{3,17} = 2.31$, $P = 0.121$), $\delta^{15}N$ (ANOVA: $F_{3,17} = 2.72$, $P = 0.084$) or molar C:N ratios (ANOVA: $F_{3,17} = 2.32$, $P = 0.119$) between treatments (Table 6). Samples were then binned by final collection depth (22 and 61 m) and significant differences between the two depths for $\delta^{13}C$ (ANOVA: $F_{3,17} = 5.47$, P =

0.0326), $\delta^{15}N$ (ANOVA: $F_{3,17} = 7.36$, $P = 0.0153$) and molar C:N ratios (ANOVA: $F_{3,17} = 6.61$, $P = 0.02$) were observed. There was enrichment in both $\delta^{13}C$ and $\delta^{15}N$ and a lower molar C:N ratio in the 61 m samples (Fig. 13, Table 6)

Table 6. $\delta^{13}C$ and $\delta^{15}N$ stable isotope, and molar C:N ratios (mean ± SE) for sponge tissue from each treatment and binned by depth (22 and 61 m)

Treatment or Depth	$\delta^{13}C$	$\delta^{15}N$	C:N
DD	-17.17 (0.12)	4.02 (0.17)	3.61 (0.06)
DS	-18.00 (0.39)	3.23 (0.21)	3.89 (0.18)
SD	-17.46 (0.17)	3.67 (0.31)	3.74 (0.06
SS	-17.70 (0.21)	3.28 (0.21)	3.95 (0.08)

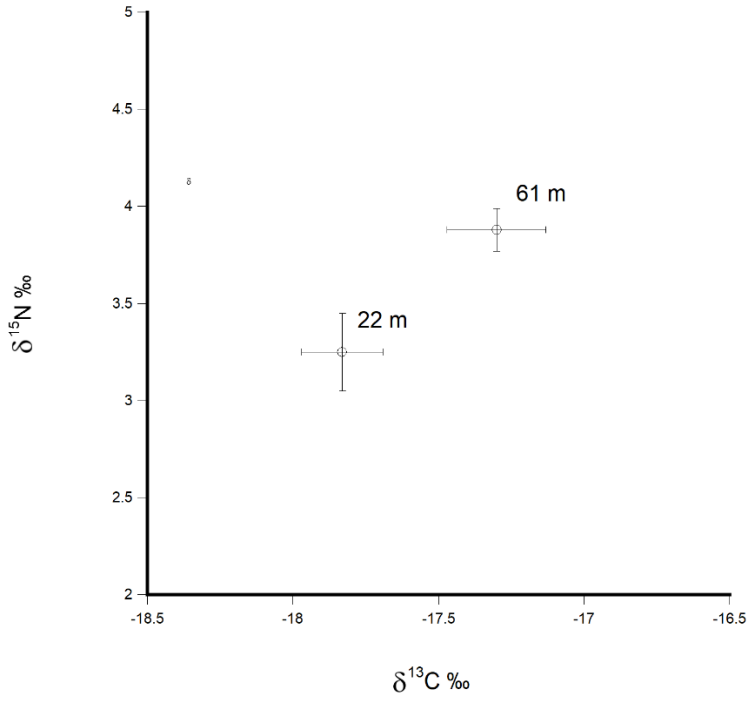

Figure 13. Bivariate plot of $\delta^{13}C$ and $\delta^{15}N$ bulk tissue stable isotopes binned by depth (mean ± SE) from the *Agelas tubulata* transplant experiment.

Proximate Biochemical Composition

There were no significant treatment effects observed for the concentration of carbohydrates (ANOVA: $F_{3,16} = 0.24$, $P = 0.867$), lipids (ANOVA: $F_{3,16} = 1.12$, $P = 0.378$), soluble proteins (ANOVA: $F_{3,16} = 0.36$, $P = 0.787$) normalized to AFDW, or total energetic content in J mg^{-1} AFDW (ANOVA: $F_{3,16} = 0.78$, $P = 0.535$) (Fig. S4)

Bite scars on experimental samples

There were no bite scars observed on any *A. tubulata* experimental samples during the feeding measurements, or at their time of collection for processing.

Discussion

The biodiversity and abundances of sponges on Caribbean mesophotic coral reefs (30-150 m) show a repeatable pattern of increased abundances and biodiversity (Lesser 2006; Trussell et al. 2006; Lesser & Slattery 2013, 2018; Slattery & Lesser 2015; Lesser & Slattery 2018; Lesser et al. 2018, 2019). Populations of *Agelas tubulata* on the Cayman Islands also show a significant

increase in percent cover with increasing depth (Macartney et al. in review). The results of this reciprocal transplant study show that for the emergent HMA sponge, *A. tubulata,* populations from mesophotic depths have a higher growth rate relative to its conspecifics located at depths <30 m. Both the transplanted sponge and the natural sponge growth rate data support data from previous studies showing that sponges exhibit increased growth as depth increases on shallow and upper mesophotic coral reefs (Lesser 2006; Trussell et al. 2006; Lesser & Slattery, 2013), and here we show that this pattern of growth extends into the mesophotic for *A. tubulata* on Grand Cayman reefs. The apical tag growth rates of both the transplanted and natural growth sponges are comparable to previous measurements of *A. tubulata* growth (Lesser 2006). The transplanted sponges display increased growth rates in the DD and SD treatments, while the SS and DS treatments show significantly less growth. This supports the hypothesis that the growth rate of these sponges is a response to the net effects of both biotic and abiotic factors that vary with increasing depth. In particular, no bite scars were noted on any treatment sponges suggesting that predation was not a significant factor affecting the growth of these sponges. In fact, the DS sponges actually show negative growth rate (i.e., de-growth) in terms of total length, potentially due to their inability to regrow tissue from the initial experimental disturbance as rapidly when compared to SD sponges. This could be the result of the reductions in their food supply when they were moved to shallow depths as previously suggested (Lesser et al. 2018). Interestingly, while the deep transplanted sponges show increasing osculum width growth rates relative to their shallow counterparts, there is no change in the natural sponge osculum width growth rates as depth increases. The apparent disparity between the experimental and natural growth rates may be due to the transplanted sponges reacting to the disturbance of transplantation by thickening their osculum walls rather than increasing apical growth. This

disturbance may be reflected in the high concentrations of soluble proteins in the sponges (Fig. S4). However, the relative osculum wall thickness growth rates in the transplant treatments were comparable to the natural sponge's osculum wall growth rates (Fig. 8b, 3b). So, undisturbed *A. tubulata* are potentially prioritizing apical and linear growth over the thickening of its osculum walls as an increase in the thickness of a sponge's cell wall may limit pumping rate (Weisz 2008; de Goeij et al. 2017), and therefore the ability to consume POM, while increasing size on the vertical axis provides more potential choanocyte chambers without the inhibition of flow rate.

The increased consumption of POM, and PON in particular, has been proposed as a primary cause for the increased abundance, diversity and growth rates in Caribbean mesophotic coral reef sponges (Lesser 2006; Trussell et al. 2006; Lesser & Slattery 2013, 2018; Slattery & Lesser 2015; Lesser & Slattery 2018; Lesser et al. 2018, 2019, 2020). As depth increases into the mesophotic zone, picoplankton with low C:N ratios increase in abundance in this study, and others (Lesser 2006; Lesser et al. 2019), which provides an important resource of nitrogen for active suspension feeders such as *A. tubulata* (Ribes et al., 2003, 2005). The available resources to sponges in this study show a steady increase in POC and PON into the mesophotic zone (Fig. 10 a, b), with concurrent decreases in DOC and DON (Fig. 10 c, d). This pattern of trophic resource availability has been observed throughout the Caribbean basin (Lesser 2006; Trussell et al. 2006; Lesser et al., 2019, 2020). Interestingly, this is the first time that both yearly and seasonal differences in the depth-dependent increase in POM concentration have been demonstrated for the shallow to mesophotic depth gradient in Grand Cayman, or any other location. Additionally, while DOM appears to be stable over time in terms of its decrease in concentration with depth, POM availability has an inverse relationship with the availability of DIN (Fig. 11 a) which is most likely a result of changes in water column primary productivity

and subsequently in the DIN pool. The DIN pool does increase with depth in both sampling periods, which can also contribute to the greater abundances of POM along the depth gradient. In this study, the experimental sponges were producers of NO_x except in July 2018 in the SS treatment (Table S2). A similar pattern has been observed in the *Xestospongia muta* in the Caribbean (Southwell et al. 2008, Fiore et al. 2013), but NO_x production (i.e., whether the sponge is a source or sink) does appear to vary by site (Fiore et al. 2013). Based on the results reported here, NO_x production in *A. tubulata* could also be affected by season (Table S2). Sponges were also sources for NH_4 and SiO_2 at both shallow and deep depths, indicating that these sponges and their microbiomes can play important roles in the cycling of these compounds at both shallow and mesophotic depths (Pita et al. 2018) (Table S2). Interestingly, while there was no significant effect of depth, sponges were generally sources for PO_4 at mesophotic depths and sinks at shallow depths (Table S2). This may mean that there are fundamental differences in the cycling of this key nutrient by the sponge's microbiome between shallow and mesophotic depths.

The availability of POM is well known to have an effect on both distributions and growth rates of a variety of active suspension feeders (Menge 2000; Gili & Coma 1998; Lesser et al. 2004; Lesser 2006; Trussell et al. 2006) and the observed patterns in this study (Fig. 10) reflects the general pattern observed for many active suspension feeders. While there is consistently an increasing amount of POM available to sponges in the mesophotic, the quality of that food changes along the depth gradient, and therefore could have an effect on growth and abundance. It has been postulated that emergent sponges in the Caribbean are nitrogen limited on shallow reefs, and the increased nitrogen in the form of PON may allow for increased growth after respiratory demands have been met (Slattery and Lesser 2015; Lesser and Slattery 2018, Lesser

et al. 2018, 2019, 2020). Many studies have identified DOC as contributing the majority of carbon to sponge diets (De Goeij et al. 2008b, 2013, 2017; Mueller et al. 2014; Rix et al. 2017, 2018, 2020; McMurray et al. 2018; Gantt et al. 2019; Wooster et al. 2019), such that carbon is unlikely to ever be limiting for sponges where DOC is utilized (Lesser et al. 2018, 2020). In this study it also appears that *Agelas tubulata* is not carbon limited (Figure 4 a, c), This may, however, result in sponges becoming nitrogen limited (Lesser et al. 2020).

Our expectations were that the growth results from the transplant experiment on *A. tubulata*, would be reflected in an increased consumption of POC and PON with increasing depth as reported in previous studies (Lesser 2006; Trussell et al. 2006; Slattery and Lesser 2015), but there were no significant treatment differences in POM consumption observed in this experiment. There is an effect 6 months post transplantation in July where a significant difference in DOC uptake between SD and DS transplants is observed, with SD sponges taking up approximately 3 times the DOC compared to DS (Fig. 12 c). This same pattern between SD and DS treatments is also observed in the uptake of DON, POC and PON but the differences between the DS and SD groups were not significant (Fig. 12 a, b, d). This treatment effect was not observed in January 2019, 12 months post transplantation. Surprisingly, in July, the SS treatment had the highest rate of POC and PON consumption, but in January had rates of POM uptake similar to the rest of the treatments (Fig. 12 a, b). This effect could be the result of increased POM availability in July relative to January (Fig 4. a, b). Shallow sponges are consistently exposed to lower concentrations of POM relative to mesophotic sponges, so shallow sponges may adjust pumping rates to utilize this resource when it becomes more abundant (Lesser 2006, de Goeij et al. 2008, Lesser & Slattery 2013). While increased food concentrations have been suggested to limit the pumping of active suspension feeders (Frost 1980; Robins 1983;

Petersen & Riisgård 1992; Petersen et al. 1999), a recent study by Morganti et al. (2019) found that there was no reduction in sponge pumping under natural oligotrophic conditions, which was also observed in a study on sponges by Ribes et al. (1999). Similarly, increased feeding rates were observed when resource availability increased for active suspension feeders in nutrient replete environments such as Antarctica (Orejas et al. 2000).

A source of variability in this experiment, the absence of any attachment by *A. tubulata* sponges to the PVC frame and closing of the base of the sponge, was not observed in a previous transplant study by Trussell et al. (2006) using *Callyspongia vaginalis*. The transplanted sponges, while partially closed off at the bottom with upright PVC into the tube, still resulted in a hollow tube. This could have affected their pumping rate due to a reduction in overall head pressure in the tube. To assess for potential influence due to this effect, natural feeding measurements were taken (Table 5). The size adjusted pumping rates of the natural sponges were higher on average (~ 270 ml s^{-1}) compared to the transplanted sponges (~25 ml s^{-1}) (Table 5, Figure S3). It appears that the morphology of the transplanted sponges had a large effect on the transplanted sponge feeding measurements. While there were no significant differences in the natural sponge feeding rates on any resource, the 61 m natural sponges did show a pattern of increased consumption of all those resources (Table 5) with small sample sizes (n=3) from each depth. Future transplant studies should combine both transplant and natural feeding with higher sampling sizes to account for potential transplantation variability and the variation observed in individual sponge pumping rates.

The results of our feeding measurements confirm that *A. tubulata* and its microbiome utilizes significant quantities of DOM in their diets. While it has been shown that sponge cells can utilize DOM (Achlatis et al. 2019), the experimental evidence also shows that the primary

consumers of DOM within the sponge, particularly algal derived DOM, is the prokaryotic microbiome (Rix et al. 2020, Zhang et al. 2019) which can then transform and translocate DOM to the host (Shih et al. 2020). Given that the kinetics of DOM uptake in bacteria show a much higher affinity, as much as three orders of magnitude, than eukaryotic cells (Manahan and Crisp 1982), it should not be surprising even though the maximum uptake kinetics for DOM uptake favor the sponge. This is because 35-50% of sponge biomass is made up of the prokaryotic microbiome (Webster and Thomas 2016, Hentschel et al 2006, Thomas et al. 2016). The microbiome of *A. tubulata*, particularly the high proportion of *Chloroflexi* bacteria, has also been shown to have a broad metabolic potential for the use of labile, semi-labile and refractory DOM. However, it is unknown what proportion of this DOM is provided to *A. tubulata* from its microbiome in the form of translocated products or via the phagocytosis of symbionts (Leys et al. 2018; Shih et al. 2020). The proportional uptake of POC to DOC (2-4% and 96-98% respectively) found in this experiment is similar to values on emergent HMA sponges on coral reefs (de Goeij et al. 2017; Wooster et al. 2019) but the POC proportion was lower than observed in other studies (McMurray et al. 2018; Rix et al. 2020). It is clear that pumping rates and feeding rates of individual sponges are highly variable over time so increasing the number of measurements over time and increasing sample sizes in future studies would be essential to account for this variability.

The increased use of POM as a nutritional resource for sponge communities in the mesophotic zone of the Caribbean is reflected in the stable isotopic signatures of *A. tubulata* tissue. Stable isotopes are generally considered a time integrated metric for assessing the diet of an organism (Fry 2006), and while there are no published studies on stable isotope turn over in sponges, we can estimate their half-life in sponges using the equation for whole body

invertebrate samples provided by Zanden et al. (2015). Our sponges had an average mass of 29.15 g AFDW giving an estimated half-life of a stable isotope in the sponge's tissue of ~10 days. The small increase in $\delta^{13}C$ may be a result of reduced consumption of photoautotrophically derived DOM and POM. It is unlikely to be because of depth-dependent changes in symbiont function, as *A. tubulata* has no known photoautotrophic symbionts (Gantt et al. 2019; Macartney & Lesser, unpublished) where the fractionation of carbon would have been affected by decreasing E_d with depth. The increased $\delta^{15}N$ at the deep site mirrors significant patterns observed in other sponges along a shallow to mesophotic depth gradient (Slattery et al. 2011; Morrow et al. 2016). The stable $\delta^{15}N$ isotope is often used as a measure of heterotrophy and changes in trophic position (Peterson & Fry 1987). In *A. tubulata*, heterotrophy increases with increasing depth (Slattery et al. 2011), and the increased $\delta^{15}N$ suggests an increased reliance by mesophotic sponges on resources such as heterotrophic picoplankton or procholorphytes, both of which increase in the mesophotic in this study and others (e.g. Lesser et al. 2019, 2020), compared to isotopically lighter eukaryotic phytoplankton and autotrophic picoplankton such as *Synechococcus* (Lesser 2006; Lesser et al. 2019, 2020; this study). The decrease in C:N ratios at the deep site also indicates that deep sponges have a more stoichiometrically balanced diet to start with, relative to shallow sponges (Lesser et al. 2020). Taken together, the stable isotope data and ambient POM concentrations provide compelling evidence that the observed differences in growth is driven by the consumption of nitrogen-rich POM over time on mesophotic reefs relative to shallow reefs. This increased consumption of an abundant, nitrogen-rich resource with greater bioavailability at mesophotic depths allows for higher growth rates on MCEs. This is the most parsimonious explanation based on the data presented here, previously published literature on Caribbean sponges (Lesser 2006; Trussell et al. 2006; Lesser and Slattery 2013; Slattery and

Lesser 2015; Wulff 2017) and literature on other active suspension feeders from a variety of environments (Lesser et al. 1994; Menge 1994, 2000; Gili & Coma 1998; Gili 2001; Lesser & Slattery 2015).

In some cases, other factors have been shown to regulate the distribution and abundance of active suspension feeder such as predation or physical disturbances (Menge & Sutherland 1976, Summerson & Peterson 1984, Wulff 2017), but the results of this study reflect bottom-up forces (i.e., food availability) as the primary factor regulating sponge biomass and growth rates. Top-down control, at least in the form of predation, also seems unlikely here as *Agelas tubulata* is a chemically defended sponge that produces a wide variety of secondary metabolites, resulting in tissue extracts from this sponge becoming less palatable to spongivores relative to other sponge species (Chanas et al., 1997, Assman et al. 2000, Pawlik et al. 2006, Pawlik 1997, 2011). In this experiment, no bite scars were observed during regular checks and final handling of the transplanted sponges. Since these sponges were exposed to all abiotic and biotic factors, the lack of bite scars suggests that predation was not a confounding factor affecting the growth rates observed during this experiment. This is further supported by the observations of Wulff (2017) who found that predation was not a significant regulator of sponge populations between depths on coral reefs but did structure sponge populations between ecotypes (mangrove vs. coral reef). It is also unlikely the light environment had any effect on this sponge's growth rates or metabolic requirements due to the lack of photoautotrophic symbionts in *A. tubulata* (Gantt et al. 2019, Macartney & Lesser, unpublished). *Agelas tubulata* does harbor dense *Chloroflexi* populations (Olson 2010, Gantt et al. 2019), as observed in many Caribbean sponges (Hentschel et al. 2012; Thomas et al. 2016; Pita et al. 2018) and while these bacteria have the potential for phototrophic

metabolism (3-Hydroxypropionate pathway), this was not reflected in the sponge tissue isotopic composition (Canfeld et al. 2005).

Conclusions

The results of this study show that *Agelas tubulata* in the mesophotic have higher growth rates relative to their shallow conspecifics. Particulate organic matter was also significantly higher at mesophotic depths in both July and January, which provides evidence that the increased growth rates at mesophotic depths were a result of the increased quantities and consumption of POM available to the mesophotic sponges, which was then reflected in the sponge tissue $\delta^{15}N$ values. We have also shown that *A. tubulata* consumes significant concentrations of DOC and DON but given the higher C:N ratios and lower bioavailability of DOM for sponges how much of this DOM actually goes into sponge biomass accumulation (*sensu* Shih et al. 2020) is unknown. The pumping and feeding rates of *A. tubulata* showed high individual variability during this study, illustrating that multiple measurements of feeding on both DOM and POM over time are required to better understand the variability in the feeding ecology of these sponges as a function of depth. These sponges were found to be sources of inorganic and organic compounds such as NO_x, NH_4 and SiO_2 at our site and were sources for PO_4 at mesophotic depths, illustrating the important role *A. tubulata* may also play in the local cycling of these essential constituents for many community members on shallow and mesophotic coral reefs (*sensu* Slattery et al. 2013). Additionally these sponges produced large quantities of phytodetrital matter. This warrants further study into detrital production in *A. tubulata*. Further study on the cycling of inorganic and organic compounds by sponges on MCEs, the chemical composition and microbial community structure along the shallow to mesophotic depth gradient are necessary to help identify other

potential factors controlling the growth, biomass and distribution of this Caribbean coral reef sponge.

Acknowledgements

We thank E. Kintzing and D. Gochfeld for field and laboratory support. We thank A. Weinheimer for insightful comments on the manuscript draft and statistical analyses. We thank S. Pankey for field and laboratory support and assistance with statistical analyses. All sample collections complied with the laws of the Cayman Islands and the United States of America. Support was provided by NSF Biological Oceanography (OCE–1632348/1632333) to MPL and MS respectively, and the University of New Hampshire Marine Biology Small Grants fund to KJM.

Literature Cited

Assmann, M., Lichte, E., Pawlik, J. R., & Köck, M. (2000). Chemical defenses of the Caribbean sponges *Agelas wiedenmayeri* and *Agelas conifera*. Marine Ecology Progress Series, 207, 255-262.

Bell, J. J. (2008). The functional roles of marine sponges. Estuarine, coastal and shelf science, 79(3), 341-353.

Bertilsson, S., Berglund, O., Karl, D. M., & Chisholm, S. W. (2003). Elemental composition of marine *Prochlorococcus* and *Synechococcus*: Implications for the ecological stoichiometry of the sea. Limnology and oceanography, 48(5), 1721-1731.

Boudreaux, M. L., Stiner, J. L., & Walters, L. J. (2006). Biodiversity of sessile and motile macrofauna on intertidal oyster reefs in Mosquito Lagoon, Florida. Journal of Shellfish Research, 25(3), 1079-1089.

Bourne, D. G., Morrow, K. M., & Webster, N. S. (2016). Insights into the coral microbiome: underpinning the health and resilience of reef ecosystems. Annual Review of Microbiology, 70.

Bradford, M. M. (1976). A rapid and sensitive method for the quantitation of microgram quantities of protein utilizing the principle of protein-dye binding. Analytical biochemistry, 72(1-2), 248-254.

Campbell, L., Nolla, H. A., & Vaulot, D. (1994). The importance of Prochlorococcus to community structure in the central North Pacific Ocean. Limnology and Oceanography, 39(4), 954-961.

Canfield, D. E., Kristensen, E., & Thamdrup, B. (2005). Carbon fixation and phototrophy. In Advances in marine biology (Vol. 48, pp. 95-127). Academic Press.

Cattaneo-Vietti, R., Chiantore, M., Misic, C., Povero, P., & Fabiano, M. (1999). The role of pelagic-benthic coupling in structuring littoral benthic communities at Terra Nova Bay (Ross Sea) and in the Straits of Magellan. Scientia Marina, 63(S1), 113-121.

Coppari, M., Gori, A., Viladrich, N., Saponari, L., Canepa, A., Grinyó, J., ... & Rossi, S. (2016). The role of Mediterranean sponges in benthic–pelagic coupling processes: *Aplysina aerophoba* and *Axinella polypoides* case studies. Journal of Experimental Marine Biology and Ecology, 477, 57-68.

Dayton, P. K., Robilliard, G. A., Paine, R. T., & Dayton, L. B. (1974). Biological accommodation in the benthic community at McMurdo Sound, Antarctica. Ecological Monographs, 44(1), 105-128.

de Goeij, J. M., & Van Duyl, F. C. (2007). Coral cavities are sinks of dissolved organic carbon (DOC). Limnology and Oceanography, 52(6), 2608-2617.

de Goeij, J. M., Lesser, M. P., & Pawlik, J. R. (2017). Nutrient fluxes and ecological functions of coral reef sponges in a changing ocean. In Climate change, ocean acidification and sponges (pp. 373-410). Springer, Cham.

de Goeij, J. M., Moodley, L., Houtekamer, M., Carballeira, N. M., & Van Duyl, F. C. (2008). Tracing 13C-enriched dissolved and particulate organic carbon in the bacteria-containing coral reef sponge *Halisarca caerulea*: Evidence for DOM-feeding. Limnology and Oceanography, 53(4), 1376-1386.

de Goeij, J. M., Van Den Berg, H., van Oostveen, M. M., Epping, E. H., & Van Duyl, F. C. (2008). Major bulk dissolved organic carbon (DOC) removal by encrusting coral reef cavity sponges. Marine Ecology Progress Series, 357, 139-151.

de Goeij, J. M., Van Oevelen, D., Vermeij, M. J., Osinga, R., Middelburg, J. J., De Goeij, A. F., & Admiraal, W. (2013). Surviving in a marine desert: the sponge loop retains resources within coral reefs. Science, 342(6154), 108-110.

Diaz, M. C., & Rützler, K. (2001). Sponges: an essential component of Caribbean coral reefs. Bulletin of Marine Science, 69(2), 535-546.

Ducklow, H. W., Kirchman, D. L., Quinby, H. L., Carlson, C. A., & Dam, H. G. (1993). Stocks and dynamics of bacterioplankton carbon during the spring bloom in the eastern North Atlantic Ocean. Deep Sea Research Part II: Topical Studies in Oceanography, 40(1-2), 245-263.

Fagerbakke, K. M., Heldal, M., & Norland, S. (1996). Content of carbon, nitrogen, oxygen, sulfur and phosphorus in native aquatic and cultured bacteria. Aquatic Microbial Ecology, 10(1), 15-27.

Fiore, C. L., Baker, D. M., & Lesser, M. P. (2013a). Nitrogen biogeochemistry in the Caribbean sponge, *Xestospongia muta*: a source or sink of dissolved inorganic nitrogen?. PLoS One, 8(8), e72961.

Fiore, C. L., Jarett, J. K., & Lesser, M. P. (2013b). Symbiotic prokaryotic communities from different populations of the giant barrel sponge, *Xestospongia muta*. Microbiology open, 2(6), 938-952.

Fiore, C. L., Jarett, J. K., Steinert, G., & Lesser, M. P. (2020). trait-Based comparison of coral and Sponge Microbiomes. Scientific reports, 10(1), 1-16.

Freeman, C. J., & Thacker, R. W. (2011). Complex interactions between marine sponges and their symbiotic microbial communities. Limnology and Oceanography, 56(5), 1577-1586.

Freeman, N. K., Lindgren, F. T., Ng, Y. O., & Nichols, A. V. (1952). Infrared spectra of some lipoproteins and related lipids. J. Biol. Chem., Vol. 203, pp. 293-304.

Frost, T. M. (1980). Clearance rate determinations for the fresh-water sponge *Spongilla-Lacustris* effects of temperature, particle type and concentration, and sponge size. Arch. Hydrobiol. 90, 330–356

Gantt, S. E., McMurray, S. E., Stubler, A. D., Finelli, C. M., Pawlik, J. R., & Erwin, P. M. (2019). Testing the relationship between microbiome composition and flux of carbon and nutrients in Caribbean coral reef sponges. Microbiome, 7(1), 124.

Gili, J. M., & Coma, R. (1998). Benthic suspension feeders: their paramount role in littoral marine food webs. Trends in ecology & evolution, 13(8), 316-321.

Gili, J. M., Coma, R., Orejas, C., López-González, P. J., & Zabala, M. (2001). Are Antarctic suspension-feeding communities different from those elsewhere in the world?. Polar Biology, 24(7), 473-485.

Griffiths, J. R., Kadin, M., Nascimento, F. J., Tamelander, T., Törnroos, A., Bonaglia, S., ... & Kotta, J. (2017). The importance of benthic–pelagic coupling for marine ecosystem functioning in a changing world. Global change biology, 23(6), 2179-2196.

Griffiths, J. R., Kadin, M., Nascimento, F. J., Tamelander, T., Törnroos, A., Bonaglia, S., ... & Kotta, J. (2017). The importance of benthic–pelagic coupling for marine ecosystem functioning in a changing world. Global change biology, 23(6), 2179-2196.

Hadas, E., Shpigel, M., & Ilan, M. (2009). Particulate organic matter as a food source for a coral reef sponge. Journal of Experimental Biology, 212(22), 3643-3650.

Hentschel, U., Piel, J., Degnan, S. M., & Taylor, M. W. (2012). Genomic insights into the marine sponge microbiome. Nature Reviews Microbiology, 10(9), 641-654.

Jaschinski, S., Hansen, T., & Sommer, U. (2008). Effects of acidification in multiple stable isotope analyses. Limnology and Oceanography: Methods, 6(1), 12-15.

Kolasinski, J., Rogers, K., & Frouin, P. (2008). Effects of acidification on carbon and nitrogen stable isotopes of benthic macrofauna from a tropical coral reef. Rapid Communications in Mass Spectrometry, 22(18), 2955-2960.

Lesser, M. P. (2006). Benthic–pelagic coupling on coral reefs: feeding and growth of Caribbean sponges. Journal of Experimental Marine Biology and Ecology, 328(2), 277-288.

Lesser, M. P., & Kruse, V. A. (2004). Seasonal temperature compensation in the horse mussel, *Modiolus modiolus*: metabolic enzymes, oxidative stress and heat shock proteins. Comparative Biochemistry and Physiology Part A: Molecular & Integrative Physiology, 137(3), 495-504.

Lesser, M. P., & Slattery, M. (2013). Ecology of Caribbean sponges: are top-down or bottom-up processes more important? PloS one, 8(11), e79799. doi:10.1371/journal.pone.0079799

Lesser, M. P., & Slattery, M. (2015). Picoplankton consumption supports the ascidian *Cnemidocarpa verrucosa* in McMurdo Sound, Antarctica. Marine Ecology Progress Series, 525, 117-126.

Lesser, M. P., & Slattery, M. (2018). Sponge density increases with depth throughout the Caribbean. Ecosphere, 9(12), e02525.

Lesser, M. P., Slattery, M., & Leichter, J. J. (2009). Ecology of mesophotic coral reefs. Journal of Experimental Marine Biology and Ecology, 375(1-2), 1-8.

Lesser, M. P., Slattery, M., & Mobley, C. D. (2018). Biodiversity and functional ecology of mesophotic coral reefs. Annual Review of Ecology, Evolution, and Systematics, 49, 49-71.

Lesser, M. P., Slattery, M., Laverick, J. H., Macartney, K. J., & Bridge, T. C. (2019). Global community breaks at 61 m on mesophotic coral reefs. Global Ecology and Biogeography, 28(10), 1403-1416.

Lesser, M. P., B. Mueller, M. S. Pankey, K. J. Macartney, M. Slattery, and J. M. Goeij. (2020) Depth-dependent detritus production in the sponge, *Halisarca caerulea*. Limnol. Oceanogr. lno.11384. doi:10.1002/lno.11384

Lesser, M. P., Witman, J. D., & Sebnens, K. P. (1994). Effects of flow and seston availability on scope for growth of benthic suspension-feeding invertebrates from the Gulf of Maine. The Biological Bulletin, 187(3), 319-335.

Leys, S. P., Kahn, A. S., Fang, J. K. H., Kutti, T., & Bannister, R. J. (2018). Phagocytosis of microbial symbionts balances the carbon and nitrogen budget for the deep-water boreal sponge *Geodia barretti*. Limnology and Oceanography, 63(1), 187-202.

Longhurst, A. (1993). Seasonal cooling and blooming in tropical oceans. Deep Sea Research Part I: Oceanographic Research Papers, 40(11-12), 2145-2165.

Loya, Y., Eyal, G., Treibitz, T., Lesser, M. P., & Appeldoorn, R. (2016). Theme section on mesophotic coral ecosystems: advances in knowledge and future perspectives.

Maldonado, M., Ribes, M., & van Duyl, F. C. (2012). Nutrient fluxes through sponges: biology, budgets, and ecological implications. In Advances in marine biology (Vol. 62, pp. 113-182). Academic Press.

Marie, D., Simon, N., & Vaulot, D. (2005). Phytoplankton cell counting by flow cytometry. Algal culturing techniques, 1, 253-267.

Masuko, T., Minami, A., Iwasaki, N., Majima, T., Nishimura, S. I., & Lee, Y. C. (2005). Carbohydrate analysis by a phenol–sulfuric acid method in microplate format. Analytical biochemistry, 339(1), 69-72.

McMurray, S. E., Johnson, Z. I., Hunt, D. E., Pawlik, J. R., & Finelli, C. M. (2016). Selective feeding by the giant barrel sponge enhances foraging efficiency. Limnology and Oceanography, 61(4), 1271-1286.

McMurray, S. E., Pawlik, J. R., & Finelli, C. M. (2014). Trait-mediated ecosystem impacts: how morphology and size affect pumping rates of the Caribbean giant barrel sponge. Aquatic Biology, 23(1), 1-13.

McMurray, S. E., Stubler, A. D., Erwin, P. M., Finelli, C. M., & Pawlik, J. R. (2018). A test of the sponge-loop hypothesis for emergent Caribbean reef sponges. Marine Ecology Progress Series, 588, 1-14.

Menge, B. A. (2000). Top-down and bottom-up community regulation in marine rocky intertidal habitats. Journal of experimental marine biology and ecology, 250(1-2), 257-289.

Menge, B. A., Berlow, E. L., Blanchette, C. A., Navarrete, S. A., & Yamada, S. B. (1994). The keystone species concept: variation in interaction strength in a rocky intertidal habitat. Ecological monographs, 64(3), 249-286.

Morel, A., Ahn, Y. H., Partensky, F., Vaulot, D., & Claustre, H. (1993). Prochlorococcus and Synechococcus: a comparative study of their optical properties in relation to their size and pigmentation. Journal of Marine Research, 51(3), 617-649.

Morganti, T. M., Ribes, M., Yahel, G., & Coma, R. (2019). Size is the major determinant of pumping rates in marine sponges. Frontiers in physiology, 10, 1474.

Morrow, K. M., Fiore, C. L., & Lesser, M. P. (2016). Environmental drivers of microbial community shifts in the giant barrel sponge, *Xestospongia muta*, over a shallow to mesophotic depth gradient. Environmental Microbiology, 18(6), 2025-2038.

Mueller, B., de Goeij, J. M., Vermeij, M. J., Mulders, Y., van der Ent, E., Ribes, M., & van Duyl, F. C. (2014). Natural diet of coral-excavating sponges consists mainly of dissolved organic carbon (DOC). PloS one, 9(2), e90152.

Olson, J. B., & Gao, X. (2013). Characterizing the bacterial associates of three Caribbean sponges along a gradient from shallow to mesophotic depths. FEMS microbiology ecology, 85(1), 74-84.

Orejas, C., Gili, J. M., Arntz, W. E., Ros, J., López, P. J., Teixidó, N., & Filipe, P. (2000). Benthic suspension feeders, key players in Antarctic marine ecosystems? Contributions to Science, 2000, vol. 1, num. 3, p. 299-311.

Packard, G. C., & Boardman, T. J. (1988). The misuse of ratios, indices, and percentages in ecophysiological research. Physiological Zoology, 61(1), 1-9.

Page, H. M., & Hubbard, D. M. (1987). Temporal and spatial patterns of growth in mussels *Mytilus edulis* on an offshore platform: relationships to water temperature and food availability. Journal of Experimental Marine Biology and Ecology, 111(2), 159-179.

Pawlik, J. R. (2011). The chemical ecology of sponges on Caribbean reefs: natural products shape natural systems. Bioscience, 61(11), 888-898.

Pawlik, J. R., Loh, T. L., & McMurray, S. E. (2018). A review of bottom-up vs. top-down control of sponges on Caribbean fore-reefs: what's old, what's new, and future directions. PeerJ, 6, e4343.

Pawlik, J. R., Loh, T. L., McMurray, S. E., & Finelli, C. M. (2013). Sponge communities on Caribbean coral reefs are structured by factors that are top-down, not bottom-up. PLoS One, 8(5), e62573.

Perea-Blazquez, A., Davy, S. K., & Bell, J. J. (2012). Estimates of particulate organic carbon flowing from the pelagic environment to the benthos through sponge assemblages. PloS one, 7(1), e29569.

Petersen, J. K., & Riisgård, H. U. (1992). Filtration capacity of the ascidian *Ciona intestinalis* and its grazing impact in a shallow fjord. Marine Ecology Progress Series, 9-17.

Petersen, J. K., Mayer, S., & Knudsen, M. Å. (1999). Beat frequency of cilia in the branchial basket of the ascidian *Ciona intestinalis* in relation to temperature and algal cell concentration. Marine Biology, 133(2), 185-192.

Pile, A. J., Patterson, M. R., Savarese, M., Chernykh, V. I., & Fialkov, V. A. (1997). Trophic effects of sponge feeding within Lake Baikal's littoral zone. 2. Sponge abundance, diet, feeding efficiency, and carbon flux. Limnology and Oceanography, 42(1), 178-184.

Pita, L., Rix, L., Slaby, B. M., Franke, A., & Hentschel, U. (2018). The sponge holobiont in a changing ocean: from microbes to ecosystems. Microbiome, 6(1), 46.

Ribes, M., Coma, R., & Gili, J. M. (1999). Natural diet and grazing rate of the temperate sponge *Dysidea avara* (Demospongiae, Dendroceratida) throughout an annual cycle. Marine Ecology Progress Series, 176, 179-190.

Ribes, M., Coma, R., Atkinson, M. J., & Kinzie III, R. A. (2003). Particle removal by coral reef communities: picoplankton is a major source of nitrogen. Marine Ecology Progress Series, 257, 13-23.

Ribes, M., Coma, R., Atkinson, M. J., & Kinzie III, R. A. (2005). Sponges and ascidians control removal of particulate organic nitrogen from coral reef water. Limnology and oceanography, 50(5), 1480-1489.

Rix, L., de Goeij, J. M., van Oevelen, D., Struck, U., Al-Horani, F. A., Wild, C., & Naumann, M. S. (2018). Reef sponges facilitate the transfer of coral-derived organic matter to their associated fauna via the sponge loop. Marine Ecology Progress Series, 589, 85-96.

Rix, L., de Goeij, J. M., van Oevelen, D., Struck, U., Al-Horani, F. A., Wild, C., & Naumann, M. S. (2017). Differential recycling of coral and algal dissolved organic matter via the sponge loop. Functional Ecology, 31(3), 778-789.

Rix, L., Ribes, M., Coma, R. Jahn, M… (2020) Heterotrophy in the earliest gut: a single-cell view of heterotrophic carbon and nitrogen assimilation in sponge-microbe symbioses. ISME J https://doi.org/10.1038/s41396-020-0706-3

Robbins, I. J. (1983). The effects of body size, temperature, and suspension density on the filtration and ingestion of inorganic particulate suspensions by ascidians. Journal of Experimental Marine Biology and Ecology, 70(1), 65-78.

Rohde, S., Nietzer, S., & Schupp, P. J. (2015). Prevalence and mechanisms of dynamic chemical defenses in tropical sponges. PLoS One, 10(7), e0132236.

Saier, B. (2002). Subtidal and intertidal mussel beds (*Mytilus edulis L*.) in the Wadden Sea: diversity differences of associated epifauna. Helgoland Marine Research, 56(1), 44-50.

Scott, A. R., & Pawlik, J. R. (2019). A review of the sponge increase hypothesis for Caribbean mesophotic reefs. Marine Biodiversity, 49(3), 1073-1083.

Shih, J. L., Selph, K. E., Wall, C. B., Wallsgrove, N. J., Lesser, M. P., & Popp, B. N. (2020). Trophic ecology of the tropical pacific sponge *Mycale grandis* inferred from amino acid compound-specific isotopic analyses. Microbial ecology, 79(2), 495-510.

Slattery, M., & Lesser, M. P. (2015). Trophic ecology of sponges from shallow to mesophotic depths (3 to 150 m): comment on Pawlik et al. (2015). Marine Ecology Progress Series, 527, 275-279.

Slattery, M., & Lesser, M. P. (2019). The Bahamas and Cayman Islands. In Mesophotic coral ecosystems (pp. 47-56). Springer, Cham.

Slattery, M., Gochfeld, D. J., Diaz, M. C., Thacker, R. W., & Lesser, M. P. (2016). Variability in chemical defense across a shallow to mesophotic depth gradient in the Caribbean sponge *Plakortis angulospiculatus*. Coral Reefs, 35(1), 11-22.

Slattery, M., Lesser, M. P., Brazeau, D., Stokes, M. D., & Leichter, J. J. (2011). Connectivity and stability of mesophotic coral reefs. Journal of Experimental Marine Biology and Ecology, 408(1-2), 32-41.

Slattery, M., Gochfeld, D. J., Easson, C. G., & O'Donahue, L. R. (2013). Facilitation of coral reef biodiversity and health by cave sponge communities. Marine Ecology Progress Series, 476, 71-86.

Stanley Jr, G. D. (2006). Photosymbiosis and the evolution of modern coral reefs. Science, 312, 3857-858.

Thacker, R. W., and C. J. Freeman. 2012. Sponge-Microbe Symbioses. Recent Advances and New Directions, Adv. Mar. Biol. 62:57-111. doi: 10.1016/B978-0-12-394283-8.00002-3

Thomas, T., Moitinho-Silva, L., Lurgi, M., Björk, J. R., Easson, C., Astudillo-García, C., ... & Chaves-Fonnegra, A. (2016). Diversity, structure and convergent evolution of the global sponge microbiome. Nature communications, 7(1), 1-12.

Trussell, G. C., Lesser, M. P., Patterson, M. R., & Genovese, S. J. (2006). Depth-specific differences in growth of the reef sponge *Callyspongia vaginalis*: role of bottom-up effects. Marine Ecology Progress Series, 323, 149-158.

Vafeiadou, A. M., Adão, H., De Troch, M., & Moens, T. (2013). Sample acidification effects on carbon and nitrogen stable isotope ratios of macrofauna from a *Zostera noltii* bed. Marine and Freshwater Research, 64(8), 741-745.

Verity, P. G., Robertson, C. Y., Tronzo, C. R., Andrews, M. G., Nelson, J. R., & Sieracki, M. E. (1992). Relationships between cell volume and the carbon and nitrogen content of marine photosynthetic nanoplankton. Limnology and Oceanography, 37(7), 1434-1446.

Weisz, J. B., Lindquist, N., & Martens, C. S. (2008). Do associated microbial abundances impact marine demosponge pumping rates and tissue densities? Oecologia, 155(2), 367-376.

Wooster, M. K., McMurray, S. E., Pawlik, J. R., Morán, X. A., & Berumen, M. L. (2019). Feeding and respiration by giant barrel sponges across a gradient of food abundance in the Red Sea. Limnology and Oceanography, 64(4), 1790-1801.

Wulff, J. (2017). Bottom-up and top-down controls on coral reef sponges: disentangling within-habitat and between-habitat processes. Ecology, 98(4), 1130-1139.

Vander Zanden, M. J., Clayton, M. K., Moody, E. K., Solomon, C. T., & Weidel, B. C. (2015). Stable isotope turnover and half-life in animal tissues: a literature synthesis. PloS one, 10(1), e0116182.

Zhang, F., Jonas, L., Lin, H., & Hill, R. T. (2019). Microbially mediated nutrient cycles in marine sponges. FEMS microbiology ecology, 95(11), 115.

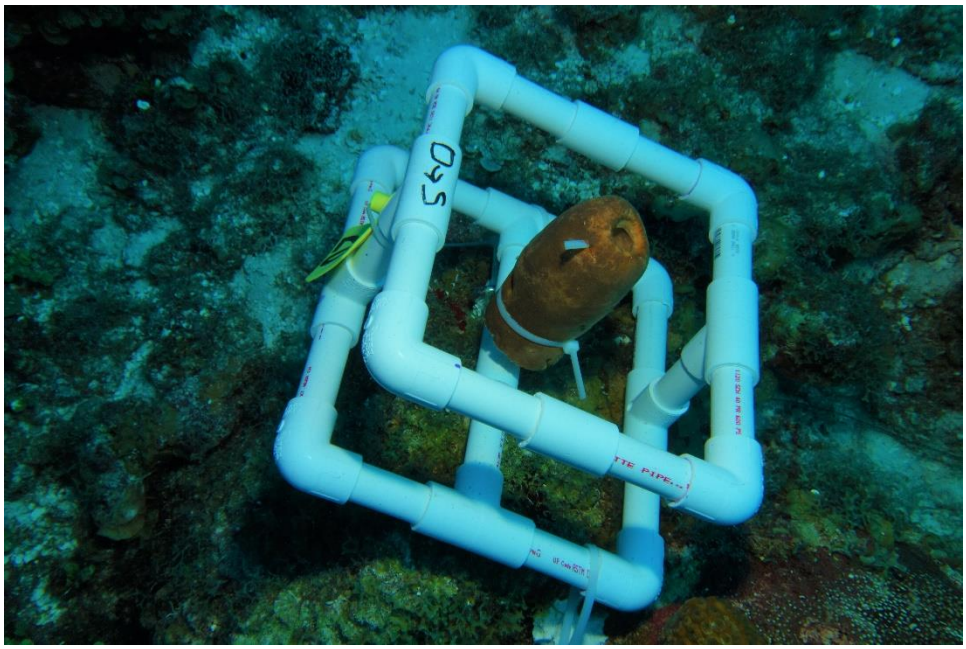

Figure 14 (S1). Photo of a transplanted *Agelas tubulata* on the experimental PVC rack (Photo: Liz Kintzing).

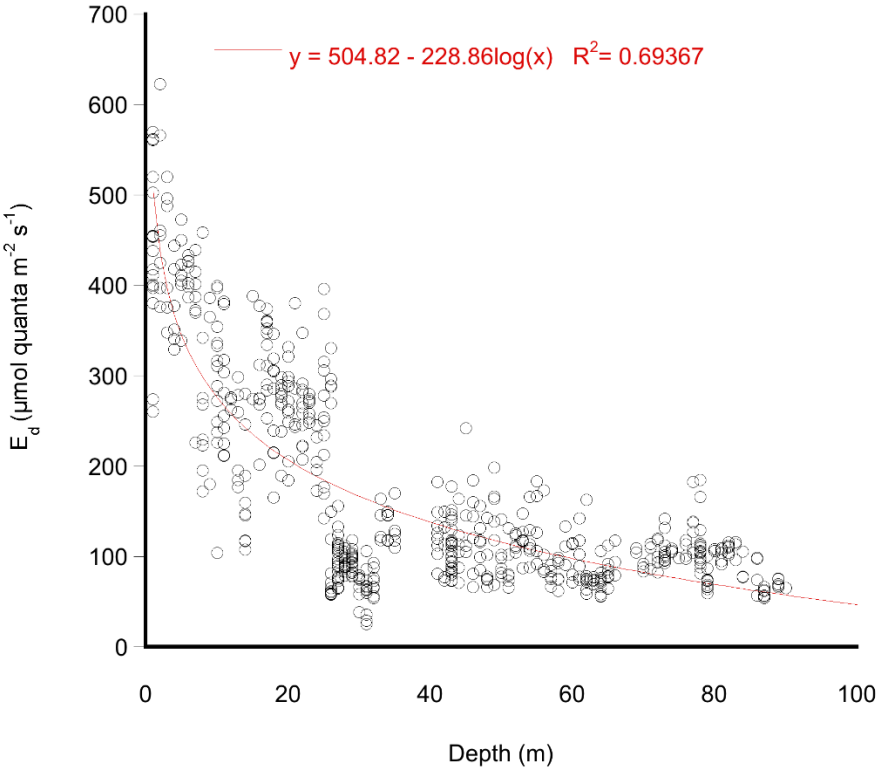

Figure 15 (S2). The effect of depth on downwelling irradiances (PAR: µmol quanta m^{-2} s^{-1}) at the experimental transplant site.

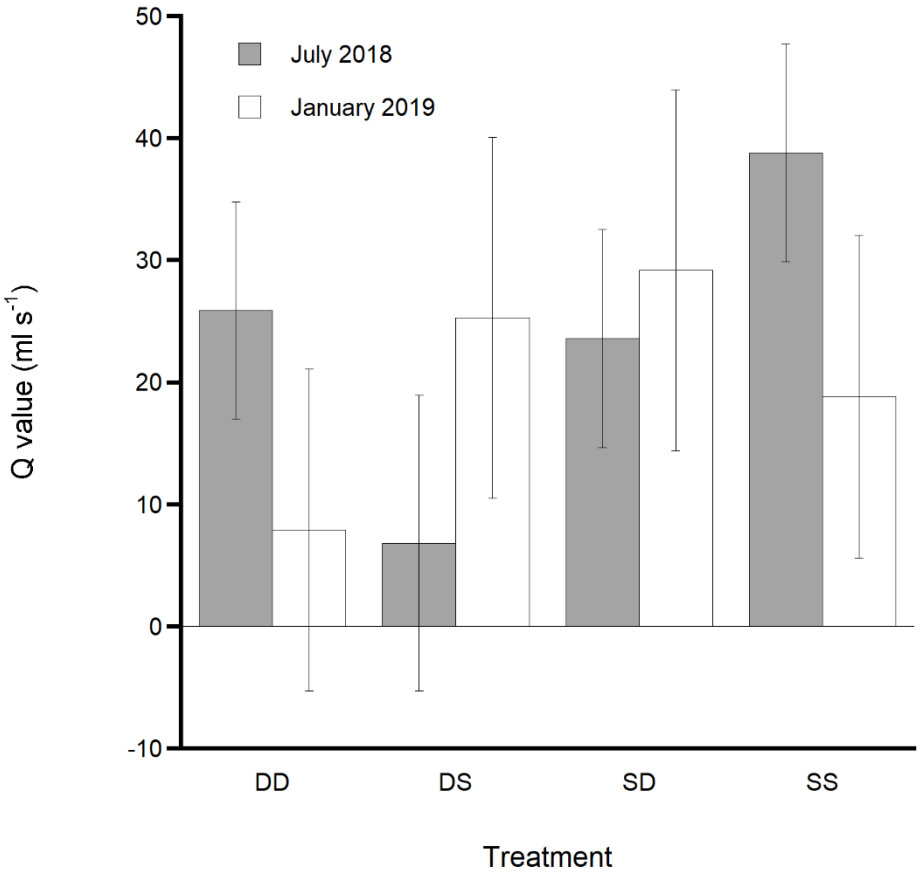

Figure 16 (S3). Mean (± SE) Q values (volumetric flux, ml s^{-1}) collected during the feeding assessments on experimental sponges.

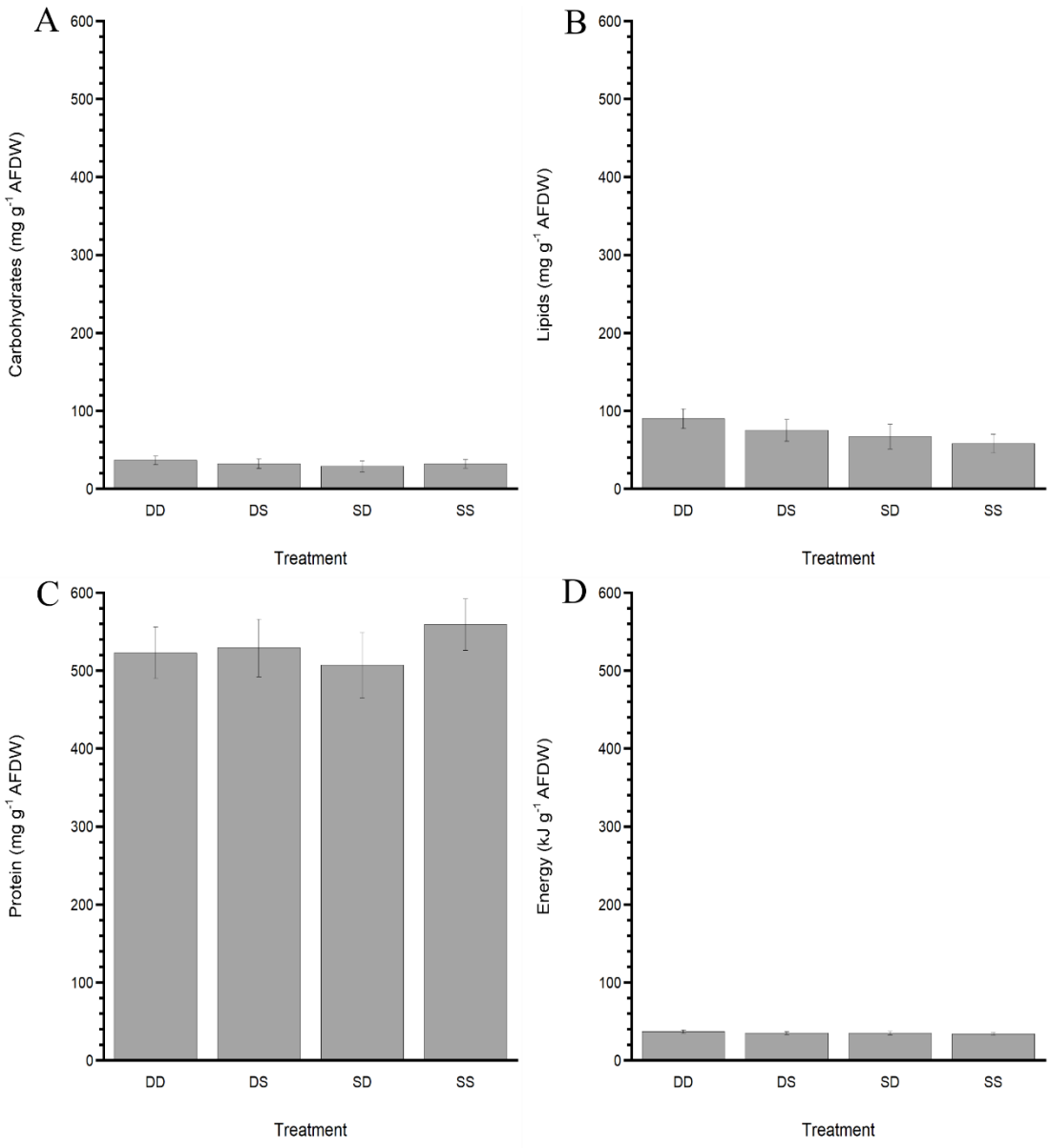

Figure 17 (S4). Experimental effects of proximate biochemical composition normalized to grams of ash free dry weight (g AFDW) for mean (± SE) **A)** carbohydrates, **B)** lipids, **C)** soluble protein and **D)** total energetic content in Joules.

Table 7 (S1). Monthly mean temperatures (± SD) at each depth for one continuous year during study period on Grand Cayman.

Year	Month	Depth	Temperature ℃
2018	7	15m	29.75 ± 0.41
2018	7	22m	29.5 ± 0.45
2018	7	30m	29.25 ± 0.5
2018	7	46m	28.51 ± 0.3
2018	7	61m	28.09 ± 0.19
2018	7	76m	27.7 ± 0.24
2018	7	91m	27.47 ± 0.22
2018	8	15m	29.35 ± 0.29
2018	8	22m	29.21 ± 0.29
2018	8	30m	29.15 ± 0.3
2018	8	46m	28.69 ± 0.28
2018	8	61m	28.38 ± 0.2
2018	8	76m	28.07 ± 0.17
2018	8	91m	27.89 ± 0.17
2018	9	15m	29.88 ± 0.16
2018	9	22m	29.79 ± 0.18
2018	9	30m	29.79 ± 0.19
2018	9	46m	29.36 ± 0.21
2018	9	61m	28.55 ± 0.27
2018	9	76m	27.75 ± 0.22
2018	9	91m	27.21 ± 0.2
2018	10	15m	29.23 ± 0.15
2018	10	22m	29.18 ± 0.13
2018	10	30m	29.21 ± 0.11
2018	10	46m	29.06 ± 0.09
2018	10	61m	28.79 ± 0.28
2018	10	76m	28.1 ± 0.55
2018	10	91m	27.46 ± 0.47
2018	11	15m	28.9 ± 0.17
2018	11	22m	28.87 ± 0.15
2018	11	30m	28.91 ± 0.15
2018	11	46m	28.79 ± 0.14
2018	11	61m	28.7 ± 0.22
2018	11	76m	28.28 ± 0.32
2018	11	91m	27.71 ± 0.47
2018	12	15m	28.14 ± 0.34
2018	12	22m	28.13 ± 0.34
2018	12	30m	28.18 ± 0.34
2018	12	46m	28.09 ± 0.33
2018	12	61m	28.15 ± 0.32
2018	12	76m	28.03 ± 0.31
2018	12	91m	27.87 ± 0.36
2019	1	15m	27.11 ± 1.12

2019	1	22m	27.1 ± 1.14
2019	1	30m	27.04 ± 1.28
2019	1	46m	27.32 ± 0.3
2019	1	61m	27.39 ± 0.32
2019	1	76m	27.49 ± 0.18
2019	1	91m	27.4 ± 0.22
2019	2	15m	27.09 ± 0.1
2019	2	22m	27.07 ± 0.1
2019	2	30m	27.04 ± 0.09
2019	2	46m	27 ± 0.09
2019	2	61m	27 ± 0.08
2019	2	76m	27.01 ± 0.09
2019	2	91m	26.91 ± 0.12
2019	3	15m	27.19 ± 0.17
2019	3	22m	27.16 ± 0.16
2019	3	30m	27.13 ± 0.15
2019	3	46m	27.08 ± 0.14
2019	3	61m	27.07 ± 0.13
2019	3	76m	27.03 ± 0.14
2019	3	91m	26.85 ± 0.14
2019	4	15m	27.6 ± 0.17
2019	4	22m	27.52 ± 0.15
2019	4	30m	27.47 ± 0.15
2019	4	46m	27.35 ± 0.15
2019	4	61m	27.23 ± 0.11
2019	4	76m	27.13 ± 0.08
2019	4	91m	26.92 ± 0.08
2019	5	15m	28.51 ± 0.31
2019	5	22m	28.43 ± 0.31
2019	5	30m	28.36 ± 0.31
2019	5	46m	28.12 ± 0.33
2019	5	61m	27.68 ± 0.24
2019	5	76m	27.42 ± 0.18
2019	5	91m	27.11 ± 0.16
2019	6	15m	29.04 ± 1.04
2019	6	22m	28.96 ± 1
2019	6	30m	28.91 ± 1.03
2019	6	46m	28.56 ± 0.97
2019	6	61m	27.83 ± 0.92
2019	6	76m	27.45 ± 0.18
2019	6	91m	27.11 ± 0.15

Table 8 (S2). Fluxes (mean ± SE) of nitrate and nitrite (NO_3 + NO_2= NO_x), ammonium (NH_4), phosphate (PO_4) and silica dioxide (SiO_2) between two sampling periods and depths.

Date	Depth (m)	NO_x Flux ($\mu mol\ s^{-1}$)	NH_4 Flux ($\mu mol\ s^{-1}$)	PO_4 Flux ($\mu mol\ s^{-1}$)	SiO2 Flux ($\mu mol\ s^{-1}$)
July 2018	22	-0.00141 (0.0128)	0.0027 (0.0081)	-0.0016 (0.0028)	0.0042 (0.0046)
July 2018	61	0.0023 (0.0007)	0.032 (0.009)	0.00005 (0.00009)	0.0028 (0.016)
January 2019	22	0.0057 (0.0025)	0.022 (0.017)	-0.0007 (0.0004)	-0.032 (0.014)
January 2019	61	0.067 (0.029)	0.021 (0.087)	0.0013 (0.0012)	0.057 (0.079)

Chapter 3

Depth Dependent Shifts in Sponge Microbial Communities and Trophic Strategies on Mesophotic Coral Reefs

Keir J. Macartney[1], M. Sabrina Pankey[1], Amelia Clayshute[2], Marc Slattery[2], Michael P. Lesser[1]

[1]University of New Hampshire, Department of Molecular, Cellular and Biomedical Sciences and School of Marine Science and Ocean Engineering, Durham, NH 03824 USA

kjm1049@wildcats.unh.edu

[2]University of Mississippi, Department of BioMolecular Science, Oxford, MS 38677 USA

Abstract

Sponges play crucial ecological roles in a wide variety of marine ecosystems, particularly with respect to benthic-pelagic coupling and biogeochemical cycling. In the Caribbean, sponge microbiomes can have a significant influence on coral reef carbon and nitrogen cycling and are responsible for a large quantity of the dissolved organic matter (DOM) consumed by sponges. As sponges increase abundance on Caribbean mesophotic coral reef ecosystems (MCEs), the microbiomes may have an effect on their trophic ecology or biogeochemical cycling between depths. Caribbean MCEs are characterized by gradients in photosynthetically active radiation (PAR), temperature and nutrients. As depth increases, particulate organic matter (POM) increases, while DOM decreases and this increase in bioavailable POM is most likely responsible for the increase in sponge abundances and growth rates on mesophotic coral reefs. However, decreases in the availability of PAR and DOM could change the microbiome community structure and function of these sponges between shallow reefs and MCEs. We characterized the microbiome community structure and function, stable isotopic composition and proximate biochemical composition of four Caribbean reef sponges (*Amphimedon compressa, Agelas tubulata, Plakortis angulospiculatus* and *Xestospongia muta*) between shallow to mesophotic depths on Grand Cayman MCEs. We found that there were species-specific changes in microbial community composition as depth increased and that Kyoto Encyclopedia of Genes and Genomes (KEGG) genes associated with nitrogen and carbon cycling also underwent species-specific changes between depths. Additionally, there were significant increases in the $\delta^{15}N$ of all the sponge species as depth increased, indicating that the sampled sponges consume more heterotrophic bacterioplankton on MCEs. We also observed phenotypic plasticity in sponge

trophic ecology and energetic state between shallow and mesophotic depths, likely as a result of the increased bioavaliable POM available on MCEs.

Introduction

Marine sponges are ubiquitous in marine ecosystems and play important roles in benthic-pelagic coupling, biogeochemical cycling and substrate consolidation in these habitats (Diaz & Rützler, 2001; Lesser 2006; Trussell 2006; Bell 2008; Maldonado et al. 2012; Slattery & Lesser 2015; de Goeij et al. 2017; Maldonado et al. 2017). In the Caribbean sponges are common members of coral reef ecosystems and their roles in nutrient cycling and habitat or food provision for a variety of important reef flora and fauna are well known (Diaz & Rützler 2001; Bell 2008; Fiore et al. 2010; de Goeij et al. 2013, 2017). Sponges, like many benthic marine fauna, form diverse and often species-specific associations with microbial communities and these communities can play important roles in nutrient cycling on coral reefs (Thacker & Freeman, 2012; Fiore et al., 2013 a, b, 2020; Morrow et al. 2016; Bourne et al. 2016; Pita et al. 2018). These host-specific communities have also been shown to have high spatial and temporal stability but can be influenced by abiotic or biotic factors at specific locations (Hardoim & Costa 2014; Morrow et al. 2016; Pita et al. 2018; Batista et al. 2018). Sponge associated microbes can comprise 35-50% of the total mass of a sponge (Webster and Thomas 2016, Hentschel et al 2006, Thomas et al. 2016) and have been documented to provide inorganic and organic resources to their host through photosynthesis, heterotrophy or chemosynthesis (Freeman & Thacker, 2011, 2012; Fiore et al., 2013a, Fiore et al. 2015; Rubin-Blum et al. 2019; Zhang et al. 2019; Rix et al. 2020). Interestingly, sponges appear to have evolved two different modes of symbiont association which are categorized based on the relative density of microbes within the mesohyl of the host sponge. High microbial abundance sponges (HMA) generally harbor 10^8 to 10^9 bacteria per gram of sponge tissue while low microbial abundance sponges (LMA) typically harbor 10^5 to 10^6 bacteria per gram of sponge tissue, similar to the

densities of microbes found in the surrounding seawater (Weisz et al. 2008; Hentschel et al. 2012, Gloeckner et al. 2014; Pita et al. 2018).

The different densities of microbes in these HMA and LMA sponges may be the result of their morphology and is reflected in their feeding strategies, and thus can affect the trophic ecology of sponges. One of the key differences between HMA and LMA sponges is the density of the mesohyl, which is greater in HMA sponges compared to LMA sponges (Weisz et al. 2008). Additionally, LMA have a higher proportion of the mesohyl (μm^2) dedicated to choanocyte chamber formations compared to LMA sponges. These chambers are responsible for pumping water through the sponge aquiferous system (Poppell et al. 2014). This results in a lower flow rate in HMA species relative to LMA species, and these differences are thought to drive a higher reliance on dissolved organic matter (DOM) in HMA sponges, whereas LMA sponges consume comparatively greater quantities of particulate organic matter (POM) (Weisz et al. 2007; Freeman & Thacker 2011, 2012; Mueller et al. 2014; de Goeij et al. 2017; Morganti et al. 2017). The higher densities of microbes, and lower pumping rates (=longer residence times of seawater) in HMA sponges result in the removal of greater concentrations of DOM in sponges where they get most of their carbon requirements (de Goeij et al. 2017). The HMA-LMA continuum in trophic resource utilization can also facilitate the maintenance of dense coral reef sponge communities (Morganti et al. 2017). The microbiomes of these sponges can also produce secondary metabolites that can be utilized for chemical defense of sponge tissue from predators or allelopathic interactions with other members of the benthic community (Assman et al. 2000, Pawlik et al. 2006, Pawlik 1997, 2011; Pita et al. 2018). Indeed, HMA sponges are generally observed to more chemically defended relative to LMA sponges (de Goeij et al. 2017). Due to the potentially significant effects that sponge associated microbes have on the chemical and trophic ecology of sponges, considering

both the structure and function of sponge microbiomes is crucial when assessing ecological factors that affect sponge distributions. This is particularly important in the case of sponge abundances between shallow coral reefs and the mesophotic zone of coral reefs, as there are clear differences in sponge distributions between shallow and mesophotic depths, with sponges increasing in density and percent cover with increasing depths (Lesser, 2006, Garcia-Sias 2010; Lesser and Slattery 2013, 2018, Lesser et al. 2011, 2018; Slattery et al. 2011, Slattery and Lesser 2012).

Mesophotic coral ecosystems are currently defined as reef systems occurring below 30 m and extending to ~150 m depth, and have received significant attention recently due to their potential role as refuges for threatened shallow reef species (Lesser et al. 2009, 2018; Loya et al. 2016; Bongaerts et al. 2010; but see Bongaerts et al. 2017). In the Caribbean MCEs are characterized by gradients in abiotic factors, such as decreasing photosynthetically active radiation (PAR) and temperature (Lesser 2006; Lesser et al. 2018). They also show repeatable patterns in trophic resource availability, such as increases in POM and a concurrent decrease in DOM as depth increases (Lesser 2006; Trussell et al. 2006; Lesser et al. 2019; Lesser et al. 2020; Chapter 2). While it has been argued that top-down processes can govern the increased abundances and diversity of sponges in the mesophotic (Pawlik et al. 2013; Pawlik et al. 2018; Scott and Pawlik 2019), the preponderance of evidence shows these ecological patterns are driven primarily by bottom-up forces, particularly the increased consumption of organic matter, both DOM and POM, (Chapter 1, 2; Lesser 2006; Trussell et al. 2006; Lesser & Slattery 2013, 2018; Slattery & Lesser 2015; Lesser & Slattery 2018; Lesser et al. 2018, 2019, 2020). While POM is critical for sponge growth through the provision of bioavailable nitrogen (Ducklow et al. 1993; Campbell et al. 1994; Lesser 2006), the DOM component of their diets has been found to be the major source of carbon for sponges (de Goeij et al. 2017). This component of their diet can comprise up to 95% of their

trophic carbon uptake (de Goeij et al. 2013, 2017; Mueller et al. 2014; McMurray et al. 2016, 2018; Wooster et al. 2019) and may be responsible for important sponge driven processes such as the "Sponge Loop Hypothesis" (de Goeij et al. 2013). While recent studies have shown that sponge cells (i.e., the choanocytes) can take up DOM, the majority of this resource is consumed by the microbiome of the sponge (Achlatis et al. 2019, Rix et al. 2020) and potentially translocated to the sponge host (Shih et al. 2020). However, the proportion of this resource that is transferred by the heterotrophic microbiome to the sponge host is still unknown (Achlatis et al. 2019, Rix et al. 2020). Given this, our understanding of how the microbial community changes along environmental gradients may provide insight into different trophic strategies between shallow and mesophotic conspecifics, particularly with respect to nitrogen and carbon cycling.

While the microbiome of sponges is often considered stable over large temporal or spatial scales, it appears that environmental gradients may change the community composition of the sponge microbiome, and the degree of this change can be site dependent (Morrow et al., 2016, Pita et al. 2018). Generally, evidence supports a species specific "core" microbiome in sponges that is stable throughout its distribution, but that changes in environmental conditions may affect the "variable" portion of the microbiome (Morrow et al. 2016; Pita et al. 2018). Given that there are gradients in both abiotic and biotic factors along a shallow to mesophotic depth gradient, it is likely that the variable portion of the microbiome of a sponge may change between depths. Studies in the Caribbean and the Pacific have shown that changes in depth can affect the community composition of the microbiome that is driven by both abiotic and biotic factors (Olson & Gao, 2013; Morrow et al. 2016; Steinert et al. 2016;). In the case of *Xestospongia muta*, Morrow et al. (2016) observed stability in the microbiome over a shallow to mesophotic depth gradient correlated with increased dissolved inorganic nitrogen (DIN) availability on MCE reefs at Lee Stocking

Island, Bahamas. Increased DIN availability at mesophotic depths supported the cyanobacterial symbionts present in *X. muta*'s microbiome despite reductions in PAR. Conversely, at a sampling site with reduced DIN at Little Cayman Island, symbiont community underwent reductions in abundance of cyanobacterial OTU's at mesophotic depths due to the decreased available PAR and decrease in DIN compared to populations in the Bahamas. Changes in abiotic and biotic factors along the MCE gradient obviously do have the potential to affect microbial community structure, and thus potentially affect the trophic ecology of the sponge through reductions or increases in both photoautotrophic and heterotrophic contributions from associated microbes.

Here we present a "natural experiment" on three HMA sponges (*Agelas tubulata, Plakortis angulospiculatus* and *Xestospongia muta*) and one LMA sponge (*Amphimedon compressa*), along a shallow to mesophotic depth gradient on Grand Cayman Island. Our goal is to assess if natural gradients in environmental factors such as PAR, temperature, POM, DOM, DIN and phosphate (PO_4) availability has an effect on the microbial community composition, predicted functional profile of the microbiome and/or trophic ecology of these sponges. These sponges represent a broad variety of morphologies, microbial associations and trophic strategies, such as symbiosis with known photoautotrophic symbionts (*X. muta*) (Morrow et al. 2016) or sponges that have low relative abundances of photoautotrophic symbionts (*A. tubulata*) (Gannt et al. 2019) and another sponge species that likely relies more heavily on POM relative to DOM (*A. compressa*) due to its LMA status (Weisz et al. 2007; Gloeckner et al. 2014; Morganti et al 2017). Additionally, there is known variability in the chemical defenses of *P. angulospiculatus* between shallow and mesophotic depths (Slattery et al. 2016). We hypothesize that photoautotrophic symbionts will decrease in relative abundance as depth increases into the mesophotic, and that increases in sponge and microbiome heterotrophy (i.e., increased POM consumption and decreased photoautotrophy)

will be reflected in their stable isotopic signatures and predicted microbiome functional profiles. We also hypothesize that the increase in POM as depth increases at this site will cause an increase in bioenergetic reserves for mesophotic sponges.

Methods

Study site

All sampling was done at the Kittiwake Anchor Buoy site, Grand Cayman (Lat: 19.362756, Long: -81.402437). This site exhibits a spur and grove structure with a sloping reef structure between 15 – 60 m, at which point the reef topography turns into a vertical wall. As depth increases into the mesophotic zone at this site, concentrations of POC and PON (μmol l^{-1}) increase significantly (Chapter 2, Fig. 10) while DOC and DON (μmol l^{-1}) decreases significantly (Chapter 2, Fig. 10). Dissolved inorganic nitrogen (DIN) as NO_x (i.e., NO_3^- + NO_2^-) increased significantly with depth at this site but ammonium (NH_4), phosphate (PO_4) and silica dioxide (SiO_2) do not vary significantly with increasing depth (Chapter 2, Fig. 11). Photosynthetically active radiation also shows a significant decrease as depth increases into the mesophotic zone (Chapter 2, Fig. 7).

Sample collection

Sponge tissue samples of *Agelas tubulata, Amphimedon compressa, Plakortis angulospiculatus* and *Xestospongia muta* were collected along a depth gradient at 15, 22, 30, 46, 61, 76 and 91 m, where sponges were found at these depths (*n* = 3-8 sponges per depth). Larger sponges such as *A. tubulata, P. angulospiculatus* and *X. muta* were sampled by cutting a "pie-slice" of sponge tissue from the apical lip of the osculum including both pinacoderm and mesohyl as described in Morrow et al. (2016) and placed in labeled bags filled with seawater. Whole "branches" were collected for

A. compressa and placed in labeled bags filled with seawater, with care taken to leave some sponge tissue at the base for regrowth after sampling. All sponges were kept in a shaded cooler and submerged in seawater until returned to shore for processing of samples for 16s rRNA metabarcoding, biochemical and stable isotope analysis. For metabarcoding, a small subsample was taken using a sterile razor and stored in DNAlater for subsequent analysis. Subsamples of tissue were also collected for stable isotope analyses and were immediately frozen at -20℃ and transported frozen to the University of New Hampshire, where they were frozen at -80℃ until analysis. The remaining sponge tissue was frozen at -20℃ and transported frozen to the University of Mississippi, where they were frozen at -80℃ until proximate biochemical analyses were conducted. Seawater samples were also taken at the surface and at 22, 30, 46, 61, 76 and 91 m (n = 3 per depth). Acid-washed 180 ml syringes were used to take samples approximately 1 m from the benthos at each depth, taking care to avoid any benthic organisms or sediment. Water samples were then filtered through a 0.2 μm baked GF/F filter and the filter stored in DNAlater. Seawater DNA samples were immediately frozen at -20℃ and transported frozen to the University of New Hampshire, where they were frozen at -80℃ until analysis.

DNA Isolation and 16s rRNA amplicon sequencing

To obtain microbial genomic DNA, approximately 200-300 mg of sponge tissue was taken from a subsample stored in DNAlater, with care taken to dab away any of the preservative using a sterile Kim-wipe. Tissue was then cut into small pieces using a sterile razor for further anaylsis. Sponge DNA was isolated using a Qiagen DNeasy PowerSoil extraction kit with the manufacture's protocol modified as follows. Sponge tissue was added to the PowerSoil bead tubes with 5 μl of

Proteinase K (20 mg ml^{-1} stock in 10% SDS) and 2 µl of RNAse (Qiagen) before incubation at 55◦C for 18 hours. After incubation, PowerSoil Kit Solution 1 was added, and samples subsequently underwent a bead beating step using a Qiagen Tissue Lyser for 5 min at 50 hertz. The Qiagen DNeasy PowerSoil kit standard instructions were followed post bead beating to produce DNA samples.

Microbial DNA was amplified using the polymerase chain reaction (PCR) with primer sets targeting the universal prokaryotic 16S rRNA gene. Degenerate primers designed to amplify the hypervariable region V3-V4 of the 16S rRNA gene were used and included a forward primer 515F (5'- GTGYCAGCMGCCGCGGTAA; Parada et al. (2016)) and reverse primer 806R (5'- GGACTACN- VGGGTWTCTAAT; Apprill et al. (2015)). Fluidigm linker sequences CS1 (5'- ACACTGACGACATGGTTC- TACA) and CS2 (5'- TACGGTAGCAGAGACTTGGTCT) were added to the 5' end of both forward and reverse primers to facilitate Illumina MiSeq. The 16S rRNA gene PCR consisted of a 25 µl reaction with 12.5 µl AmpliTaq Gold 360 Master Mix (Applied Biosystems), 1.0 µl GC-enhancer, 0.5 µl 515F (10 µM) and 0.5 µl 806R (10 µM), 2.0 µl of DNA template (40-60 ng) and 8.5 µl nuclease free water (Integrated DNA Technologies, Coralville, Iowa). Reactions were performed using the following protocol: initial denaturation for 10 min at 95◦C, 30 cycles of 95◦C for 45 s, 50◦C for 60 s, and 72◦C for 90 s, followed by a 10 min extension at 72°C. The PCR products were then electrophoresed on a 1% agarose gel. The 16S rRNA PCR amplicons containing Fluidigm linkers were sequenced on an Illumina MiniSeq System employing V2 chemistry (2 x 150 bp reads) at the University of Illinois at Chicago (UIC) Research Resources Center's Sequencing Core. The amplicon sequence variants (ASVs) were inferred and tabulated across sponge samples using "DADA2" (Callahan et al, 2016) using an established bioinformatic pipeline (Lesser et al. 2020).

Analyses of the microbial communities of the sponges were completed utilizing the R package "PhyloSeq" (McMurdie et al. 2016) in R *sensu* (Lesser et al. 2020). Samples with fewer than 10,000 counts were filtered from the ASV count table. Additionally, ASVs detected in more than 2 samples and had at least 10 occurrences across samples were retained during the filtering process. The samples were then rarefied in order to account for sampling effort. To test alpha diversities, the Shannon richness index was used. Ordination plots were produced based on Bray-Curtis distances using nonmetric multidimensional scaling (NMDS) (Stress value = <0.0001). To assess compositional differences at varying taxonomic scales, the rarefied ASV count table was consolidated by rank using the PhyloSeq "tax_glom" function and then raw counts were transformed to center log rations using the "transform" function (CLR) from the R package "microbiome" (Callahan et al. 2016). Phylum and class compositional differences between depths were tested using PERMANOVA with the Adonis function from the R package "vegan". Any differences observed during post hoc testing at class level for taxa between depths were tested using ANOVA and Tukey's HSD on dominant taxa (>1% reads).

Metagenomic functional abundances were predicted using "PICRUSt2" v2.1.0–b (https://github.com/picrust/picrust2/wiki)(Langille et al. 2013; Langille 2018). The 16S rRNA ASVs inferred by DADA2 were aligned with "HMMER" (Eddy 2008)and then placed in a reference tree provided by PICRUSt2 using "EPA–ng" and "GAPPA" (Barbera et al. 2019). Gene family numbers were predicted for 16S rRNA as well as KEGG functions (*i.e.*, EC and KO accessions) using Hidden State Prediction ("castor*"*) based on 16S rRNA ASV abundances and phylogenetic proximity to reference taxa with available genomes. In order to minimize error in gene content prediction due to poor matches to available genomes, any ASVs receiving Nearest-Sequenced-Taxon-Index (NSTI) scores below two were removed from subsequent analyses.

Abundances of biological pathways encoded by microbiomes were then predicted using *MinPath* (Ye and Doak 2009). Abundances of KEGG genes of interest (Table 9) were assessed for the effect of depth with linear regression on relative abundances normalized to the total reads in the sample. KEGG genes of interest were selected to assess carbon and nitrogen metabolism.

Table 9. Selected KEGG orthology genes from the predictive functional analysis of the sampled sponge microbiomes.

KEGG	Function Type	Process	Specific Function
K01602	Carbon metabolism	Calvin Cycle	Ribulose-bisphosphate carboxylase small chain
K01601	Carbon metabolism	Calvin Cycle	Ribulose-bisphosphate carboxylase large chain
K01681	Carbon metabolism	Citrate Cycle	Aconitate hydratase (acnA)
K00134	Carbon metabolism	Glycolysis	Glyceraldehyde 3-phosphate dehydrogenase (gapA)
K01638	Carbon metabolism	Glyoxylate cycle	Malate synthase (carbohydrate metabolism)
K01965	Carbon metabolism	Propionyl CoA cylce	Propionyl-CoA carboxylase alpha chain
K02707	Carbon metabolism	Photosynthesis	Photosystem II cytochrome b559 subunit alpha (psbE)
K02705	Carbon metabolism	Photosynthesis	Photosystem II CP43 chlorophyll apoprotein
K01428	Nitrogen metabolism	Ammonification	Urease subunit alpha (ureC)
K00370	Nitrogen metabolism	Denitrification	Nitrate reductase / nitrite oxidoreductase, alpha subunit (narG, NarZ)
K00376	Nitrogen metabolism	Denitrification	Nitrous-oxide reductase (nosZ)
K02588	Nitrogen metabolism	N fixation	Nitrogenase iron protein NifH (nifH)
K02586	Nitrogen metabolism	N fixation	Nitrogenase molybdenum-iron protein alpha chain (nifD)
K02584	Nitrogen metabolism	N fixation	Nif-specific regulatory protein (nifA)
K10944	Nitrogen metabolism	Nitrification	Methane/ammonia monooxygenase subunit A (amoA)
K03385	Nitrogen metabolism	N reduction	Nitrite reductase (cytochrome c-552) (nrfA)
K04561	Nitrogen metabolism	N reduction	Nitric oxide reductase subunit B (norB)
K00366	Nitrogen metabolism	N reduction	Ferredoxin-nitrite reductase (nirA)
K00368	Nitrogen metabolism	N reduction	Nitrite reductase (NO-forming) (nirK)
K01507	Phosphorus metabolism	Phosphate production and lipid degradation	Inorganic pyrophosphatase (ppA)

Stable isotope analyses

Subsamples of sponge tissue were collected using a sterile razor. Tissue samples were then dried at 55°C for 24 h before pulverizing into a powder using a mortar and pestle. Samples of tissue were sent to the Marine Biological Laboratory (Woods Hole, MA) for the bulk analysis of particulate C and N as well as the natural abundance of the stable isotopes $\delta^{15}N$ and $\delta^{13}C$. Prior to analysis samples were acidified using 1N HCL. We did not observe any significant differences in $\delta^{15}N$ due to acidification, using paired samples of acidified and acidified tissues (*sensu* Chapter 2, 4) Samples were analyzed using a Europa ANCA-SL elemental analyzer-gas chromatograph attached to a continuous-flow Europa 20-20 gas source stable isotope ratio mass spectrometer. The carbon isotope results are reported relative to Vienna Pee Dee Belemnite and nitrogen isotope results are reported relative to atmospheric air and both are expressed using the delta (δ) notation in units per mil (‰). The analytical precision of the instrument is ± 0.1‰, and the mean precision of sample replicates for $\delta^{13}C$ was ± 0.4 ‰ and $\delta^{15}N$ was ± 0.2 ‰.

Proximate Biochemical Composition

When samples arrived at the University of Mississippi, sample wet mass and volume were recorded. Samples were then freeze dried, pulverized, and dry sample mass recorded. Carbohydrates were extracted via incubation of 10 mg freeze dried tissue in 5 mL 5% trichlororacetic acid (TCA) for 4 h. Concentration of carbohydrates was determined using the phenol-sulfuric acid method in microplate format described in Masuko et al. (2005). Briefly, 50 µl of TCA digested sample solution or glucose standard, 150 µl of sulfuric acid, and 30 µl of 5%

phenol was pipetted in triplicate on a 96 well plate and incubated for 10-15 min at 90°C. Absorbance at 490 nm was then measured using a microplate reader. A standard curve was derived from glucose standards and used to calculate the concentration of carbohydrates in samples. Protein was extracted via incubation of 10 mg of freeze-dried tissue in 5 ml of 1 M sodium hydroxide (NaOH) for 24 h. Soluble protein concentration was then analyzed using the Bradford Method (Bradford, 1976). 40 ul of NaOH digested sample or BioRad Bovine Serum Albumin (BSA) standard was mixed with 2 ml of BioRad Quick StartTM Bradford reagent. Absorbance at 600 nm was measured using a spectrophotometer. A standard curve was derived from BSA standards and used to calculate the concentration of protein in samples. Lipids were extracted using a modified version of the gravimetric protocol described by Freeman et al. (1957). A 50 mg sample of freeze-dried tissue was sonicated for 15 min in a 2:1 chloroform to methanol solution and then filtered into a 50 ml conical tube containing ~20 mL of distilled water. The bottom organic layer was then pipetted into a pre-weighed scintillation vial. This process was repeated twice per sample. The methanol-chloroform solution was then evaporated off over a period of 12 h via vacuum centrifugation and the extracted lipids weighed. Inorganic tissue constituents (i.e., ash) were measured using methods described by McClintock et al., 1992. A 100 mg sample of freeze-dried sponge tissue was placed in a pre-weighed aluminum foil weigh-boat that was baked at 500°C in a muffle furnace for 5 h. All concentrations of proximate biochemical composition were normalized to ash-free dry weight (AFDW).

Statistical analyses

All statistical analyses were completed in either JMP (v. 14) or R (v. 3.6.2). The effects of depth and species on microbial community were assessed with PERMANOVA and ANOVA as

described above. The effects of depth and species on stable isotope ratios and proximate biochemical composition were assessed using linear regression with depth treated as a continuous variable. Any variables not meeting the assumptions of normality were log transformed before analysis.

RESULTS

16s rRNA metabarcoding

A total of 5,908,265 16S rRNA MiniSeq read-pairs were initially recovered from sequencing of the four sponge species, seawater and sediment pore water. After merging and quality trimming with DADA2, 5,572,585 read-pairs remained. These ranged from 67,833 to 11,001 with a mean of 31,483 ± 7,860 reads per sample. A total of 8,507 unique ASVs were initially recovered, but ASVs unique to two or less samples or with fewer than 10 total observations were removed from the dataset, resulting in a total of 3,709 unique ASVs for downstream analyses.

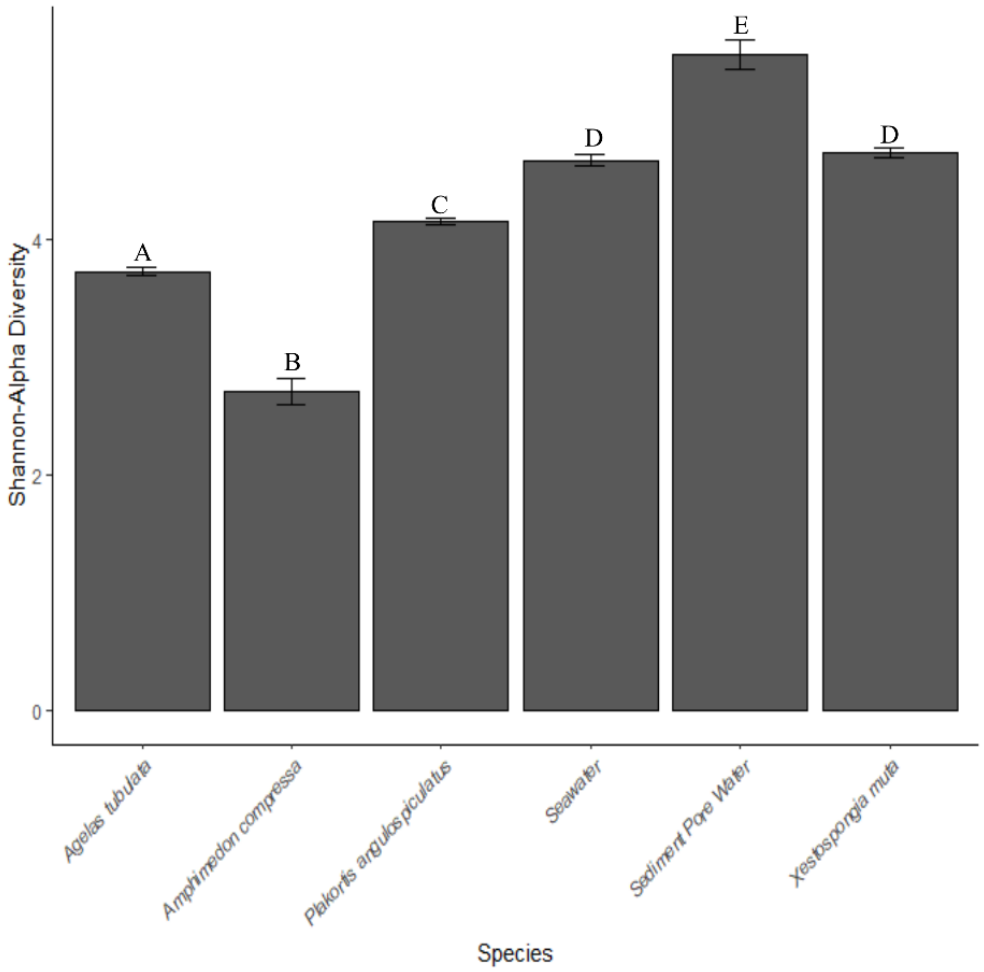

Figure 18. Mean (± SE) alpha diversity quantified using the Shannon diversity index for *Amphimedon compressa, Agelas tubulata, Plakortis angulospiculatus, Xestospongia muta*, sediment pore water and seawater samples from shallow to mesophotic depths. Species or sample with common superscripts are not significantly different from each other (Tukey's HSD, $P<0.05$)

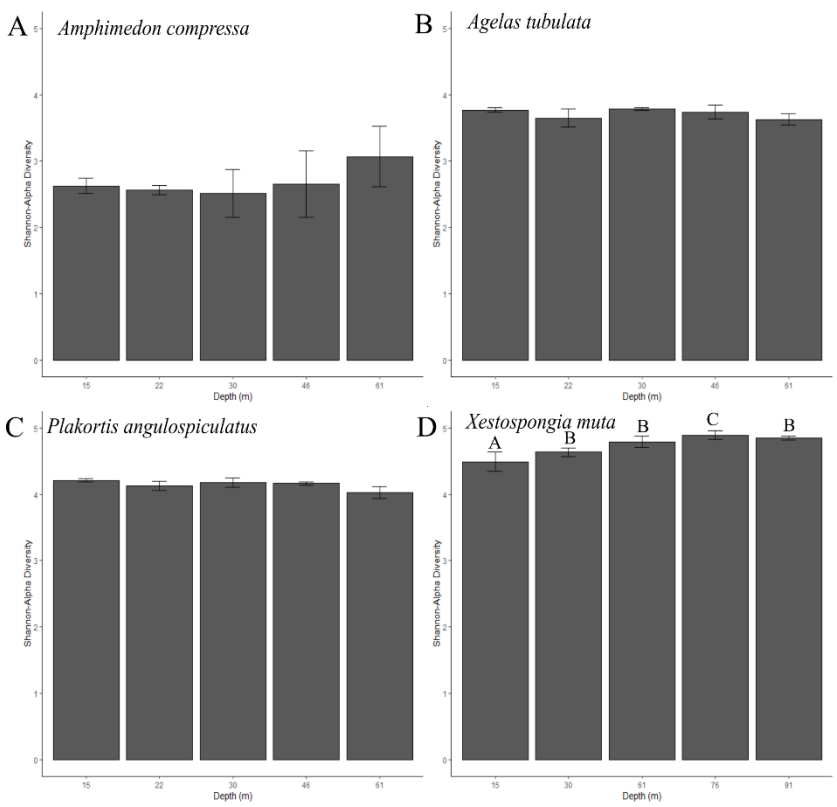

Figure 19. A) Mean (± SE) Shannon-alpha diversity index for *Amphimedon compressa* between depths. **B)** Mean (± SE) Shannon-alpha diversity index for *Agelas tubulata* between depths. **C)** Mean (± SE) Shannon-alpha diversity index for *Plakortis angulospiculatus* between depths. **D)** Mean (± SE) Shannon-alpha diversity index for *Xestospongia muta* between depths. Depths with common superscripts are not significantly different from each other (Tukey's HSD, $P<0.05$)

There were significant differences in mean Shannon-Alpha diversity between different sponge species, seawater and sediment pore water (ANOVA: $F_{5,125} = 192.63$, $P < 0.0001$) (Fig. 18) with all species and water types significantly different from each other, with the exception of *X. muta* and the filtered seawater samples (Tukey's HSD <0.05) (Fig. 18a). Between the sponge species, *X. muta* had the highest mean Shannon-Alpha diversity (4.73 ± 0.07 SE), followed by *P. angulospiculatus* (4.15 ± 0.05 SE) and *A. tubulata* (3.17 ± 0.04 SE), while *A. compressa* displayed the lowest mean Shannon-Alpha diversity (2.66 ± 0.06 SE). There was no significant effect of depth on Shannon-Alpha diversity for *A. compressa* (ANOVA: $F_{4,22} = 0.52$, $P = 0.71$) (Fig. 19a)

For *A. tubulata*, there was no significant effect of depth on mean Shannon-Alpha diversity (ANOVA: $F_{5,30} = 0.71$, P = 0.623) (Fig. 19b). There was no significant effect of depth on Shannon-Alpha diversity for *P. angulospiculatus* (ANOVA: $F_{4,22} = 1.77$, P = 0.17) (Fig. 19c). For *X. muta*, there was a significant effect of depth on mean Shannon-Alpha diversity (ANOVA: $F_{4,25} = 3.81$, P = 0.017), with the highest mean Shannon-Alpha diversity at 76 m and the lowest at 15 m, with all other depths as intermediates (Tukey's HSD <0.05) (Fig. 19d).

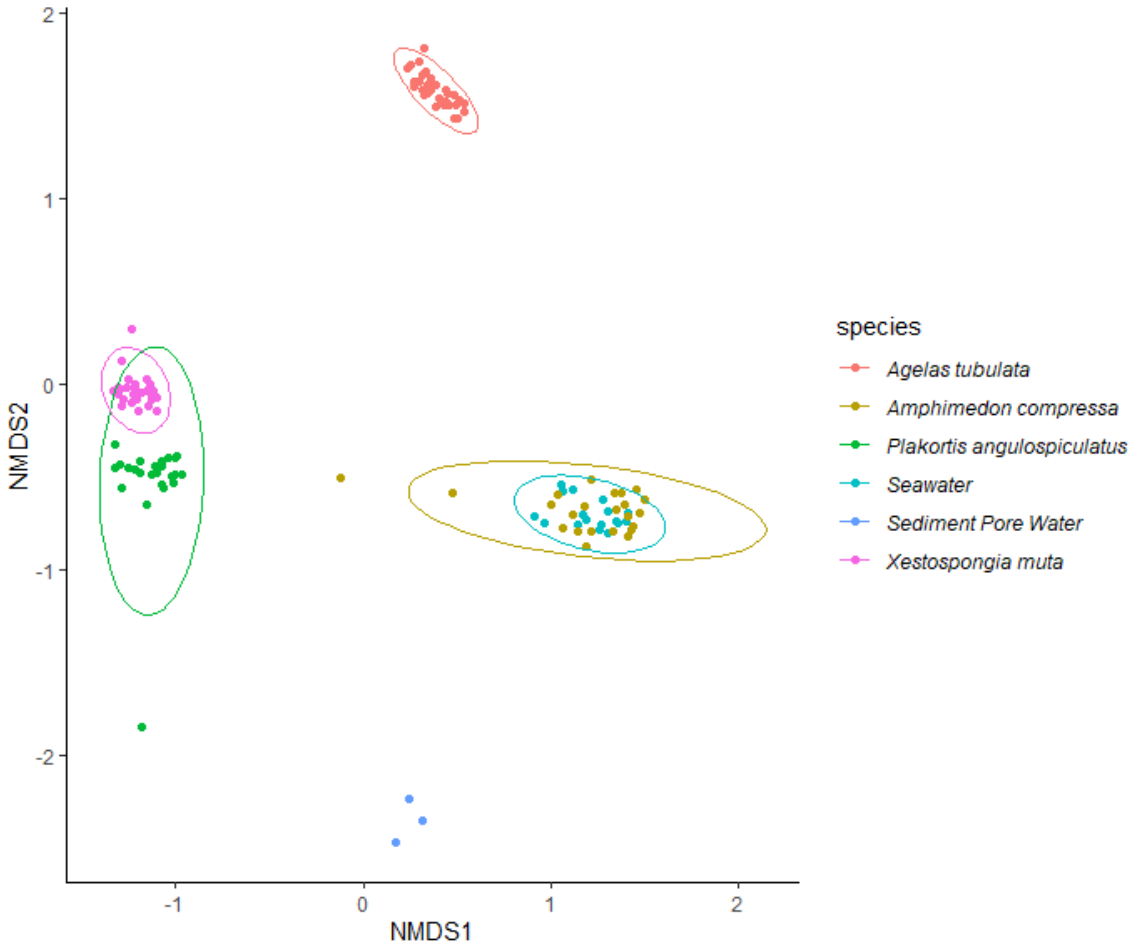

Figure 20. Multidimensional analysis of the β-diversity estimates using Bray–Curtis distance matrices of ASV composition for *Amphimedon compressa, Agelas tubulata, Plakortis angulospiculatus, Xestospongia muta*, sediment pore water and seawater microbial community composition. The 95% confidence interval (CI) ellipses are drawn to show the species or sample type groupings.

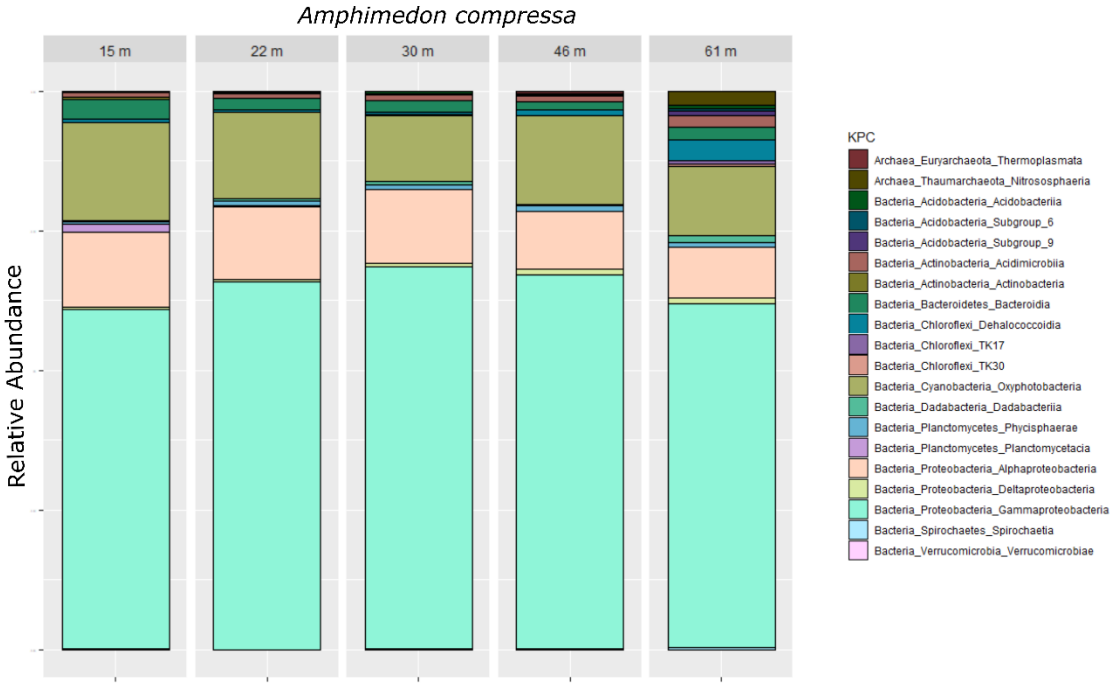

Figure 21. Mean relative abundance (percentage) from the dominant Classes (comprising > 1% of reads) in the *Amphimedon compressa* microbiome along a shallow to mesophotic depth gradient.

The non-metric multidimensional scaling analysis of the Beta diversity using Bray-Curtis distance matrixes showed significant differences in microbial community ASV composition between sponge species or sample type (PERMANOVA: $F_{5,125}$ = 44.68, P = 0.001) (Fig. 20). Seawater samples showed an effect of depth on microbial community composition at Class level (PERMANOVA: $F_{5,125}$ = 44.68, P = 0.001) but not at the phylum level (Fig. S1). There were significant reductions in the classes *Oxyphotobacteria, Bacteriodia, Gammaproteobacteria* and *Alphaproteobacteria* with depth (Tukey's HSD <0.05), while there were significant increases in the *Dehalococcidia*, *Deltaproteobacteria* and *Acidimicrobiia* with depth (Tukey's HSD <0.05) (Fig. S1). In the LMA sponge, *A. compressa*, both phylumphylum composition (PERMANOVA: $F_{4,22}$ = 1.93, P = 0.048) and class level composition (PERMANOVA: $F_{4,22}$ = 1.90, P = 0.009) of the microbiome were significantly different between depths (Fig. 21). This was driven by increases of the class *Nitrososphaeria* within the phylum *Thaumarchaeota* as depth increased and decreases

in the class *Planctomycetacia* (phylum *Plantomyctes*) as depth increased (Tukey's HSD <0.05). No significant differences were observed between depths in phylumphylum composition (PERMANOVA: $F_{4,30} = 0.96$, P = 0.511) or class level composition (PERMANOVA: $F_{4,30} = 1.08$, P = 0.31) in the microbiome of *A. tubulata* (Fig. 22).

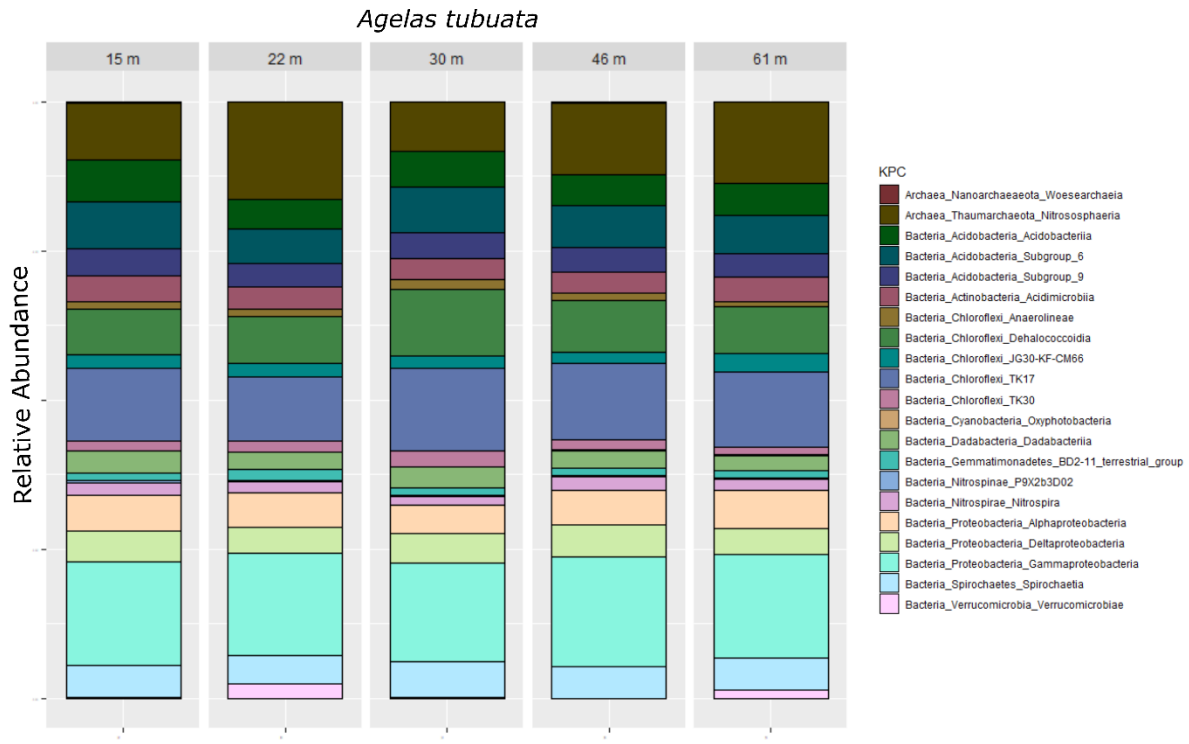

Figure 22. Mean relative abundance (percentage) from the dominant Classes (comprising > 1% of reads) in the *Agelas tubulata* microbiome along a shallow to mesophotic depth gradient.

In the microbiome of *P. angulospiculatus*, there was no significant differences between depths in phylum composition (PERMANOVA: $F_{4,25} = 1.93$, P = 0.234) but there was a significant effect of depth on class level composition (PERMANOVA: $F_{4,25} = 1.56$, P = 0.006) (Fig. 23). Post-hoc testing showed that the class *Nitrososphaeria* within the phylum *Thaumarchaeota* increased as depth increased to 61 m (Tukey's HSD <0.05). There were significant decreases in the classes *Entotheonellia* (phylum *Entotheonellaeota*) and *Acidobacteriia* (phylum *Acidobacteria*) at 46 m

relative to all other depths, while the class *Alphaproteobacteria* (phylum *Proteobacteria*) increased at 46 m relative to all other depths (Tukey's HSD <0.05). The class *Spirochaetia* (phylum *Spirochaetes*) showed a significant increase between 30 m and 46 m, but all other depths showed no significant differences (Tukey's HSD <0.05). The class "P9X2b3D02" of the phylum *Nitrospinae* significantly decreased at 61 m compared to 15 m and 46 m, and it was found in its highest abundance at 46 m (Tukey's HSD <0.05) (Fig. 23).

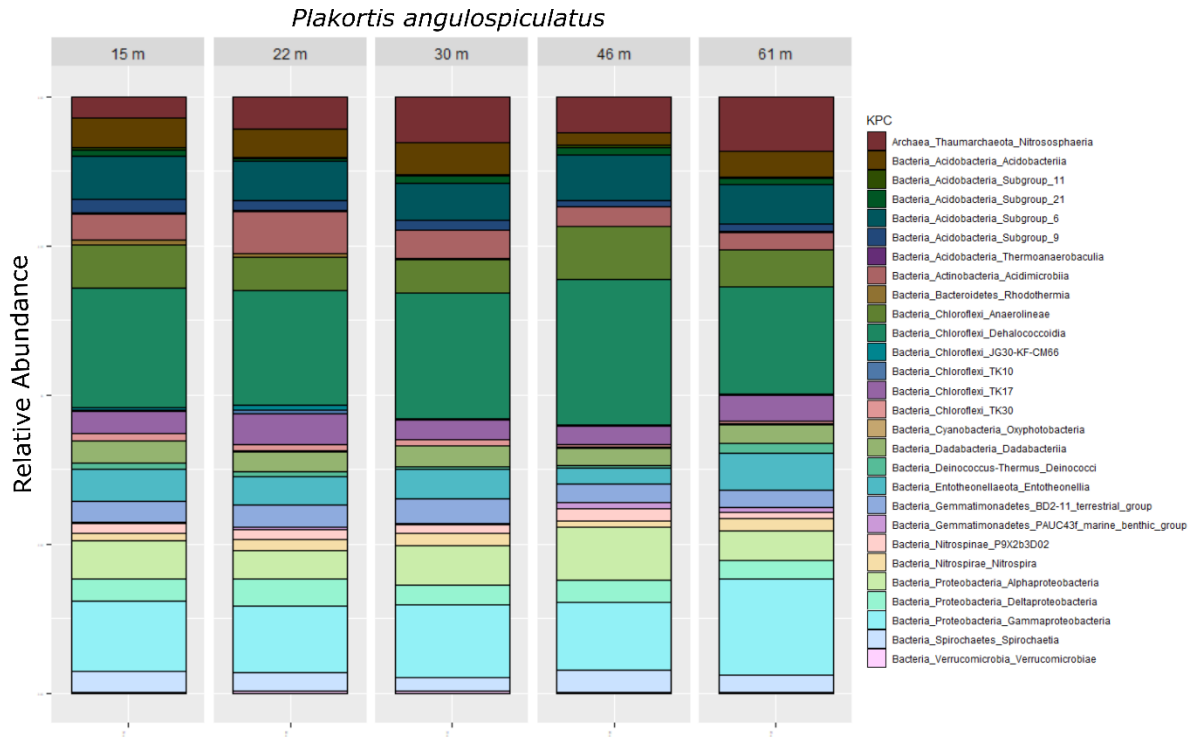

Figure 23. Mean relative abundance (percentage) from the dominant Classes (comprising > 1% of reads) in the *Plakortis angulospiculatus* microbiome along a shallow to mesophotic depth gradient.

For *X. muta*, both phylum composition (PERMANOVA: $F_{4,25} = 2.98$, P = 0.001) and class level composition (PERMANOVA: $F_{4,25} = 2.22$, P = 0.001) of the microbiome were significantly different between depths (Fig. 24). Post-hoc testing showed that the classes "TK17" and *Anaerolineae* of the phylum *Chloroflexi*, the class *Thermoanaerobaculia* of the phylum

Acidiobacteria and the *Alphaproteobacteria* of the phylum *Proteobactieria* showed significant decreases in abundance with increasing depth to 91 m (Tukey's HSD <0.05). The classes *Nitrospira* (phylum Nitrospirae), *Deinococci* (phylum *Deinoccocus*), *Entotheonellia* (phylum *Entotheonellaeota*) and *Spirochaetia* (phylum *Spirochaetes*) showed significant increases in abundance as depth increased (Tukey's HSD <0.05). The class *Rhodothermia* (Phylum *Bacteriodites*) were showed significant increases in abundance after after 30 m (Tukey's HSD <0.05). The class "Sub Group 6" of the *Acidobacteria* was significantly higher at 91 m compared to all other depths (Tukey's HSD <0.05) (Fig. 24).

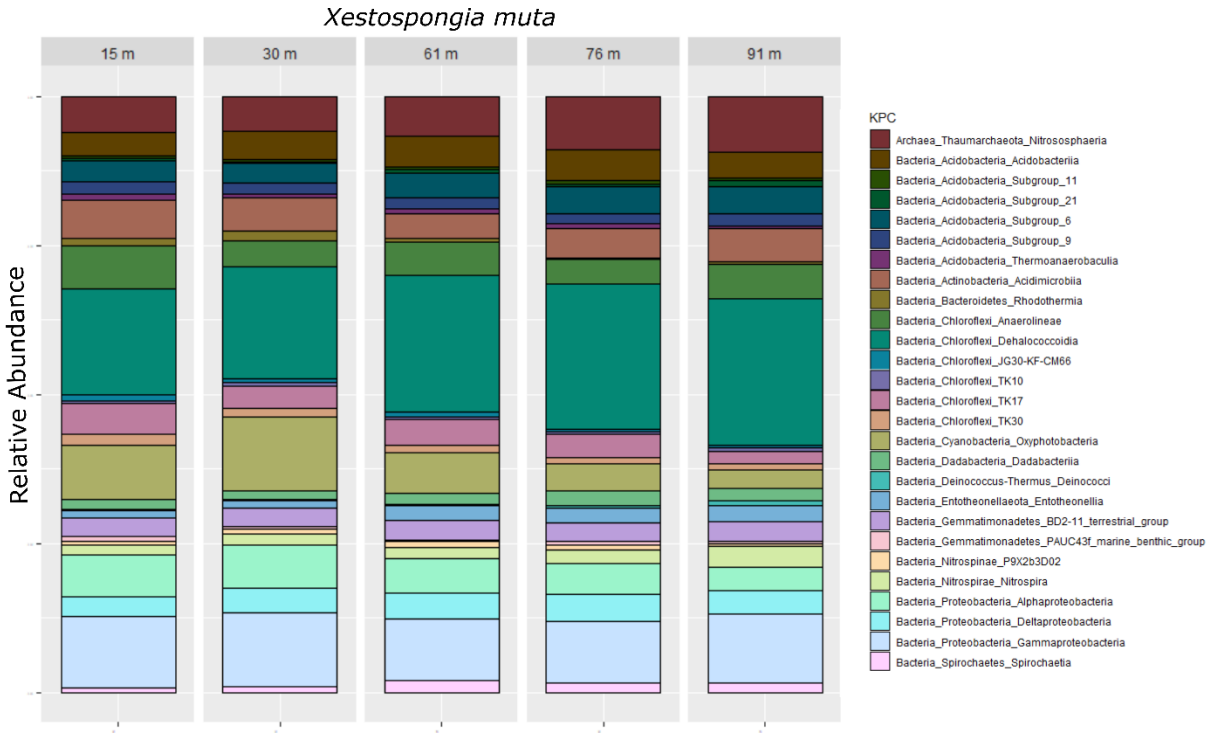

Figure 24. Mean relative abundance (percentage) from the dominant Classes (comprising > 1% of reads) in the *Xestospongia muta* microbiome along a shallow to mesophotic depth gradient.

Functional profiling of selected KEGG orthologs

The mean NSTI score for the sampled sponges was 0.41 (± 0.09 SE) and ranged from 0.03 to 0.53. In samples from *Amphimedon compressa*, KEGG genes for Aconitate hydratase (K01681), Propionyl-CoA carboxylase alpha chain (K01965), Nitrous-oxide reductase (K00376), Methane/ammonia monooxygenase subunit A (K10944), Nitric oxide reductase subunit B (K04561), Nif-specific regulatory protein (nifA) (K02584) and Nitrite reductase (K00368) showed a significant decrease in relative abundance with increasing depth (linear regression $P < 0.05$, summarized in Table 9). KEGG genes for Ribulose-bisphosphate carboxylase small chain (K01602), Ribulose-bisphosphate carboxylase large chain (K01601) and Inorganic pyrophosphatase (K01507) showed a significant increase in relative abundance with increasing depth (linear regression $P < 0.05$, summarized in Table 9).

In samples from *Agelas tubulata*, KEGG genes for Aconitate hydratase (K01681), Glyceraldehyde 3-phosphate dehydrogenase (K00134), Nitrate reductase / nitrite oxidoreductase (K00370), Nitrous-oxide reductase (K00376), Methane/ammonia monooxygenase (K10944), Nitric oxide reductase (K04561), Nif-specific regulatory protein (nifA) (K02584) and Nitrite reductase (K00368) showed a significant decrease in relative abundance with increasing depth (linear regression $P < 0.05$, summarized in Table 10). KEGG genes for Ribulose-bisphosphate carboxylase large chain (K01601), Photosystem II cytochrome b559 subunit alpha (K02707), Photosystem II CP43 chlorophyll apoprotein (K02705), Inorganic pyrophosphatase (K01507), Nitrite reductase (K0385) showed a significant increase in relative abundance with increasing depth (linear regression $P < 0.05$, summarized in Table 10).

In samples from *Plakortis angulospiculatus*, KEGG genes for Glyceraldehyde 3-phosphate dehydrogenase (K00134), Malate synthase (K01638), Propionyl-CoA carboxylase alpha chain

(K01965), Photosystem II cytochrome b559 subunit alpha (K02707), Photosystem II CP43 chlorophyll apoprotein (K02705), Urease subunit alpha (K01428), Inorganic pyrophosphatase (K01507), Nitrogenase iron protein NifH (K02588), Nitrogenase molybdenum-iron protein alpha chain (K02586), Nitrite reductase (K03385) and Ferredoxin-nitrite reductase (K00366) showed a significant decrease in relative abundance as with increasing depth (linear regression $P < 0.05$, summarized in Table 11). KEGG genes for Aconitate hydratase (K01681), Nitrite reductase (K00368), Nif-specific regulatory protein (nifA) (K02584) and Methane/ammonia monooxygenase subunit A (K10944) showed a significant increase in relative abundance with increasing depth (linear regression $P < 0.05$, summarized in Table 11).

In samples from *Xestospongia muta*, KEGG genes for Ribulose-bisphosphate carboxylase small chain (K01602), Ribulose-bisphosphate carboxylase large chain (K01601), Photosystem II cytochrome b559 subunit alpha (K02707), Photosystem II CP43 chlorophyll apoprotein (K02505) and Nitrite reductase (K03385) showed a significant decrease in relative abundance as with increasing depth (linear regression $P < 0.05$, summarized in Table 12). The KEGG genes for Aconitate hydratase (K01681), Nif-specific regulatory protein (nifA) (K02584) and nitrate reductase / nitrite oxidoreductase (K0370) showed a significant increase in relative abundance with increasing depth (linear regression $P < 0.05$, summarized in Table 12).

Table 10. Selected KEGG orthology genes from the predictive functional analysis of the *Amphimedon compressa* microbiome and the effect of increasing depth on the relative abundance of the KEGG genes.

KEGG	Function Type	Process	Specific Function	Depth Regression (*t*:23)	Effect of Increasing Depth
K01602	Carbon metabolism	Calvin Cycle	Ribulose-bisphosphate carboxylase small chain	$P < 0.001$, $R^2 = 0.410$	Increase

K01601	Carbon metabolism	Calvin Cycle	Ribulose-bisphosphate carboxylase large chain	$P < 0.001$, $R^2 = 0.398$	Increase
K01681	Carbon metabolism	Citrate Cycle	Aconitate hydratase (acnA)	$P = 0.003$, $R^2 = 0.337$	Decrease
K00134	Carbon metabolism	Glycolysis	Glyceraldehyde 3-phosphate dehydrogenase (gapA)	$P = 0.121$, $R^2 = 0.111$	N/A
K01638	Carbon metabolism	Glyoxylate cycle	Malate synthase (carbohydrate metabolism)	$P = 0.839$, $R^2 = 0.002$	N/A
K01965	Carbon metabolism	Propionyl CoA cylce	Propionyl-CoA carboxylase alpha chain	$P = 0.006$, $R^2 = 0.304$	Decrease
K02707	Carbon metabolism	Photosynthesis	Photosystem II cytochrome b559 subunit alpha (psbE)	$P = 0.085$, $R^2 = 0.134$	N/A
K02705	Carbon metabolism	Photosynthesis	Photosystem II CP43 chlorophyll apoprotein	$P = 0.085$, $R^2 = 0.135$	N/A
K01428	Nitrogen metabolism	Ammonification	Urease subunit alpha (ureC)	$P = 0.569$, $R^2 = 0.015$	N/A
K00370	Nitrogen metabolism	Denitrification	Nitrate reductase / nitrite oxidoreductase, alpha subunit (narG, NarZ)	$P = 0.056$ $R^2 = 0.163$	N/A
K00376	Nitrogen metabolism	Denitrification	Nitrous-oxide reductase (nosZ)	$P = 0.001$, $R^2 = 0.386$	Decrease
K02588	Nitrogen metabolism	N fixation	Nitrogenase iron protein NifH (nifH)	$P = 0.633$, $R^2 = 0.011$	N/A
K02586	Nitrogen metabolism	N fixation	Nitrogenase molybdenum-iron protein alpha chain (nifD)	$P = 0.995$, $R^2 = 0$	N/A
K02584	Nitrogen metabolism	N fixation	Nif-specific regulatory protein (nifA)	$P = 0.009$, $R^2 = 0.28$	Decrease
K10944	Nitrogen metabolism	Nitrification	Methane/ammonia monooxygenase subunit A (amoA)	$P < 0.001$, $R^2 = 0.412$	Decrease

K03385	Nitrogen metabolism	N reduction	Nitrite reductase (cytochrome c-552) (nrfA)	P = 0.756, R^2 = 0.005	N/A
K04561	Nitrogen metabolism	N reduction	Nitric oxide reductase subunit B (norB)	P = 0.024, R^2 = 0.219	Decrease
K00366	Nitrogen metabolism	N reduction	Ferredoxin-nitrite reductase (nirA)	P = 0.967, R^2 = 0	N/A
K00368	Nitrogen metabolism	N reduction	Nitrite reductase (NO-forming) (nirK)	P < 0.001, R^2 = 0.425	Decrease
K01507	Phosphorus metabolism	Phosphate degradation	Inorganic pyrophosphatase (ppA)	P < 0.001, R^2 = 0.606	Decrease

Table 11. Selected KEGG orthology genes from the predictive functional analysis of the *Agelas tubulata* microbiome and the effect of increasing depth on the relative abundance of the KEGG genes.

KEGG	Function Type	Process	Specific Function	Depth Regression (*t*:29)	Effect of Increasing Depth
K01602	Carbon metabolism	Calvin Cycle	Ribulose-bisphosphate carboxylase small chain	P < 0.001, R^2 = 0.409	Increase
K01601	Carbon metabolism	Calvin Cycle	Ribulose-bisphosphate carboxylase large chain	P < 0.001, R^2 = 0.416	Increase
K01681	Carbon metabolism	Citrate Cycle	Aconitate hydratase (acnA)	P < 0.001, R^2 = 0.414	Decrease
K00134	Carbon metabolism	Glycolysis	Glyceraldehyde 3-phosphate dehydrogenase (gapA)	P = 0.002, R^2 = 0.281	Decrease
K01638	Carbon metabolism	Glyoxylate cycle	Malate synthase (carbohydrate metabolism)	P = 0.463, R^2 = 0.019	N/A
K01965	Carbon metabolism	Propionyl CoA cylce	Propionyl-CoA carboxylase alpha chain	P = 0.007, R^2 = 0.221	Decrease
K02707	Carbon metabolism	Photosynthesis	Photosystem II cytochrome b559 subunit alpha (psbE)	P = 0.006, R^2 = 0.232	Increase

K02705	Carbon metabolism	Photosynthesis	Photosystem II CP43 chlorophyll apoprotein	$P = 0.006$, $R^2 = 0.232$	Increase
K01428	Nitrogen metabolism	Ammonification	Urease subunit alpha (ureC)	$P = 0.083$, $R^2 = 0.100$	N/A
K00370	Nitrogen metabolism	Denitrification	Nitrate reductase / nitrite oxidoreductase, alpha subunit (narG, NarZ)	$P = 0.002$, $R^2 = 0.273$	Decrease
K00376	Nitrogen metabolism	Denitrification	Nitrous-oxide reductase (nosZ)	$P < 0.001$, $R^2 = 0.352$	Decrease
K02588	Nitrogen metabolism	N fixation	Nitrogenase iron protein NifH (nifH)	$P = 0.937$, $R^2 = 0$	N/A
K02586	Nitrogen metabolism	N fixation	Nitrogenase molybdenum-iron protein alpha chain (nifD)	$P = 0.655$, $R^2 = 0.007$	N/A
K02584	Nitrogen metabolism	N fixation	Nif-specific regulatory protein (nifA)	$P < 0.001$, $R^2 = 0.42$	Decrease
K10944	Nitrogen metabolism	Nitrification	Methane/ammonia monooxygenase subunit A (amoA)	$P < 0.001$, $R^2 = 0.354$	Decrease
K03385	Nitrogen metabolism	N reduction	Nitrite reductase (cytochrome c-552) (nrfA)	$P = 0.001$, $R^2 = 0.302$	Increase
K04561	Nitrogen metabolism	N reduction	Nitric oxide reductase subunit B (norB)	$P = 0.011$, $R^2 = 0.200$	Decrease
K00366	Nitrogen metabolism	N reduction	Ferredoxin-nitrite reductase (nirA)	$P = 0.851$, $R^2 = 0.001$	N/A
K00368	Nitrogen metabolism	N reduction	Nitrite reductase (NO-forming) (nirK)	$P < 0.001$, $R^2 = 0.498$	Decrease
K01507	Phosphorus metabolism	Phosphate degradation	Inorganic pyrophosphatase (ppA)	$P < 0.001$, $R^2 = 0.516$	Decrease

Table 12. Selected KEGG orthology genes from the predictive functional analysis of the *Plakortis angulospiculatus* microbiome and the effect of increasing depth on the relative abundance of the KEGG genes.

KEGG	Function Type	Process	Specific Function	Depth Regression (*t*:25)	Effect of Increasing Depth
K01602	Carbon metabolism	Calvin Cycle	Ribulose-bisphosphate carboxylase small chain	$P = 0.933$, $R^2 = 0$	N/A
K01601	Carbon metabolism	Calvin Cycle	Ribulose-bisphosphate carboxylase large chain	$P = 0.933$, $R^2 = 0.028$	N/A
K01681	Carbon metabolism	Citrate Cycle	Aconitate hydratase (acnA)	$P < 0.001$, $R^2 = 0.503$	Increase
K00134	Carbon metabolism	Glycolysis	Glyceraldehyde 3-phosphate dehydrogenase (gapA)	$P < 0.001$, $R^2 = 0.437$	Decrease
K01638	Carbon metabolism	Glyoxylate cycle	Malate synthase (carbohydrate metabolism)	$P < 0.001$, $R^2 = 0.412$	Decrease
K01965	Carbon metabolism	Propionyl CoA cylce	Propionyl-CoA carboxylase alpha chain	$P < 0.001$, $R^2 = 0.481$	Decrease
K02707	Carbon metabolism	Photosynthesis	Photosystem II cytochrome b559 subunit alpha (psbE)	$P < 0.001$, $R^2 = 0.483$	Decrease
K02705	Carbon metabolism	Photosynthesis	Photosystem II CP43 chlorophyll apoprotein	$P < 0.001$, $R^2 = 0.483$	Decrease
K01428	Nitrogen metabolism	Ammonification	Urease subunit alpha (ureC)	$P < 0.001$, $R^2 = 0.490$	Decrease
K00370	Nitrogen metabolism	Denitrification	Nitrate reductase / nitrite oxidoreductase, alpha subunit (narG, NarZ)	$P = 0.089$ $R^2 = 0.111$	N/A
K00376	Nitrogen metabolism	Denitrification	Nitrous-oxide reductase (nosZ)	$P < 0.001$, $R^2 = 0.010$	Decrease
K02588	Nitrogen metabolism	N fixation	Nitrogenase iron protein NifH (nifH)	$P < 0.001$, $R^2 = 0.406$	Decrease

K02586	Nitrogen metabolism	N fixation	Nitrogenase molybdenum-iron protein alpha chain (nifD)	P = 0.01, R^2 = 0.203	Increase
K02584	Nitrogen metabolism	N fixation	Nif-specific regulatory protein (nifA)	P = 0.0332, R^2 = 0.17	Increase
K10944	Nitrogen metabolism	Nitrification	Methane/ammonia monooxygenase subunit A (amoA)	P = 0.03, R^2 = 0.162	Increase
K03385	Nitrogen metabolism	N reduction	Nitrite reductase (cytochrome c-552) (nrfA)	P < 0.001, R^2 = 0.513	Decrease
K04561	Nitrogen metabolism	N reduction	Nitric oxide reductase subunit B (norB)	P = 0.051, R^2 = 0.144	N/A
K00366	Nitrogen metabolism	N reduction	Ferredoxin-nitrite reductase (nirA)	P = 0.021, R^2 = 0.196	Decrease
K00368	Nitrogen metabolism	N reduction	Nitrite reductase (NO-forming) (nirK)	P = 0.022, R^2 = 0.192	Increase
K01507	Phosphorus metabolism	Phosphate degradation	Inorganic pyrophosphatase (ppA)	P = 0.009, R^2 = 0.239	Decrease

Table 13. Selected KEGG orthology genes from the predictive functional analysis of the *Xestospongia muta* microbiome and the effect of increasing depth on the relative abundance of the KEGG genes.

KEGG	Function Type	Process	Specific Function	Depth Regression (*t*:24)	Effect of Increasing Depth
K01602	Carbon metabolism	Calvin Cycle	Ribulose-bisphosphate carboxylase small chain	P = 0.008, R^2 = 0.254	Decrease
K01601	Carbon metabolism	Calvin Cycle	Ribulose-bisphosphate carboxylase large chain	P = 0.099, R^2 = 0.246	Decrease
K01681	Carbon metabolism	Citrate Cycle	Aconitate hydratase (acnA)	P = 0.008, R^2 = 0.253	Increase

K00134	Carbon metabolism	Glycolysis	Glyceraldehyde 3-phosphate dehydrogenase (gapA)	P = 0.553, R^2 = 0.015	N/A
K01638	Carbon metabolism	Glyoxylate cycle	Malate synthase (carbohydrate metabolism)	P = 0.347, R^2 = 0.037	N/A
K01965	Carbon metabolism	Propionyl CoA cylce	Propionyl-CoA carboxylase alpha chain	P = 0.923, R^2 = 0	N/A
K02707	Carbon metabolism	Photosynthesis	Photosystem II cytochrome b559 subunit alpha (psbE)	P = 0.001, R^2 = 0.366	Decrease
K02705	Carbon metabolism	Photosynthesis	Photosystem II CP43 chlorophyll apoprotein	P = 0.001, R^2 = 0.366	Decrease
K01428	Nitrogen metabolism	Ammonification	Urease subunit alpha (ureC)	P = 0.01, R^2 = 0.244	Decrease
K00370	Nitrogen metabolism	Denitrification	Nitrate reductase / nitrite oxidoreductase, alpha subunit (narG, NarZ)	P = 0.007, R^2 = 0.266	Increase
K00376	Nitrogen metabolism	Denitrification	Nitrous-oxide reductase (nosZ)	P = 0.348, R^2 = 0.037	N/A
K02588	Nitrogen metabolism	N fixation	Nitrogenase iron protein NifH (nifH)	P = 0.075, R^2 = 0.126	N/A
K02586	Nitrogen metabolism	N fixation	Nitrogenase molybdenum-iron protein alpha chain (nifD)	P = 0.142, R^2 = 0.088	N/A
K02584	Nitrogen metabolism	N fixation	Nif-specific regulatory protein (nifA)	P = 0.0152, R^2 = 0.23	Increase
K10944	Nitrogen metabolism	Nitrification	Methane/ammonia monooxygenase subunit A (amoA)	P = 0.567, R^2 = 0.014	N/A
K03385	Nitrogen metabolism	N reduction	Nitrite reductase (cytochrome c-552) (nrfA)	P = 0.025, R^2 = 0.192	Decrease
K04561	Nitrogen metabolism	N reduction	Nitric oxide reductase subunit B (norB)	P = 0.249, R^2 = 0.055	N/A

K00366	Nitrogen metabolism	N reduction	Ferredoxin-nitrite reductase (nirA)	P = 0.057, R^2 = 0.143	N/A
K00368	Nitrogen metabolism	N reduction	Nitrite reductase (NO-forming) (nirK)	P = 0.54, R^2 = 0.016	N/A
K01507	Phosphorus metabolism	Phosphate degradation	Inorganic pyrophosphatase (ppA)	P = 0.31, R^2 = 0.043	

Stable isotope analyses

In isotopic niche space, the HMA sponges *P. angulospiculatus* and *X. muta* grouped separately from each other. The HMA sponge *A. tubulata* grouped with the LMA sponge *A. compressa*. (Fig. 25). In *A. compressa*, there was a significant effect of depth on $\delta^{15}N$ ($t(17) = 2.21$, P = 0.042), with increased $\delta^{15}N$ as depth increased into the mesophotic zone (Fig. 26a, Table 14). There was no significant effect of depth on the $\delta^{13}C$ ($t(17) = 0.972$, P = 0.338) or molar C:N ratios ($t(17) = 0.007$, P = 0.933) (Fig. 26b, Table 14). For *A. tubulata*, there was a significant effect of depth on molar C:N ratios ($t(23) = 3.08$, P = 0.005), with increased C:N ratios as depth increased (Table 14). There were no significant effects of depth for $\delta^{13}C$ ($t(23) = -1.40$, P = 0.174) or $\delta^{15}N$ ($t(23) = 1.78$, P = 0.08) (Fig. 26b). There were significant effects of depth in the $\delta^{13}C$ ($t(28) = -2.88$, P = 0.007) and $\delta^{15}N$ ($t(28) = 3.93$, P = 0.02) of *P. angulospiculatus*, as $\delta^{13}C$ decreased with increasing depth, while $\delta^{15}N$ increased as depth increased (Fig. 25c, Table 14). There was no significant effect of depth on the molar C:N ratios of this sponge ($t(28) = 1.43$, P = 0.164) (Table 14). There was a significant effect of depth on *X. muta* $\delta^{15}N$ ($t(28) = 3.12$, P = 0.002), with increased $\delta^{15}N$ as depth increased (Fig. 26d, Table 14). There were no significant effects of depth on $\delta^{13}C$ ($t(21) = 0.99$, P = 0.334) or molar C:N ratios ($t(21) = 0.25$, P = 0.803) (Fig. 26d, Table 14).

Table 14. Mean (± SE) $\delta^{13}C$, $\delta^{15}N$ and molar C:N ratios from *Amphimedon compressa*, *Agelas tubulata*, *Plakortis angulospiculatus* and *Xestospongia muta* along the sampling depth gradient.

Species	Depth (m)	$\delta^{13}C$	$\delta^{15}N$	Molar C:N Ratio
Amphimedon compressa	15 (*n*=8)	-17.76 (0.28)	3.31 (0.11)	4.01 (0.07)
	22 (*n*=3)	-17.97 (0.15)	3.48 (0.16)	4.13 (0.08)
	30 (*n*=3)	-18.76 (0.28)	2.75 (0.05)	4.54 (0.17)
	46 (*n*=3)	-17.93 (0.18)	3.49 (0.13)	4.13 (0.08)
	61 (*n*=3)	-17.25 (0.41)	3.90 (0.04)	4.04 (0.12)
Agelsa tubulata	15 (*n*=8)	-18.00 (0.13)	2.67 (0.11)	4.10 (0.12)
	22 (*n*=5)	-16.91 (0.18)	4.05 (0.15)	3.89 (0.09)
	30 (*n*=5)	-17.08 (0.21)	3.91 (0.23)	3.9 (0.16)
	46 (*n*=5)	-18.26 (0.25)	3.43 (0.17)	4.82 (0.06)
	61 (*n*=5)	-17.78 (0.28)	4.02 (0.18)	4.38 (0.17)
Plakortis angulospiculatus	15 (*n*=5)	-19.43 (0.24)	1.41 (0.38)	8.41 (0.65)
	22 (*n*=5)	-19.48 (0.06)	1.55 (0.17)	8.12 (0.52)
	30 (*n*=5)	-19.54 (0.21)	2.61 (0.20)	9.12 (0.75)
	46 (*n*=5)	-19.77 (0.19)	1.71 (0.03)	8.75 (0.45)
	61 (*n*=5)	-20.05 (0.19)	3.21 (0.31)	9.61 (0.81)
Xestospongia muta	15 (*n*=7)	-19.08 (0.12)	3.37 (0.19)	4.97 (0.18)
	30 (*n*=6)	-19.47 (0.26)	4.18 (0.09)	5.49 (0.16)
	61 (*n*=6)	-20.13 (0.27)	4.28 (0.23)	7.07 (0.39)
	76 (*n*=5)	-20.17 (0.11)	4.86 (0.17)	7.32 (0.07)
	91 (*n*=5)	-18.59 (0.14)	4.92 (0.21)	4.98 (0.10)

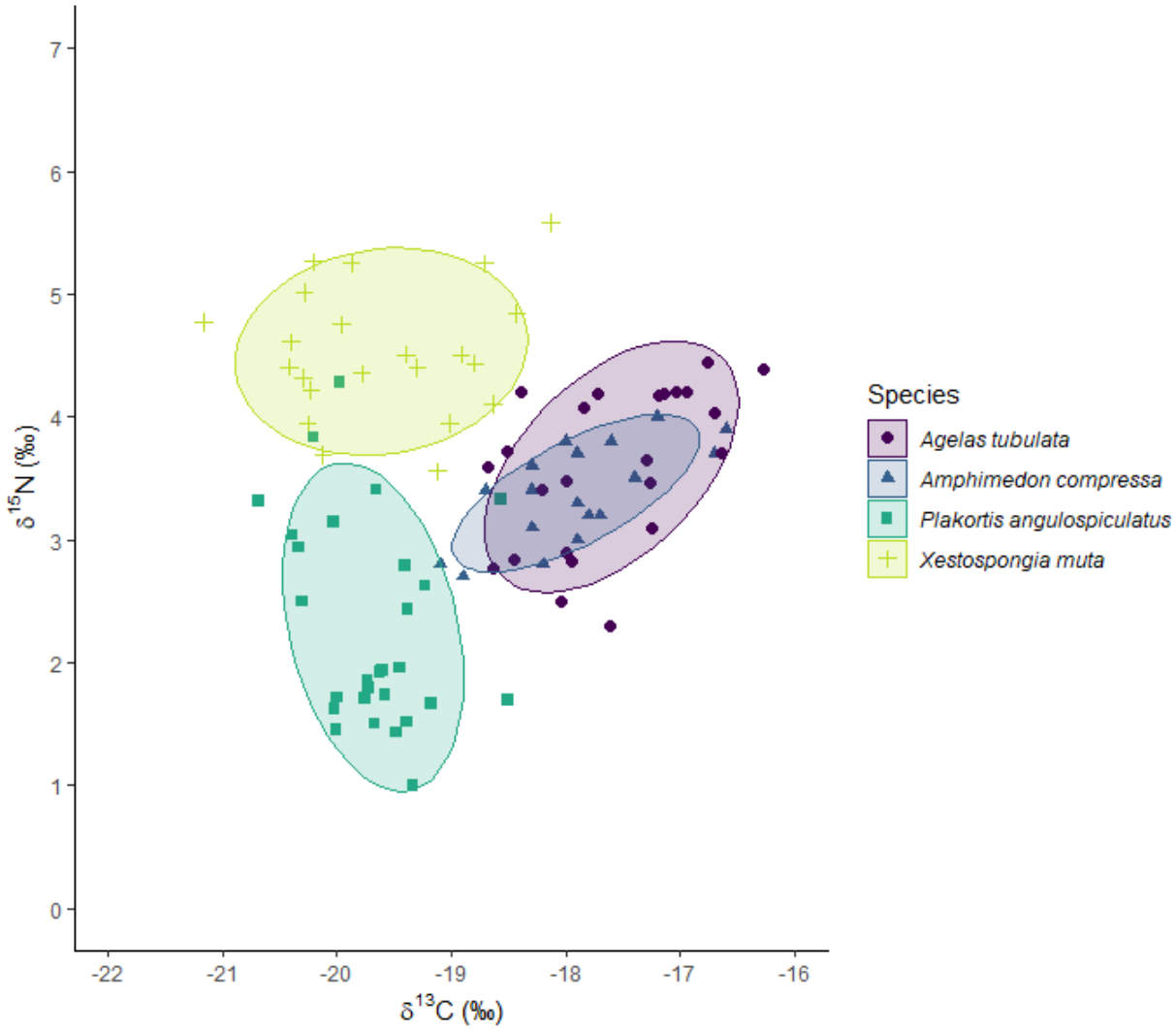

Figure 25. Bivariate plot of $\delta^{13}C$ and $\delta^{15}N$ of *Amphimedon compressa*, *Agelas tubulata*, *Plakortis angulospiculatus* and *Xestospongia muta.* The 95% confidence interval (CI) ellipses show the species groupings.

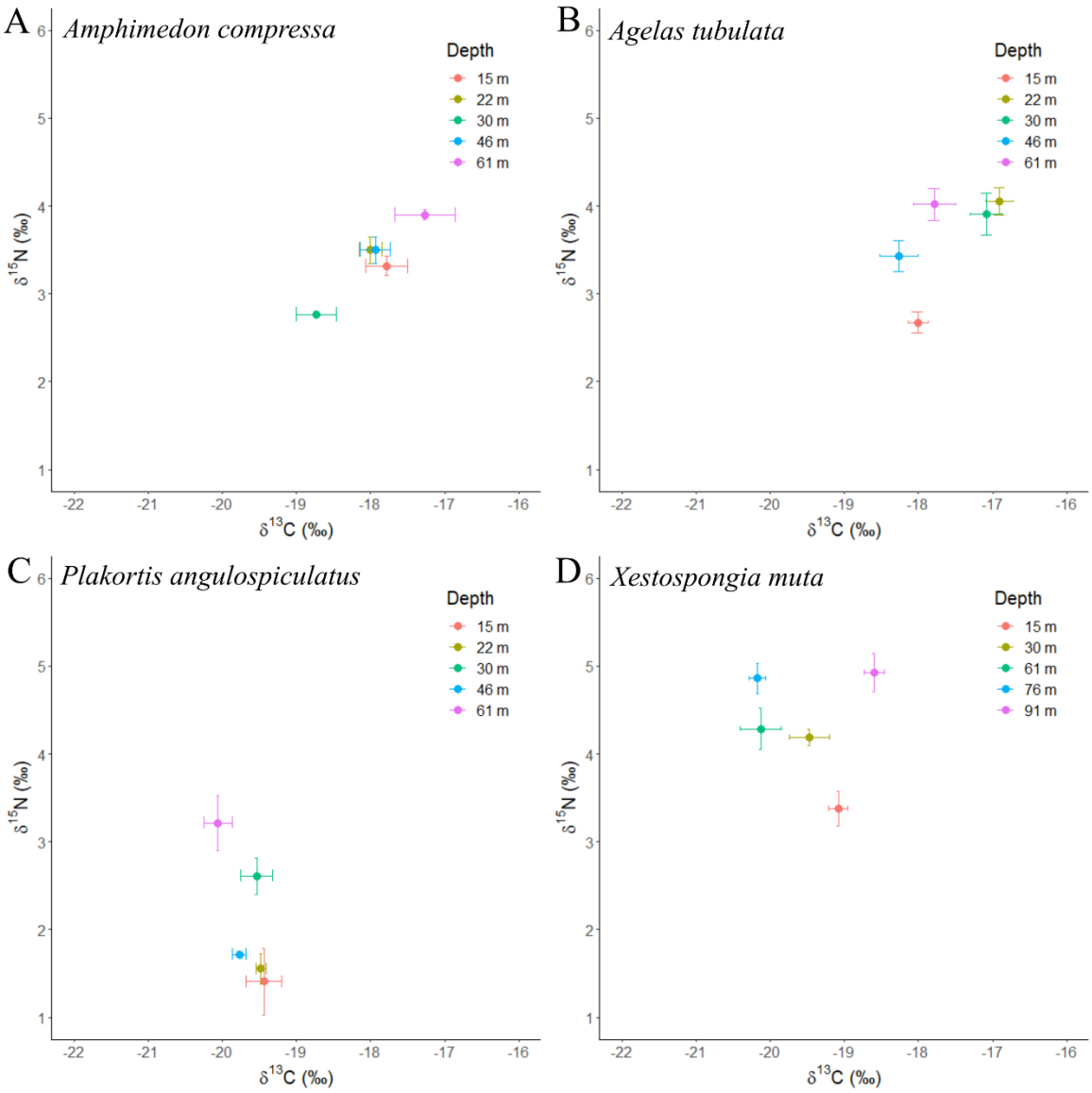

Figure 26. A) Bivariate plot of mean (± SE) $\delta^{13}C$ and $\delta^{15}N$ from *Amphimedon compressa* between depths. **B)** Bivariate plot of mean (± SE) $\delta^{13}C$ and $\delta^{15}N$ from *Agelas tubulata* between depths. **C)** Bivariate plot of mean (± SE) $\delta^{13}C$ and $\delta^{15}N$ from *Plakortis angulospiculatus* between depths. **D)** Bivariate plot of mean (± SE) $\delta^{13}C$ and $\delta^{15}N$ from *Xestospongia muta* between depths.

Proximate Biochemical Composition

There were significant effects of depth on concentration of carbohydrates (mg g^{-1} AFDW) ($t(21) = 4.42$, $P = 0.0003$), soluble protein (mg g^{-1} AFDW) ($t(21) = 3.25$, $P = 0.004$) and lipids (mg g^{-1} AFDW) ($t(21) = -4.84$, $P < 0.0001$) in *A. compressa*. As depth increased, carbohydrates and soluble protein increased while lipids decreased in concentration (Table 15). There was no significant effect of depth on total energetic content (kJ g^{-1} AFDW) ($t(21) = -1.26$, $P = 0.22$) in *A. compressa.* For *A. tubulata,* there were significant effects of depth on concentration of carbohydrates (mg g^{-1} AFDW) ($t(29) = 4.29$, $P = 0.0002$), soluble protein (mg g^{-1} AFDW) ($t(29) = 3.40$, $P = 0.0021$), lipids (mg g^{-1} AFDW) ($t(29) = -6.45$, $P < 0.0001$) and total energetic content (kJ g^{-1} AFDW) ($t(29) = -2.23$, $P = 0.034$). As depth increased, carbohydrates and soluble protein concentrations increased while lipids and total energetic content decreased (Table 15). In *P. angulospiculatus*, there were no significant effects of depth on concentration of carbohydrates (mg g^{-1} AFDW) ($t(29) = 0.91$, $P = 0.375$), soluble protein (mg g^{-1} AFDW) ($t(29) = -0.11$, $P = 0.911$), lipids (mg g^{-1} AFDW) ($t(29) = -0.64$ $P = 0.526$) and total energetic content (kJ g^{-1} AFDW) ($t(29) = 1.96$, $P = 0.062$). In *X. muta,* there were significant effects of depth on concentration of carbohydrates (mg g^{-1} AFDW) ($t(29) = 7.11$, $P = 0.0001$), soluble protein (mg g^{-1} AFDW) ($t(29) = 3.63$, $P = 0.0013$), lipids (mg g^{-1} AFDW) ($t(29) = -3.05$, $P < 0.0055$) and total energetic content (kJ g^{-1} AFDW) ($t(29) = 3.72$, $P = 0.0011$). As depth increased, carbohydrates, soluble protein and total energetic content concentrations increased while lipid concentrations decreased (Table 15).

Table 15. Mean (± SE) carbohydrates (mg g^{-1} AFDW), soluble protein (mg g^{-1} AFDW), Lipids (mg g^{-1} AFDW) and energetic content (kJ g^{-1} AFDW) from in sponge tissue from *Amphimedon compressa*, *Agelas tubulata*, *Plakortis angulospiculatus* and *Xestospongia muta* as a function of depth.

Species	Depth (m)	Carbohydrates	Protein	Lipids	Energetic Content
Amphimedon compressa	15 (*n*=10)	6.36 (2.62)	42.25 (8.90)	270.14 (12.43)	36.02 (0.93)
	22 (*n*=3)	125.69 (5.42)	173.45 (8.41)	33.90 (8.72)	36.27 (1.22)
	30 (*n*=3)	128.78 (10.18)	119.70 (8.18)	27.15 (3.59)	38.15 (0.51)
	46 (*n*=3)	125.46 (9.97)	152.20 (9.06)	62.42 (29.71)	36.35 (0.50)
	61 (*n*=3)	118.32 (21.99)	130.42 (22.40)	20.61 (9.92)	33.13 (1.82)
Agelas tubulata	15 (*n*=10)	14.54 (1.43)	336.17 (13.82)	154.23 (9.13)	35.43 (1.45)
	22 (*n*=5)	109 (5.64)	423.08 (15.22)	132.63 (19.57)	32.37 (0.16)
	30 (*n*=5)	96.43 (3.90)	458.36 (11.57)	60.75 (5.52)	32.89 (0.65)
	46 (*n*=5)	98.39 (8.50)	474.58 (15.26)	75.79 (9.90)	30.95 (0.22)
	61 (*n*=5)	97.70 (3.94)	418.92 (11.11)	45.28 (7.09)	32.37 (0.70)
Plakortis angulospiculatus	15 (*n*=5)	182.16 (10.09)	186.55 (12.46)	102.43 (4.64)	33.25 (0.58)
	22 (*n*=5)	208.18 (36.84)	271.50 (79.03)	99.54 (19.14)	33.31 (0.45)
	30 (*n*=5)	190.83 (15.69)	220.56 (39.75)	103.21 (15.50)	34.82 (0.36)
	46 (*n*=5)	253.70 (54.08)	237.30 (46.21)	94.77 (11.83)	33.21 (0.80)
	61 (*n*=5)	219.08 (63.58)	205.15 (24.59)	93.44 (9.56)	38.49 (3.73)
Xestospongia muta	15 (*n*=4)	66.92 (5.62)	182.72 (22.85)	223.98 (18.22)	45.14 (1.98)
	30 (*n*=6)	184.57 (12.95)	242.46 (20.71)	83.86 (9.56)	48.13 (2.31)
	61 (*n*=6)	184.07 (11.70)	310.03 (13.17)	124.95 (24.51)	46.25 (1.57)
	76 (*n*=5)	220.71 (15.47)	284.82 (15.30)	72.29 (6.26)	49.33 (1.34)
	91 (*n*=5)	322.73 (21.04)	280.82 (14.27)	84.67 (8.00)	61.33 (1.64)

Discussion

While Caribbean MCEs are characterized by steep gradients in available PAR (Chapter 2, Lesser et al. 2009; Morrow et al. 2016; Lesser et al. 2018) which results in transitions in trophic strategy from photoautotrohpy to heterotrophy as depth increases in corals and sponges (Lesser et al. 2009, 2010, 2018, 2019; Slattery et al. 2011), there are also predictable gradients in the principle food sources for both sponges and their associated microbiota. At the sampling site in Grand Cayman, three sampling periods over 18 months showed increasing POC and PON at this site during each sampling (Chapter 2; Lesser et al. 2019) and while the overall abundance of those resources changed between samplings, there was consistently more POC and PON available to sponges at mesophotic depths. The increase in sponge growth rates and sponge abundances is driven primarily by this POM availability (Chapter 1, 2; Lesser 2006; Trussell et al. 2006; Slattery & Lesser 2015) However, the principle trophic resources for the microbiome of Caribbean reef sponges, DOC and DON, showed significant reductions in concentration as depth increased from 0 m to 91 m (~ 50% and 80% respectively), which could have an impact on the community structure and function of these associated microbes and the biogeochemical cycling by sponges on MCEs. Interestingly, another important resource for sponge associated microbiota, DIN, increased with depth by 1 to 2 orders of magnitude (Chapter 2, Fig. 11) which has been previously shown to confer stability on the microbiome of *X. muta* (Morrow et al. 2016). This pattern on Grand Cayman is contrary to observations at the neighboring island of Little Cayman, which had no such increase in DIN with depth (Morrow et al. 2016) highlighting the importance of assessing environmental variables in conjunction to microbial studies in sponges, even between reefs in the same biogeographic province. As these gradients in resources will likely have an effect on trophic utilization patterns of both the sponge and its microbiome, or the biogeochemical cycling by a sponge microbiome,

quantifying these resources is crucial. We found that the gradients in abiotic and biotic factors resulted in species-specific shifts in associated microbe community structure and function, and that increased consumption of POM affected energetic strategy between depths. Additionally, all sponges increased consumption of POM at mesophotic depths.

The sponges sampled in this study show a similar pattern of species-specific microbial communities (Fig. 20) previously observed in many species (Thomas et al. 2016; Pita et al. 2018). The HMA sponge microbiomes are significantly separated at the species level using Bray Curtis Diversity metrics, while the microbiome of the LMA sponge, *A. compressa*, displays higher similarity to the microbial community of seawater from this site. This pattern has also been observed previously in LMA sponges, which generally show a higher similarity to seawater microbial communities compared to HMA sponges (Gloeckner et al. 2014; Moitinho-Silva et al. 2014). Interestingly, there is some disparity in the alpha diversity metric (Shannon's) between *A. compressa* and seawater (Fig. 18), which is likely driven by a higher abundance of unique ASVs that could be present in the seawater samples relative to samples from *A. compressa*. The alpha diversity scores of the HMA sponges are significantly higher relative to the LMA sponge, which is not surprising given the microbial diversity these sponges harbor (Thacker & Freeman, 2012; Fiore et al. 2013, 2015, 2020; Morrow et al. 2016; Pita et al. 2018; Gannt et al. 2019). Additionally, the alpha and beta diversity metrics reinforce the HMA-LMA dichotomy and indicate that there are clear differences in the microbial composition and abundances of the microbiome between the two functional classifications. The highest mean Shannon-alpha diversity score was recorded in *X. muta*, which is known to harbor dense and diverse communities of symbionts, and this diversity increased significantly with depth (Fig. 19d), while all other sponge species showed no significant changes between the sampled depths. The small but significant change with depth in *X. muta* is

most likely a reflection of a shift in symbionts towards heterotrophy as there is a steep gradient in PAR availability at this site (Chapter 2, Fig. 7) or increases in more rare microbial fauna occupying trophic niches not available to them in the sponge on shallow coral reefs.

The microbial community structure of the HMA sponges in this study is similar to previous studies on the same species, with the dominant phyla consisting of the *Proteobacteria*, *Thaumarchaeota*, *Acidobacteria*, *Actinobacteria* and *Chloroflexi*, while the LMA sponge *A. compressa* was associated primarily with the *Proteobacteria* and *Cyanobacteria* (Thomas et al. 2016; Pita et al. 2018) (Fig. 21-24). These phyla are commonly associated with a wide range of marine sponges and have been described as the "core" phyla of marine sponges (Pita et al. 2018). The similarity of the *A. compressa* microbiome to sea water appears to be associatied primarily with the presence of *Proteobacteria* and *Cyanobacteria* (Fig. 21, S1), which also concurs with previous studies on a variety of LMA sponges (Thacker & Freeman 2012; Steinert et al. 2016; Thomas et al. 2016; Pita et al. 2018; Gannt et al. 2019). While HMA sponges share many of the same phyla, the relative abundance of each varies for each species (Fig. 22-24), indicating that while these phyla play important roles in sponges overall their contributions to the trophic ecology, or chemical ecology, will likely vary between species based on their relative abundances. This may facilitate trophic niche separation as suggested by Morganti et al. (2017) which is reflected in the stable isotopic composition of the sampled sponges from this study (Fig. 25). The microbial associations of sponges remain species-specific at both local and regional biogeographic scales (Thacker & Freeman 2012; Steinert et al. 2016; Pita et al. 2018), and our results along the depth gradient show the same pattern of species-specificity in the sponge microbiomes. However, along local gradients such as our depth series, the microbiomes within each species can undergo

significant changes as a result of the changing biotic or abiotic factors as depth increases into mesophotic environments (Olson & Gao 2013; Steinert et al. 2016; Morrow et al. 2016).

Of the four sponge species sampled, only the community structure of the *A. tubulata* microbiome remained unchanged with depth (Fig. 21). This may be a result of similar trophic or chemical strategies at all depths in this sponge but, there were significant differences due to depth in the predicted functions of the *A. tubulata* microbiome. Changes in nitrogen and carbon cycling did occur as a function of depth (Table 11) which indicates that while the community structure of a sponge may remain stable along a depth gradient, the microbiome itself can alter its function in relation to different environmental conditions between depths. Indeed, the microbiome of *A. tubulata* has a significant population of microbes from the phyla *Proteobacteria* and *Chloroflexi* (Fig. 22), which have been shown previously to have high physiological diversity (Bayer et al. 2018; Pita et al. 2018; Fiore et al. 2020). The other sponges, *A. compressa*, *X. muta* and *P. angulospiculatus*, were observed to have significant changes in their microbiomes, but these were species-specific with regards to both the microbial classes that underwent changes in abundance relative to depth. These changes are likely driven by a combination of PAR and reductions or increases in certain trophic resources. While DOC decreases with depth, it is highly unlikely that the sponge holobiont is carbon limited at any depth based on the concentrations observed (Chapter 2, Fig. 10). Decreases in DON with concurrent increases in DIN (Chapter 2, Fig. 10, 11) may cause changes in community composition due to the importance of nitrogen in cell growth. Increased heterotrophic microbes can be found in increased densities where DIN concentrations are higher as DIN is an important component of their diet (Lesser 2006; Voss et al. 2013) so changes in microbial trophic strategies and thus community composition within the sponge is also likely. While these changes were significant, many of the microbes within the microbiome did not

vary with depth, which may have been a result of the increased DIN between depths conferring stability. So, while there are broad and generalizable gradients in abiotic and biotic factors (i.e., food or PAR) between shallow and mesophotic depths, they do not appear to have a universal effect on sponge microbial composition with depth. The functional predictions for these microbiomes also reflect the species-specific function of the microbiome between depths. While the predictions show a variety of complex nitrogen and carbon cycling pathways are present in all the sampled species (Tables 10-13), none of the selected KEGG genes showed the same effect of depth between any species (Tables 10-13). It would appear that the effect of the sponge microbiome on carbon and nitrogen cycling along shallow to mesophotic depth gradients must be interpreted carefully,and may not be generalizable. The biogeochemical cycling by sponges between depths must be assessed on species by species basis to truly understand overall nutrient and elemental cycling by sponges on mesophotic coral reefs.

The $\delta^{13}C$ of both *X. muta* and *P. angulospiculatus* reflect photoautotrophic carbon inputs to the sponge's carbon budget (Fry 2006; Slattery et al. 2011), potentially by translocation of photoautotrophically produced carbon from symbionts in *X. muta* (Morrow et al. 2016; Gannt et al. 2019). However, *P. angulospiculatus* does not appear to contain large communities of cyanobacteria, so the $\delta^{13}C$ signature of both of these sponges may reflect the trophic resources available to them (POM and DOM), and subsequent carbon cycling within the microbiome. While there are large communities of *Chloroflexi* in all of the HMA sponges, there is no clear signal of photoautotrophy by the *Chloroflexi* in the $\delta^{13}C$ of *X. muta* and *P. angulospiculatus* (Canfeld et al. 2005). Using compound specific isotope analysis of amino acids techniques (CSIA-AA) it has been shown that the translocation of resynthesized amino acids from symbionts in both *X. muta* and *P. angulospiculatus* can occur based on EV values, which quantifies the potential for

translocation of resynthesized amino acids from microbes to host (Shih et al. 2020) (Chapter 1, Fig. 5). Interestingly, we expected to see significant reductions in the cyanobacteria symbionts of *X. muta* but it appears that the increased DIN with depth at this site might have provided the environment supporting the relative stability between depths for this symbiont community (*sensu* Morrow et al. 2016). Additionally, reduced photoautotrophic inputs are also not reflected in any significant increases in the $\delta^{13}C$ of *X. muta* as depth increases (Fig. 26d, Table 14). The $\delta^{13}C$ of both *A. compressa* and *A. tubulata* reflect a more heterotrophic diet, and they are ~2 ‰ higher relative to *X. muta* and *P. angulospiculatus*. Both *A. compressa* and *A. tubulata* likely rely more heavily on POM, which is common for LMA sponges (Thacker & Freeman 2012; Weisz et al. 2008) and in the case of *A. tubulata*, its EV value is low relative to the other HMA sponges sampled in this study (Chapter 1, Table 1). Additionally, *A. compressa* and *A. tubulata* both share a similar isotopic niche (Fig. 25), so while *A. tubulata* and *A. compressa* may be classified as an HMA or LMA sponge respectively, they may both rely more heavily on the POM portion of their diets for tissue growth.

While this study has shown that there is high variability between species in multiple metrics, all the sampled species in this study show a statistically significant pattern of increasing $\delta^{15}N$ as depth increases (Fig. 26, Table 14). This increase in $\delta^{15}N$ has been observed in multiple studies of sponges along a shallow to mesophotic depth gradient at multiple sites in the Caribbean (Chapter 1, 2; Slattery et al. 2011; Morrow et al. 2016; Lesser et al. 2020). The pattern of increased $\delta^{15}N$ with depth reflects the increased consumption of POM, in particular heterotrophic picoplankton which are more abundant in the mesophotic (Chapter 2; Lesser 2006; Trussell 2006; Lesser et al. 2019; 2020). It may also reflect increased heterotrophic inputs instead of photoautotrophic inputs from the microbiome as depth increases due to reductions in PAR

(Chapter 1, 2; Slattery et al. 2011). Increased availability of POM at mesophotic depths is associated with higher growth rates and abundances in a variety of Caribbean sponge species as depth increases (Chapter 1, 2; Lesser 2006; Trussell et al. 2006; Slattery & Lesser 2015). While there are clear differences between both species and HMA/LMA status in potential microbial community structure and function as a result of increasing depth, it is highly likely that all sponges in this study consume more POM as depth increases into the mesophotic. Within species, there are species specific differences $\delta^{15}N$ which likely reflects the unique microbial communities and functions of each sponge species.

In *P. angulospiculatus* particularly low $\delta^{15}N$ are observed on shallow reefs (Fig. 26c, Table 14), that reflects potential inputs of nitrogen produced via nitrogen fixation pathways (N-fixation $\delta^{15}N$: -2 to 2‰), and KEGG genes were observed in this sponge in the functional predictions (Table 12). The potential for N-fixation has been observed in sponges previously (Mohammed et al. 2008), which would likely occur during cessation of pumping leading to hypoxic compartments within the tissue (Mohammed et al. 2008; Fiore et al. 2010). In *P. angulospiculatus*, the *nifH* gene shows reduced expression (Table 12) as depth increases while *nifA* (a *nif* regulatory gene) shows increases which follows the pattern of the increased $\delta^{15}N$ for this sponge along the depth gradient. N_2 fixation, however, is an energetically expensive process, and sponges are exposed to higher levels of DON at shallow depths, so further study is required to understand why this process may occur at shallow instead of mesophotic depths where DON is significantly lower. Another explanation of the low $\delta^{15}N$ relative to other species, may be a result of different microbial transformations of assimilated nitrogen in *P. angulospiculatus* since mineralization, denitrification and nitrification can cause variability in the $\delta^{15}N$ signal (Kendall & McDonell 1998), these processes may be occurring at different rates in this sponge species relative to other species.

The proximate biochemical composition of *A. compressa*, *A. tubulata* and *X. muta* showed significant differences as a function of increasing depth, with lipids decreasing and carbohydrates and soluble protein increasing at mesophotic depths (Table 15). This was unexpected as an organism exposed to increased food, such as POM for mesophotic sponges, would be expected to increase their lipid reserves (Sokolova 2013). Lipid stores are often mobilized during periods of starvation, reproduction or growth. It is highly unlikely that sponges at mesophotic depths are under stress or starvation conditions as they are consistently exposed to more POM than their shallow conspecifics (Chapter 2; Lesser 2006; Trussell et al. 2006; Lesser et al. 2019, 2020) and are generally buffered from potential abiotic stressors (Lesser et al. 2009). As some sponges are known to exhibit phenotypic plasticity in chemical defense, metabolic rate, morphology and spicule size (Bavestrello et al. 1993; Hill & Hill 2001; Morley et al. 2016; Slattery et al. 2016), it is possible that sponges may exhibit phenotypic plasticity in their trophic ecology and energetic state. Indeed, it is well known that many invertebrates can exhibit phenotypic plasticity, including energetic strategies (Padilla & Savedo 2013). Previous studies have shown that sponges increase their growth rates as depth increases (Chapter 2; Lesser 2006; Trussell et al. 2006; Lesser & Slattery 2013; Slattery & Lesser 2015) and that appears to be a function of the increased picoplankton available to them (Chapter 2; Lesser 2006; Trussell et al. 2006; Slattery et al. 2011; Lesser et al. 2018, 2019, 2020) which may also result in an increase in the mobilization of macromolecules, such as lipids, with their high energetic content..

Mesophotic sponges in this study may prioritize their higher growth rates over maintaining lipid stores which requires the use of energy reserves despite the fact that they are consistently exposed to higher levels of particulate resources which can be used for increasing biomass (i.e., low C:N ratio bacterioplankton that increase with depth). Conversely, shallow sponges have

slower growth rates and are exposed to significantly less POM at this site (Chapter 2, Fig. 10), so these sponges may prioritize lipid storage as their energetic demand is also lower. The higher abundance of low C:N ratio picoplankton in the mesophotic may also account for the increased concentrations of soluble proteins available in mesophotic sponges as nitrogen is crucial for protein synthesis. Interestingly the effect of decreasing lipids with depth was observed in all HMA sponges and the LMA sponge, *A. compressa*. As LMA sponges generally utilize more POM in their diet over DOM (Morganti et al. 2017), this suggests that POM availability may be causing the observed changes in proximate biochemical composition.

An alternate explanation is that the sponges on shallow reefs are exposed to more cyanobacteria which have higher lipid content relative to other heterotrophic bacterioplankton (da Silva et al. 2008; Olsen 2009; Karatay & Donmez 2011) while sponges in the mesophotic are exposed to bacterioplankton populations with significantly less cyanobacteria (Chapter 2; Lesser 2006; Trussell 2006; Lesser 2019, 2020). The observed differences in proximate biochemical composition are likely a combination of both plasticity in energetic strategy and shifts in the types of picoplankton as depth changes. However, Luskow et al. (2019) found that potential starvation did not affect sponge lipid concentrations in temperate sponges, so further study over an extended time period, accounting for seasonal changes in POM abundance as observed in Chapter 2, would be important to understand this pattern. It is also interesting that the observed pattern in PBC with depth is species-specific as PBC in *P. angulopsiculatus* did not vary with depth. The largely unknown contributions from heterotrophic symbionts to sponge energetic budgets (Rix et al. 2020), but see Shih et al. (2020), leaves a large gap in our understanding of the contributions from DOM to sponge energetics.

It is also possible that the concentrations of lipids are a reflection of the microbiome of these sponges. However, the lipid concentration of bacteria is low (0.5-2 mg g^{-1} DW) (Gillan et al. 1988; da Silva et al. 2008) relative to the values for the sponge holobionts (Table 14) and thus the majority of the variability in the biochemical composition we see in this study is a reflection of the sponge tissue and not microbial biomass. Additionally, this pattern was observed in both HMA and LMA sponges, so the density of associated microbes does not play a role in the depth dependent changes either. Reproduction is known to mobilize and utilize significant quantities of lipids (Koojiman 2010). Very little is known about reproduction in sponges, but it is likely tied to lunar cycle (Nozawa et al. 2016) or temperature (Caralt et al. 2018). It is possible the disparity between these sponge's PBC may be a result of mesophotic sponges spawning before their shallow conspecifics. While this seems unlikely given that this pattern was observed in multiple species, the influence of reproduction on the seasonal changes in PBC is unknown. This highlights the need to quantify the reproductive state of sponge tissue when assessing PBC in future studies. Predation pressure may also result in a sponge changing its overall biochemical composition to become less nutritionally favorable for a predator (Duffy & Paul 1992). The sampled sponges in this study are chemically defended (Albrizo et al. 1995; Chanas & Pawlik 1995; Chanas et al. 1995) so it is unlikely that nutritionally quality played a role here. However, assessing potential changes in chemical defense along the studied gradient in these sponges is also required to fully understand if top-down effects has any role in the distribution and abundance of these sponges.

Conclusion

In this study we have shown that sponges show species specific patterns in microbial community structure and that these microbiomes do undergo significant compositional changes along a shallow to mesophotic depth gradient, regardless of HMA or LMA status. These species-specific

microbiomes have complex carbon and nitrogen cycling potential, that changes along the depth gradient. These patterns are, again, species-specific so generalizations about nutrient cycling of sponge holobionts between shallow to MCE should be approached with caution. Additionally, in the sponge *A. tubulata*, the community composition did not undergo any significant changes in its community composition between depths, but the predicted function of that community did change significantly with depth. The gradients in PAR, DOM and DIN are likely factors in these compositional and functional changes, highlighting the importance of collecting environmental data when assessing sponge microbiome along environmental gradients. The increased POM and the composition of that POM on MCEs appears to be reflected in both the $\delta^{15}N$ and PBC signatures of sponge tissue that potentially relates to phenotypic plasticity in the trophic ecology and energetic state between shallow and mesophotic depths. It is probable that sponges prioritize growth over energetic reserves in the mesophotic due to increased POM availability. Gradients in abiotic factors can change sponge microbial communities and their function at a local scale, but broad generalizations regarding sponge biogeochemical cycling, trophic strategy and energetics should be approached carefully given the species-specificity observed in this study. While species specific patterns were clear in this study, it also appears that the sponges in this study do consume more heterotrophic picoplankton at depth, providing increased evidence that bottom-up processes play a significant role in sponge distributions.

Acknowledgements

We thank E. Kintzing, A. Chavez and D. Gochfeld for field and laboratory support. We thank A. Weinheimer for assistance and advice on statistical analyses of 16s rRNA metabarcoding data. All sample collections complied with the laws of the Cayman Islands and the United States of America. Support was provided by NSF Biological Oceanography (OCE–1632348/1632333) to

MPL and MS respectively, and the University of New Hampshire Marine Biology Small Grants fund to KJM.

Literature Cited

Achlatis, M., Pernice, M., Green, K., de Goeij, J. M., Guagliardo, P., Kilburn, M. R., ... & Dove, S. (2019). Single-cell visualization indicates direct role of sponge host in uptake of dissolved organic matter. Proceedings of the Royal Society B, 286(1916), 20192153.

Albrizio, S., Ciminiello, P., Fattorusso, E., Magno, S., & Pawlik, J. R. (1995). Amphitoxin, a new high molecular weight antifeedant pyridinium salt from the Caribbean sponge *Amphimedon compressa*. Journal of Natural Products, 58(5), 647-652.

Apprill A, McNally S, Parsons R, Weber L (2015) Minor revision to V4 region SSU rRNA 806R gene primer greatly increases detection of SAR11 bacterioplankton. Aquatic Microbial Ecology 75:129–137

Assmann, M., Lichte, E., Pawlik, J. R., & Köck, M. (2000). Chemical defenses of the Caribbean sponges *Agelas wiedenmayeri* and *Agelas conifera*. Marine Ecology Progress Series, 207, 255-262.

Barbera P, Kozlov AM, Czech L, Morel B, Darriba D, Flouri T, Stamatakis A (2019) EPA-ng: massively parallel evolutionary placement of genetic sequences. System Biology 68:365–369

Batista, D., Costa, R., Carvalho, A. P., Batista, W. R., Rua, C. P., de Oliveira, L., ... & Dobretsov, S. (2018). Environmental conditions affect activity and associated microorganisms of marine sponges. Marine environmental research, 142, 59-68.

Bavestrello, G., Bonito, M., & Sarà, M. (1993). Influence of depth on the size of sponge spicules. Scientia Marina (Barcelona), 57(4), 415-420.

Bayer, K., Jahn, M. T., Slaby, B. M., Moitinho-Silva, L., & Hentschel, U. (2018). Marine sponges as *Chloroflexi* hot spots: genomic insights and high-resolution visualization of an abundant and diverse symbiotic clade. MSystems, 3(6).

Bell, J. J. (2008). The functional roles of marine sponges. Estuarine, coastal and shelf science, 79(3), 341-353.

Bossier, P., Dierckens, K., van Delsen, B., Defoirdt, T., de Schryver, P., Vadstein, O., ... & Skjermo, J. (2009, August). The role of microbiota in aquaculture target organisms and their environment. In Aquaculture Europe 2009.

Bourne, D. G., Morrow, K. M., & Webster, N. S. (2016). Insights into the coral microbiome: underpinning the health and resilience of reef ecosystems. Annual Review of Microbiology, 70.

Bradford, M. M. (1976). A rapid and sensitive method for the quantitation of microgram quantities of protein utilizing the principle of protein-dye binding. Analytical biochemistry, 72(1-2), 248-254.

Callahan BJ, Sankaran K, Fukuyama JA, McMurdie PJ, Holmes SP (2016) Bioconductor workflow for microbiome data analysis: from raw reads to community analyses.

Canfield, D. E., Kristensen, E., & Thamdrup, B. (2005). Carbon fixation and phototrophy. In Advances in marine biology (Vol. 48, pp. 95-127). Academic Press.

Chanas, B., & Pawlik, J. R. (1995). Defenses of Caribbean sponges against predatory reef fish. II. Spicules, tissue toughness, and nutritional quality. Marine Ecology Progress Series, 127, 195-211.

Chanas, B., Pawlik, J. R., Lindel, T., & Fenical, W. (1997). Chemical defense of the Caribbean sponge *Agelas clathrodes* (Schmidt). Journal of Experimental Marine Biology and Ecology, 208(1-2), 185-196.

de Caralt, S., González, J., Turon, X., & Uriz, M. J. (2018). Reproductive strategies of two common sympatric Mediterranean sponges: *Dysidea avara* (*Dictyoceratida*) and *Phorbas tenacior* (*Poecilosclerida*). PeerJ, 6, e5458.

de Goeij, J. M., Lesser, M. P., & Pawlik, J. R. (2017). Nutrient fluxes and ecological functions of coral reef sponges in a changing ocean. In Climate change, ocean acidification and sponges (pp. 373-410). Springer, Cham.

de Goeij, J. M., Van Oevelen, D., Vermeij, M. J., Osinga, R., Middelburg, J. J., De Goeij, A. F., & Admiraal, W. (2013). Surviving in a marine desert: the sponge loop retains resources within coral reefs. Science, 342(6154), 108-110.

Diaz, M. C., & Rützler, K. (2001). Sponges: an essential component of Caribbean coral reefs. Bulletin of Marine Science, 69(2), 535-546.

Eddy, S.R. (2008) A Probabilistic Model of Local Sequence Alignment That Simplifies Statistical Significance Estimation. PLoS Comput Biol 4:e1000069

Fernandes Da Silva, C., Ballester, E., Monserrat, J., Geracitano, L., Wasielesky Jr, W., & Abreu, P. C. (2008). Contribution of microorganisms to the biofilm nutritional quality: protein and lipid contents. Aquaculture Nutrition, 14(6), 507-514.

Fiore, C. L., Baker, D. M., & Lesser, M. P. (2013a). Nitrogen biogeochemistry in the Caribbean sponge, *Xestospongia muta*: a source or sink of dissolved inorganic nitrogen? PLoS One, 8(8), e72961.

Fiore, C. L., Jarett, J. K., & Lesser, M. P. (2013b). Symbiotic prokaryotic communities from different populations of the giant barrel sponge, *Xestospongia muta*. Microbiology open, 2(6), 938-952.

Fiore, C. L., Jarett, J. K., Olson, N. D., & Lesser, M. P. (2010). Nitrogen fixation and nitrogen transformations in marine symbioses. Trends in microbiology, 18(10), 455-463.

Fiore, C. L., Jarett, J. K., Steinert, G., & Lesser, M. P. (2020). Trait-Based comparison of coral and Sponge Microbiomes. Scientific reports, 10(1), 1-16.

Freeman, C. J., & Thacker, R. W. (2011). Complex interactions between marine sponges and their symbiotic microbial communities. Limnology and Oceanography, 56(5), 1577-1586.

Freeman, N. K., Lindgren, F. T., Ng, Y. O., & Nichols, A. V. (1952). Infrared spectra of some lipoproteins and related lipids. J. Biol. Chem., Vol. 203, pp. 293-304.

Gantt, S. E., McMurray, S. E., Stubler, A. D., Finelli, C. M., Pawlik, J. R., & Erwin, P. M. (2019). Testing the relationship between microbiome composition and flux of carbon and nutrients in Caribbean coral reef sponges. Microbiome, 7(1), 124.

Gillan, F. T., Stoilov, I. L., Thompson, J. E., Hogg, R. W., Wilkinson, C. R., & Djerassi, C. (1988). Fatty acids as biological markers for bacterial symbionts in sponges. Lipids, 23(12), 1139-1145.

Gloeckner, V., Wehrl, M., Moitinho-Silva, L., Gernert, C., Schupp, P., Pawlik, J. R., ... & Hentschel, U. (2014). The HMA-LMA dichotomy revisited: an electron microscopical survey of 56 sponge species. The Biological Bulletin, 227(1), 78-88.

Hardoim, C. C., & Costa, R. (2014). Microbial communities and bioactive compounds in marine sponges of the family *Ircinidae*: a review. Marine Drugs, 12(10), 5089-5122.

Hentschel, U., Piel, J., Degnan, S. M., & Taylor, M. W. (2012). Genomic insights into the marine sponge microbiome. Nature Reviews Microbiology, 10(9), 641-654.

Hill, M. S., & Hill, A. L. (2002). Morphological plasticity in the tropical sponge *Anthosigmella varians*: responses to predators and wave energy. The Biological Bulletin, 202(1), 86-95.

Karatay, S. E., & Dönmez, G. (2011). Microbial oil production from thermophile cyanobacteria for biodiesel production. Applied Energy, 88(11), 3632-3635.

Kooijman, B., & Kooijman, S. A. L. M. (2010). Dynamic energy budget theory for metabolic organisation. Cambridge university press.

Langille MGI (2018) Exploring Linkages between taxonomic and functional profiles of the human microbiome. mSystems 3:e00163-17

Langille, M.G.I., Zaneveld. J., Caporaso. J.G., McDonald D., Knights D., Reyes J.A., Clemente J.C., Burkepile D.E., Thurber R.L.V., Knight R., Beiko R.G., Huttenhower C. (2013)

Predictive functional profiling of microbial communities using 16S rRNA marker gene sequences. Nat Biotechnol 31:814

Lesser, M. P. (2006). Benthic–pelagic coupling on coral reefs: feeding and growth of Caribbean sponges. Journal of Experimental Marine Biology and Ecology, 328(2), 277-288.

Lesser, M. P., & Slattery, M. (2013). Ecology of Caribbean sponges: are top-down or bottom-up processes more important? PloS one, 8(11), e79799. doi:10.1371/journal.pone.0079799

Lesser, M. P., & Slattery, M. (2015). Picoplankton consumption supports the ascidian *Cnemidocarpa verrucosa* in McMurdo Sound, Antarctica. Marine Ecology Progress Series, 525, 117-126.

Lesser, M. P., & Slattery, M. (2018). Sponge density increases with depth throughout the Caribbean. Ecosphere, 9(12), e02525.

Lesser, M. P., B. Mueller, M. S. Pankey, K. J. Macartney, M. Slattery, and J. M. Goeij. (2020) Depth-dependent detritus production in the sponge, Halisarca caerulea. Limnol. Oceanogr. lno.11384. doi:10.1002/lno.11384

Lesser, M. P., Slattery, M., & Leichter, J. J. (2009). Ecology of mesophotic coral reefs. Journal of Experimental Marine Biology and Ecology, 375(1-2), 1-8.

Lesser, M. P., Slattery, M., & Mobley, C. D. (2018). Biodiversity and functional ecology of mesophotic coral reefs. Annual Review of Ecology, Evolution, and Systematics, 49, 49-71.

Lesser, M. P., Slattery, M., Laverick, J. H., Macartney, K. J., & Bridge, T. C. (2019). Global community breaks at 61 m on mesophotic coral reefs. Global Ecology and Biogeography, 28(10), 1403-1416.

Lüskow, F. T., Kløve-Mogensen, K., Tophøj, J., Pedersen, L. H., Riisgård, H. U., & Eriksen, N. T. (2019). Seasonality in lipid content of the demosponges *Halichondria panicea* and *H. bowerbanki* at two study sites in temperate Danish waters. Frontiers in Marine Science, 6, 328.

Maldonado, M., Aguilar, R., Bannister, R. J., Bell, J. J., Conway, K. W., Dayton, P. K., ... & Leys, S. P. (2017). Sponge grounds as key marine habitats: a synthetic review of types, structure, functional roles, and conservation concerns.

Maldonado, M., Ribes, M., & van Duyl, F. C. (2012). Nutrient fluxes through sponges: biology, budgets, and ecological implications. In Advances in marine biology (Vol. 62, pp. 113-182). Academic Press.

Masuko, T., Minami, A., Iwasaki, N., Majima, T., Nishimura, S. I., & Lee, Y. C. (2005). Carbohydrate analysis by a phenol–sulfuric acid method in microplate format. Analytical biochemistry, 339(1), 69-72.

McClintock J., Heine J., Slattery M., and Weston J. (1991). Biochemical and Energetic Composition, Population Biology, and Chemical Defense of the Antarctic Ascidian *Cnemidocarpa verrucosa* lesson. Journal of Experimental Marine Biology and Ecology, 147, 163-175. doi:10.1016/0022-0981(91)90180-5.

McMurdie P.J., Holmes S. (2015) Shiny-phyloseq: web application for interactive microbiome analysis with provenance tracking. Bioinformatics 31:282-283

McMurray, S. E., Johnson, Z. I., Hunt, D. E., Pawlik, J. R., & Finelli, C. M. (2016). Selective feeding by the giant barrel sponge enhances foraging efficiency. Limnology and Oceanography, 61(4), 1271-1286.

McMurray, S. E., Stubler, A. D., Erwin, P. M., Finelli, C. M., & Pawlik, J. R. (2018). A test of the sponge-loop hypothesis for emergent Caribbean reef sponges. Marine Ecology Progress Series, 588, 1-14.

Mohamed, N. M., Colman, A. S., Tal, Y., & Hill, R. T. (2008). Diversity and expression of nitrogen fixation genes in bacterial symbionts of marine sponges. Environmental Microbiology, 10(11), 2910-2921.

Moitinho-Silva, L., Steinert, G., Nielsen, S., Hardoim, C. C., Wu, Y. C., McCormack, G. P., ... & Hentschel, U. (2017). Predicting the HMA-LMA status in marine sponges by machine learning. Frontiers in Microbiology, 8, 752.

Morganti, T., Coma, R., Yahel, G., & Ribes, M. (2017). Trophic niche separation that facilitates co-existence of high and low microbial abundance sponges is revealed by in situ study of carbon and nitrogen fluxes. Limnology and Oceanography, 62(5), 1963-1983.

Morley, S. A., Berman, J., Barnes, D. K., de Juan Carbonell, C., Downey, R. V., & Peck, L. S. (2016). Extreme phenotypic plasticity in metabolic physiology of Antarctic demosponges. Frontiers in Ecology and Evolution, 3, 157.

Morley, S. A., Berman, J., Barnes, D. K., de Juan Carbonell, C., Downey, R. V., & Peck, L. S. (2016). Extreme phenotypic plasticity in metabolic physiology of Antarctic demosponges. Frontiers in Ecology and Evolution, 3, 157.

Morrow, K. M., Fiore, C. L., & Lesser, M. P. (2016). Environmental drivers of microbial community shifts in the giant barrel sponge, *Xestospongia muta*, over a shallow to mesophotic depth gradient. Environmental Microbiology, 18(6), 2025-2038.

Mueller, B., de Goeij, J. M., Vermeij, M. J., Mulders, Y., van der Ent, E., Ribes, M., & van Duyl, F. C. (2014). Natural diet of coral-excavating sponges consists mainly of dissolved organic carbon (DOC). PloS one, 9(2), e90152.

Olson, J. B., & Gao, X. (2013). Characterizing the bacterial associates of three Caribbean sponges along a gradient from shallow to mesophotic depths. FEMS microbiology ecology, 85(1), 74-84.

Padilla, D. K., & Savedo, M. M. (2013). A systematic review of phenotypic plasticity in marine invertebrate and plant systems. In Advances in marine biology (Vol. 65, pp. 67-94). Academic Press.

Parada A.E., Needham D.M., Fuhrman J.A. (2016) Every base matters: Assessing small subunit rRNA primers for marine microbiomes with mock communities, time series and global field samples. Environ Microbiol 18:1403–1414

Pawlik, J. R. (2011). The chemical ecology of sponges on Caribbean reefs: natural products shape natural systems. Bioscience, 61(11), 888-898.

Pawlik, J. R., Loh, T. L., & McMurray, S. E. (2018). A review of bottom-up vs. top-down control of sponges on Caribbean fore-reefs: what's old, what's new, and future directions. PeerJ, 6, e4343.

Pawlik, J. R., Loh, T. L., McMurray, S. E., & Finelli, C. M. (2013). Sponge communities on Caribbean coral reefs are structured by factors that are top-down, not bottom-up. PLoS One, 8(5), e62573.

Pita, L., Rix, L., Slaby, B. M., Franke, A., & Hentschel, U. (2018). The sponge holobiont in a changing ocean: from microbes to ecosystems. Microbiome, 6(1), 46.

Poppell, E., Weisz, J., Spicer, L., Massaro, A., Hill, A., & Hill, M. (2014). Sponge heterotrophic capacity and bacterial community structure in high-and low-microbial abundance sponges. Marine Ecology, 35(4), 414-424.

Rix, L., Ribes, M., Coma, R. Jahn, M… (2020) Heterotrophy in the earliest gut: a single-cell view of heterotrophic carbon and nitrogen assimilation in sponge-microbe symbioses. ISME J https://doi.org/10.1038/s41396-020-0706-3

Rubin-Blum, M., Antony, C. P., Sayavedra, L., Martínez-Pérez, C., Birgel, D., Peckmann, J., ... & Sahling, H. (2019). Fueled by methane: deep-sea sponges from asphalt seeps gain their nutrition from methane-oxidizing symbionts. The ISME journal, 13(5), 1209-1225.

Scott, A. R., & Pawlik, J. R. (2019). A review of the sponge increase hypothesis for Caribbean mesophotic reefs. Marine Biodiversity, 49(3), 1073-1083.

Slattery, M., & Lesser, M. P. (2015). Trophic ecology of sponges from shallow to mesophotic depths (3 to 150 m): comment on Pawlik et al. (2015). Marine Ecology Progress Series, 527, 275-279.

Slattery, M., Gochfeld, D. J., Diaz, M. C., Thacker, R. W., & Lesser, M. P. (2016). Variability in chemical defense across a shallow to mesophotic depth gradient in the Caribbean sponge *Plakortis angulospiculatus*. Coral Reefs, 35(1), 11-22.

Slattery, M., Lesser, M. P., Brazeau, D., Stokes, M. D., & Leichter, J. J. (2011). Connectivity and stability of mesophotic coral reefs. Journal of Experimental Marine Biology and Ecology, 408(1-2), 32-41.

Sokolova, I. M. (2013). Energy-limited tolerance to stress as a conceptual framework to integrate the effects of multiple stressors. Integrative and comparative biology, 53(4), 597-608.

Steinert, G., Taylor, M. W., Deines, P., Simister, R. L., De Voogd, N. J., Hoggard, M., & Schupp, P. J. (2016). In four shallow and mesophotic tropical reef sponges from Guam the microbial community largely depends on host identity. PeerJ, 4, e1936.

Thacker, R. W., and C. J. Freeman. 2012. Sponge-Microbe Symbioses. Recent Advances and New Directions, Adv. Mar. Biol. 62:57-111. doi: 10.1016/B978-0-12-394283-8.00002-3

Thomas, T., Moitinho-Silva, L., Lurgi, M., Björk, J. R., Easson, C., Astudillo-García, C., ... & Chaves-Fonnegra, A. (2016). Diversity, structure and convergent evolution of the global sponge microbiome. Nature communications, 7(1), 1-12.

Trussell, G. C., Lesser, M. P., Patterson, M. R., & Genovese, S. J. (2006). Depth-specific differences in growth of the reef sponge *Callyspongia vaginalis*: role of bottom-up effects. Marine Ecology Progress Series, 323, 149-158.

Voss, M., Bange, H. W., Dippner, J. W., Middelburg, J. J., Montoya, J. P., & Ward, B. (2013). The marine nitrogen cycle: recent discoveries, uncertainties and the potential relevance of climate change. Philosophical Transactions of the Royal Society B: Biological Sciences, 368(1621), 20130121.

Weisz, J. B., Lindquist, N., & Martens, C. S. (2008). Do associated microbial abundances impact marine demosponge pumping rates and tissue densities? Oecologia, 155(2), 367-376.

Wooster, M. K., McMurray, S. E., Pawlik, J. R., Morán, X. A., & Berumen, M. L. (2019). Feeding and respiration by giant barrel sponges across a gradient of food abundance in the Red Sea. Limnology and Oceanography, 64(4), 1790-1801.

Ye Y, Doak TG (2009) A parsimony approach to biological pathway reconstruction/inference for genomes and metagenomes. PLoS Comput Biol 5:e1000465

Zhang, F., Jonas, L., Lin, H., & Hill, R. T. (2019). Microbially mediated nutrient cycles in marine sponges. FEMS microbiology ecology, 95(11), 115.

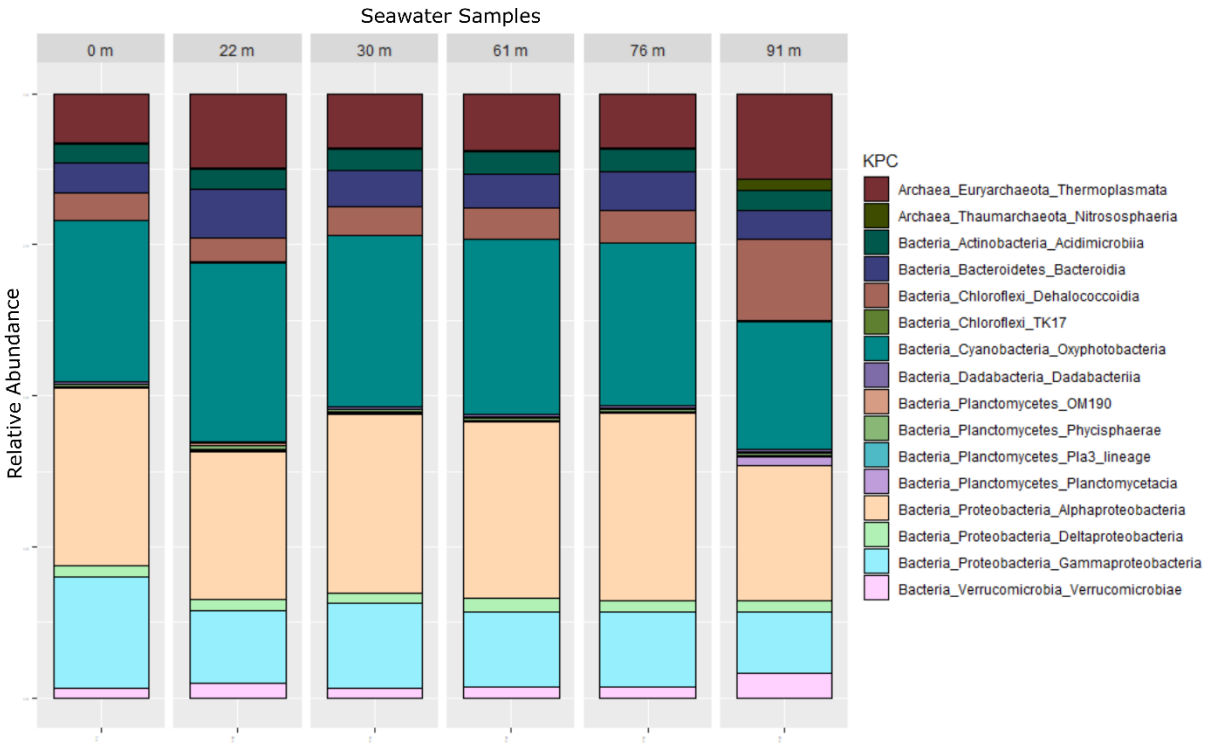

Figure 27 (S1). Average relative abundance (percentage) from the dominant Classes (comprising > 1% of reads) in the seawater sample microbiomes along a shallow to mesophotic depth gradient.

Chapter 4

Trophodynamics of the Sclerosponge *Ceratoporella nicholsoni* Along a Shallow to Mesophotic Depth Gradient

Revision submitted to *Coral Reefs*

Keir J. Macartney[1], M. Sabrina Pankey[1], Marc Slattery[2], Michael P. Lesser[1]

[1]University of New Hampshire, Department of Molecular, Cellular and Biomedical Sciences and School of Marine Science and Ocean Engineering, Durham, NH 03824 USA

kjm1049@wildcats.unh.edu

[2]University of Mississippi, Department of BioMolecular Science, Oxford, MS 38677 USA

Abstract

The sclerosponge *Ceratoporella nicholsoni* is a hyper-calcifying high microbial abundance (HMA) sponge. This sponge has been observed at high densities throughout the Caribbean in the mesophotic zone (30-150 m), as well as cryptic environments in shallow (<30 m) depths. Given the densities of this sponge, it could play an important role in the cycling of inorganic and organic sources of carbon and nitrogen at mesophotic depths. Additionally, there is broad interest in this sponge as a tool for paleobiology, paleoclimatology and paleoceanography. As a result, it is increasingly important to understand the ecology of these unique sponges in the underexplored Caribbean mesophotic zone. Here we show that this sponge increases in abundance from shallow depths into the mesophotic zone of Grand Cayman Island. We observed no significant differences in the stable isotope signatures of δ^{15}N and δ^{13}C of sponge tissue between depths. A predictive model of sponge diet with increasing depth shows that these sponges consume dissolved organic matter of algal and coral origin, as well as the consumption of particulate organic matter consistent with the interpretation of the stable isotope data. The taxonomic composition of the sclerosponge microbiome was invariant across the shallow to mesophotic depth range but did contain the Phylum *Chloroflexi*, known to degrade a variety of dissolved organic carbon sources. These data suggest that the depth distribution of this sponge may not be driven by changes in trophic strategy and is potentially regulated by other biotic or abiotic factors which is contrary to previous observations on emergent, open reef sponges found in the previous chapters.

Introduction

It is well-known that cryptic spaces in coral reefs are a crucial component of overall coral reef productivity (de Goeij and van Duyl 2007; de Goeij et al. 2013, 2017). These habitats may comprise up to 75-90% of total reef volume in the Caribbean (Ginsburg 1983; de Goeij et al. 2017) and are known to be net sinks of dissolved organic matter (DOM), and in particular dissolved organic carbon (DOC). Cryptic spaces also play a significant role in overall productivity of coral reefs and may improve adjacent coral reef health (Slattery et al. 2013). The primary components of cryptobenthic fauna in these habitats are sponges, primarily encrusting species, and the study of cryptic sponges has increased significantly in the last decade due to their potential role as major ecosystem engineers through the sponge loop (de Goeij et al. 2013; 2017). The "Sponge Loop Hypothesis" proposes that sponges consume DOM and produce large concentrations of cellular detritus, such as choanocyte cells, that are subsequently consumed by reef organisms.

The majority of these studies, however, have focused on shallow coral reefs (<30m), with far fewer studies on mesophotic coral reef ecosystems (MCEs; 30-150 m) where endemic communities of sponges can be found in the lower mesophotic (>60 m) zone of the Caribbean (Lesser et al. 2009; Slattery et al. 2011; Loya et al. 2016). Once exception is a recent study by Lesser et al. (2020) which showed that the encrusting sponge *Halisarca caerulea* produces significantly less detritus at mesophotic depths (~50 m) compared to conspecifics at shallow depths (~10 m). Since the production of detritus is a prerequisite for a functional sponge loop it demonstrated the broader need to understand the trophic ecology of the sponge fauna found in

the low-light environment of MCEs, which may mimic shallow water cryptic spaces, for our overall understanding of the functional ecology of sponges in MCEs.

One of the most understudied members of the sponge community are sclerosponges. Sclerosponges are slow-growing and deposit a calcium carbonate exoskeleton in sequential layers over time, and recent studies have suggested that the symbiotic prokaryotic microbiome of sclerosponges may have an important role in calcification (Garate et al. 2017; Germer et al. 2017). Sclerosponges are found throughout the tropics across a 1000 m depth range and can live for centuries (Lang and Hartman 1975; Benavides and Druffel 1986; Böhm et al. 1996; Swart et al. 1998). One species of sclerosponge, *Ceratoporella nicholsoni* (Fig. 28a), is commonly found within the reef framework, overhangs and small caves of Caribbean MCEs (Lang and Hartman 1975; Santavy et al. 1990; Vacelet et al. 2015). *Ceratoporella nicholsoni* produces a thin layer of siliceous spicule supported tissue over a dense aragonite skeleton (Lang and Hartman 1975; Vacelet et al. 2015). This species of sponge is commonly used for paleooceanographic reconstructions as it produces its skeleton at isotopic equilibrium with surrounding seawater (Benavides and Druffel 1986; Swart et al. 1998, 2002, 2010; Haase-Schramm et al. 2003), but relatively little is known about its general ecology, and trophic ecology in particular. While *C. nicholsoni* can be found at depths shallower than 30 m deep in the reef framework, it is much more common in MCEs below 30 m, where it grows openly on wall faces and overhangs (Lang and Hartman 1975; Vacelet et al. 2015). This particular species is the most conspicuous of the Caribbean sclerosponges (Lang and Hartman 1975; Vacelet et al. 2015) and forms dense communities in the low-light environments of MCEs, in some cases comprising 25-50% of total cover in overhangs and small caves (Lang and Hartman 1975). At depths below 70 m, this sponge and potentially other less common sclerosponge species may contribute significantly to

the emergent deep reef community and its structure (Lang and Hartman 1975; Swart et al. 1998; Vacelet et al. 2015) by assuming the functional role of scleractinian corals as a three-dimensional reef structure. Since this sponge is classified as a high microbial abundance (HMA) sponge (Santavy et al. 1990), it is very likely utilizing DOM in its diet (Yahel et al. 2003; de Goeij et al. 2013, 2017; Mueller et al. 2014). As a result, these sponges may contribute to DOM cycling (i.e.,

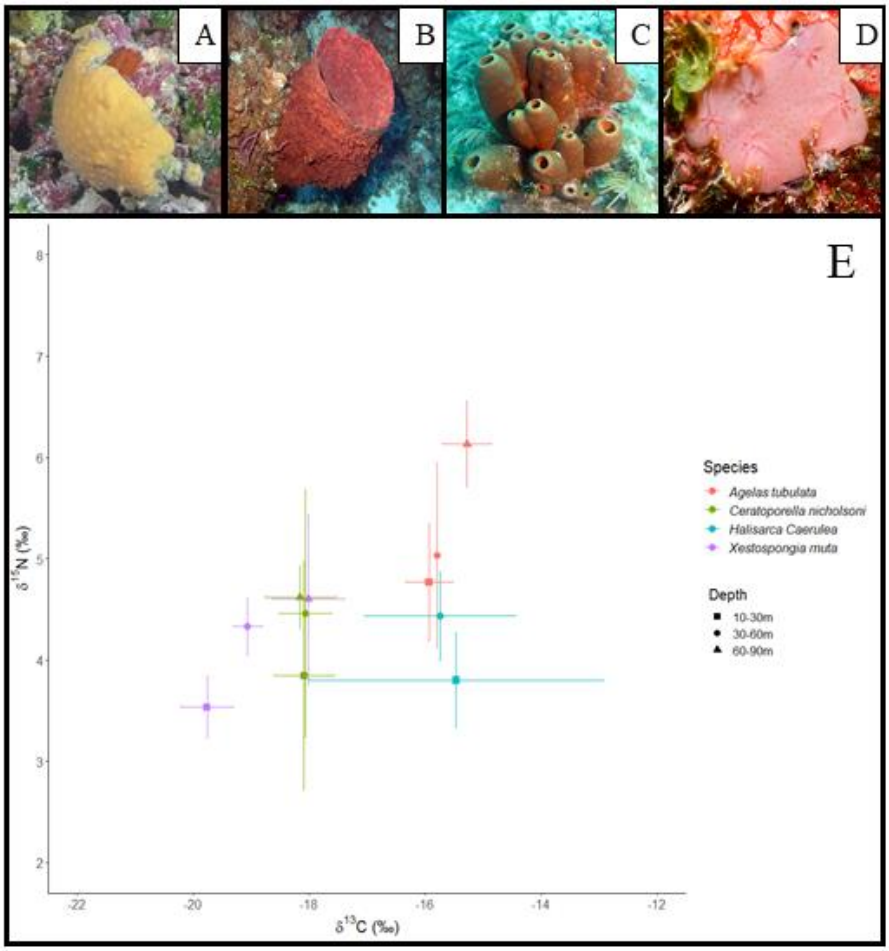

Figure 28. *In-situ* photos of **A)** *Ceratoporella nicholsoni* (photo: Keir Macartney), **B)** *Xestospongia muta* (photo: Michael Lesser), **C)** *Agelas tubulata* (photo: Liz Kintzing) and **D)** *Halisarca caerulea* (photo: Sabrina Pankey). **E)** Comparative bivariate plot of Caribbean coral reef sponge bulk $\delta^{13}C$ and $\delta^{15}N$ values (mean ± SD) along a shallow to mesophotic depth gradient from published literature. All data was binned to match the binning of depths in this publication. Data for *X. muta* were taken from Morrow et al. (2016), data for *A. tubulata* was taken from Slattery et al. (2011) and data for *H. caerulea* was taken from Lesser et al. (2020).

Sponge Loop) on MCEs.

As an HMA sponge the prokaryotic microbiome of *Ceratoporella nicholsoni* likely plays a significant role in its trophic ecology as reported for many HMA sponges (Hentschel et al. 2012; Pita et al. 2018), and specifically its ability to assimilate and translocate particulate organic matter (POM) and DOM for growth. Recent research has shown that detritus production is linked to the quantity of the POM and DOM available, and consumption of these resources relies on both the host and its microbiome (de Goeij et al. 2013, 2017; Mueller et al. 2014; Rix et al. 2016; Lesser et al. 2020). Additionally, the microbiome in many sponges is responsible for the production of secondary metabolites (Engel and Pawlik 2000; Taylor et al. 2007; Hentschel et al. 2012; Pita et al. 2018), and given the slow growth of *C. nicholsoni*, these compounds could be important in the prevention of overgrowth by competitors. While previous studies have analyzed the C. *nicholsoni* microbiome using traditional media-based isolation techniques (Santavy et al. 1990), many sponge associated microbes are nonculturable. The use of metagenetic techniques can increase both the recovery and resolution of the *C. nicholsoni* microbiome, and its potential function. Here we utilize bulk stable isotope techniques (SIA) and a diet reconstruction model, as well as 16s rRNA amplicon sequencing and predicted metagenomic content in order to characterize the community composition, potential function and the trophic ecology of these unique sponges at both shallow and mesophotic depths in the Cayman Islands. We hypothesize that this sponge will increase in abundance in the Grand Cayman mesophotic zone, that its diet will be a reflection of the available food resources and that it's microbiome will have broad metabolic potential, as observed in other sponges.

Methods

Site Description

Samples of the sclerosponge *Ceratoporella nicholsoni* were collected on reefs in the vicinity of the Kittiwake Anchor Buoy site, Grand Cayman (Lat: 19.362756, Long: -81.402437) along a shallow to mesophotic (10-100 m) depth gradient on Grand Cayman Island (Fig. S1). This site exhibits a spur and grove structure with a sloping reef structure between 15 – 60 m, at which point reef topography turns into a vertical wall. Additionally, based on data collected previously at this site (Lesser et al. 2019) the concentrations ($\mu mol\ l^{-1}$) of POC and PON increase significantly as depth increases into the mesophotic zone while DOC and DON decreases significantly as depth increases (Lesser et al. 2019).

Sample Collection

Samples were collected in January 2019 by divers utilizing mixed gas closed circuit rebreather systems and technical diving procedures for collection deeper than 30 m while open circuit SCUBA was used to collect samples above 30 m. Whole sponges were removed from the substrate using a hammer and chisel, brought to the surface in plastic bags, transported in seawater to a wet lab and immediately frozen at -4°C. Samples were transported to the University of New Hampshire while frozen for further analysis and stored at -80°C. Samples were binned into groups from 10-30 m (shallow) (n = 8), 31-60 m (upper mesophotic) (n = 5) and 61-90 m (lower mesophotic) (n = 9) where the seawater temperatures at approximately the mid-point of each depth grouping was 27.12°C at 22 m, 27.32°C at 46 m and 27.49°C at 76 m with temperatures measured as described in Lesser et al. (2009). Photosynthetically active

radiation (PAR: μmol quanta m^{-2} s^{-1}) decreases significantly at this site as depth increases into the mesophotic with irradiances at approximately the midpoint of each depth bin of 22 m = 263 μmol quanta m^{-2} s^{-1}, 46 m = 126 μmol quanta m^{-2} s^{-1}, and 76 m = 61 μmol quanta m^{-2} s^{-1} measured as described in Lesser et al. (2018).

Sclerosponge surveys

Sclerosponge abundance and percent cover were measured using replicate transects (n = 3) of 30 m length at depths of 37, 49, 67, 81 and 97 m, with1 m^2 quadrats (n = 5) positioned at random points along each transect. Since sclerosponges are primarily found in more cryptic environments (e.g., overhangs), these depths were chosen based on the presence of relevant habitat. It was not possible to enumerate sclerosponges with any degree of accuracy in the cryptic habitat at < 30 m. Specifically, each transect line began at an identified overhang where a 1 m^2 quadrat was placed. Following that, a random number generator was used to determine the next overhang to be analyzed (i.e., using numbers from one to five if the random number was "3" then the third overhang from the transect origin was measured). For each transect, at all depths, the number of overhangs analyzed was n = 5. All sclerosponges within each m^2 quadrat were counted, and the percent cover of these sclerosponges was estimated using the point intercept method.

Stable Isotope Analysis

Samples of *C. nicholsoni* tissue were taken by using a sterile razor to scrape tissue from the surface of the sponge. Tissue samples were dried at 55℃ for 24 h before pulverizing into a powder using a mortar and pestle. Samples of tissue were sent to the Marine Biological Laboratory (Woods Hole, MA) for the bulk analysis of particulate C and N as well as the natural abundance of the stable isotopes δ^{15}N and δ^{13}C. Prior to analysis samples were acidified using 1N HCL. Samples were analyzed using a Europa ANCA-SL elemental analyzer-gas chromatograph attached to a continuous-flow Europa 20-20 gas source stable isotope ratio mass spectrometer. The carbon isotope results are reported relative to Vienna Pee Dee Belemnite and nitrogen isotope results are reported relative to atmospheric air and both are expressed using the delta (δ) notation in units per mil (‰). The analytical precision of the instrument is ± 0.1‰, and the mean precision of sample replicates for δ^{13}C was ± 0.4 ‰ and δ^{15}N was ± 0.2 ‰. In order to avoid changes in δ^{15}N due to acidification (Schubert and Nielsen 2000), non-acidified tissue samples were sent to the Stable Isotope Laboratory at the University of Miami's Rosenstiel School of Marine Geosciences. The δ^{15}N of non-acidified samples was determined using a Costech CN analyzer interfaced to a Thermo Advantage V with δ^{15}N standards supplied from the International Atomic Energy Authority (IAEA) (*sensu* Mackenzie et al. 2015). Statistical analyses for differences between depths for all SIA variables were conducted utilizing ANOVA in R statistical software (version 3.4.2). Any variables not meeting the assumptions of normality were log transformed before analysis. The relative diet contribution was assessed using the R package "SIAR4" (Parnell et al. 2010) *sensu* Lesser et al. (2020). Source endmember values for algal DOM (δ^{13}C: -15.42‰, δ^{15}N: 0.80‰), coral DOM (δ^{13}C: -18.19‰, δ^{15}N: 0.26‰), and coral reef POM (δ^{13}C: -24.91‰, δ^{15}N: 5.62‰) were taken from (van Duyl et al. 2011a; van Duyl et al. 2018) and values for sponge derived detritus (δ^{13}C: --19.54‰, δ^{15}N: 2.56‰) were taken from

(Lesser et al. 2020). For the effects of depth in the mixing model both $\delta^{13}C$ and $\delta^{15}N$ stable isotope values for *Lobophora variegata* (Slattery and Lesser 2014) and *Montastraea cavernosa*, *Montastraea annularis* (now *Orbicella annularis*) and *Agaricia agaricities* (Lesser et al. 2010, Muscatine et al. 1989, Muscatine and Kaplan 1994) were included as averaged source end members for algal and coral DOM for their respective depths. The source end member data were taken from different sites in the Caribbean and are consistent with the known variation of these end member isotope values throughout the region and between depths (e.g., Lesser et al. 2020). The trophic enrichment factor applied for $\delta^{13}C$ was 0.5 ± 0.5%, and for $\delta^{15}N$ a trophic enrichment factor of 3.0 ± 0.5% was applied *sensu* van Duyl et al. (2018) and Lesser et al. (2020).

DNA Isolation and 16s rRNA amplicon sequencing

To obtain microbial genomic DNA, *C. nicholsoni* tissue was removed from the calcareous skeleton using a sterile razor with care taken to avoid inclusion of $CaCo_3$ debris from the skeleton into the sample. Approximately 200-300 mg of tissue were removed. Sponge DNA was isolated using a Qiagen DNeasy PowerSoil extraction kit with the manufacture's protocol modified as follows. Sponge tissue was added to the PowerSoil bead tubes with 5 µl of Proteinase K (20mg/ml stock in 10% SDS) and 2 µl of RNAse (Qiagen) before incubation at 55◦C for 18 hours. After incubation, PowerSoil Kit Solution 1 was added, and samples subsequently underwent a bead beating step using a Qiagen Tissue Lyser for 5 minutes at 50 hertz. The Qiagen DNeasy PowerSoil kit standard instructions were followed post bead beating to produce DNA samples.

Microbial DNA was amplified using the polymerase chain reaction (PCR) with primer sets targeting the universal prokaryotic 16S rRNA gene. Degenerate primers designed to amplify the hypervariable region V3-V4 of the 16S rRNA gene were used and included a forward primer 515F (5'- GTGYCAGCMGCCGCGGTAA; Parada et al. (2016)) and reverse primer 806R (5'- GGACTACN- VGGGTWTCTAAT; Apprill et al. (2015)). Fluidigm linker sequences CS2 (5'- ACACTGACGACATGGTTC- TACA) and CS2 (5'- TACGGTAGCAGAGACTTGGTCT) were added to the 5' end of both forward and reverse primers to facilitate Illumina MiSeq. The 16S rRNA gene PCR consisted of a 25 µl reaction with 12.5 µl AmpliTaq Gold 360 Master Mix (Applied Biosystems), 1.0 µl GC-enhancer, 0.5 µl 515F (10 µM) and 0.5 µl 806R (10 µM), 2.0 µl of DNA template (40-60 ng) and 8.5 µl nuclease free water (Integrated DNA Technologies, Coralville, Iowa). Reactions were performed using the following protocol: initial denaturation for 10 min at 95◦C, 30 cycles of 95◦C for 45 s, 50◦C for 60 s, and 72◦C for 90 s, followed by a 10 min extension at 72°C. The PCR products were then electrophoresed on a 1% agarose gel. The 16S rRNA PCR amplicons containing Fluidigm linkers were sequenced on an Illumina MiniSeq System employing V2 chemistry (2 x 150 bp reads) at the University of Illinois at Chicago (UIC) Research Resources Center's Sequencing Core. The amplicon sequence variants (ASVs) were inferred and tabulated across sclerosponge samples using "DADA2" (Callahan et al, 2016) using an established bioinformatic pipeline (Lesser et al. 2020).

Analyses of the microbial communities of *C. nicholosoni* were done utilizing the R package "PhyloSeq" (McMurdie et al. 2016) in R *sensu* (Lesser et al. 2020). Samples with fewer than 10,000 counts were filtered from the ASV count table. Additionally, ASVs detected in more than 2 samples and had at least 10 occurrences across samples were retained during the filtering process. The samples were then rarefied in order to account for sampling effort. To test alpha

diversities, the Shannon richness index was used. Ordination plots were produced based on Bray-Curtis distances using nonmetric multidimensional scaling (NMDS) (Stress value = <0.0001). To assess compositional differences at varying taxonomic scales, the rarefied ASV count table was consolidated by rank using the PhyloSeq "tax_glom" function and then raw counts were transformed to center log rations using the "transform" function (CLR) from the R package "microbiome" (Callahan et al. 2016). Compositional differences between depths were tested using PERMANOVA with the Adonis function from the R package "vegan". Any differences observed during post hoc testing at phylum level for taxa between depths were tested using ANOVA and Tukey's HSD. Raw 16S rRNA reads were submitted to the NCBI Sequence Read Archive under BioProject accession number PRJNA555077.

Metagenomic functional abundances were predicted using "PICRUSt2" v2.1.0–b (https://github.com/picrust/picrust2/wiki) (Langille et al. 2013; Langille 2018). The 16S rRNA ASVs inferred by DADA2 were aligned with "HMMER" (Eddy 2008) and then placed in a reference tree provided by PICRUSt2 using "EPA–ng" and "GAPPA" (Barbera et al. 2019). Gene family numbers were predicted for 16S rRNA as well as KEGG functions (*i.e.*, EC and KO accessions) using Hidden State Prediction ("castor*"*) based on 16S rRNA ASV abundances and phylogenetic proximity to reference taxa with available genomes. In order to minimize error in gene content prediction due to poor matches to available genomes, any ASVs receiving Nearest-Sequenced-Taxon-Index (NSTI) scores below two were removed from subsequent analyses. Abundances of biological pathways encoded by microbiomes were then predicted using *MinPath* (Ye and Doak 2009). Abundances of KEGG genes of interest and all pathways from "MetaCyc" inferences were assessed for differences between depth zones using ANOVA on relative abundances normalized to the total reads in the sample. KEGG genes of interest were selected to

assess carbon and nitrogen metabolism, secondary metabolite production and indications of stress, such as genes encoding for heat shock proteins.

Results

Sclerosponge surveys

Both percent cover (ANOVA: $F_{4,14} = 82.33$, $P<0.0001$) and abundance per m^{-2} (ANOVA: $F_{4,14} = 100.01$, $P<0.0001$) of *C. nicholsoni* significantly increased with depth from the upper mesophotic zone (31-60 m) to the lower mesophotic zone (61-90m) (Fig. 29). At lower mesophotic depths sponges were both more abundant and had significantly greater percent cover than those found in the upper mesophotic zone (Tukey's HSD, $P<0.05$), and were qualitatively larger than their shallow water counterparts inferred based on fewer individuals per m m^{-2} but increased percent cover.

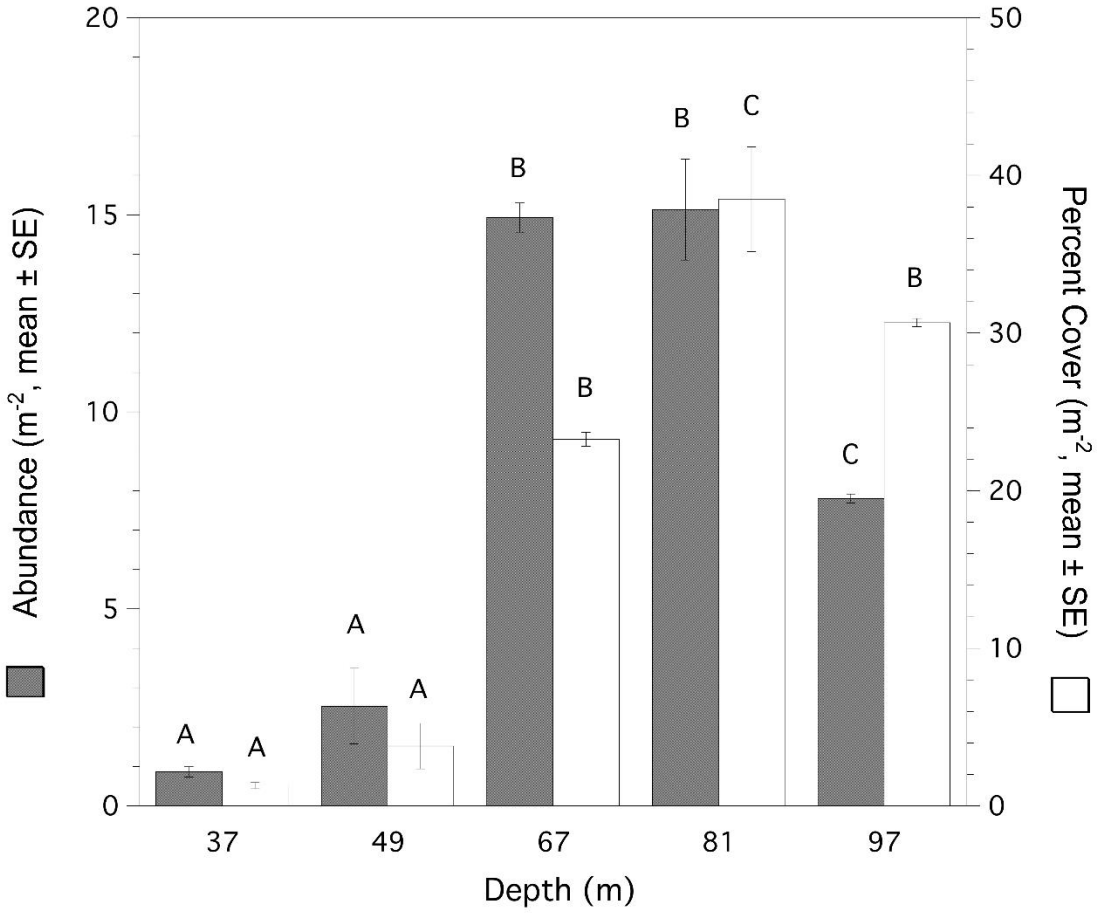

Figure 29. Depth dependent mean abundance (± SE) and percent cover (± SE) per m² of *Ceratoporella nicholsoni* in the Grand Cayman mesophotic zone. Depths with common superscripts are not significantly different from each other (Tukey's HSD, $P<0.05$).

Stable isotopes

There were no significant differences between the sclerosponge tissue $\delta^{13}C$ (ANOVA: $F_{2,19} = 0.061$, $P = 0.941$), $\delta^{15}N$ (ANOVA: $F_{2,19} = 1.4907$, $P = 0.25$) or C:N ratios (ANOVA: $F_{2,19} = 0.912$, $P = 0.418$) as a function of depth (Fig. 28e, Table S1). A non-significant enrichment between ~0.5-1.0‰ was found for acidified samples (Table S2), similar to previous results (Kolasinski et al. 2008). We used the results from non-acidified samples for all downstream

analyses. The SIAR4 diet reconstruction shows high variability in source contributions to sclerosponge diets and there were no significant differences between depths in the reconstructed diets (Fig. 30, Table S3). There is, however, a larger contribution of benthic derived DOM in *C. nicholosoni*, with coral and algal DOM contributing approximately 40-70% to the total diet compared to POM. And there is an increase in both algal and coral DOM in the diet of these sponges as depth increases into the mesophotic zone (Fig. 30, Table S3), while live and detrital POM contributes approximately 20-50% to the diet which decreases with increasing depth (Fig. 30, Table S3).

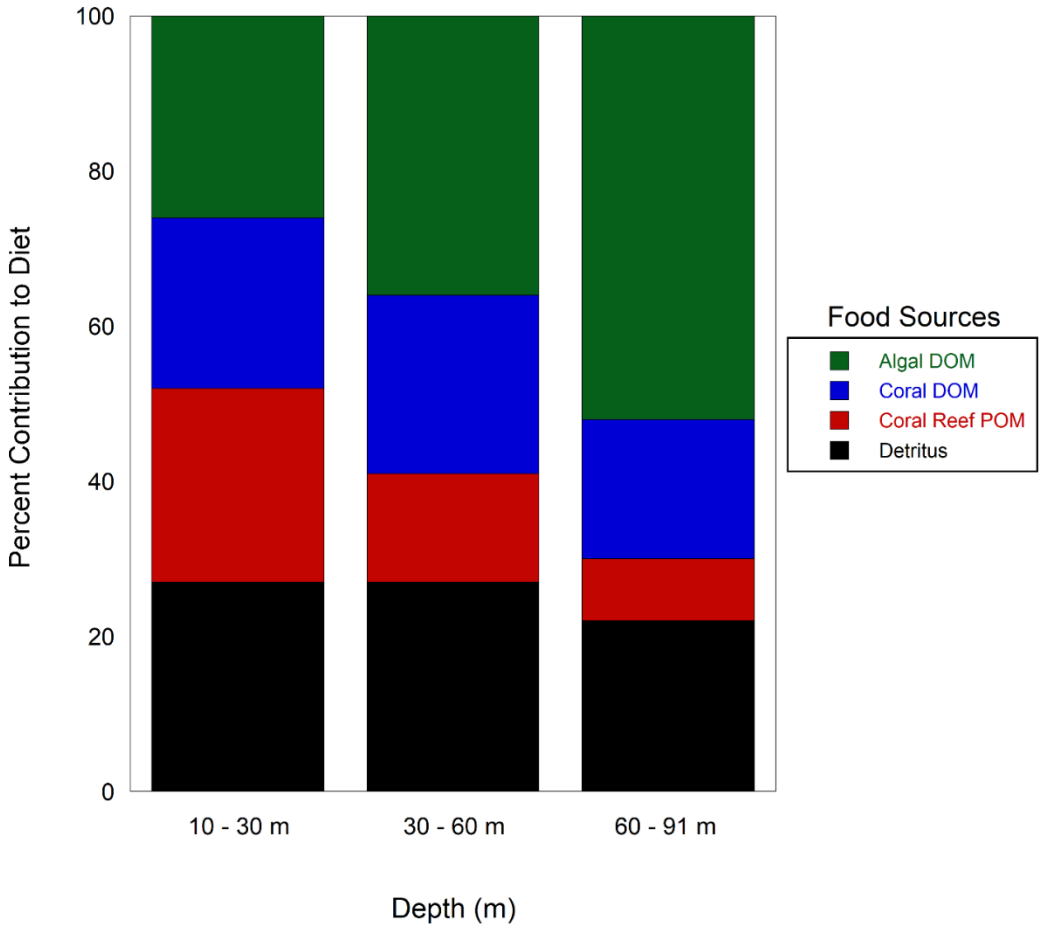

Figure 30. Bayesian diet reconstruction of *Ceratoporella nicholsoni* diet along a shallow to mesophotic depth gradient showing the mean percent contribution of each food source to the sclerosponge diet.

16s rRNA metabarcoding and predictive functional profiling

A total of 805,756 16S rRNA MiniSeq read-pairs were initially recovered from sequencing. After merging and quality trimming with DADA2, 692, 894 read-pairs remained. These ranged from 37,833 to 19,217 with a mean of 30,125 ± 3,720 reads per sample. A total of 858 unique ASVs were initially recovered, but ASVs unique to a single sample or with fewer than 5 total observations were removed from the dataset, resulting in a total of 412 unique ASVs for downstream analyses.

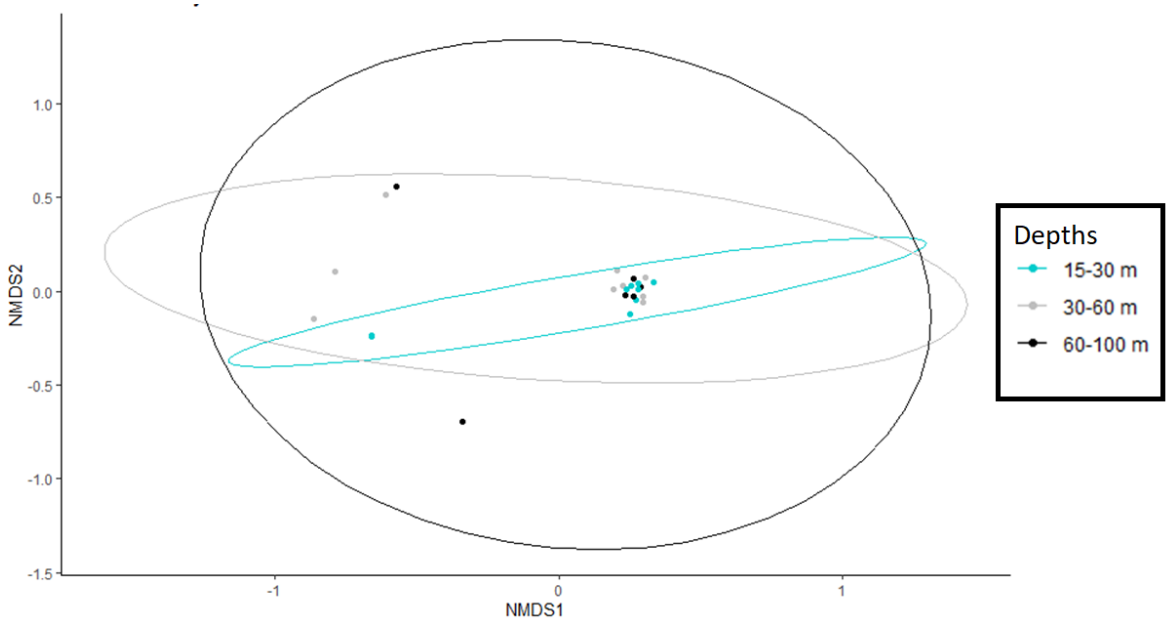

Figure 31. Multidimensional analysis of the β-diversity estimates using Bray–Curtis distance matrices of ASV composition for *Ceratoporella nicholsoni* microbial community composition between depths. The 95% confidence interval (CI) ellipses are drawn to show the depth groupings.

The multidimensional analysis of the Beta diversity using Bray-Curtis distance matrixes showed no significant difference between microbial community ASV composition between depth zones (PERMANOVA: $F_{2,19} = 0.893$, $P = 0.54$) (Fig. 31). Both phyletic composition (PERMANOVA: $F_{2,19} = 1.597$, $P = 0.063$) and class level composition (PERMANOVA: $F_{2,19}$ =

0.901, P = 0.578) did not differ significantly between depths With the exception of the Phylum *Dadabacteria*, no significant differences in overall phyletic abundance between depth zones were found in *C. nicholsoni* (Fig. S2). There were significant differences between depths in the *Dadabacteria* (PERMANOVA: $F_{2,19}$ = 5.13, P = 0.015) (Fig. S2), for which higher total counts were observed in mesophotic compared to shallow depths (Tukey's HSD <0.05). In the microbiomes of sampled *C. nicholsoni* 84% of the reads belong to ASVs of the following 5 phyla; *Chloroflexi* (32%, ± 5%, mean ± SD), *Thaumarcheaota* (16% ± 5%), *Proteobacteria* (15%, ± 3%), *Acidobacteria* (12%, ± 4%) and *Actinobacteria* (9%, ± 2%) (Fig. S3). Within the *Chloroflexi* phylum, classes "TK17" and *Dehalococcoidia* made up 12% ± 3% and 10% ± 4% of the total microbiome respectively (Fig. 32, S4). Within the *Thaumarcheota*, the *Nitrososphaeria* comprise 15%± 4% of the total microbiome (Fig. 32, S4). The Proteobacteria are dominated by the *Gammaproteobacteria* and the *Alphaproteobacteria*, comprising 7% ± 2% and 4% ± 1%, respecitively, of the total microbiome. Within the *Acidobacteria*, dominant classes include the *Acidobacteriia* (3% ± 2% of total microbiome) and "Subgroup 9" (4% ± 2% of total microbiome). The *Actinobacteria* are almost exclusively composed of the class *Acidimicrobiia*, which is 8% ± 3% of the total microbiome of *C. nicholsoni* (Fig. 32, S4). The Shannon-Alpha diversity of all sponges ranged between 4.78 and 3.42 but there were no significant differences between depths (ANOVA: $F_{2,19}$ = 0.282, P = 0.758) (Fig. S5)

Functional profiling between depths was accomplished with PICRUSt2. The mean NSTI score was 0.41 ± 0.061 (mean ± SD) and ranged between 0.31 to 0.54. There were significant differences in mean NSTI scores between depths (ANOVA: $F_{2,19}$ = 5.931, P = 0.009), with shallow samples returning higher scores (0.47) compared to the lower and upper mesophotic samples (Tukey's HSD = <0.05). The analysis returned 238 MetaCyc pathways and 4,051

unique KO genes. Of the 238 pathways, only pathway "GLYCOGENSYNTH-PWY" (glycogen biosynthesis I (from ADP-D-Glucose)) had significant enrichment in the pathway for shallow depths compared to lower mesophotic depths (ANOVA: $F_{2,19} = 0.971$, FDR adjusted P = 0.022). KEGG genes of interest (Table 1) were tested for differences between depths and while no significant differences were found (ANOVA: FDR adjusted P>0.05), all genes of interest (Table S4) were present in the inferred metagenome of the samples.

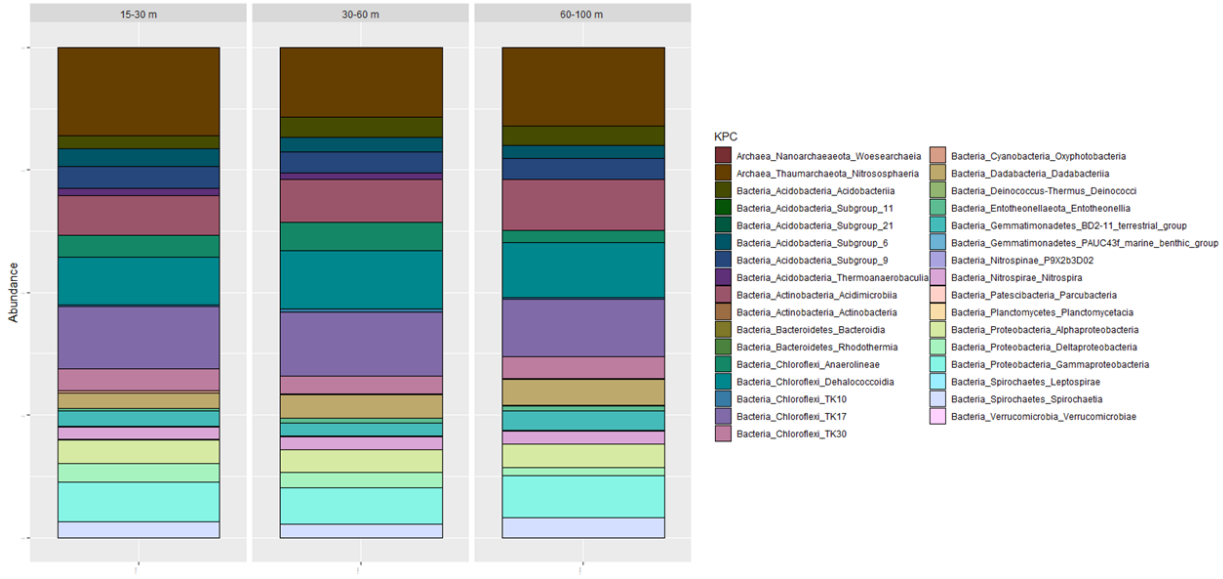

Figure 32. Mean relative abundance (percentage) at the Class level for the community composition of the *Ceratoporella nicholsoni* microbiome along a shallow to mesophotic depth gradient.

Discussion

The percent cover surveys of *C. nicholsoni* in Grand Cayman follow a similar pattern to the percent cover observed for *C. nicholsoni* in Discovery Bay, Jamaica described by Lang and Hartman (1975). Our study shows *C. nicholsoni* occupies approximately 25% to 35% of relevant habitat space (i.e., wall overhangs and small caverns) between the depths of 67 to 97 m, making it one of the dominant members of the community on Grand Cayman lower mesophotic reefs

(Fig. 29). This pattern of distribution is similar to those seen in non-calcareous siliceous sponges on open habitat space in the mesophotic throughout the Caribbean (Lesser 2006; Lesser et al. 2009, 2019; Slattery and Lesser 2015; Lesser and Slattery 2018). That distribution is influenced by food availability, both DOM and POM, but nitrogen rich POM that increases in quantity with depth is believed to be essential for the development and maintenance of increasing sponge biomass with increasing depth. (Lesser 2006; Trussell et al. 2006; Lesser et al. 2009, 2018; Slattery et al. 2011; Slattery and Lesser 2015; Morrow et al. 2016). As sclerosponges are considered low-light species, found primarily in the reef framework at depths shallower than 50 m (Lang and Hartman 1975; Vacelet et al. 2015), and below large overhangs and caverns in the lower mesophotic (Lang and Hartman 1975) the factors that influence emergent sponge distributions may not regulate sclerosponge distributions. Here we addressed whether the trophic ecology of these sponges is similar to that of open reef sponges where food quality and quantity play an important role in the ecological depth distributions of sponges throughout the Caribbean (Lesser and Slattery, 2018; Lesser et al. 2018).

The stable isotopes of *C. nicholsoni* do not reveal any significant depth-dependent changes (Fig. 28e) in trophic strategy, which is contrary to previous studies of sponges where stable isotopic signatures in the mesophotic show clear patterns of enrichment with depth, and often transitions from photoautotrophy to heterotrophy (Slattery et al. 2011; Morrow et al. 2016; Lesser et al. 2020). Previous studies have shown significant increases in $\delta^{15}N$ between shallow and mesophotic depths (Fig. 28e) in *Xestospongia muta* (Fig. 28b), *Agelas tubulata* (Fig. 28c) and *Halisarca caerulea* (Fig. 28d) indicating a shift from photoautotrophic resources to heterotrophic resources such as bacterioplankton, which are more abundant in the mesophotic (Lesser 2006; Lesser et al. 2019, 2020). The emergent sponges *X. muta* and *A. tubulata* also

showed significant increases in $\delta^{13}C$ (Fig. 28e) which in *X. muta* has been hypothesized to be the result of the decrease of photoautotrophic cyanobacteria in the microbiome as depth increases (Morrow et al. 2016). The encrusting and generally cryptic sponge *H. cearulea* did not have a significant decrease in $\delta^{13}C$ (Fig. 28e) in a study by Lesser et al. (2020), which is similar to the patterns observed for *C. nicholsoni*, and potentially due to the low-light environments they are found in.

The close grouping of the isotopic signatures from *C. nicholsoni* (Fig. 28e, Table S1) indicates that contributions to their diet from their microbiome and the consumption of DOM and POM in these sponges are similar throughout their depth distribution. The values for these sponges $\delta^{13}C$ (~ -18‰) are slightly higher than those typically found in marine phytoplankton (-19 to -24‰) but within the typical range for DOM (-16 to -23‰) (Fry 2006; Slattery et al. 2011; van Duyl et al. 2011b, 2018; Lesser et al. 2020). The $\delta^{15}N$ (~ 4.5‰) of the sampled sclerosponges is similar to the range for both bulk POM and DOM (1-6‰) (Fry 2006; Slattery et al. 2011; van Duyl et al. 2011, 2018; Ren et al. 2012). Taken together, it appears this sponge is dependent primarily on DOM as a carbon source, as observed in the diet reconstruction, but does consume picoplankton as do many HMA sponges (de Goeij et al. 2017; McMurray et al. 2018). The $\delta^{13}C$ and $\delta^{15}N$ values for this sponge are similar to open reef HMA sponges from shallow waters (Fig. 28e) (Freeman and Thacker 2011; van Duyl et al. 2011, 2018; Morrow et al. 2016; Lesser et al. 2020). The diet reconstruction for the sclerosponges indicates a reliance on DOM (60-70%) from benthic primary producers with the remainder of the diet made up of live and detrital POM. While there is a large amount of variation in the diet reconstruction model (Table S3), it supports the stable isotope results, and its interpretation. However, this sponge does appear to consume more detrital matter and POM (Fig 30) compared to a diet reconstruction

from *H. caerulea* (Lesser et al. 2020) which is likely a reflection of this sponge's unique microbial community and the nutrient cycling processes found within that community. For instance, we do not know whether the microbiome of *C. nicholsoni* is involved in the uptake of DOM and its re-synthesis and translocation to the host as amino acids as observed in other sponge species (Fiore et al. 2013, 2015; Shih et al. 2020). It should be noted that the diet reconstruction (Fig. 30) is based on end member values from other taxa or geographic areas, but no direct feeding measurements were made in this study and none are available from the literature for sclerosponges. Feeding studies should be done to validate the diet reconstruction model presented here.

The amplicon sequencing of 16s rRNA provides some insights into the metabolic functions and nutrient cycling in the sponge holobiont. The microbial community and the dominant taxa found in *C. nicholsoni* are similar to other prokaryotic microbiome communities in the Demospongiae (Thomas et al. 2016; Bayer et al. 2018; Pita et al. 2018) (Fig. 32). Interestingly, the *Chloroflexi* are the most abundant phyla in these sclerosponges, with higher abundances then observed in other HMA sponge microbiomes (Thomas et al. 2016; Pita et al. 2018). Specifically, in the order *Agelasida*, where *C. nicholsoni* is classified, *Chloroflexi* are often found in high abundances in sponges, generally between 10-29% (Bayer et al. 2018). The metagenomes of *Chloroflexi* from sponges shows wide metabolic diversity that includes the ability to fix carbon under aerobic an anaerobic conditions, conduct ammonia and nitrite uptake, as well as other precursors for multiple biosynthetic pathways including amino acid syntheses (Bayer et al. 2018) which could be translocated to the host (*sensu* Shih et al. 2020). In particular, complex carbohydrate degradation pathways have been reported in *Chloroflexi*, and other members of the prokaryotic microbiome of sponges, which may enhance their ability to utilize

the DOM pool on coral reefs (Slaby et al. 2017; Bayer et al. 2018). Bayer et al. (2018) also found that the *Chloroflexi* have the genomic potential for degradation of DOM, both its recalcitrant and labile forms. Additionally, the presence of *Thaumarcheota* in *C. nicholsoni* is not surprising as it is the most abundant archaeal phyla in HMA sponges (Thomas et al. 2016; Pita et al. 2018). Recent research on the *Thaumarchaeota* has shown that this phylum may be a keystone microbial taxa in some sponges, where it has the ability for ammonia oxidation (e.g., Engelberts et al. 2020).

The functional inference provided by the PICRUSt2 analysis of the prokaryotic microbiome supports the potential of these sponges to use multiple complex carbon, nitrogen and sulfur cycling pathways. Weighted NSTI scores serve as a method of testing the reliability of such predictions (Langille et al. 2013), which calculates dissimilarity between available reference genomes and the predicted metagenome. The NSTI scores in this study were high, with a mean score of 0.41 and shallow scores being the highest, at 0.47, compared to 0.37 for upper mesophotic and 0.38 for lower mesophotic samples. These particular scores are relatively high compared to previous PICRUSt analyses on sponge samples, being twice as high as those analyzed by Cleary et al. (2015). Higher NSTI scores generally result in lower predictive accuracy, but a recent study by Fiore et al. (2020) showed that despite moderate NSTI values (0.15 - 0.32), a PICRUSt analysis of the sponge *Xestospongia muta*, showed a strong correlation between the functional profiles of its metatranscriptome and the functional predictions for both coverage and abundance. This suggests that functional analyses such as PICRUSt2 may still provide meaningful predictions, even in some poorly characterized communities (i.e., sponge microbiomes).

The only significant difference between depths for both MetaCyc pathways and selected KEGG genes was the glycogen synthesis pathway, which was enriched in shallow samples relative to the lower mesophotic. However, multiple pathways and KEGG genes related to nitrogen, carbon, sulfur and phosphorous cycling were found to be abundant (Table S4), with the exception of photoautotrophic pathways. Genes for polyketide synthase and non-ribosomal peptides synthesis were also found (Table S4), indicating the sponge microbiome has the capability for chemical defense of this sponge, potentially for prevention of predation or allelopathic interactions with faster growing competitors (Pawlik 2011; Trindade-Silva et al. 2013; Slattery et al. 2016; Gutleben et al. 2019). The *Chloroflexi* also have the potential to participate in sponge chemical defense (Gutleben et al. 2019), and their high abundances may provide this slow growing sponge secondary metabolites to prevent overgrowth. These chemical compounds may be present at all depths, based on the predictive functional profiling, which would indicate that this sclerosponge does not require an increase in chemical defenses along the depth gradient. Such a finding would imply that predation or competitive allelopathic interactions are similar at all depths, unlike previous observations of varying chemical defenses in sponges from the shallow to mesophotic zone (e.g., Slattery et al. 2016).

Conclusions

Here we have shown that the sclerosponge, *C. nicholsoni*, similar to observations of sponge communities on coral reefs in the Caribbean (Lesser and Slattery 2018), does show an increase in percent cover and abundance into the mesophotic zone but that its microbiome community is invariant along the shallow to mesophotic depth gradient. The abundance of this sponge, and the metabolic diversity of its microbiome, at mesophotic depths suggests that this sponge may play a

previously underappreciated role in DOM cycling in these deep, low-light habitats. Additionally, it appears that this sponge does not change its trophic strategy with depth based on the stable isotope analyses and diet reconstruction model, which is contrary to previous studies on sponges, and some scleractinian corals, in the mesophotic. Factors such as its preference for low-light habitats and the energetic requirements (i.e., ion pumping) of calcification may be why this sponge exhibits an unexpected pattern in its trophic ecology compared to siliceous demosponges in the Caribbean. Other factors such as changes in sedimentation rates (given their preference for overhangs and vertical walls in the mesophotic), competition or mesophotic reef geomorphology (vertical wall versus slopes) could regulate this sponge's distribution as suggested by Lang and Hartman (1975). In particular, direct feeding studies on this sponge will be necessary for validating the diet reconstruction and isotope signatures presented here. Given the continuing interest in this sponge as an indicator species for paleobiology, paleoclimatology and paleoceanography, understanding its ecology and potential roles it plays on coral reefs at all depths will be critical for understanding the dynamics of MCEs.

Acknowledgements

We thank K. Morrow, E. Kintzing, and D. Gochfeld for field and laboratory support. We thank A. Weinheimer for insightful comments on the manuscript draft and statistical analyses. We thank Dr. Peter Swart for his comments on the manuscript, and for re-running non-acidified sponge tissue samples at the University of Miami's Rosenstiel School of Marine Geosciences. All sample collections complied with the laws of the Cayman Islands and the United States of America. Support was provided by NSF Biological Oceanography (OCE–1632348/1632333) to

MPL and MS respectively, and the University of New Hampshire Marine Biology Small Grants fund to KJM.

Conflict of Interest Statement

On behalf of all authors, the corresponding author states that there is no conflict of interest.

Literature Cited

Apprill A, McNally S, Parsons R, Weber L (2015) Minor revision to V4 region SSU rRNA 806R gene primer greatly increases detection of SAR11 bacterioplankton. Aquat Microb Ecol 75:129–137

Barbera P, Kozlov AM, Czech L, Morel B, Darriba D, Flouri T, Stamatakis A (2019) EPA-ng: massively parallel evolutionary placement of genetic sequences. Syst Biol 68:365–369

Bayer K, Jahn MT, Slaby BM, Moitinho-Silva L, Hentschel U (2018) Marine sponges as *Chloroflexi* hot spots: genomic insights and high-resolution visualization of an abundant and diverse symbiotic clade . mSystems 3:1–19

Benavides LM, Druffel ERM (1986) Sclerosponge growth rate as determined by 210Pb and Δ14C chronologies. Coral Reefs 4:221–224

Böhm F, Joachimski MM, Lehnert H, Morgenroth G, Kretschmer W, Vacelet J, Dullo WC (1996) Carbon isotope records from extant Caribbean and South Pacific sponges: Evolution of δ13C in surface water DIC. Earth Planet Sci Lett 139:291–303

Bongaerts P, Ridgway T, Sampayo EM, Hoegh-Guldberg O (2010) Assessing the "deep reef refugia" hypothesis: Focus on Caribbean reefs. Coral Reefs 29:1–19

Bongaerts P, Riginos C, Brunner R, Englebert N, Smith SR, Hoegh-Guldberg O (2017) Deep reefs are not universal refuges: Reseeding potential varies among coral species. Sci Adv 3:e1602373

Bongaerts P, Smith TB (2019) Beyond the "Deep Reef Refuge" Hypothesis: A Conceptual Framework to Characterize Persistence at Depth. Springer, Cham, pp 881–895

Callahan BJ, Sankaran K, Fukuyama JA, McMurdie PJ, Holmes SP (2016) Bioconductor workflow for microbiome data analysis: from raw reads to community analyses. F1000Research 5:1492

Cleary DFR, de Voogd NJ, Polónia ARM, Freitas R, Gomes NCM (2015) composition and predictive functional analysis of bacterial communities in seawater, sediment and sponges in the Spermonde Archipelago, Indonesia. Microb Ecol 70:889–903

Corredor JE, Wilkinson CR, Vicente VP, Morell JM, Otero E (1988) Nitrate release by Caribbean reef sponges,. Limnol Oceanogr 33:114–120

de Goeij JM, van Duyl FC (2007) Coral cavities are sinks of dissolved organic carbon (DOC). Limnol Oceanogr 52:2608–2617

de Goeij JM, Lesser MP, Pawlik JR (2017) Nutrient Fluxes and Ecological Functions of Coral Reef Sponges in a Changing Ocean. Climate Change, Ocean Acidification and Sponges. Springer International Publishing, pp 373–410

de Goeij JM, van Oevelen D, Vermeij MJA, Osinga R, Middelburg JJ, de Goeij AFPM, Admiraal W (2013) Surviving in a Marine Desert: The Sponge Loop Retains Resources Within Coral Reefs. Science 342:108–110

Eddy SR (2008) A Probabilistic Model of Local Sequence Alignment That Simplifies Statistical Significance Estimation. PLoS Comput Biol 4:e1000069

Engel S, Pawlik JR (2000) Allelopathic activities of sponge extracts. Mar Ecol Prog Ser 207:273–281

Engelberts JP, Robbins SJ, Goeij JM de, Webster NS, Aranda M, Bell SC, Webster NS (2020) Characterization of a sponge microbiome using an integrative genome-centric approach. ISME J 14:1100-1110

Fan L, Reynolds D, Liu M, Stark M, Kjelleberg S, Webster NS, Thomas T (2012) Functional equivalence and evolutionary convergence in complex communities of microbial sponge symbionts. Proc Natl Acad Sci USA 109:1878-1887

Fiore CL, Baker DM, Lesser MP (2013) Nitrogen Biogeochemistry in the Caribbean Sponge, Xestospongia muta: A Source or Sink of Dissolved Inorganic Nitrogen? PLoS One 8:e72961

Fiore CL, Jessica KJ, Steinert G, Lesser MP (2020) Trait-based comparison of coral and sponge microbiomes. Sci Rep 10:2340

Fiore CL, Labrie M, Jarett JK, Lesser MP (2015) Transcriptional activity of the giant barrel sponge, *Xestospongia muta* Holobiont: molecular evidence for metabolic interchange. Front Microbiol 6:364

Freeman CJ, Thacker RW (2011) Complex interactions between marine sponges and their symbiotic microbial communities. Limnol Oceanogr 56:1577–1586

Fry B (2006) Stable isotope ecology. Springer, New York

Garate L, Sureda J, Agell G, Uriz MJ (2017) Endosymbiotic calcifying bacteria across sponge species and oceans. Sci Rep 7:43674

Germer J, Cerveau N, Jackson DJ (2017) The holo-transcriptome of a calcified early branching metazoan. Front Mar Sci 4:81

Ginsburg RN (1983) Geological and biological roles of cavities in coral reefs. In: Perspectives on Coral Reefs, Barnes DJ, (ed), Australian Institute of Marine Sciences, Townsville, Australia, pp 148–153

Grottoli AG, Adkins JF, Panero WR, Reaman DM, Moots K (2010) Growth rates, stable oxygen isotopes ($\delta^{18}O$), and strontium (Sr/Ca) composition in two species of Pacific sclerosponges (*Acanthocheatetes wells*i and *Astrosclera willeyana*) with $\delta^{18}O$ calibration and application to paleoceanography. J Geophys Res Ocean 115:1–14

Gutleben J, Koehorst JJ, McPherson K, Pomponi S, Wijffels RH, Smidt H, Sipkema D (2019) Diversity of tryptophan halogenases in sponges of the genus *Aplysina*. FEMS Microbiol Ecol 95:fiz108

Haase-Schramm A, Böhm F, Eisenhauer A, Dullo W-C, Joachimski MM, Hansen B, Reitner J (2003) Sr/Ca ratios and oxygen isotopes from sclerosponges: temperature history of the Caribbean mixed layer and thermocline during the Little Ice Age. Paleoceanogr Paleoclimat

18:3

Hentschel U, Piel J, Degnan SM, Taylor MW (2012) Genomic insights into the marine sponge microbiome. Nat Rev Microbiol 10:641–654

Kolasinski J, Rogers K, Frouin P (2008) Effects of acidification on carbon and nitrogen stable isotopes of benthic macrofauna from a tropical coral reef. Rap Comm Mass Spec 22:2955-2960

Lang JC, Hartman WD (1975) Sclerosponges: primary framework constructors on the Jamaican deep fore-reef. J Mar Res 33:223-231

Langille MGI (2018) Exploring Linkages between taxonomic and functional profiles of the human microbiome. mSystems 3:e00163-17

Langille MGI, Zaneveld J, Caporaso JG, McDonald D, Knights D, Reyes JA, Clemente JC, Burkepile DE, Thurber RLV, Knight R, Beiko RG, Huttenhower C (2013) Predictive functional profiling of microbial communities using 16S rRNA marker gene sequences. Nat Biotechnol 31:814

Laverick JH, Andradi-Brown DA, Exton DA, Bongaerts P, Bridge TCL, Lesser MP, Pyle RL, Slattery M, Wagner D, Rogers AD (2016) To what extent do mesophotic coral ecosystems and shallow reefs share species of conservation interest? Environ Evid 5:16

Lesser MP (2006) Benthicpelagic coupling on coral reefs: Feeding and growth of Caribbean sponges. J Exp Mar Bio Ecol 328:277–288

Lesser MP, Mueller B, Pankey MS, Macartney KJ, Slattery M, Goeij JM (2020) Depth-dependent detritus production in the sponge, *Halisarca caerulea* . Limnol Oceanogr 65:1200-1216

Lesser MP, Slattery M (2018) Sponge density increases with depth throughout the Caribbean. Ecosphere 9:e02525

Lesser MP, Slattery M, Laverick JH, Macartney KJ, Bridge TC (2019) Global community breaks at 60 m on mesophotic coral reefs. Glob Ecol Biogeogr 28:1403–1416

Lesser MP, Slattery M, Leichter JJ (2009) Ecology of mesophotic coral reefs. J Exp Mar Bio Ecol 375:1–8

Lesser MP, Slattery M (2011). Phase shift to algal dominated communities at mesophotic depths associated with lionfish (*Pterois volitans*) invasion on a Bahamian coral reef. Biol Invasions 13:1855-1868.

Lesser MP, Slattery M, Stat M, Ojimi M, Gates RD, and Grottoli A (2010). Photoacclimatization by the coral Montastraea cavernosa in the mesophotic zone: light, food, and genetics. Ecology, 91, 990-1003.Lesser MP, Slattery M, Mobley CD (2018) Biodiversity and functional ecology of mesophotic coral reefs. Ann Rev Ecol Evol Syst 49:49–71

Loya Y, Eyal G, Treibitz T, Lesser MP, Appeldoorn R (2016) Theme section on mesophotic coral ecosystems: advances in knowledge and future perspectives. Coral Reefs 35:1–9

Mackenzie GJ, Schaffner FC, Swart PK (2015) The stable isotopic composition of carbonate (C and O) and the organic matrix (C and N) in waterbird eggshells from South Florida: insights into feeding ecology, timing of egg formation, and geographic range. Hydrobiologia, 743:89-108

McMurdie PJ, Holmes S (2015) Shiny-phyloseq: web application for interactive microbiome analysis with provenance tracking. Bioinformatics 31:282-283

McMurray, SE, Stubler AD, Erwin PM, Finelli CM, Pawlik JR (2018). A test of the sponge-loop hypothesis for emergent Caribbean reef sponges. Mar Ecol Prog Ser 588:1-14

Mohamed NM, Colman AS, Tal Y, Hill RT (2008) Diversity and expression of nitrogen fixation genes in bacterial symbionts of marine sponges. Environ Microbiol 10:2910–2921

Morrow KM, Fiore CL, Lesser MP (2016) Environmental drivers of microbial community shifts in the giant barrel sponge, *Xestospongia muta*, over a shallow to mesophotic depth gradient. Environ Microbiol 18:2025–2038

Mueller B, de Goeij JM, Vermeij MJA, Mulders Y, van der Ent E, Ribes M, van Duyl FC (2014) Natural diet of coral-excavating sponges consists mainly of dissolved organic carbon (DOC). PLoS One 9:e90152

Muscatine L, Porter JW, Kaplan IR (1989) Resource partitioning by reef corals as determined from stable isotope composition - I. $\delta^{13}C$ of zooxanthellae and animal tissue vs depth. Mar Biol 100:185–193.

Muscatine, L, Kaplan, IR (1994). Resource partitioning by reef corals as determined from stable isotope composition II. $\delta^{15}N$ of zooxanthellae and animal tissue versus depth. Pac Sci 48:304-312.

Parada AE, Needham DM, Fuhrman JA (2016) Every base matters: Assessing small subunit rRNA primers for marine microbiomes with mock communities, time series and global field samples. Environ Microbiol 18:1403–1414

Parnell AC, Inger R, Bearhop S, Jackson AL (2010) Source partitioning using stable isotopes: coping with too much variation. PloS one 5.3: e9672

Pawlik JR (2011) The chemical ecology of sponges on caribbean reefs: natural products shape natural systems. Bioscience 61:888–898

Pita L, Rix L, Slaby BM, Franke A, Hentschel U (2018) The sponge holobiont in a changing ocean: from microbes to ecosystems. Microbiome 6:46

Ren H, Sigman DM, Thunell RC, Prokopenko MG (2012) Nitrogen isotopic composition of planktonic foraminifera from the modern ocean and recent sediments. Limnol Oceanogr 57:1011–1024

Rix L, de Goeij JM, Mueller CE, Struck U, Middelburg JJ, van Duyl FC, Al-Horani FA, Wild C, Naumann MS, van Oevelen D (2016) Coral mucus fuels the sponge loop in warm- and cold-water coral reef ecosystems. Sci Rep 6:18715

Rocha LA, Pinheiro HT, Shepherd B, Papastamatiou YP, Luiz OJ, Pyle RL, Bongaerts P (2018)

Mesophotic coral ecosystems are threatened and ecologically distinct from shallow water reefs. Science 361:281–284

Santavy DL, Willenz P, Colwell RR (1990) Phenotypic study of bacteria associated with the Caribbean sclerosponge, *Ceratoporella nicholsoni*. Appl Environ Microbiol 56:1750–1762

Schubert CJ, Nielsen B (2000) Effects of decarbonation treatments on $\delta^{13}C$ values in marine sediments. Mar Chem 72:55-59

Shih JL, Selph KE, Wall CB, Wallsgrove NJ, Lesser MP, Popp BN (2020) Trophic ecology of the tropical Pacific sponge *Mycale grandis* inferred from amino acid compound-specific isotopic analyses. Microb Ecol 79:495-510

Slaby BM, Hackl T, Horn H, Bayer K, Hentschel U (2017) Metagenomic binning of a marine sponge microbiome reveals unity in defense but metabolic specialization. ISME J 11:2465–2478

Slattery M, Lesser MP (2014). Allelopathy in the tropical alga *Lobophora variegata* (P haeophyceae): mechanistic basis for a phase shift on mesophotic coral reefs?. Journal of Phycology, 50:493-505.

Slattery M, Lesser MP (2015) Trophic ecology of sponges from shallow to mesophotic depths (3 to 150 m): Comment on Pawlik et al. (2015) Mar Ecol Prog Ser 527:275–279

Slattery M, Gochfeld DJ, Diaz MC, Thacker RW, Lesser MP (2016) Variability in chemical defense across a shallow to mesophotic depth gradient in the Caribbean sponge *Plakortis angulospiculatus*. Coral Reefs 35:11–22

Slattery M, Gochfeld DJ, Easson CG, O'Donahue LRK (2013) Facilitation of coral reef biodiversity and health by cave sponge communities. Mar Ecol Prog Ser 476:71–86

Slattery M, Lesser MP, Brazeau D, Stokes MD, Leichter JJ (2011) Connectivity and stability of mesophotic coral reefs. J Exp Mar Bio Ecol 408:32–41

Swart PK, Greer L, Rosenheim BE, Moses CS, Waite AJ, Winter A, Dodge RE, Helmle K (2010) The ^{13}C Suess effect in scleractinian corals mirror changes in the anthropogenic CO_2 inventory of the surface oceans. Geophys Res Lett 37:5

Swart PK, Rubenstone JL, Charles C, Reitner J (1998) Sclerosponges : A new proxy indicator of climate. NOAA Climate and Global Change Program: Special Report 12:19

Swart PK, Thorrold S, Rosenheim B, Eisenhauer A, Harrison CGA, Grammer M, Latkoczy C (2002) Intra-annual variation in the stable oxygen and carbon and trace element composition of sclerosponges. Paleoceanogr Paleoclimat 17:1045

Taylor MW, Radax R, Steger D, Wagner M (2007) Sponge-associated microorganisms: evolution, ecology, and biotechnological potential. Microbiol Mol Biol Rev 71:295–347

Thomas T, Moitinho-Silva L, Lurgi M, Björk JR, Easson C, Astudillo-García C, Olson JB, Erwin PM, López-Legentil S, Luter H, Chaves-Fonnegra A, Costa R, Schupp PJ, Steindler L, Erpenbeck D, Gilbert J, Knight R, Ackermann G, Victor Lopez J, Taylor MW, Thacker RW, Montoya JM, Hentschel U, Webster NS (2016) Diversity, structure and convergent

evolution of the global sponge microbiome. Nat Commun 7:1–12

Trindade-Silva AE, Rua CPJ, Andrade BGN, Vicente ACP, Silva GGZ, Berlinck RGS, Thompson FL (2013) Polyketide synthase gene diversity within the microbiome of the sponge Arenosclera brasiliensis, endemic to the southern Atlantic Ocean. Appl Environ Microbiol 79:1598–1605

Trussell GC, Lesser MP, Patterson MR, Genovese SJ (2006) Depth-specific differences in growth of the reef sponge *Callyspongia vaginalis*: role of bottom-up effects. Mar Ecol Prog Ser 323:149–158

Vacelet J, Willenz P, Hartman WD (2015) Living hypercalcified sponges: Treatise on invertebrate palaeontology, part E(revised), Porifera, vol. 4–5, pp. 1–14. Lawrence, KS: The University of Kansas Palaeontological Institute

van Duyl FC, Moodley L, Nieuwland G, van Ijzerloo L, van Soest RWM, Houtekamer M, Meesters EH, Middelburg JJ (2011) Coral cavity sponges depend on reef-derived food resources: stable isotope and fatty acid constraints. Mar Biol 158:1653–1666

van Duyl FC, Mueller B, Meesters EH (2018) Spatio-temporal variation in stable isotope signatures (δ13C and δ15N) of sponges on the Saba Bank. PeerJ 2018:1–25

Yahel G, Sharp JH, Marie D, Häse C, Genin A (2003) In situ feeding and element removal in the symbiont-bearing sponge *Theonella swinhoei*: Bulk DOC is the major source for carbon. Limnol Oceanogr 48:141-149.

Ye Y, Doak TG (2009) A parsimony approach to biological pathway reconstruction/inference for genomes and metagenomes. PLoS Comput Biol 5:e1000465

Zhang F, Blasiak LC, Karolin JO, Powell RJ, Geddes CD, Hill RT, Karl DM (2015) Phosphorus sequestration in the form of polyphosphate by microbial symbionts in marine sponges. Proc Natl Acad Sci USA 112:4381–4386

Figure 33 (S1). Map showing study location on Grand Cayman (Google Maps, 2020). The inset map shows the Kittiwake Artificial Reef site and the dashed line is where samples were collected along the depth gradient.

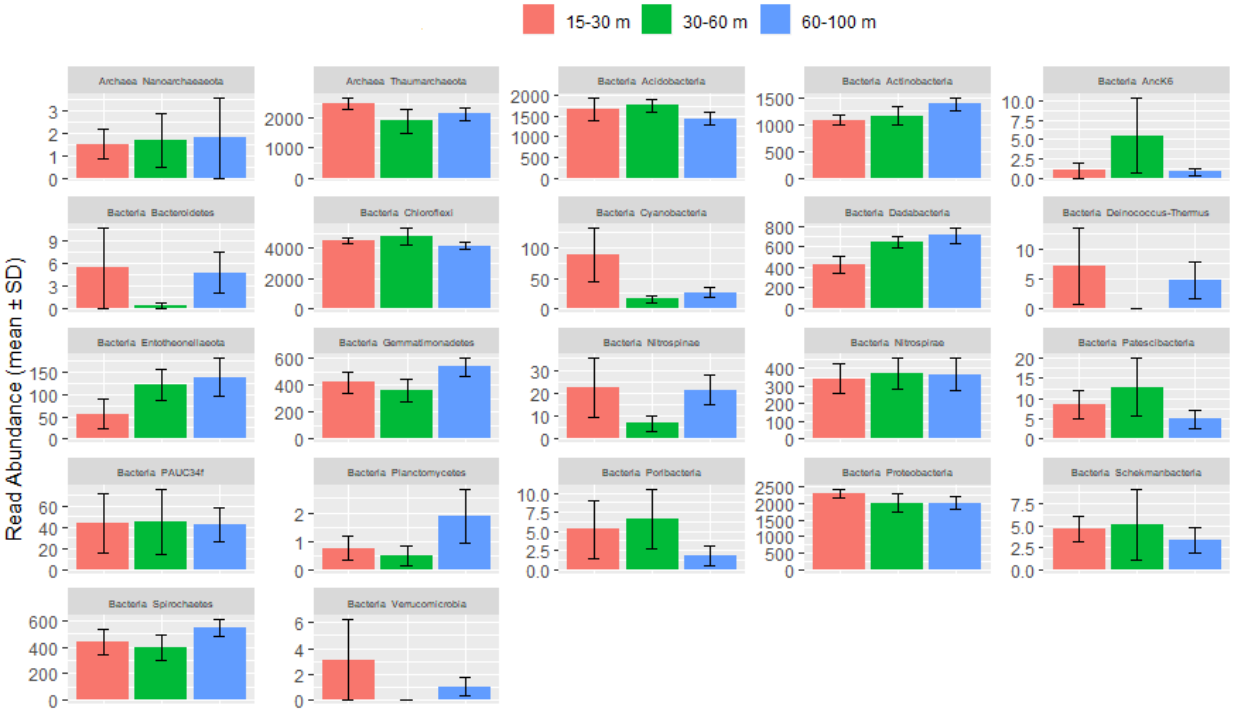

Figure 34 (S2). Mean (± SD) read abundance of phyla in *Ceratoporella nicholsoni* samples from shallow to mesophotic depths.

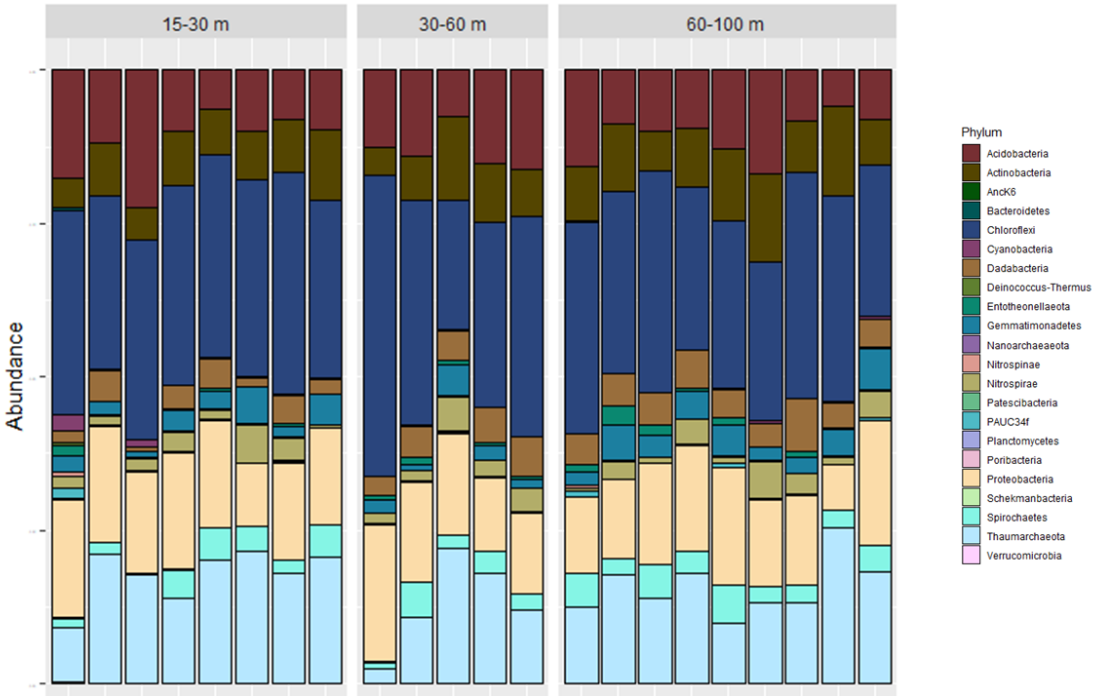

Figure 35 (S3). Relative abundance (percentage) at the Phylum level for the community composition of the *Ceratoporella nicholsoni* microbiome along a shallow to mesophotic depth gradient.

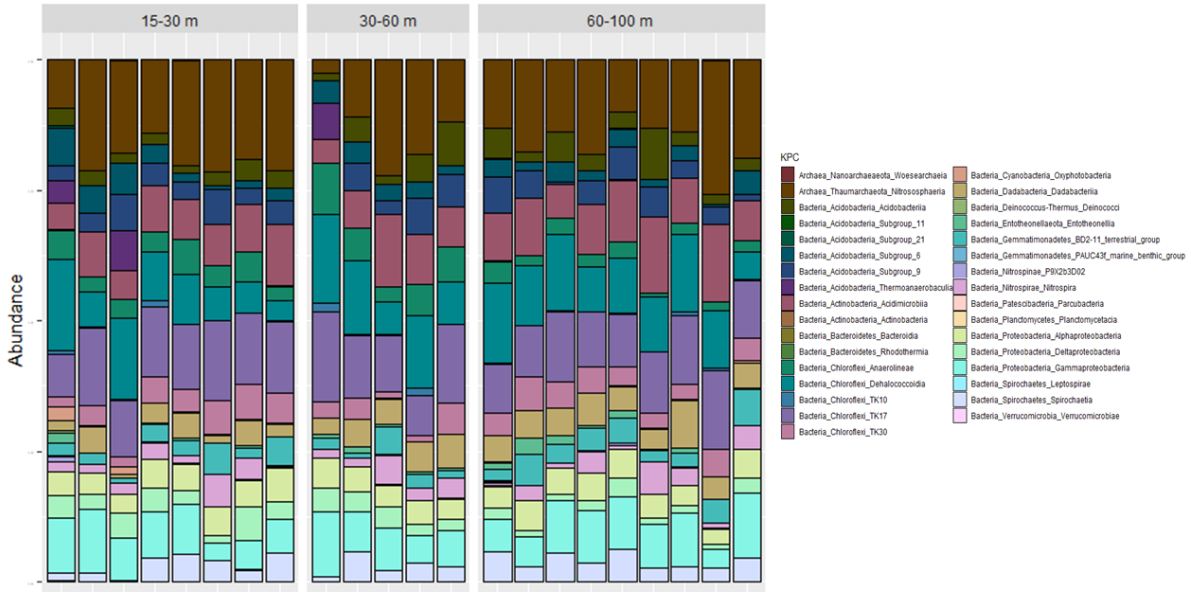

Figure 36 (S4). Relative abundance (percentage) at the Class level for the community composition of the *Ceratoporella nicholsoni* microbiome along a shallow to mesophotic depth gradient.

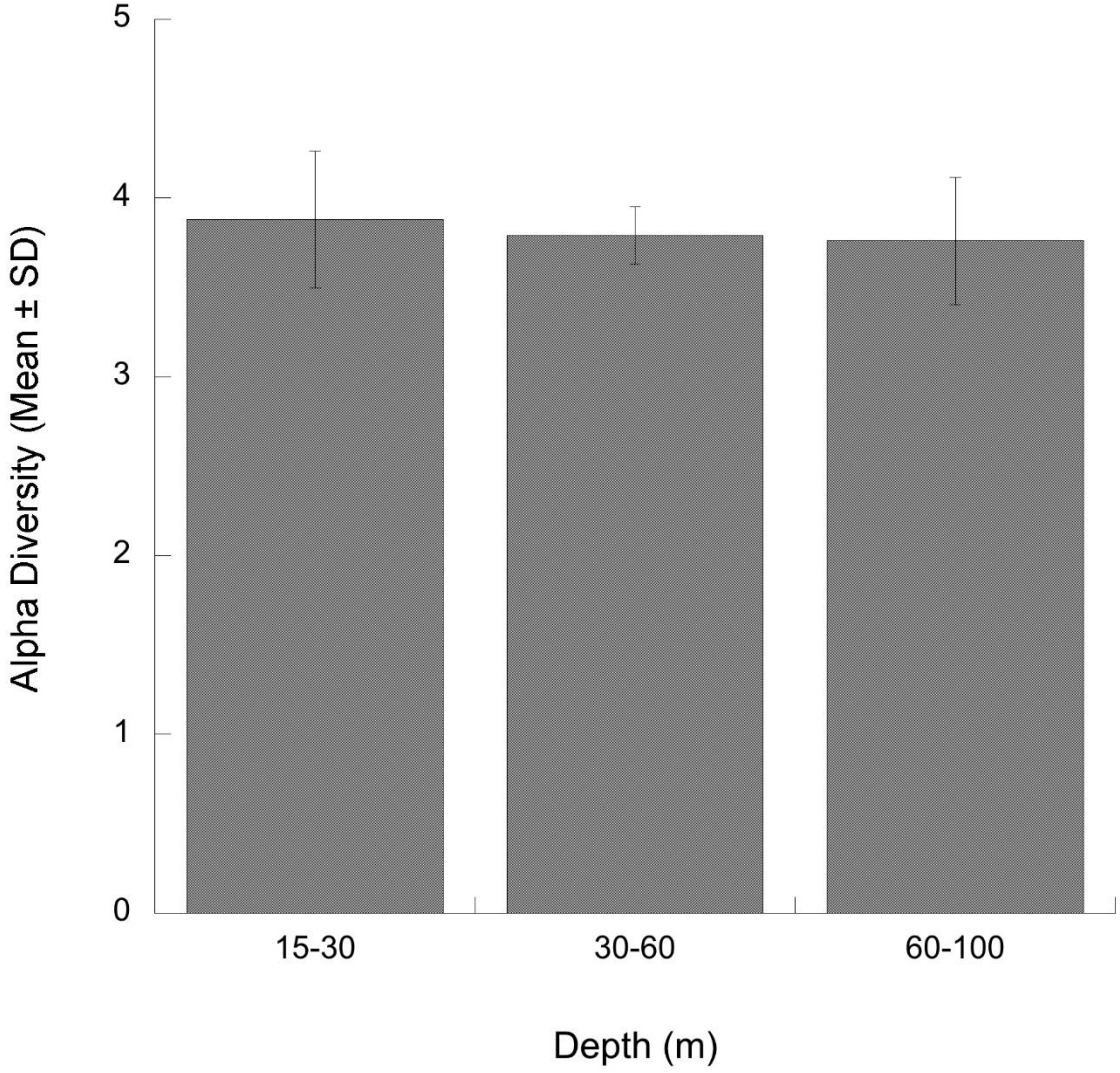

Figure (37) S5. Alpha diversity quantified using the Shannon diversity index for *Ceratoporella nicholsoni* samples from shallow to mesophotic depths.

Table 16 (S1). Mean values of $\delta^{13}C$, $\delta^{15}N$ and C:N ratios **(±** SE**)** for *Ceratoporella nicholsoni* along the shallow to mesophotic depth gradient in Grand Cayman, Cayman Islands.

Depth (m)	$\delta^{13}C$ (± SE)	$\delta^{15}N$ (± SE)	C:N (± SE)
15-30 m	-18.09 (0.19)	3.84 (0.34)	4.88 (0.05)
30-60 m	-18.07 (0.18)	4.46 (0.37)	4.86 (0.06)
60-90 m	-18.16 (0.20)	4.61(0.31)	4.96 (0.06)

Table 17 (S2). Comparison between paired non-acidified and acidified $\delta^{15}N$ values from *Ceratoporella nicholsoni* tissue showing on average 0.53‰ (± 0.58‰ SD) enrichment in the acidified samples.

Depth Zone	$\delta^{15}N$ Acidified	$\delta^{15}N$ No Acidification	Percent Difference Acidified - No Acidification)
10-30m	5.09	4.57	0.52
10-30m	5.04	4.66	0.38
10-30m	5.05	3.68	1.37
10-30m	5.34	5.08	0.26
10-30m	4.64	4.28	0.36
10-30m	2.63	2.09	0.54
10-30m	3.57	2.55	1.02
30-60m	6.24	5.53	0.71
30-60m	6.30	5.81	0.49
30-60m	5.84	4.57	1.27
30-60m	2.74	2.38	0.36
30-60m	4.68	4.08	0.60
30-60m	5.09	4.39	0.70
60-90m	5.16	4.94	0.22
60-90m	3.47	5.06	-1.59
60-90m	4.90	4.55	0.35
60-90m	5.04	4.52	0.52
60-90m	5.87	4.95	0.92
60-90m	4.99	4.53	0.46
60-90m	5.16	4.49	0.67
60-90m	4.97	4.45	0.52
60-90m	5.13	4.07	1.06

Table 18 (S3). Contributions of most likely coral reef source end members to *Ceratoporella nicholsoni* diets. Bayesian means with 95% credibility intervals (in brackets) of source contributions (%) to sponge diets based on SIAR4.

Depth (m)	Macroalgae (%)	Coral (%)	Live POM (%)	Detritus POM (%)
15 - 30	26 (0-48)	22(0-35)	25 (0-44)	27 (0-47)
30 - 60	36 (0-84)	23 (0-43)	14 (0-30)	27 (1-48)
60 - 90	52 (30-82)	18 (0-36)	8 (0-18)	22 (0-39)

Table 19 (S4). Selected KEGG orthology genes from the predictive functional analysis of the *Ceratoporella nicholsoni* microbiome.

KEGG Gene	Function Type	Specific Function	Total Sum Counts
K00626	Carbon metabolism	Acetyl-CoA C-acetyltransferase	1,537,056
K01602	Carbon metabolism	Ribulose-bisphosphate carboxylase small chain	21,786
K01601	Carbon metabolism	Ribulose-bisphosphate carboxylase large chain	22,988
K01681	Carbon metabolism	Aconitate hydratase (acnA)	658,476
K00134	Carbon metabolism	Glyceraldehyde 3-phosphate dehydrogenase (gapA)	608,505
K01638	Carbon metabolism	Malate synthase (carbohydrate metabolism)	72,093
K01965	Carbon metabolism	Propionyl-CoA carboxylase alpha chain	29,351
K02707	Carbon metabolism	Photosystem II cytochrome b559 subunit alpha (psbE)	1,411
K01428	Nitrogen metabolism	Urease subunit alpha (ureC)	15,925
K00370	Nitrogen metabolism	Nitrate reductase / nitrite oxidoreductase, alpha subunit (narG, NarZ)	21,049
K00376	Nitrogen metabolism	Nitrous-oxide reductase (nosZ)	3,623
K02588	Nitrogen metabolism	Nitrogenase iron protein NifH (nifH)	1,977
K02586	Nitrogen metabolism	Nitrogenase molybdenum-iron protein alpha chain (nifD)	1,976
K10944	Nitrogen metabolism	Methane/ammonia monooxygenase subunit A (amoA)	54,842
K03385	Nitrogen metabolism	Nitrite reductase (cytochrome c-552) (nrfA)	360
K04561	Nitrogen metabolism	Nitric oxide reductase subunit B (norB)	1,221
K00366	Nitrogen metabolism	Ferredoxin-nitrite reductase (nirA)	860
K00368	Nitrogen metabolism	Nitrite reductase (NO-forming) (nirK)	184,632
K10150	Sulfur metabolism	Sulfate transport system substrate-binding protein (cysP)	9,346
K03119	Sulfur metabolism	Taurine dioxygenase (tauD)	37,764
K01507	Phosphorus metabolism	Inorganic pyrophosphatase (ppA)	407,648

K00912	Secondary metabolites	Tetraacyldisaccharide 4'-kinase (Lipopolysaccaride biosynthesis.	275,863
K05356	Secondary metabolites	All-trans-nonaprenyl-diphosphate synthase (Terpenoid backbone synthesis)	1062
K01582	Secondary metabolites	Lysine decarboxylase (Tropane, piperidine and pyridine alkaloid biosynthesis)	202
K14266	Secondary metabolites	Tryptophan 7-halogenase	2,168
K04517	Secondary metabolites	Prephenate dehydrogenase (Novobiocin biosynthesis)	537,918
K05555	Secondary metabolites	Cyclase (actIV) (Type 2 polyketide products)	33,265
K01779	Secondary metabolites	Aspartate racemase (Nonribosomal peptide structure synthesis)	31,858
K00801	Secondary metabolites	Farnesyl-diphosphate farnesyltransferase (Sesquiterpenoid and triterpenoid biosynthesis)	17,873
K06045	Secondary metabolites	Squalene-hopene/tetraprenyl-beta-curcumene cyclase (Metabolism of terpenoids and polyketides)	35,516
K00812	Secondary metabolites	Aspartate aminotransferase	425,144
K01692	Secondary metabolites	Enoyl-CoA hydratase (Geraniol degradation)	440,635
K03969	Stress response	Phage shock protein A	46,663
K03799	Stress response	Heat shock protein (htpX)	573,562